HERIOT-WATT UNIVERSITY
&
NATIONAL LASER CENTRE, CSIR

Mid-Infrared Diode-Pumped Solid-State Lasers

M.J. Daniel Esser

Thesis submitted
as part of the Engineering Doctorate in Photonics
at Heriot-Watt University.

Dr. Christoph Bollig, Local Supervisor
National Laser Centre, Council for Scientific and Industrial Research, South Africa

Prof. Denis R. Hall, Academic Supervisor
Heriot-Watt University, Edinburgh, Scotland

October 2010

Abstract

The concept of a diode-end-pumped Tm^{3+} laser pumping a Ho^{3+} laser was utilised to develop mid-infrared solid-state laser devices. After presenting an in-depth literature study of the promising material Tm:$GdVO_4$, it was theoretically predicted and experimentally verified that a diode-end-pumped Tm:$GdVO_4$ laser can be operated over a 100 nm wavelength range merely through the appropriate selection of the resonator output coupling value. The output at 1818 nm is the shortest wavelength demonstrated for a multi-watt Tm:$GdVO_4$ laser, while the quasi-continuous-wave output power of 8.7 W at 1915 nm is the highest reported for a diode-end-pumped Tm:$GdVO_4$ laser.

A dual-end-pumped Tm:$GdVO_4$ laser operating at 1892 nm was subsequently designed as pump source for a Ho:YLF laser, the implementation of which was demonstrated for the first time. The *Q*-switched Ho:YLF laser, pumped with a 83 mJ quasi-continuous-wave pulse of 19 ms duration at 5 Hz repetition rate, produced 1.9 mJ in a 17.6 ns pulse at 2051 nm on the π-polarisation, and 2.1 mJ in a 47.7 ns pulse on the σ-polarisation.

This initial research work directed the way towards the development of high-energy Ho^{3+} lasers and amplifiers pumped with alternative high average power Tm^{3+} laser devices.

Aan my geliefde vrou,

Irene-marié

Acknowledgements

I would firstly like to thank God for the creation of light, and for His abundant grace in my life. Further, I would like to acknowledge and pose my sincere gratitude towards:

- The CSIR National Laser Centre that fully sponsored my part-time formal studies.
- The CSIR Young Researcher Establishment Fund for awarding me the grant that formed the seed funding for 2 µm laser development in South Africa, also of the work presented here.
- ARMSCOR for their substantial and continued financial support of laser development projects at the CSIR National Laser Centre, which also formed part of the research presented in this thesis and additional publications.
- Hardus Greyling and Lourens Botha at the National Laser Centre for your moral support and faith in my ability to complete this work in due time.
- The Laser Sources Group members, Christoph Bollig, Dieter Preussler, Cobus Jacobs, Hencharl Strauss, Wayne Koen, Oliver Collett, Edward Bernhardi, and Kwanele Nyangaza for your technical ideas and acceptance of my work methods. Your technical contributions resound in our joint publications.
- Caroline Howes for your personalised support of the Laser Sources Group and Corrie van der Westhuizen for your professional opto-mechanical design drawings, which have also been presented in this work.
- Martin Shellhorn of the French-German Research Institute in Saint Louis, for your experience that you shared during your sabbatical at the National Laser Centre and for the successful research collaboration, the work of which is also reported here.
- My local supervisor, Dr Christoph Bollig, for extensively sharing your knowledge since we started working together in 2002. Thank you for allowing me to grow into a researcher of my own right.
- Professor Denis Hall, for your unwavering commitment towards building Photonics in South Africa, which has also been exemplified by your encouragement and contribution to the completion of this thesis.
- My family and friends who encouraged me up to the end. In particular my father, Jan Esser, who moved mountains and who taught me to continue to give my best.

Finally, I want to thank my wife, Irene-marié. Without you it would have simply not been possible.

ACADEMIC REGISTRY

Research Thesis Submission

Name*:*	M J Daniel Esser		
School/PGI:	EPS		
Version:	Final	Degree Sought	Engineering Doctorate in Photonics

Declaration

In accordance with the appropriate regulations I hereby submit my thesis and I declare that:

1) the thesis embodies the results of my own work and has been composed by myself.
2) where appropriate, I have made acknowledgement of the work of others and have made reference to work carried out in collaboration with other persons.
3) the thesis is the correct version of the thesis for submission and is the same version as any electronic versions submitted.
4) my thesis for the award referred to, deposited in the Heriot-Watt University Library, should be made available for loan or photocopying and be available via the Institutional Repository, subject to such conditions as the Librarian may require.
5) I understand that as a student of the University I am required to abide by the Regulations of the University and to conform to its discipline.

Signature of Candidate		Date	

Submission

Submitted By	M J Daniel Esser
Signature of Individual Submitting:	
Date Submitted:	

For Completion in Academic Registry

Received in the Academic Registry by *(name in capitals):*			
Method of Submission			
E-thesis Submitted			
Signature:		Date	

Contents

List of figures

List of tables

Chapter 1

Introduction

Mid-infrared solid-state laser systems have existed since the dawn of laser development [1, 2], but due to the improvement of diode laser technology and new laser materials, the interest in these lasers has grown significantly over the last few years. High power diode lasers with controlled beam quality opened up the opportunity to develop mid-infrared solid-state laser systems that are efficient and compact. However, to develop such a laser system requires a detailed study of suitable solid-state laser materials, laser excitation schemes, mounting techniques of laser crystals, resonator designs, as well as an in-depth analysis of experimental results. The objective of this thesis is to present the outcomes of the research study as defined below.

1.1 Research problem

The mid-infrared spectral region is generally accepted to be in the range of 2 µm to 5 µm [3]. One approach to produce laser output in this region is to develop a Thulium (Tm^{3+}) doped solid-state laser operating at 1.9 µm which provides the pump energy for a Holmium (Ho^{3+}) doped laser which operates at 2 µm. In turn, the Ho^{3+} doped laser can be used as pump source for generating coherent radiation further in the mid-infrared.

The Tm^{3+} laser system can be operated with high efficiency when pumped with one or more laser diodes. In addition, good beam quality can be achieved when such a solid-state laser is end-pumped with diode lasers (e.g. pumped longitudinally along the optical axis). However, the research problem remains of how to design a solid-state 2 µm laser system which is compact and efficient, especially when an attempt is made

to scale it to high power levels and if it is to be used for practical, non-laboratory applications.

The project scope was limited to Ho:YLF as gain material at 2 µm due to a number of favourable properties of this material. In particular, it has a long upper laser level lifetime of 14 ms, which is well suited for energy storage when operated in *Q*-switched mode. Further, the host crystal YLF has a weak negative thermal lens on the σ-polarisation, which can result in diffraction limited laser beams even under intense end-pumping. Finally, the range of output wavelengths obtainable with Ho:YLF, namely from 2050 nm on π-polarisation to 2064 nm on σ-polarisation was desired for a particular application for which the 2 µm laser system was being developed.

The purpose of this research project was therefore the development of a suitable Tm^{3+} pump laser for a *Q*-switched Ho:YLF laser, as well as the experimental implementation of the 2 µm laser system.

After careful consideration of which Tm^{3+} laser material to focus on, all the literature available on the chosen material, Tm:$GdVO_4$, has been studied and evaluated in detail. This knowledge was used to design and construct a novel diode-end-pumped Tm:$GdVO_4$ laser, which was ultimately used to pump a *Q*-switched Ho:YLF laser.

1.2 Overview of the thesis

In *Chapter 2* an introduction to Tm^{3+} and Ho^{3+} solid-state lasers is given, with a brief description of different schemes employed to produce 2 µm laser radiation. These include flash lamp pumped Cr:Tm:Ho co-doped lasers, diode-pumped Tm:Ho co-doped lasers, and diode-pumped Tm^{3+} lasers pumping Ho^{3+} lasers, including Tm:fibre laser pumped Ho^{3+} lasers. An overview of wavelengths obtained with crystalline Tm^{3+} lasers is also given. The concepts of diode end-pumping and diode side-pumping are compared, and the challenge of scaling diode-end-pumped lasers to high pump powers is discussed. The conclusion is reached that a diode-end-pumped Tm^{3+} laser pumping a Ho:YLF laser warrants further research and development.

An in-depth literature study and the history of the Tm:$GdVO_4$ laser material are presented in *Chapter 3*, including a description of the favourable properties of this material for diode-pumped operation. Power scaling experiments, as reported in the

literature, are evaluated to conclude that the most promising approach to develop a high power Tm:$GdVO_4$ laser is to implement a diode-end-pump design with high power laser diode modules as pump sources.

Chapter 4 is a detailed description of the design, development and experimental evaluation of a diode-end-pumped Tm:$GdVO_4$ laser, pumped with a single fibre-coupled laser diode. Both continuous-wave operation, as well as quasi-continuous-wave (QCW) operation are described and the performance parameters of the Tm:$GdVO_4$ laser with two different output coupler mirrors are evaluated against the theoretically expected wavelengths, polarisations and oscillation threshold values. It is shown that by careful analysis of the emission spectra, the Tm:$GdVO_4$ laser can be tuned over a 100 nm wavelength range simply by appropriate selection of the reflectivity of the output coupler.

Since it was experimentally verified that a Tm:$GdVO_4$ laser can be efficiently operated with multi-watt output over a wavelength range that is suitable for pumping a Ho:YLF laser, a modified dual-end-pumped Tm:$GdVO_4$ laser was developed to operate at 1892 nm to be specifically used as pump source for a Ho:YLF laser, which is described in *Chapter 5*.

The experiments which represent the first reported demonstration of a Tm:$GdVO_4$ laser pumping a Ho:YLF laser are presented in *Chapter 6*. In this chapter the optical layout to couple the Tm:$GdVO_4$ laser output into the 40 mm long, 0.5% doped Ho:YLF crystal is described. In addition, two Ho:YLF resonator designs are presented, the first being a simple linear resonator with low internal loss, but with limited performance when *Q*-switched. By implementing an improved folded three-mirror resonator *Q*-switched Ho:YLF laser, output energies of 1.9 mJ and 2.1 mJ were demonstrated with the Ho:YLF laser operating on π-polarisation and σ-polarisation, respectively. The conclusion is made that the research goal of developing a solid-state 2 µm laser system was accomplished in the form of the Ho:YLF laser end-pumped by the custom-developed Tm:$GdVO_4$ laser.

Chapter 7 provides a summary of the significant results achieved with the Tm:$GdVO_4$ laser material in different configurations, and also highlights the importance of the first demonstration of a Tm:$GdVO_4$ pumped Ho:YLF laser. Several recommendations are

made to scale the power and energy of the demonstrated laser devices. These recommendations for Tm:$GdVO_4$ include the use of crystals of higher quality, with lower doping concentration and in slab geometry. Finally, a conclusion is reached regarding the approach of a diode-pumped Tm^{3+} laser pumping a Ho^{3+} laser to obtain 2 µm laser output.

A short description of the mid-infrared laser systems that were subsequently developed by the research team at the National Laser Centre, and in which the author played a significant role in terms of design, experiment and analysis is presented in *Chapter 8*. These laser systems include:

- a novel approach to efficiently pump a Ho:YLF oscillator-amplifier with a randomly polarised Tm:Fibre laser [4];
- a world-leading single-frequency Ho:YLF oscillator-amplifier system producing 70 mJ per pulse at 50 Hz [5];
- a high power continuous-wave Tm:YLF slab laser with more than 200 W output at 1.9 µm [6, 7, 8];
- a high-energy 2 µm amplifier simultaneously utilising both a Ho:YLF and a Ho:LuLF slab crystal as gain media, pumped by a modified Tm:YLF slab laser producing 180 W at 1892 nm [9];
- a hybrid stable-unstable slab oscillator using the same Tm:YLF pump laser and slab Ho:YLF and Ho:LuLF crystals [10].
- a molecular hydrogen bromide laser which produced pulsed laser output at 4 µm wavelength, pumped with the custom-developed single-frequency Ho:YLF oscillator-amplifier system [11].

The *Publication List* at the end of the thesis provides a list of published work by the author and co-workers on the research presented in this thesis and additional collaborative research that followed the initial project. The publication list also includes reference to a comprehensive series of *Monthly Technical Reports* and *Project Technical Reports* which were prepared for the principal external sponsor of the research. In practice, these reports were accompanied by detailed oral presentations describing technical progress and achievements.

1.3 References

[1] L. F. Johnson, G.D. Boyd, and K. Nassau "Optical maser characteristics of Ho^{3+} in $CaWO_4$," Proceedings of IRE **50**, 87 (1962).

[2] L. F. Johnson, G.D. Boyd, and K. Nassau "Optical maser characteristics of Tm^{3+} in $CaWO_4$," Proceedings of IRE **50**, 86 (1962).

[3] I.T. Sorokina, K.L. Vodopyanov (Eds.), Solid-State Mid-Infrared Sources, Topics in Applied Physics, vol. 89, Springer, Berlin, Heidelberg, (2003).

[4] W. Koen, C. Bollig, H. Strauss, M. Schellhorn, C. Jacobs and M. J. D. Esser, "Compact Fibre-Laser-Pumped Ho:YLF Oscillator-Amplifier System," *Applied Physics B* **99** (1-2) 101-106 (April 2010).

[5] C. Bollig, M. J. D. Esser, C. Jacobs, W. Koen, D. Preussler, K. Nyangaza and M. Schellhorn, "70 mJ Single-Frequency Q Switched Ho:YLF Ring Laser – Amplifier System Pumped by a Single 82-W Tm Fibre Laser," *Middle-Infrared Coherent Sources,* Trouville, France, 8-12 June 2009, Mo3 **(*invited*)** (2009).

[6] M. Shellhorn, S. Ngcobo, and C. Bollig, "High-power diode-pumped Tm:YLF slab laser" *Applied Physics B* **94** (2) 195-198 (2008).

[7] E. H. Bernhardi, C. Bollig, M. Eichhorn, M. J. D. Esser, P. Fuhrberg, A. Hirth, C. Kieleck, M. Schellhorn and K. Scholle, "High-Power Diode-Pumped 2 µm Lasers," *17th International Laser Physics Workshop (LPHYS'08), Trondheim, Norway,* p. 232, June/July 2008 **(*invited*)** (2008).

[8] M. Schellhorn, S. Ngcobo, C. Bollig, M. J. D. Esser, D. Preussler, K. Nyangaza, "High-power diode-pumped Tm:YLF slab laser," *CLEO Europe*, Munich, Germany, 14-19 June 2009, CA1.3 (2009).

[9] W. Koen, H. J. Strauss, C. Bollig, M. J. D. Esser**,** C. Jacobs, O. J. P. Collett, K. Nyangaza and D. Preussler "200 mJ Single Frequency Ho:YLF & Ho:LuLF Slab Amplifier System at 2064 nm" in *4th EPS-QEOD Europhoton Conference,*

Hamburg, Germany, WeC4, Europhysics Conference Abstract Volume 34C, ISBN 2-914771-64-9, (2010).

[10] M. J. D. Esser**,** H. J. Strauss, W. Koen, O. J. P. Collett and C. Bollig "End-pumped Ho:YLF & Ho:LuLF Slab Laser" in *4th EPS-QEOD Europhoton Conference*, Hamburg, Germany, WeP29, Europhysics Conference Abstract Volume 34C, ISBN 2-914771-64-9, (2010).

[11] L. R. Botha, C. Bollig, M. J. D. Esser, R. N. Campbell, C. Jacobs and D. R. Preussler "Ho:YLF pumped HBr Laser," *Optics Express*, **17** (22) 20615–20622 (Oct 2009).

Chapter 2

Introduction to diode-pumped Tm and Ho lasers

Solid-state lasers in the mid-infrared can be classified into three main groups, depending on whether the laser gain medium is a rare-earth-based ionic crystal, a transition-metal-based ionic crystal, or a colour-centre-medium-based laser. The most commonly used rare-earth ions for laser action in the mid-infrared are Tm^{3+}, Ho^{3+} or Er^{3+}, while transition-metal lasers and colour-centre solid-state lasers are of much less interest. Such lasers and Er^{3+} based lasers will not be discussed further since they offer less promise to realise compact high power laser devices in the mid-infrared spectral region. More information on these lasers can be found in [1, 2].

When considering Tm^{3+} and Ho^{3+} ions as the basis of potential diode-pumped lasers, it is important to note the wavelength bands where these materials can be optically pumped, as well as the emission wavelength ranges. Tm^{3+} doped solid-state lasers can be pumped with laser diodes emitting at around 0.8 µm, and produce laser oscillation at 1.9 – 2.0 µm. Ho^{3+} doped lasers cannot be pumped directly by typical near-infrared laser diodes, but is best pumped at 1.9 µm to subsequently produce laser oscillation in the wavelength range from 2.0 – 2.1 µm.

An important application of diode-pumped Tm^{3+} lasers is therefore to pump Ho^{3+} lasers. This approach has been followed, as described later in this thesis, to develop a Tm:$GdVO_4$ laser to pump a *Q*-switched Ho:YLF laser. However, it was considered worthwhile to evaluate a range of different possibilities to produce laser output at 2 µm from a Ho^{3+} doped or Ho^{3+} co-doped system, as described in the next sections.

The following schemes can be employed to produce 2 µm laser output from a Ho^{3+} doped or co-doped system, and are discussed in detail below:

- Flash lamp pumped, Tm:Ho co-doped systems
- Diode-pumped, Tm:Ho co-doped systems
- Diode-pumped Tm-doped laser pumping a Ho-doped laser or amplifier
- Tm:fibre laser pumped Ho-doped systems

2.1 Flash lamp pumped, Tm:Ho co-doped systems

The most traditional method for "pumping" light energy into a solid-state laser medium is to use high-voltage flash lamps and arc lamps. The very first laser that was demonstrated in 1960 used this technique [3]. This method of coupling flash lamp energy into a laser medium, which can be used for stimulated emission at 2 µm, is conceptually shown in Figure 2.1.

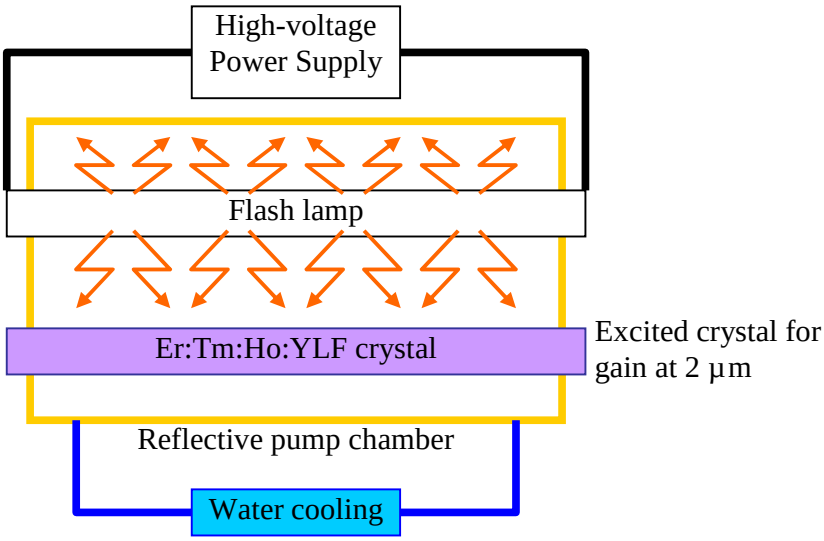

Figure 2.1: Concept of a flash lamp pumped 2 µm gain module.

Flash lamps and arc lamps usually consist of a quartz tube sealed at the ends by two electrodes. The tube is filled with a gas, for example xenon or krypton at a suitable pressure such that when a high voltage is applied to the electrodes, an arc discharge can take place in the gas. The light emission from the gas discharge can be coupled into a laser medium, thereby storing energy in the medium. The stored energy can be extracted from the laser medium by laser oscillation in a resonator or by amplifying a laser pulse passing through the crystal. In the 2 µm system presented above, the laser medium is an YLF crystal co-doped with Er, Tm and Ho.

Unfortunately with this technique, the coupling efficiency of pump light into the medium is usually low, since the incoherent pump light cannot be coupled with high optical density into the laser medium and only a small portion of the omni-directional radiation from a lamp source can be focussed into the gain crystal [4]. This is illustrated in Figure 2.2 below, where only a small portion of the light emitted from the flash lamp is coupled into the laser medium in a reflective pump chamber. Although the coupling efficiency can be improved by elaborate pump chamber designs, it is always less than what can be achieved with more modern technologies.

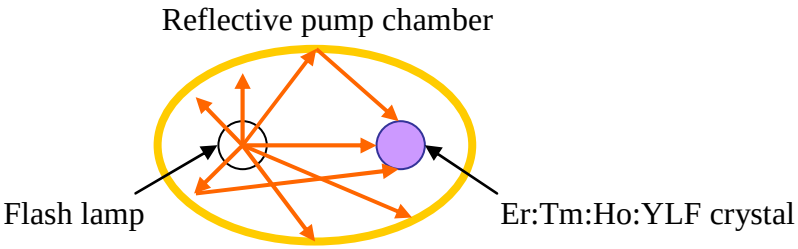

Figure 2.2: End-view of the flash-lamp pumped 2 µm gain module. Some portion of the light emitted by the flash lamp is reflected by the pump chamber into the laser medium.

An additional disadvantage of this scheme is that, usually, the broad spectral output of flash lamps and arc lamps overlap poorly with the absorption spectrum of solid-state laser materials. This is of particular concern for the type of laser medium required in for a 2 µm laser system. For example, the Ho^{3+} ion cannot be efficiently excited by flash lamp energy directly, making it necessary for the laser medium to also consist of co-dopants. The energy levels of the co-doped system and energy transfer processes are indicated in Figure 2.3.

The Cr^{3+} ion (or Er^{3+} if the host crystal is YLF) needs to be present in order to absorb the broad wavelength emission from the flash lamp into the pump energy band. From the high-lying Cr^{3+} pump bands ^2E and $^4T_2$, the energy can be transferred to the $^3F_3$ level of Tm^{3+} from where it decays non-radiatively to the $^3F_4$ level. If the Tm^{3+} concentration is sufficiently high the cross-relaxation process $^3F_4 \rightarrow {}^3H_4$, $^3H_6 \rightarrow {}^3H_4$ can take place which leaves two Tm^{3+} ions excited in the $^3H_4$ level. From here the energy can be subsequently transferred to the $^5I_7$ level of the Ho^{3+} active ion, which can ultimately provide stimulated emission at 2 µm wavelength in the transition $^5I_7 \rightarrow {}^5I_8$ [2]. The presence of these additional ions is detrimental for high-energy operation due to additional complex energy transfer processes in the laser medium,

which could lead to inefficiencies and the deposition of a significant heat load into the laser crystal [5].

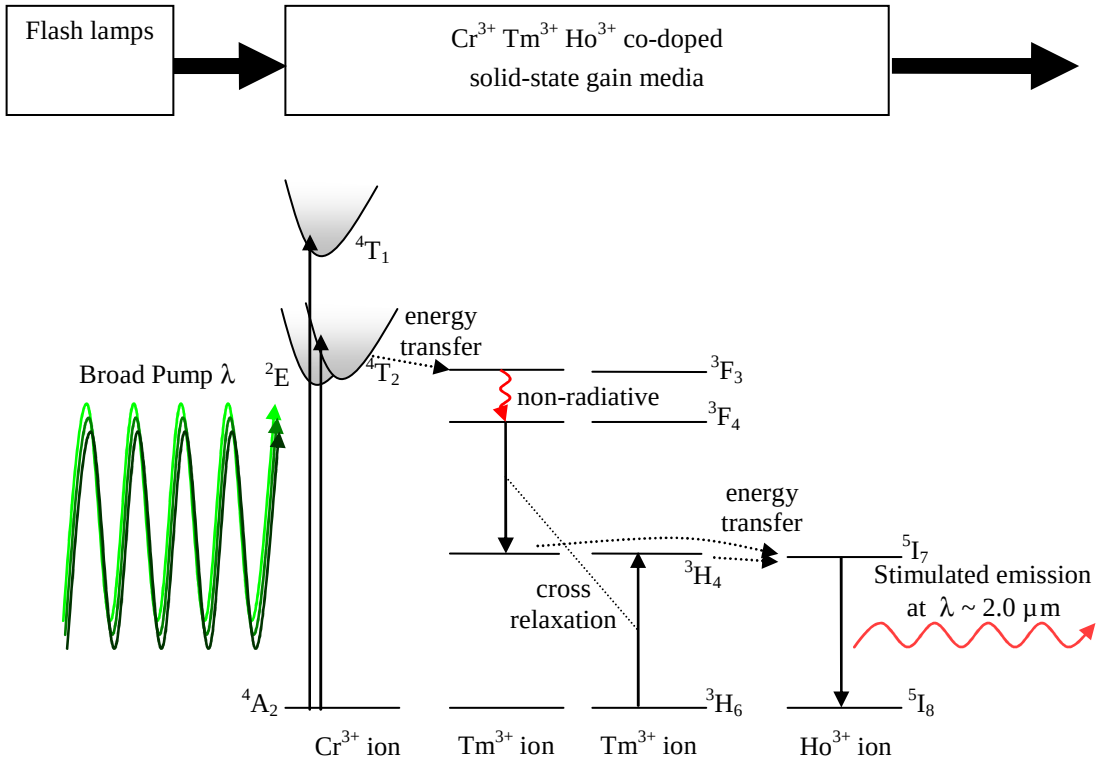

Figure 2.3: Energy levels and transfer mechanisms in a flash lamp pumped Cr:Tm:Ho co-doped 2 µm system [2].

The main reason why flash lamp pumped systems were able to develop as far as they did, is the fact that the electrical-to-optical efficiency of arc discharges is high, in the order of 70%. With suitable power supplies, tens of mega joules of pulsed energy and hundreds of kilowatts of power can be delivered by lamp sources. Therefore, the amount of power that is coupled into the laser medium, although a small portion of the total pump power, can be significant. The other advantage of flash lamps is that the technology is not expensive, and the price per watt or, alternatively, the price per joule is very low.

However, the overall electrical-to-optical efficiency of high power lamp-pumped solid-state lasers is in the order of a few percent only [e.g. 6]. A large proportion of the wasted energy is converted into heat, which necessitates water cooling of the pump chamber that houses the flash lamps and crystals. Additional disadvantages of lamp-pumped systems include the limited lifetime of flash lamps and arc lamps, the

elaborate power supplies necessary to drive high voltage discharges in short pulses, and instabilities in the laser output due to the statistical nature of gas discharges [7].

It can be concluded that these disadvantages are the limiting factors when considering this technology for modern 2 µm solid-state laser systems. The design and implementation of such a flash lamp pumped system does not require significant research and development but would only utilise existing methods and techniques, the limitations of which are well known. Several other options are available for the design of a modern 2 µm solid-state laser system, as discussed in the remainder of this chapter.

2.2 Diode-pumped, Tm:Ho co-doped systems

It has become widely accepted that diode-pumped solid-state laser and amplifier systems, as compared to flash lamp-pumped systems, are much more efficient and produce lower thermal load in the laser medium, which generally results in laser beams with higher beam quality. This is also the case for 2 µm solid-state laser systems. The concept of a high-power diode-side-pumped 2 µm laser system based on co-doped Tm:Ho:YLF as gain medium is shown in Figure 2.4 below.

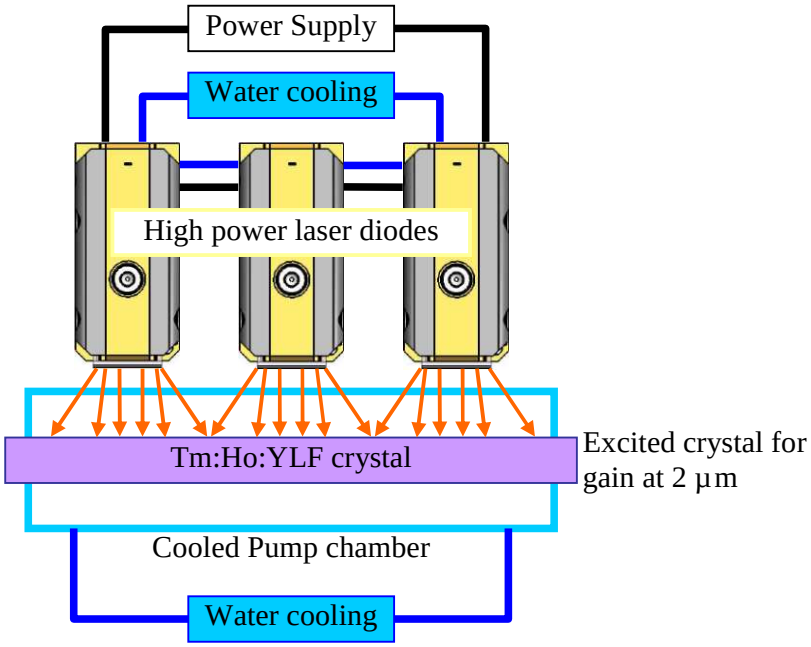

Figure 2.4: Concept for a diode-side-pumped 2 µm solid-state laser system.

Although the concept presented here at first glance seems to be very similar to the flash lamp pumped amplifier, there are very important differences which makes the diode-pumped approach more favourable. The only aspect which is the same is the side-pumping geometry, which will be critically discussed later in this section.

2.2.1 Properties of a diode-pumped 2 µm system

The favourable properties of the diode-pumped approach are the following:

- Diode laser radiation can have a good spectral overlap with the absorption band of solid-state laser media.
- The laser medium requires a less complicated composition of ions.
- The laser head and pump source can be spatially separated.

The main advantage of using diode lasers to pump solid-state lasers and amplifiers, as compared to lamp-pumped systems, is the high efficiency that can be achieved in coupling the laser diode power into the laser medium. The semiconductor material of the laser diode can be engineered such that essentially all the optical power delivered by the laser diode falls within the absorption band of the solid-state laser material. Expressed in another way, the laser medium absorbs all of the pump light because the wavelength of the pump light is chosen to match the absorption spectrum of the laser material. This improves the overall efficiency of the system, even if the typical electrical to optical efficiency of diode lasers is less than that of lamp sources. Most high-power laser diodes have an electrical to optical efficiency in the order of 25% – 50%, but, by selecting the optimum wavelength of the laser diode, all of the optical power can be absorbed by the laser material, making the system very efficient.

Additional fundamental advantages of using diode lasers to pump solid-state gain media include the following [7, 8, 9]:

- the high brightness output of a diode laser allows the pump light to be focussed with high optical density, leading to high gain in the laser medium;
- the good spectral overlap between diode radiation and the absorption spectrum of a laser medium leads to a reduction in thermal load in the medium which can lead to better beam quality;
- the high coupling efficiency can lead to the development of laser systems which are challenging as lamp pumped systems, including for example quasi-three-level 2 µm systems;

- laser diodes are quiet pump sources with good amplitude and spectral stability, leading to stable operation of the solid-state laser. This is critical for single-frequency laser oscillators, also at 2 µm wavelength.

Favourable operating conditions of diode lasers, which have led to the wide-range implementation of diode-pumped solid-state lasers and amplifiers, are notably:

- the low voltage operation, which allows power supplies to be stable, compact and safe;
- the long lifetime of the laser diodes that enables “maintenance free” operation of diode-pumped solid-state lasers and amplifiers;
- the separation of the pump source from the laser cavity due to delivery optics such as optical fibres, which allows for compact and robust system designs.

The last-mentioned favourable operating condition of laser diodes leads the discussion to the next point, namely that the laser head and pump source can be spatially separated.

The advantage of separating the laser head and the pump source is important with respect to thermal management, which is required for high average power and high-energy systems where a small percentage of waste heat can amount to a significant total value leading to low efficiency and increased optical distortion in the medium. The generated heat in laser diodes, which is a consequence of inefficiencies in the laser diodes themselves, must be managed. It is a major advantage if the pump source, where the heat is generated, is not thermally coupled to the laser head. This is even more so for quasi-three-level 2 µm laser systems because their performance will be strongly influenced by temperature. It is therefore worthwhile to explore methods by which the pump source and laser head can be separated.

Various techniques have been developed to couple the radiation of diode lasers into solid-state laser media. The technique of coupling the radiation directly into the medium without any intervening optics, which can make the system very compact, is essentially limited to diode-side-pump geometries and microchip laser designs. However, the advantage of separating the laser head and pump source is then lost.

Other techniques to couple diode radiation into solid-state laser media include the use of standard optics [10], GRIN lenses [11], micro-optics [12], lens ducts [13] and optical fibres [14]. These techniques allow the laser or amplifier medium to be side-pumped or end-pumped. The concepts of diode side-pumping and of diode end-pumping are discussed below.

2.2.2 Diode side-pumping

Consider as an example the cylindrical crystal laser rod shown in Figure 2.5 pumped from the side by diode laser radiation. The side-pump setup is usually implemented in such a way that the whole crystal is filled with diode radiation. The number of active ions excited by the radiation (the excitation density), decays exponentially from the edge of the crystal due to the Beer-Lambert absorption law. However, the diameter of the crystal is rarely more than the absorption length of the pump light. Reflective pump cavities are therefore necessary to reflect the transmitted pump light back into the solid-state laser crystal to improve the absorption efficiency of the system.

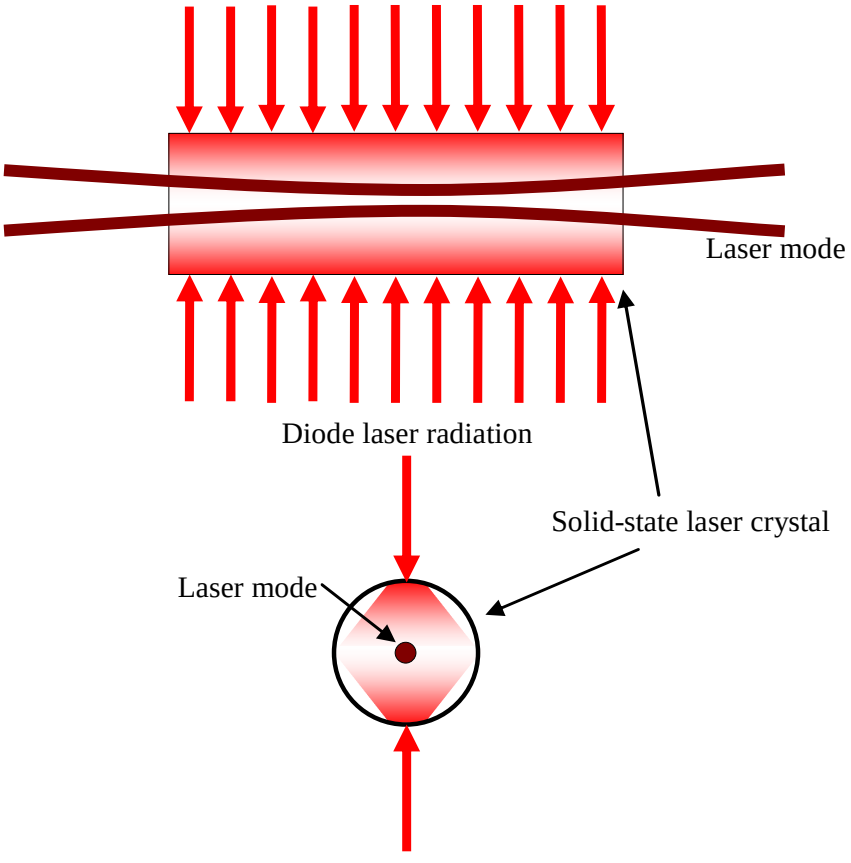

Figure 2.5: Diode-side-pumped solid-state crystal with the laser beam shown inside the crystal.

As stated, typically the whole crystal is excited and can act as the gain medium. Nevertheless, the only energy that can be extracted by the laser is the energy from the

excited ions that spatially overlaps with the laser beam inside the crystal. As seen in the example of Figure 2.5, the laser beam does not fill the whole crystal and does not overlap with the region where the gain is the highest, i.e. at the edge of the crystal.

An additional concern of the side-pumping scheme is that the beam shape and quality of the laser beam might be distorted from the fundamental TEM_{00} beam inside a laser oscillator. The outside areas of the laser beam which has a better overlap with the excited ions in the crystal, will have considerable gain as compared to the centre of the beam. This may decrease the optical quality of the laser beam, which is undesirable.

Implementing this technique will limit the energy that can be extracted from the gain medium in a fundamental TEM_{00} mode and, with this poor beam overlap efficiency, a large portion of the pump light is deposited as heat inside the crystal.

2.2.3 Diode end-pumping

If the solid-state laser crystal is pumped longitudinally, collinear with the laser beam, then it is referred to as end-pumping, as illustrated in Figure 2.6. This arrangement allows very good beam overlap efficiency because only the ions that spatially overlap with the laser beam are excited by the pump radiation.

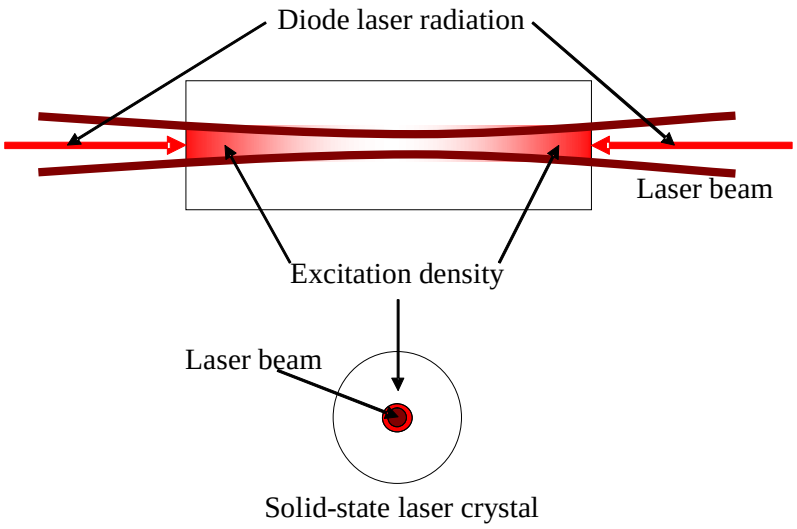

Figure 2.6: Diode end-pumped solid-state crystal showing the overlap of the excitation density and the laser beam inside the crystal.

High beam quality is ensured when only the fundamental laser mode has high gain in the crystal. This may be achieved by spatially overlapping the pump beam and the

laser beam inside the crystal. If this matching is performed successfully, the laser beam should maintain its fundamental beam shape and beam quality, while extracting power from the excited crystal.

In this arrangement good absorption efficiency of the pump light is achieved since the solid-state laser crystal is usually chosen to be significantly longer than the absorption length of the pump radiation. The absorption length is determined by the doping concentration of the active ions in the crystal, and the spectral (wavelength) overlap between the diode radiation and the crystal absorption spectra.

The practical advantage of end-pumping is that it usually facilitates a flexible system design since no additional pump cavities are necessary to reflect the pump light back into the solid-state laser crystal. This tends to lead to more compact designs since no provision needs to be made for coupling optics along the edge of the crystal. Rather, the design can be optimised for good heat extraction from the solid-state laser rod with either direct conductive or convective cooling.

The combination of the favourable properties of diode lasers and the advantages of the end-pump geometry results in the high efficiency and good beam quality of diode end-pumped solid-state laser systems. However, these advantages may be overshadowed by the onset of thermal distortions in the gain medium when scaling of these systems to high average output power or high energy is attempted, unless suitable precautions are taken. Although this geometry ensures overall less heat generation due to the good beam overlap efficiency, it does result in localised heating in the centre of the laser crystal rod. With intense pumping, the localised heating causes highly distorted thermal lensing which impairs the beam quality [15, 16, 17].

The problem of localised heating, and therefore considerable thermal lensing, is reduced for side-pumped systems. However, a balance between efficiency and thermal distortions can be found if the thermal effects in the solid-state laser crystal are well understood and are incorporated in the system design.

The optical-to-optical efficiency of well-designed diode-pumped solid-state lasers and amplifiers can be in the order of 30 - 50%, and even higher efficiencies have been demonstrated. This efficiency is considered high since energy is converted from diode

lasers at near infrared wavelength, which have “poor” beam quality with a wide spectral output, into highly coherent laser beams at, for example, 2 µm wavelength with diffraction limited beam quality. The energy from continuous or quasi-continuous diode radiation can also be stored with high efficiency in a solid-state laser crystal with a long upper laser level lifetime, such that it can be released as high-energy laser pulses.

The main disadvantage of diode-pumped systems, as compared to flash lamp pumped systems, is the relatively high cost of diode lasers. This, together with the unavailability of high power diode lasers with fair beam quality has hampered the development of diode-pumped solid-state lasers up to the middle 1990’s. However, the cost of diode laser power has decreased significantly over the last two decades. In addition to the lowering price, beam-shaping techniques have increased the brightness of diode lasers [18]. These beam-shaping techniques are increasingly used in commercial high power diodes, making the development of high power diode-pumped solid-state lasers and amplifiers feasible.

2.2.4 Limitations of diode-pumped Tm:Ho co-doped systems

Despite the advantages brought on by the use of laser diodes, the diode-pumped Tm:Ho co-doped technology is limited in efficiency at high energy operation due to the complex energy transfer processes taking place in the Tm^{3+} ion and the Ho^{3+} ion. The energy transfer processes are described with reference to Figure 2.7.

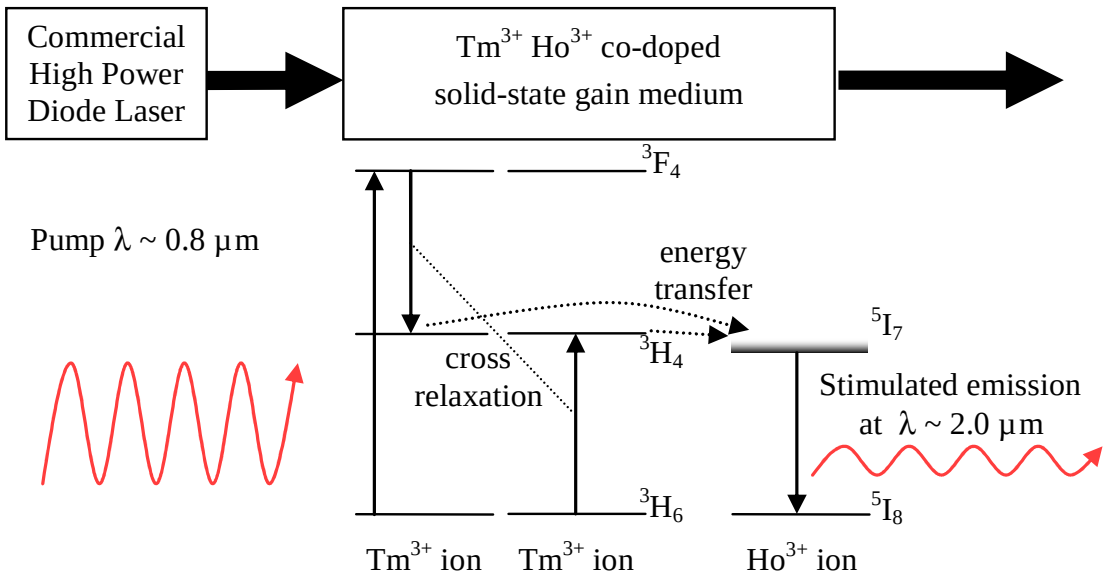

Figure 2.7: Energy transfer processes in a diode-pumped Tm:Ho co-doped system.

The Tm^{3+} ions are required for absorbing the pump wavelength at 0.8 µm. When doped in YLF, the absorption peak is at 793 nm, which requires that the laser diode wavelength should also be 793 nm. If this is the case, the Tm^{3+} ions will absorb the pump light and become excited to the upper energy level $^3F_4$. The process by which this energy can be transferred to the Ho^{3+} ion requires an additional Tm^{3+} ion which is physically close to the excited Tm^{3+} ion. The two ions can exchange approximately half of the stored energy through cross relaxation. At the end of this process two Tm^{3+} ions are excited to an intermediate energy level. From the intermediate level, it is a preferred process for the two Tm^{3+} ions to transfer the energy to close-lying Ho^{3+} ions [2, 19, 20].

For this method to be efficient, a high concentration of Tm^{3+} ions is usually required to enable cross relaxation, as well as a sufficient concentration of Ho^{3+} ions to enhance the energy transfer process. The end result of these cross relaxation and energy transfer processes is that Ho^{3+} ions are excited and are able to produce stimulated emission at 2 µm wavelength. However, there are many more energy levels of both the Tm^{3+} ions and the Ho^{3+} ions that can take part in energy transfer processes [20]. These additional processes are considered parasitic, some of which are highlighted in Figure 2.8.

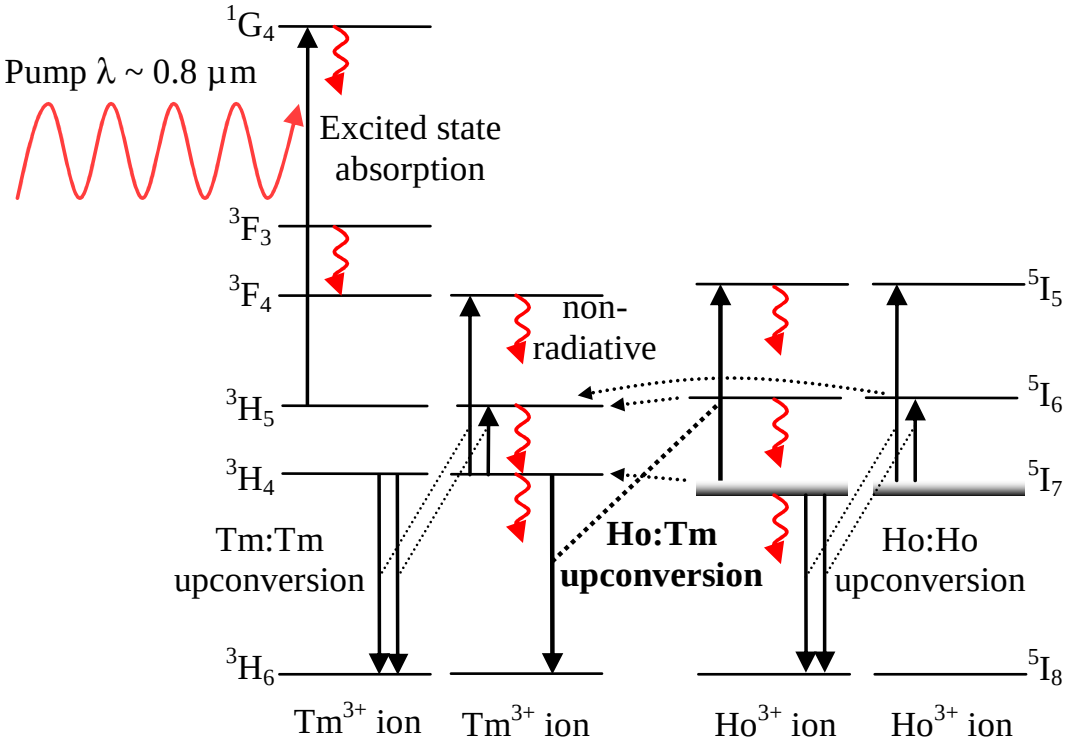

Figure 2.8: Parasitic processes in a Tm:Ho co-doped system [20].

Many of these parasitic processes are more pronounced at high-energy operation of the 2 µm laser system since energy storage is in the $^5I_7$ level of the Ho^{3+} ions which has a high population density. The upconversion processes in the system, of which the resonant Ho:Tm process is dominant, scale non-linearly with the population inversion. The consequences of the parasitic processes are that the energy storage lifetime is reduced, the stored energy is removed from the upper laser level $^5I_7$, and it can lead to significant heat load in the gain medium resulting in thermally-induced aberrations of the laser beam, and ultimately thermal fracture of the laser material.

It can be concluded that diode-pumped Tm:Ho co-doped systems are limited in their achievable output energy and efficiency due to the fundamental properties of co-doped systems. The limitations can be addressed by intensive engineering efforts to optimally design the concentration of Tm^{3+} and Ho^{3+} ions and the composition of the host crystal, as well as limiting the system to quasi-continuous-wave operation to reduce the heat load in the crystal [21]. An alternative solution for this problem is to have separate host crystals for the Tm^{3+} ion and the Ho^{3+} ion. Different approaches based on this principle are discussed below.

2.3 Diode-pumped Tm-doped laser pumping a Ho-doped system

The preferred solution to the problems associated with Tm and Ho co-doped systems is to construct a system based on a separate diode-pumped Tm-doped laser, pumping a Ho gain medium [22, 23, 24, 25]. This is indeed the best approach to scale the energy output of a 2 µm system. A schematic of this approach is indicated in Figure 2.9.

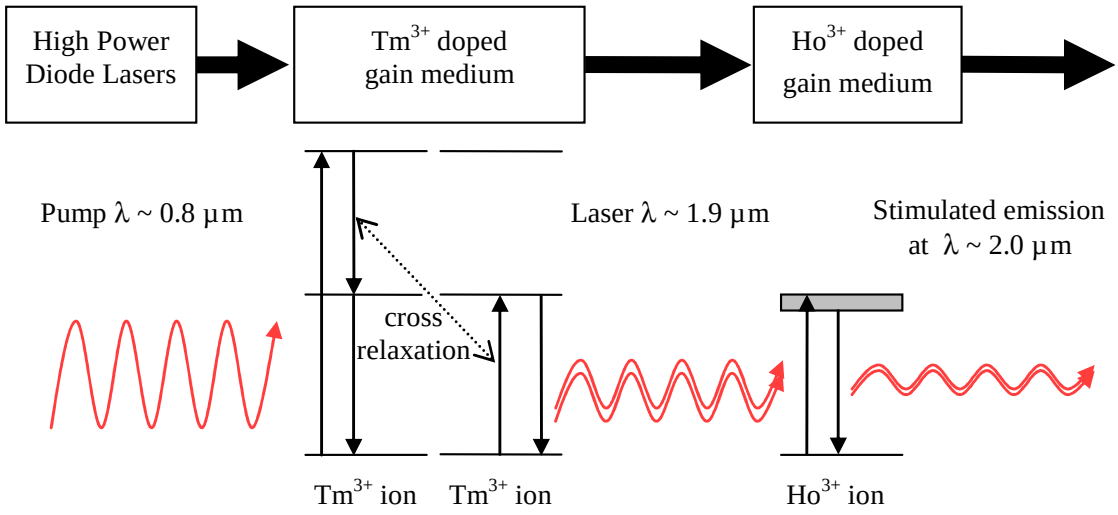

Figure 2.9: Schematic of a diode-pumped Tm-doped laser pumping a Ho-doped gain medium.

By considering the energy conversion processes taking place, the advantage of this approach can be visualised. The Tm-doped gain medium is pumped at 0.8 µm by high-power diode lasers to become excited to the upper energy level. If the Tm^{3+} ion concentration is at an optimal level, the excited Tm ions will exchange half of their stored energy with close-lying Tm ions in the ground state through the process of cross relaxation. At the end of this process the Tm ions are excited to the intermediate energy level, the so-called upper laser level.

The first part of pumping the Tm doped gain medium, is the same process as in the co-doped system described before. However, in this case, there can be no energy transfer processes to the Ho doped gain medium which is physically separated. The process that must be followed is an optical one.

In conjunction with a suitable laser resonator design, the excited Tm ions can release their stored energy by emitting laser light at 1.9 µm. This is the required wavelength at which the Ho-doped gain medium should be pumped. Through the process of optical absorption of the 1.9 µm light, the Ho ions in the gain medium become excited and store the pump energy in the upper energy level. From this level, it is possible to generate or amplify 2 µm laser light.

In this scheme of separated host media, the concentration of the Ho ions can be chosen to be optimal for energy storage by choosing a low doping level to avoid Ho:Ho upconversion. Most importantly though, the resonant Ho:Tm upconversion process cannot take place, making this scheme much more suited for energy storage in the Ho^{3+} upper laser level.

An additional advantage of this separated scheme is that most of the heat is generated in the Tm^{3+} host medium and less heat is generated in the Ho^{3+} doped crystal. The expected heat load in the system is illustrated in Figure 2.10.

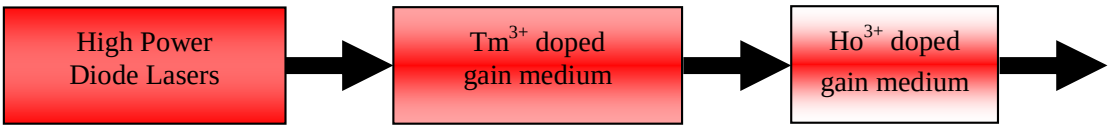

Heat load: high	Heat load: high	Heat load: low
Thermal management: optimal	Thermal management: good	Thermal management: good
Beam quality: low	Beam quality: sufficient	Beam quality: good

Figure 2.10: Heat load, thermal management and expected beam quality of a diode-pumped Tm laser, pumping a Ho-doped gain medium.

The pumping process of the Tm laser results in heat deposited in the host medium due to some inefficiency in the pumping scheme. In contrast, the heat deposited in the Ho-doped medium is only due to the quantum defect between the pump light at 1.9 µm and the laser light at 2 µm, which is minimal. The reason for this is that, in an ideal situation, the Ho ions are excited directly into the upper laser energy level, without any other energy levels being excited which could lead to unwanted heat load in the host crystal.

The consequence of the low heat load in the Ho-doped medium is that the 2 µm laser light will experience minimal thermal beam distortions in the crystal. This is important for generating or amplifying a 2 µm laser beam of good beam quality.

The heat load in the Tm pump laser is more significant, which could result in a pump beam with lower beam quality at 1.9 µm. However, this does not influence the system output too negatively, since the overall system can be designed such that the pump light for the Ho-doped medium need not have perfect beam quality. In practice, the requirement is only that a significant fraction of the available energy is pumped into the Ho-doped crystal over the typical absorption length of a few mm or cm. Additionally, since the Tm pump laser is physically separated from the Ho-doped crystal, the Tm laser can be designed such that the heat generated in the host medium is removed in the most efficient way possible.

2.3.1 Requirements of the pump laser at 1.9 µm

The research challenge of this scheme, where the Tm and Ho host materials are separate, is to be able to construct a suitable pump laser at 1.9 µm. For Ho:YLF, which

is the gain material chosen for the demonstration of a 2 µm laser system, the requirements of the pump laser at 1.9 µm are the following:

- **Operational mode:** continuous wave (CW) or quasi-continuous wave (QCW).
- **QCW pulse length:** longer than the $^5I_7$ level lifetime of Ho:YLF (14 ms).
- **Output power:** high, preferably 10 – 100 W.
- **Output wavelength:** tuned to one of the absorption peaks of Ho:YLF, i.e. at 1940 nm or 1892 nm.
- **Polarisation:** polarised output beneficial.
- **Output beam quality:** should be fair, so that the 1.9 µm pump beam can readily be focussed into the Ho-doped crystal and collimated over the absorption length.
- **Pumping scheme for Tm laser:** utilise commercially available diode lasers.

The requirements stated above drove the development of a Tm:$GdVO_4$ laser, as described in Chapter 4. However, the suitability of a number of Tm^{3+} doped solid-state laser designs was evaluated based on their output wavelength ranges and maximum output powers demonstrated in the literature, as discussed in the next section.

2.3.2 Overview of Tm^{3+} solid-state lasers at 1.9 µm

Tm^{3+} lasers are at the shorter end of the mid-infrared range, with output wavelengths ranging from 1.78 – 2.16 µm. The specific lasing wavelengths obtainable strongly depends on the host crystal within which Tm^{3+} is a dopant. Several other factors also influence the tuning range of a particular laser, including doping concentration, resonator configuration, and pump power. Shown in Figure 2.11 is a representation of the wavelength ranges attained during lasing with Tm^{3+} in different host crystals. Recent overviews of widely tuneable Tm^{3+} lasers are reported in [2, 26].

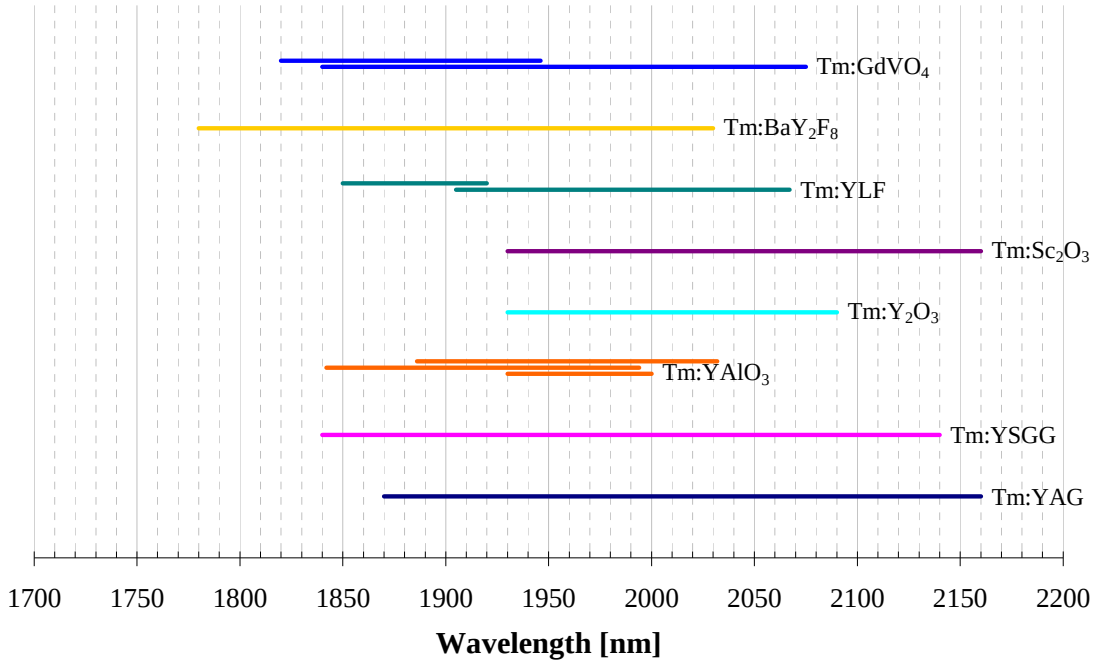

Figure 2.11: Wavelength ranges of several Tm^{3+} doped crystalline lasers [references in text].

YAG is a well known host material, and it has been demonstrated that Tm:YAG lasers can be tuned from 1.87 to 2.16 µm when pumped at 785 nm with a Ti:Sapphire laser [27]. In the same report, this material was compared with Tm:YSGG ($Y_3Sc_2Ga_3O_{12}$), which was tuned over a 300 nm range from 1.84 to 2.14 µm. The highest continuous-wave output power reported from a 2.02 µm diode-pumped Tm:YAG laser was 150W in a side-pump geometry, using a laser crystal with undoped end-caps [28].

Initial results obtained with a Tm:$YAlO_3$ laser (also known as Tm:YAP), indicated that tuneabilty from 1.93 to 2.00 µm could be achieved [29]. However, more recently this tuning range has been exceeded using a Ti:Sapphire pumped Tm:YAP laser which has been shown to be tuneable over the wavelength range from 1.842 µm to 1.994 µm [30], and by a diode-end-pumped Tm:YAP laser whose wavelength was scanned over a similar range, from 1.886 µm to 2.032 µm [31].

Rare-earth sesquioxides doped with Tm^{3+}, such as Tm:Y_2O_3 and Tm:Sc_2O_3, have been tuned from 1.93 to 2.09 µm and 1.93 to 2.16 µm, respectively [32]. They are promising new candidates as host materials for the use at high powers since they have high thermal conductivity and low phonon energy [33]. However, the sesquioxide host crystals have very high melt temperatures making reliable production of these crystals with high optical quality challenging.

Tm^{3+} doped in YLF, which is a host crystal with attractive properties, has been tuned from 1.905 to 2.067 µm in a side-pumped high-power slab geometry [34]. While earlier, a highly doped (10%), diode-end-pumped Tm:YLF laser cooled to liquid nitrogen temperatures, was tuned from 1.85 to 1.92 µm [35]. The use of the diode-end-pumped slab geometry is an attractive route for power scaling diode-pumped Tm:YLF solid-state lasers, as presented by S. So and co-workers [36]. In a research collaboration, the highest output power for Tm:YLF has been demonstrated in a diode-end-pumped slab geometry [37, 38], as discussed in Chapter 8 of this thesis.

A wide tuning range of 245 nm (from 1.785 µm to 2.03 µm) has been demonstrated in an 8% doped Tm:BaYF laser [39], and the output power of a few mW at 1.785 µm is the shortest wavelength from a diode-pumped Tm^{3+} doped crystalline laser reported to date.

The orthovanadate host crystals Tm:YVO_4, Tm:$LuVO_4$ and Tm:$GdVO_4$ are of particular interest for further research and development. For this family of crystals, the previously reported highest power laser operation has been demonstrated in Tm:$GdVO_4$ [40]. Prior to the work presented in this thesis, the maximum wavelength tuning range demonstrated was from 1.855 µm to 1.995 µm [41]. A comprehensive literature study of the laser performances and tuning ranges of Tm:$GdVO_4$ lasers is presented in Chapter 3 and the leading results obtained with quasi-continuous-wave diode-end-pumped Tm:$GdVO_4$ lasers are presented in Chapter 4 and Chapter 5 of this thesis.

2.3.3 Conclusion on diode-pumped Tm-doped laser pumping a Ho-doped system

After a detailed consideration of the options, it was concluded that a 2 µm laser system based on a separate diode-pumped Tm-doped laser, pumping a Ho laser was likely to be the best approach of those discussed thus far. Moreover, it was noted that a number of Tm^{3+} lasers have been demonstrated in a variety of host materials. The relatively new laser material, Tm:$GdVO_4$, was thought to exhibit particularly interesting possibilities for further research and development, due to its reported favourable properties, which will be discussed in detail in Chapter 3.

However, an alternative pumping scheme for the 2 µm laser system does exist, and is presented in the next section.

2.4 Tm:fibre laser pumped, Ho-doped systems

It was judged that one of the most effective methods to pump a 2 µm Ho based system when high pulse energy is the goal is to utilise the emerging technology of Tm doped fibre lasers. Tm:fibre lasers are typically high-power lasers, emitting at 1.9 µm wavelength, usually operating in continuous-wave mode.

The wavelength of the fibre laser can be engineered to overlap exactly with a strong absorption peak of the Ho^{3+} ion in the host medium, so that the Ho-doped system can be efficiently pumped to store a significant amount of energy that can be extracted as a high energy laser pulse at 2 µm.

Compared to the previously-listed methods of pumping energy into a Ho-doped gain medium, this method has by far the simplest energy transfer scheme, as indicated in Figure 2.12. However, the complexity of obtaining 1.9 µm output from the Tm:fibre laser is not presented in this scheme.

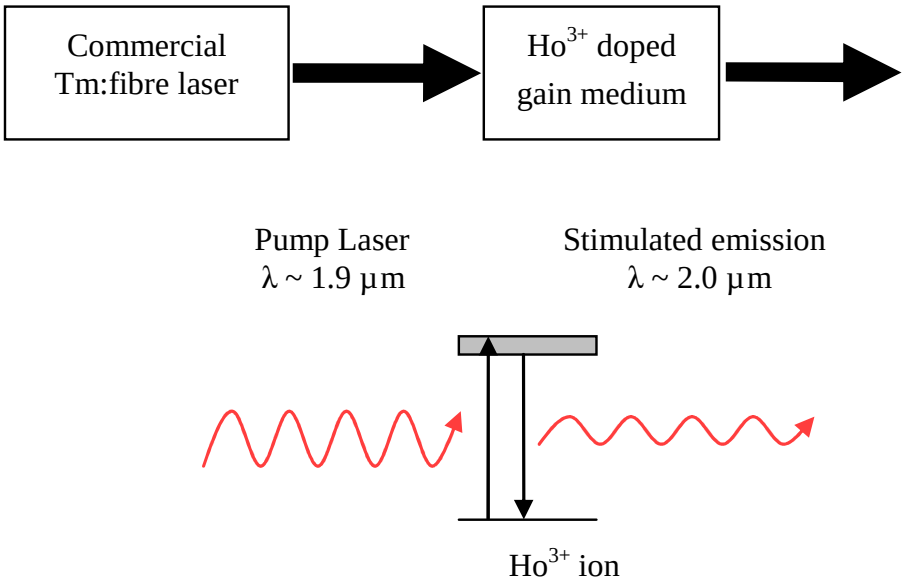

Figure 2.12: Energy level scheme of a Ho-doped gain medium, pumped by a high-power Tm:fibre laser.

The advantages of this amplifier scheme are the following:

- Commercially available, high-power 1.9 µm pump laser.
- Selectable laser pump wavelength.
- Near perfect pump beam quality.
- Potential for high optical-to-optical efficiency for the Ho^{3+} system.

- Minimal heat load in the Ho host material.
- Scalable in energy.
- Enables flexible pump designs.

The Tm:fibre lasers that are commercially available surpass all the criteria for a 1.9 µm pump laser as set out in Section 2.3.1 above, except that the output of the Tm:fibre laser is typically not polarised. This has led to significant challenges when used to pump a Ho^{3+} doped system with strongly polarised absorption spectra [42, 43].

The major disadvantage of this approach is the high cost of the Tm:fibre laser technology. This also implies that some degree of flexibility in the overall system design is reduced, since the specifications of an existing Tm:fibre laser cannot be changed by the end user. If this were to be requested of the laser supplier, major additional costs would usually be incurred. Furthermore, the electrical-to-optical efficiency of the Tm:fibre laser can be low, depending on the excitation scheme employed in the fibre.

It should be mentioned that there is a minor limitation in the way in which the Tm:fibre laser technology can be implemented when using it as pump laser for a Ho-doped laser or amplifier. The Ho-doped crystal cannot be pumped "intra-cavity" to the commercial Tm:fibre laser. This is in contrast to the diode-pumped Tm^{3+} doped laser technology discussed above, which can pump a Ho-doped amplifier crystal intra-cavity. There are, however, a number of technical challenges to be overcome with an intra-cavity pump design which are non-trivial. Intra-cavity pumping was not considered in this study for demonstrating a 2 µm laser system.

As part of the additional collaborative research development reported in Chapter 8, a Tm:fibre laser pumped Ho:YLF laser oscillator-amplifier system was developed [44] and subsequently implemented as a single-frequency Ho:YLF oscillator-amplifier [45], which is the highest single-frequency energy reported for a system pumped by a single Tm:fibre laser.

In summary it can be stated that the principles and experimental results presented above clearly demonstrate the feasibility of the approach of a Tm:fibre laser pumping a Ho-doped material. However, the high cost and general unavailability of high power

Tm:fibre lasers made this approach less attractive for the initial research study, compared to the development of a new Tm^{3+} doped solid-state laser specifically designed to pump a Ho:YLF 2 µm laser.

2.5 Conclusions

From the information presented above a qualitative analysis was made as presented in Table 2.1 comparing the feasibility and attractiveness of the different possible pumping schemes for a Ho-doped 2 µm laser system.

Table 2.1: Qualitative comparison of the evaluated concepts for 2 µm solid-state laser systems.

Pump source	**Flash lamp**	**Diode**	**Tm^{3+}**	**Tm:fibre**
2 µm gain medium	**Er:Tm:Ho:YLF**	**Tm:Ho:YLF**	**Ho:YLF**	**Ho:YLF**
Heat generation	High	High	Low	Low
Efficiency of Ho^{3+} system	Low	Medium	High	High
Research & development interest	Low	Low	High	High
Implementation costs	Medium	Medium	Low	High
Development time	Long	Long	Short	Short
Feasibility for high energy & scalability	High energy, but limits known	Limited by upconversion	Very good, limits to be determined	Very good, but limited by cost
Overall evaluation for initial research project	**Not preferred**	**Not preferred**	**Preferred**	**Preferred if affordable**

The qualitative evaluation presented in Table 2.1, compares the different technologies with relative measures for heat generation and efficiency, based on the different principles of operation, as discussed above. Furthermore, the research and development interests based on what has been demonstrated in the literature are evaluated, as well as the estimated cost and development time required during the initial research project for each technology relative to the other technologies. The feasibility for scaling to high energies is compared for each approach, leading to an overall evaluation of the approach to be followed.

The conclusion is that the diode-pumped Tm^{3+} laser, pumping a Ho:YLF laser crystal is the preferred and most feasible scheme to be implemented during the research project as the 2 µm laser system. This is based on the evaluation that the principle of operation will lead to an efficient system without major heat load in the Ho:YLF crystal. Furthermore, the Tm^{3+} laser technology requires further interesting research and development, as described in the remainder of the thesis. The implementation cost and time required to implement such technology is deemed to be significantly less than the co-doped schemes, which require development of laser crystals with sophisticated

compositions of Tm^{3+} and Ho^{3+} ions. The approach with spatially separated Tm- and Ho-doped crystals also lends itself to a scalable 2 µm oscillator-amplifier system, since it can be modular by adding additional Tm^{3+} pump lasers to the system.

The alternative approach, of using one or more Tm:fibre lasers to pump a Ho:YLF laser system, is also evaluated favourably. However, the high cost of Tm:fibre lasers limited the implementation of this preferred approach during the initial research project. Fortunately a high-power Tm:fibre laser became subsequently available for the additional 2 µm laser development, as discussed in detail in Chapter 8.

2.6 References

[1] M. J. Weber “Handbook of Lasers” Laser & Optical Science & Technology, Volume 18, CRC Press, (2000).

[2] I.T. Sorokina, K.L. Vodopyanov (Eds.), Solid-State Mid-Infrared Sources, Topics in Applied Physics, vol. 89, Springer, Berlin, Heidelberg, (2003).

[3] T. H. Maiman “Stimulated Optical Radiation in Ruby” *Nature* **187** 493-494 (6 August 1960).

[4] W. Koechner “Solid-state laser Engineering” 5th rev and updated ed. *Springer series in Optical Sciences Volume 1*, Springer-Verlag Berlin Heidelberg, Germany (1999).

[5] M. E. Storm, “Holmium YLF amplifier performance and the prospects for multi-Joule energies using diode-laser pumping,” *IEEE Journal of Quantum Electronics* **29** (2) 440-451 (February 1993).

[6] E. P. Chicklis, C. S. Naiman, R. C. Folweiler, D. R. Gabbe, H. P. Jenssen, and A. Linz “High-Efficiency Room-Temperature 2.06-µm Laser Using Sensitized Ho^{3+}:YLF” Appl. Phys. Lett. **19**, 119 (1971).

[7] T. S. O. Fan and R. L. Byer “Diode Laser-Pumped Solid-State Lasers” *IEEE Journal of Quantum Electronics* **24** (6) 895-912 (June 1988).

[8] D. W. Hughes and J. R. M. Barr “Laser diode pumped solid state lasers” *Journal of Physics D: Applied Physics* **25** 563-586 (1992).

[9] C. Hanke “High power diode lasers” *Solid-state lasers: New Developments and Applications* Edited by M. Inguscio and R. Wallenstein, Plenum Press, New York (1993).

[10] J. R. Leger and W. C. Goltsos “Geometrical Transformation of linear Diode-Laser Arrays for Longitudinal Pumping of Solid-State Lasers” *IEEE Journal of Quantum Electronics* **28** (4) (April 1992).

[11] J. M. Auerbach and R.L. Schmitt, “Diode-laser-pumped monolithic Nd:YLF laser operating at 1.053 μm” *Optics Letters* **16** (15) 1171-1173 (1991).

[12] Th. Graf and J. E. Balmer “High-power Nd:YLF laser end pumped by a diode-laser bar” *Optics Letters* **18** (16) 1317-1319 (1991).

[13] R. Beach, P. Reichert, W. Benett, B. Freitas, S. Mitchell, A. Velsko, J. Davin and R. Solarz “Scalable diode-end-pumping technology applied to a 100-mJ Q-switched Nd^{3+}:YLF laser oscillator” *Optics Letters* **18** (16) 1326-1328 (August 1993).

[14] B. Ehlers, K. Du, M. Baumann, H. Treusch, P. Loosen and R. Poprawe, “Beam shaping and fiber coupling of high-power diode laser arrays” *Lasers in Material Processing* Proc. SPIE **3097** 639-644 (1997).

[15] S. B. Sutton and G. F. Albrecht “Optical distortion in end-pumped solid-state rod lasers” *Applied Optics* **32** (27) 5256-5269 (September 1993).

[16] Y. F. Chen, C. F. Kao, T. M. Huang, C. L. Wang and S. C. Wang “Influence of Thermal Effect on Output Power Optimization in Fiber-Coupled Laser-Diode End-Pumped Lasers” *IEEE Journal of Selected Topics in Quantum Electronics* **3** (1) (February 1997).

[17] W. A. Clarkson “Thermal effects and their mitigation in end-pumped solid-state lasers” *Journal of Physics D: Applied Physics* **34** 2381-2395 (2001).

[18] W. Clarkson and D. Hanna, "Two-mirror beam-shaping technique for high-power diode bars," Opt. Lett. 21, 375-377 (1996).

[19] Fan, T.Y.; Huber, G.; Byer, R.L.; Mitzscherlich, P.; , "Spectroscopy and diode laser-pumped operation of Tm,Ho:YAG," *Quantum Electronics, IEEE Journal of* , vol.24, no.6, pp.924-933, Jun 1988.

[20] G. Rustad, and K. Stenersen, "Modeling of laser-pumped Tm and Ho lasers accounting for upconversion and ground-state depletion," *IEEE Journal of Quantum Electronics*, **32** (9) 1645-1656 (September 1996).

[21] S. Chen, J. Yu, M. Petros, Y. Bai, B. Trieu, M. Kavaya, and U. Singh, "One-Joule Double-Pulsed Ho:Tm:LuLF Master-Oscillator-Power-Amplifier (MOPA)," in Advanced Solid-State Photonics, Technical Digest (Optical Society of America, 2005), paper MD6.

[22] R. Stoneman and L. Esterowitz, "Intracavity-pumped 2.09- µm Ho:YAG laser," Opt. Lett. 17, 736-738 (1992).

[23] C. Bollig, R. Hayward, W. Clarkson, and D. Hanna, "2-W Ho:YAG laser intracavity pumped by a diode-pumped Tm:YAG laser," Opt. Lett. 23, 1757-1759 (1998).

[24] P. Budni, C. Ibach, S. Setzler, E. Gustafson, R. Castro, and E. Chicklis, "50 mJ, Q-switched, 2.09-µm holmium laser resonantly pumped by a diode-pumped 1.9-µm thulium laser," Opt. Lett. 28, 1016-1018 (2003).

[25] M. Schellhorn, "High-energy, in-band pumped Q-switched Ho^{3+}:$LuLiF_4$ 2 µm laser," Opt. Lett. 35, 2609-2611 (2010).

[26] Antoine Godard, “Infrared (2–12 µm) solid-state laser sources: a review,” C. R. Physique 8 1100–1128 (2007).

[27] R.C. Stoneman, and L. Esterowitz, “Efficient, broadly tunable, laser-pumped Tm:YAG and Tm:YSGG CW lasers,” Optics Letters 15 486–488 (1990).

[28] K. S. Lai, W. J. Xie, R. F. Wu, Y. L. Lim, Ernest Lau, Lindy Chia, and P. B. Phua, “A 150W 2-micron diode-pumped Tm:YAG laser” OSA TOPS Vol.

68, Advanced Solid-State Lasers Martin E. Fermann and Larry R. Marshall, eds. 335-339 (2002).

[29] R. C. Stonemann, and L. Esterowitz, “Efficient 1.94-μm Tm:YALO laser,” IEEE J. Sel. Topics Quantum Electronics **1** 78–80 (1995).

[30] H. Kalaycioglu, and A. Sennaroglu, “Low-threshold continuous-wave Tm^{3+}:$YAlO_3$ laser,” Optics Communications **281** 4071–4074 (2008).

[31] B. Yao, Y. Li, Y. Wang, X. Duan, G. Zhao, Y. Zong, and J. Xu “Efficient Diode-Pumped Tm:$YALO_3$ Laser with a Pump Recycling Scheme,” Chinese Physics Letters **24,** (9), 2597-2599, (September 2007).

[32] L. Fornasiero, N. Berner, B.-M. Dicks, E. Mix, V. Peters, K. Petermann, and G. Huber, “Broadly tunable laser emission from Tm:Y_2O_3 and Tm:Sc_2O_3 at 2 μm,” OSA Trends Opt. Photonics Adv. Solid-State Lasers 26, 450–453 (Opt. Soc. Am., Washington, DC 1999).

[33] J. H. Mun, A. Jouini, A. Novoselov, Y. Guyot, A. Yoshikawa, H. Ohta, H. Shibata, Y. Waseda, G. Boulon, and T. Fukuda “Growth and characterization of Tm-doped Y_2O_3 single crystals” Optical Materials **29**, (11), 1390-1393 (July 2007).

[34] A. Dergachev, K. Wall, P. F. Moulton “A CW side-pumped Tm:YLF laser,” OSA Trends Opt. Photonics 68, 343–350 (Opt. Soc. Am., Washington, DC 2002)

[35] P. A. Ketteridge, P. A. Budni, M. G. Knights and E. P. Chicklis, "All solid-state 7 watt CW, tunable Tm:YLF laser" OSA Trends in Optics and Photonics Vol. 10, Advanced Solid State Lasers, Clifford R. Pollock and Walter R. Bosenberg, eds., (Optical Society of America, Washington, D.C., 1997), pp. 197-198.

[36] S. So, J.I. Mackenzie, D.P. Shepherd, W.A. Clarkson, J.G. Betterton, and E.K. Gorton, “A power-scaling strategy for longitudinally diode-pumped Tm:YLF lasers,” Appl. Phys. B **84** (3) 389-393 (2006).

[37] M. Shellhorn, S. Ngcobo, and C. Bollig, “High-power diode-pumped Tm:YLF slab laser” *Applied Physics B* **94** (2) 195-198 (2008).

[38] M. Schellhorn, S. Ngcobo, C. Bollig, M. J. D. Esser, D. Preussler, K. Nyangaza, “High-power diode-pumped Tm:YLF slab laser,” *CLEO Europe*, Munich, Germany, 14-19 June 2009, CA1.3 (2009).

[39] N. Coluccelli, D. Gatti, G. Galzerano, F. Cornacchia, D. Parisi, A. Toncelli, M. Tonelli, and P. Laporta, “Tunability range of 245 nm in a diode pumped Tm:BaY_2F_8 laser at 1.9 μm: a theoretical and experimental investigation,” Appl. Phys. B **85** 553–555 (2006).

[40] J. Šulc, P. Černý, H. Jelínková, W. Ryba-Romanowski, R. Lisiecki, P. Solarz, G. Dominiak-Dzik, Y. Urata, and M. Higuchic, “Tm-doped vanadates under pulsed pumping with variable duty cycle: impact on lasing and fluorescence,” Proc. SPIE **6998**, 69980T, (2008).

[41] E. Sorokin, A. N. Alpatiev, I. T. Sorokina, A. I. Zagumennyi, and I. A. Shcherbakov, “Tunable efficient continuous-wave room-temperature Tm^{3+}:$GdVO_4$ laser,” OSA Trends Opt. Photonics Adv. Solid-State Lasers 68, 347–350 (Opt. Soc. Am., Washington, DC 2002).

[42] Y. Bai, M. Petros, J. Yu, P. Petzar, B. Trieu, H. Lee, and U. Singh, "Highly Efficient Ho:YLF Laser Pumped by Tm:fiber Laser," in Conference on Lasers and Electro-Optics/Quantum Electronics and Laser Science Conference and Photonic Applications Systems Technologies, Technical Digest (CD) (Optical Society of America, 2006), paper CThFF4.

[43] Y. Bai, J. Yu, P. Petzar, M. Petros, S. Chen, B. Trieu, H. Lee, and U. Singh, "Single Longitudinal Mode, High Repetition Rate, Q-Switched Ho:YLF Laser for Remote Sensing," in Conference on Lasers and Electro-Optics/International Quantum Electronics Conference, OSA Technical Digest (CD) (Optical Society of America, 2009), paper CWH5.

[44] W. Koen, C. Bollig, H. Strauss, M. Schellhorn, C. Jacobs and M. J. D. Esser, "Compact Fibre-Laser-Pumped Ho:YLF Oscillator-Amplifier System," *Applied Physics B* **99** (1-2) 101-106 (April 2010).

[45] C. Bollig, M. J. D. Esser, C. Jacobs, W. Koen, D. Preussler, K. Nyangaza and M. Schellhorn, "70 mJ Single-Frequency *Q*-Switched Ho:YLF Ring Laser – Amplifier System Pumped by a Single 82-W Tm Fibre Laser," *Middle-Infrared Coherent Sources*, Trouville, France, 8-12 June 2009, Mo3 **(*invited*)** (2009).

Chapter 3

Mid-infrared diode-pumped lasers based on Tm:$GdVO_4$

In this chapter the development of lasers based on Tm:$GdVO_4$ as the laser gain medium is discussed, as well as the relevant properties of this material. The development and evolution of Tm:$GdVO_4$ lasers as reported in the literature is also presented. The maximum output power performance previously reported with continuous-wave (CW) lasers, and the maximum energy of quasi-continuous-wave (QCW) lasers are listed. The key features of the relevant architectures employed to achieve these results, such as the crystal mounting methods, the pumping schemes, as well as the laser resonator designs are discussed. Furthermore, the challenge of power scaling Tm^{3+} doped vanadate lasers, as addressed in the literature, is also evaluated. This chapter is a comprehensive literature study which refers to all the available literature on Tm:$GdVO_4$.

3.1 Overview of Tm:$GdVO_4$ as mid-infrared laser material

Since the first recognition that $GdVO_4$ is a suitable host crystal for Tm^{3+} doped solid-state lasers it has been argued that the material has, like the other vanadate isomorphs, certain advantages over other host crystals [1, 2]. Firstly, Tm:YVO_4, Tm:$LuVO_4$ and Tm:$GdVO_4$ all have strong and broad absorption features at the emission wavelength of commercially available high power laser diodes at ~800 nm [3]. Secondly, the broad emission peak at 1.9 µm in Tm:$GdVO_4$ can be utilised for laser operation over a useful wavelength tuning range, as shown in Section 2.3.2, including wavelengths which can be used to pump Ho^{3+} doped lasers and Cr^{2+}:ZnSe lasers [4, 5]. Furthermore, Tm:$GdVO_4$ is a uniaxial, birefringent crystal which implies that an a-cut

crystal allows the polarization (***E***-field) of linearly polarized light to be either perpendicular or parallel to the crystalline c-axis. It is, therefore, possible to operate a Tm:$GdVO_4$ laser on either the π-polarisation ($\boldsymbol{E}\|$c) or on the σ-polarisation ($\boldsymbol{E}\perp$c). Finally, it has been reported that Tm:$GdVO_4$ has a higher thermal conductivity (9.7 W/m.K) along the crystalline c-axis than Tm:YVO_4 (5.1 W/m.K) [6], even though a recent report [7] has stated that it is higher for YVO_4 (12.1 W/m.K) than for $GdVO_4$ (10.5 W/m.K), which is similar to YAG (10.1 W/m.K). Nevertheless, it is clear that Tm:$GdVO_4$ is an attractive gain-material option for the design of high-power diode-pumped laser devices at 1.9 µm, especially when the 2-for-1 pumping process in Tm^{3+} is considered, as discussed in more detail later in this chapter.

The first report of a Tm^{3+} doped vanadate laser was in 1992, using a 5% doped Tm:YVO_4 crystal of length 2.5 mm that was pumped by a Ti:Sapphire laser at 797 nm [8]. The first demonstration of a mid-infrared $GdVO_4$ laser was with a device which was co-doped with 4% Tm^{3+} and 0.5% Ho^{3+} [9, 10]. These early reports already highlighted the fact that the pump absorption band of Tm^{3+} in vanadate is red shifted towards the typical emission wavelengths of high-power diode lasers, as compared with the well known YAG host material. This feature is further discussed in Section 3.2.1.

Zagumennyi *et al* from the Institute of General Physics at the Russian Academy of Sciences in Moscow pioneered the characterisation of Tm:$GdVO_4$ as laser material [1, 2]. The Tm:$GdVO_4$ crystals they studied were grown by the Czochralski method with Tm^{3+} atomic doping concentrations from 0.5.% to 15%, and in collaboration with G Huber and other researchers from Hamburg University in Germany, these crystals were tested in a monolithic microchip laser design in a series of experiments reported in 1997 [11, 12]. The 1 mm thick microchip laser was end-pumped by a Ti:Sapphire laser, and in a second series of experiments, by a diode laser at 806 nm, with the pump beam chopped at repetition frequencies of 20 to 50 Hz and a duty cycle of 50% in all experiments. The maximum QCW output power from the Ti:Sapphire-pumped laser was 180 mW, with 478 mW of pump power absorbed. However, the mirror coatings on the microchip laser crystal were damaged above 125 mW due to the high intra-cavity power density, since the output coupling of the resonator was only 0.5% at 1.9 µm. When pumped with the diode laser at 806 nm, of which 1.18 W was absorbed,

only 43 mW QCW output power was demonstrated. The authors stated that the lower efficiency was most likely due to the larger pump beam of the laser diode, which could not be made smaller due to the beam quality factor of the pump source. The Tm:$GdVO_4$ laser output wavelength was centred at 1923 nm, with a measured 20 nm full width of the output spectrum.

Subsequent to these initial laser tests, a number of publications appeared in 1998 and 1999 based on microchip lasers that were designed and tested by C P Wyss *et al* at the Institute of Applied Physics of the University of Bern in Switzerland, also using 6.9% Tm^{3+} doped $GdVO_4$ crystals grown by the researchers at the Russian Academy of Sciences [6, 13, 14, 15, 16]. Important outcomes of this widely referenced work included experimental evaluations of the microchip laser performance under different QCW pumping duty cycles, two different cooling conditions, as well as a comparison of diode laser pumping versus Ti:Sapphire laser pumping at 806 nm. Furthermore, the authors provided a reasonable description of the 2-for-1 pumping process taking place in the Tm^{3+} energy levels to explain the high laser efficiency of 58% that was obtained under Ti:Sapphire laser pumping of Tm:$GdVO_4$ [16]. The maximum QCW output power at that time was 1.4 W, for 33 W of diode input power [15].

In 2001, the first true CW Tm:$GdVO_4$ laser was reported by Zagumennyi *et al*, delivering 630 mW with a slope efficiency of 33% from a microchip laser configuration that was pumped by a fibre-coupled 3 W laser diode at 806 nm [17, 18, 19]. During this experiment, the crystal temperature was kept at 7°C. However, when the temperature was increased to 24°C, the observed output power fell to 550 mW, highlighting the quasi-three-level nature of Tm:$GdVO_4$ lasers.

The widely tuneable output of Tm:$GdVO_4$ near 1.9 µm was explored by Sorokin and Sorokina at the Technical University of Vienna in Austria, in a collaboration with Zagumennyi *et al* at the Russian Academy of Sciences [4, 20, 21]. They demonstrated for the first time that a 6.8% doped Tm:$GdVO_4$ laser, pumped by a CW Ti:Sapphire laser at 797 nm, can be tuned over 140 nm. The wide tuning from 1855 to 1995 nm was achieved with an 1.6 mm thick quartz plate inside the laser cavity that acted as a birefringent filter, together with polarisation control of the laser output. Without the birefringent filter, the maximum TEM_{00} CW laser output was 230 mW when 640 mW

of the polarised pump light was absorbed in the 1 mm thick Tm:$GdVO_4$ crystal. The authors argued that the material Tm:$GdVO_4$ is a promising candidate to fulfil the requirements of a highly efficient laser at 1.9 µm.

Independent from the results reported up to 1999, Y Urata and S Wada together with other researchers from Japan, presented an evaluation of Tm:$GdVO_4$ crystal characteristics. Initially their work focussed on Czochralski grown crystals [22, 23], but their most valuable contribution to the knowledge on Tm:$GdVO_4$ lasers was on the Floating Zone growth process of this laser material [24, 25, 26, 27]. In a collaboration with P Cerny, J Oswald, J Sulc, and H Jelinkova from the Czech Republic, they reported in 2006 a breakthrough in the CW output power with a demonstration of a multi-watt diode-end-pumped laser, based on a 2% doped Tm:$GdVO_4$ laser crystal grown by the Floating Zone technique [5]. The 2.6 W CW laser output centred at 1910 nm demonstrated by the researchers was significantly more than the 420 mW reported earlier by themselves with Czochralski grown crystals [23, 28, 29]. By implementing the high optical quality Floating Zone grown crystals, they reported for the multi-watt output of the laser a slope efficiency of 30.8%, with an overall efficiency of 26% with respect to the 10 W of absorbed pump power from the laser diode at 800-803 nm. The improved laser design that they implemented, namely a diode-end-pumped laser architecture with a lower doping level longer length crystal of 3 mm, was fundamentally different to the design of highly-doped microchip lasers of length 1 mm previously used by other researchers. During the same period, the co-workers J Sulc, and H Jelinkova from the Czech Republic reported on the widest tuning of 235 nm obtained from a Tm:$GdVO_4$ laser, from 1840-2075 nm using a birefringent filter for tuning the laser wavelength [30].

The results obtained with the Tm:$GdVO_4$ laser were later compared directly to the performance of diode-pumped Tm:$LuVO_4$ as well as Tm:YVO_4 by the same research collaboration [3, 31, 32]. It was, however, found during this study that CW lasing can only be obtained with Tm:$GdVO_4$, and not with the other Tm^{3+} doped vanadates which could only be operated in QCW lasing mode. These reports included a detailed spectroscopic analysis of Tm:YVO_4, Tm:$LuVO_4$ and Tm:$GdVO_4$ performed by Lisiecki *et al* from the Polish Academy of Sciences in Wrocław, Poland. In a more recent report, the researchers attributed the lack of CW lasing performance in

$Tm:YVO_4$ and $Tm:LuVO_4$ to the onset of parasitic upconversion processes in the Tm^{3+} laser media associated with the increase in the laser crystal temperature with QCW pumping duty cycles higher than 60% [33]. The observed upconversion fluorescence, discussed in more detail in Section 3.2.4, was significantly more for the 5% doped Czochralski grown $Tm:YVO_4$ crystals and for the 3% doped Floating Zone grown $Tm:LuVO_4$ crystals than for the 2 to 6% doped Floating Zone grown $Tm:GdVO_4$ laser crystals. Although not conclusive, the authors suggested that possible contamination with Er^{3+} impurities might have been the cause for the increased upconversion fluorescence observed in $Tm:YVO_4$ and $Tm:LuVO_4$.

The highest output power from a $Tm:GdVO_4$ laser was demonstrated by yet another research group - from the Harbin Institute of Technology in China [34]. The first report by Y Li, B Yao and Y Wang was a $Tm:GdVO_4$ laser producing 2.35 W from a diode-end-pumped laser, pumped from both ends with a single 24 W fibre-coupled laser diode at 804.5 nm, employing a 2% doped $Tm:GdVO_4$ crystal of length 10 mm cooled to cryogenic temperatures [35]. Their subsequent laser design, utilising a 5 mm long 3% doped $Tm:GdVO_4$ crystal cooled to 18°C, resulted in 2.8 W CW laser output at 1912 nm when pumped with an 18 W fibre-coupled laser diode at 795 nm, also in a double-end-pump resonator layout [34].

The most recent result of a $Tm:GdVO_4$ laser was also reported by Li *et al* at the end of 2008, which was published early 2009 [36]. This report included the demonstration of the first *Q*-switched $Tm:GdVO_4$ laser, which produced laser pulses as short as 48 ns at 5 kHz with an average output power of 2 W at 1912 nm. The compact resonator of total length 35 mm included an acousto-optic modulator (AOM) that served as *Q*-switch, as well as a 3% doped 2 mm long $Tm:GdVO_4$ crystal that was pumped from one end only with a 15 W fibre-coupled laser diode at 805 nm with a pump spot diameter in the crystal of 320 µm. They reported that the laser was also operated in CW mode in the same laser configuration, but with the AOM *Q*-switch removed from the cavity, again producing 2.8 W of CW output power.

From the literature results presented above it is clear that there is significant scope for the power scaling of $Tm:GdVO_4$ lasers. In order to do so, the fundamental properties of this laser material need to be evaluated, as discussed in the next section.

3.2 Properties of Tm:$GdVO_4$

In order to further evaluate the possibility of scaling the output power of Tm:$GdVO_4$ lasers and to calculate its expected performance, it is necessary to consider the fundamental properties of this relatively new laser material. In this section, the key laser physics issues relating to diode-pumped Tm:$GdVO_4$ lasers are discussed, including the absorption and emission cross sections of the material at 0.8 µm and at 1.9 µm, as well as the population dynamics of the Tm^{3+} ions. The optical, thermal and mechanical properties of Tm:$GdVO_4$ crystals are also presented.

3.2.1 Absorption spectra

The energy level structure of the Tm^{3+} ion in a particular crystal host can be determined by a detailed analysis of the spectroscopic properties of the laser material. Several reports on the spectroscopic properties of Tm:$GdVO_4$ are in the literature, but only a few contain a comprehensive analysis of the laser material [3, 37]. The following discussion is based on the analysis conducted by Lisiecki and co-workers from the Polish Academy of Sciences in Wrocław, Poland. The measurement data reproduced here were obtained directly from the lead author who performed the spectroscopic measurements [38].

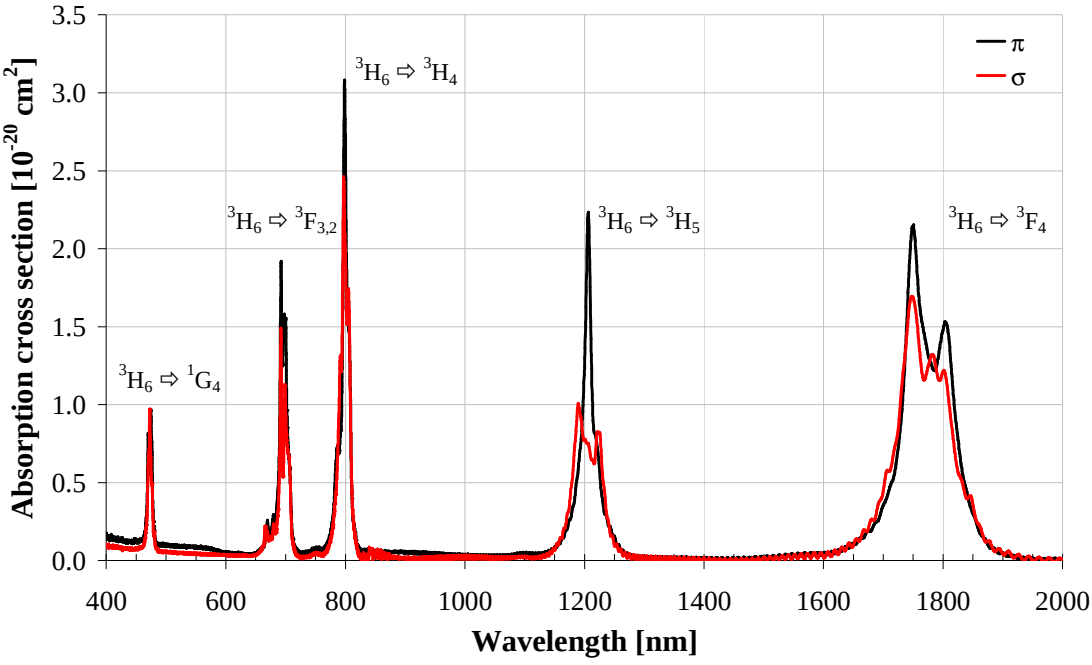

Figure 3.1: Absorption cross section of the ground state of Tm:$GdVO_4$ over the wavelength range from 400 nm to 2000 nm [3].

The polarisation resolved absorption cross section of Tm:$GdVO_4$ over the wavelength range from 400 nm to 2000 nm is shown in Figure 3.1. The researchers identified the transitions from the ground state to the different excited states of the Tm^{3+} ion responsible for the different absorption bands, as indicated on the graph.

The $^3H_6 \rightarrow {}^3H_4$ absorption band is of relevance for pumping Tm:$GdVO_4$ with laser diodes in the 0.8 µm wavelength region where high power laser diodes are commercially available. In order to demonstrate the advantage of diode-pumping the Tm:$GdVO_4$ laser material, several publications present the polarisation resolved absorption coefficients of a 3% doped Tm:$GdVO_4$ crystal, compared directly to that of a 5% doped Tm:YAG crystal in the wavelength range from 770 to 820 nm [27], as reproduced in Figure 3.2. The graph clearly shows the contrast between the strong and wide absorption band of Tm:$GdVO_4$ at 800 nm, and the weak and narrow absorption features of Tm:YAG at 778 to 786 nm, a wavelength range not readily available from high-power laser diodes.

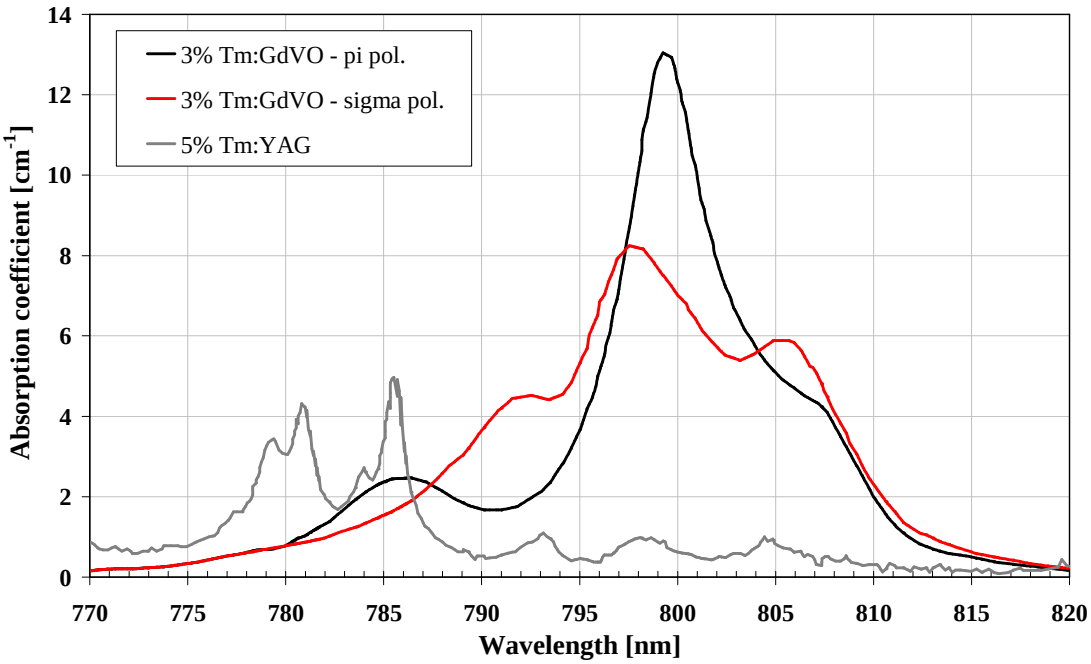

Figure 3.2: The polarisation resolved absorption coefficients of 3% Tm:$GdVO_4$ and of 5% Tm:YAG in the 0.8 µm wavelength range [27].

In terms of the absorption cross sections of the $^3H_6 \rightarrow {}^3H_4$ absorption band, the following can be noted with reference to Figure 3.3. The peak of the absorption cross section is 3×10^{-20} cm^2 on the π-polarisation ($\boldsymbol{E}\|c$) centred at 799 nm and has a full width at half maximum (FWHM) of 9 nm. The σ-polarisation ($\boldsymbol{E}\perp c$) has a lower

absorption cross section of 2.5 x 10^{-20} cm^2 located at 797 nm, but has a FWHM of 16 nm. At 804 nm the absorption cross section for the two polarisations is equal at a value of 1.6 x 10^{-20} cm^2, which is an attractive feature that will lead to strong, uniform absorption when pumped with a fibre-coupled diode-laser at 804 nm having mixed polarisation. The absorption reduces gradually to longer wavelengths, but at 809 nm it is still comparable to the peak absorption cross section of Tm:YAG (0.81 x 10^{-20} cm^2 at 785 nm, FWHM 1.5 nm) [39]. Based on the evaluation of the $^3H_6$ → $^3H_4$ absorption feature of Tm:$GdVO_4$, it is clear that there are no stringent requirements placed on the operational wavelength, bandwidth or polarisation properties of diode lasers to be used as pump sources for high-power diode-pumped Tm:$GdVO_4$ lasers. Rather, in the first instance the selection can be made from commercially available pump sources based on output power, beam quality, availability and cost.

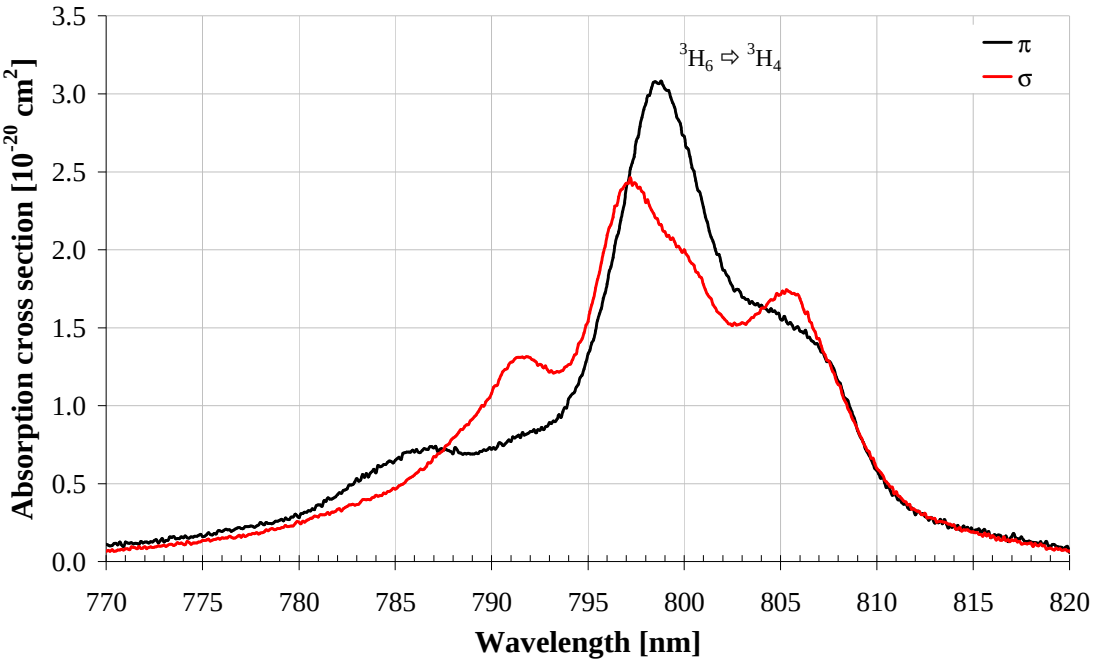

Figure 3.3: Polarisation resolved absorption cross sections for the $^3H_6$ → $^3H_4$ transition in Tm:$GdVO_4$ [3].

The absorption band from the ground state to the upper laser level $^3F_4$ is also of relevance for designing high-power Tm:$GdVO_4$ lasers, the spectroscopic detail of which is shown in Figure 3.4. The absorption data presented in Figure 3.4 was obtained directly from the lead author [38], whereas the emission cross section data is reproduced as it appeared in [3]. The slight oscillation features observed on the absorption data is most likely due to measurement inaccuracies, which was not reported in [3].

On both polarisations the peak absorption is located around 1750 nm, with the values of 2.1 x 10^{-20} cm^2 on the π-polarisation and 1.7 x 10^{-20} cm^2 on the σ-polarisation, while the peak emission occurs between 1810 – 1820 nm for both polarisations, with the peak cross section of the π-polarisation stronger at a value of 2 x 10^{-20} cm^2 at 1809 nm, compared to 1.7 x 10^{-20} cm^2 at 1806 nm on the σ-polarisation. The π-polarisation emission cross section has a smooth decay towards longer wavelengths down to 2000 nm, while on the σ-polarisation the emission cross section has a distinct spectral feature located at 1850 nm and a slight feature at 1910 nm.

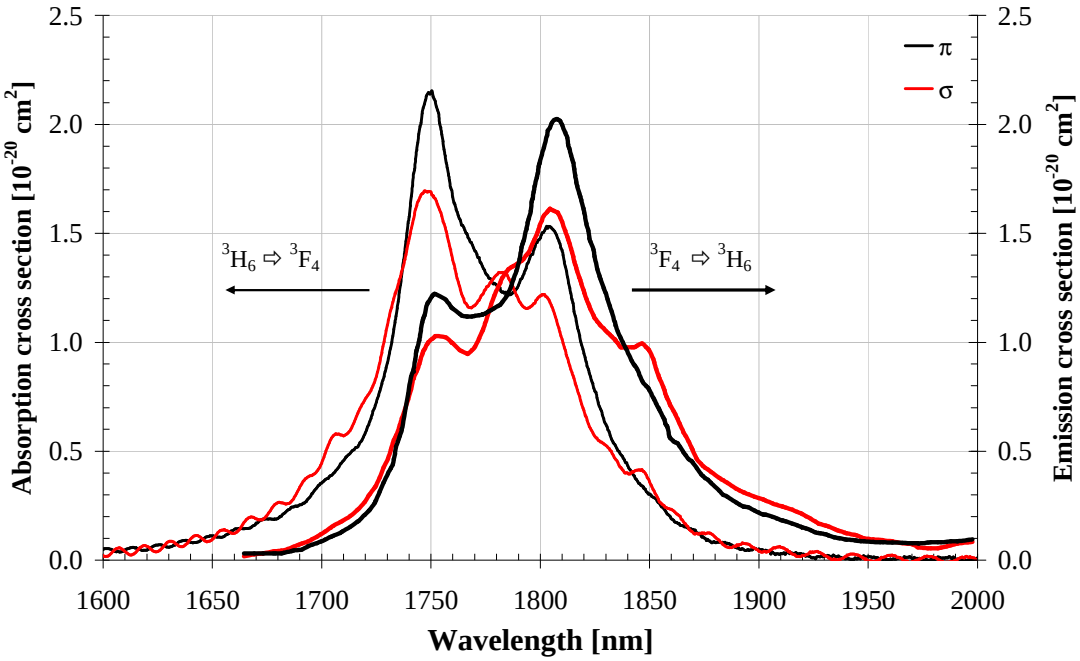

Figure 3.4: The reported absorption cross sections (thin) and emission cross sections (thick) of Tm:$GdVO_4$ for π-polarised and σ-polarised light between 1600 nm and 2000 nm [3].

Accurately measured absorption spectra, and the calculated emission spectra, are of crucial importance for the calculation of the expected threshold power and the operational wavelength of a diode-pumped Tm:$GdVO_4$ laser [3]. The data reproduced here, which is the most comprehensive data in the literature, was not sufficiently precise for the calculations that needed to be performed to predict the laser performance of a diode-pumped Tm:$GdVO_4$ laser. This is the reason why the absorption spectra were measured accurately as discussed in Chapter 4.

3.2.2 Energy levels

The energy levels identified in the spectroscopic analysis are transitions within the $4f^{12}$ configuration of Tm^{3+} ions and although these transitions are the same for all host crystals, the exact energy levels of the Tm^{3+} ion multiplets and Stark splittings are weakly influenced by the crystal structure and are therefore unique for each type of crystal. From the spectroscopic measurements and Judd-Ofelt crystal field analysis, the energy levels of the Tm^{3+} ion multiplets and Stark splittings were calculated by the researchers for the vandate host crystals, from which the data of Tm:$GdVO_4$ are reproduced in Figure 3.5 below [3]. Other researchers also presented a Judd–Ofelt analysis of spectroscopic properties of Tm:$GdVO_4$ [37], but their results are based on less detailed spectroscopic measurements that do not correspond directly with the first published results and are not further considered.

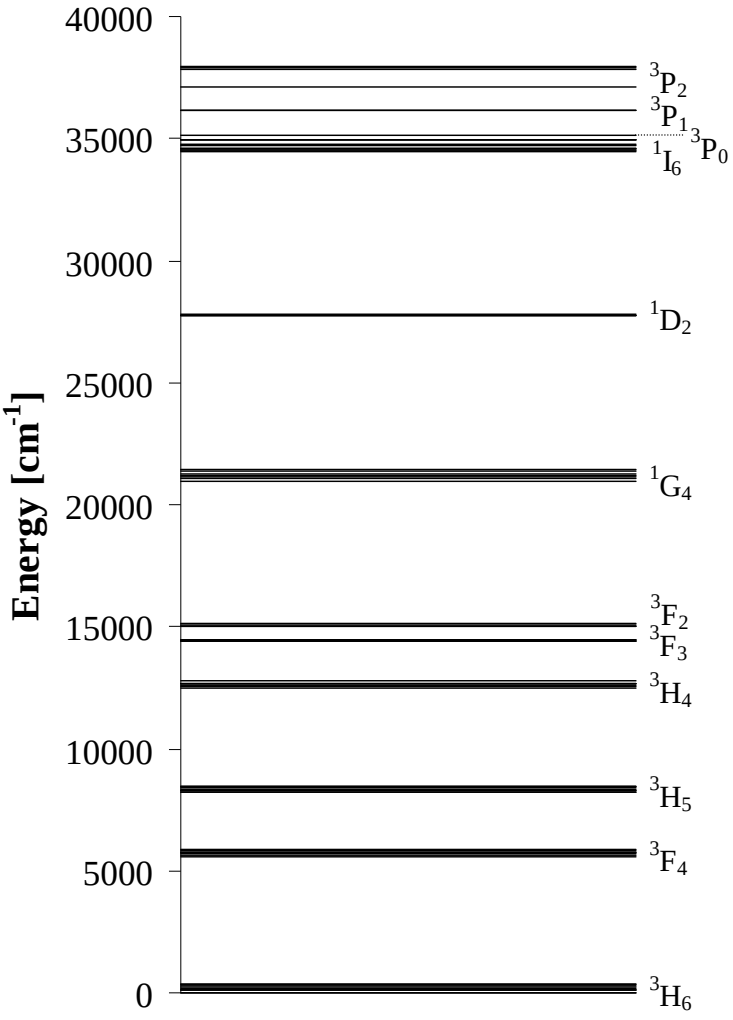

Figure 3.5: The multiplet energy levels and Stark splittings of Tm:$GdVO_4$ [3].

For mid-infrared lasing in Tm:$GdVO_4$, only the first few energy levels from the ground level $^3H_6$ up to $^3H_4$ are utilised. However, when analysing florescence spectra and upconversion processes in Tm:$GdVO_4$, the higher lying energy levels up to $^1D_2$ are taken into account, as discussed in Section 3.2.4.

3.2.3 Two-for-one pump scheme

C P Wyss and co-workers at the Institute of Applied Physics of the University of Bern in Switzerland provided a reasonable description of the pumping process to excite the Tm^{3+} ions in $GdVO_4$ to the $^3F_4$ upper laser level [13, 14], an illustration of which is shown in Figure 3.6, where the energy levels of the Tm^{3+} ion multiplets and Stark splittings in $GdVO_4$ are drawn to scale.

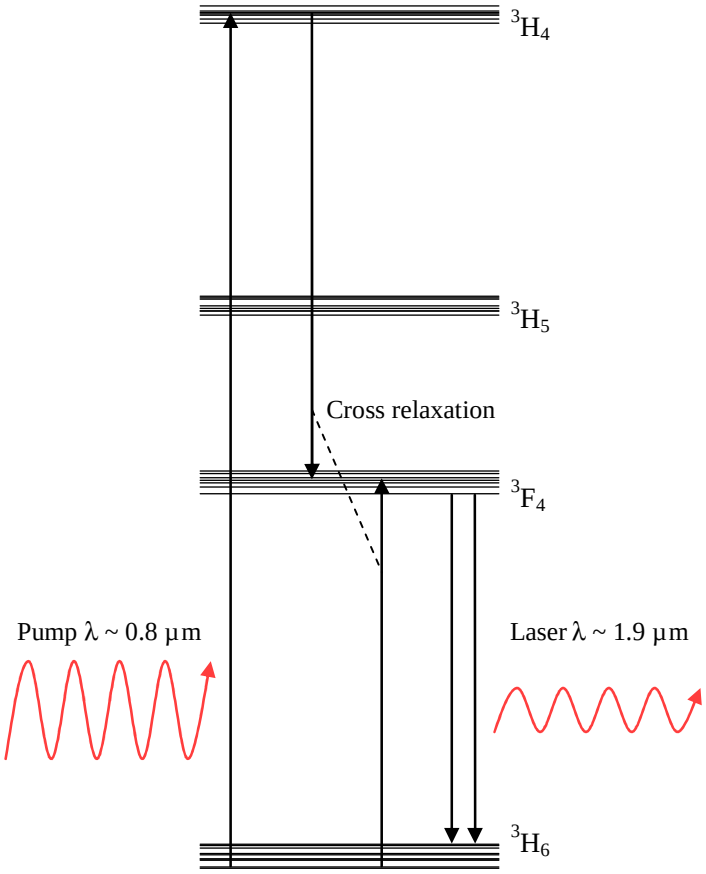

Figure 3.6: Energy levels involved in the 2-for-1 pump process and the 1.9 µm lasing transition in Tm:$GdVO_4$.

The Tm:$GdVO_4$ crystal is pumped from the $^3H_6$ ground state at the 0.8 µm absorption band to become excited to the $^3H_4$ upper energy level. If the Tm^{3+} ion concentration is at an optimal level, typically a few atomic percent, the excited Tm^{3+} ions can exchange roughly half of their stored energy with close-lying Tm^{3+} ions in the $^3H_6$ ground state

through a non-radiative cross relaxation process. At the end of this process the Tm^{3+} ions are excited to the $^3F_4$ intermediate energy level, which is the upper laser level, from where the 1.9 µm laser transition terminates in the $^3H_6$ ground state. The excitation process is often called the 2-for-1 pump scheme, since for each absorbed pump photon, it is possible to excite two Tm^{3+} ions to the upper laser level through cross relaxation, making the theoretical pump efficiency 200%. This feature is incorporated in the pump quantum efficiency parameter $\eta_{p\text{-}q}$, typically assumed to be 1.5 for practical laser configurations. Another advantage of the 2-for-1 pump process, other than high efficiency, is that less heat is deposited in the laser crystal through non-radiative transitions, thereby favouring high-power laser operation.

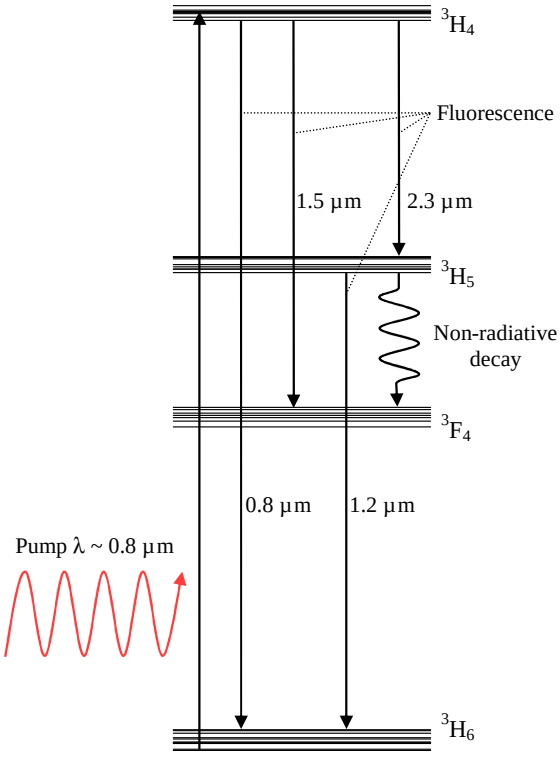

Figure 3.7: Alternative energy decay transitions following pump excitation at 0.8 µm in Tm:$GdVO_4$.

It can be seen from the schematic in Figure 3.6 that there is a slight energy difference between the $^3H_4$ → $^3F_4$ transition, and the $^3H_6$ → $^3F_4$ transition, necessitating that the cross relaxation process be phonon assisted. Since the phonon energies vary for different crystals, the cross relaxation efficiency will differ for different host crystals. This dependence has not yet been quantified for Tm:$GdVO_4$ as it has been done for Tm:YLF and other Tm^{3+} doped crystals [40]. Furthermore, since the cross relaxation process involves two close-lying Tm^{3+} ions, the probability of the process also

depends on the doping concentration of Tm^{3+} ions in the crystal. If the doping concentration is too low for efficient cross relaxation, other decay routes will be favoured, including fluorescence from $^3H_4$ to $^3F_4$, and fluorescence from $^3H_4$ to $^3H_5$ followed by non-radiative decay from $^3H_5$ to $^3F_4$, as illustrated in Figure 3.7. The reported splitting ratios of these energy transitions, however, indicate a large probability that the $^3H_4$ and $^3H_5$ levels will preferable decay directly to the $^3H_6$ ground state, which will significantly reduce the efficiency of a lowly doped Tm:$GdVO_4$ laser [3].

3.2.4 Quenching of the laser transition

It has been recognised that competing upconversion processes lead to the quenching of the 1.9 µm laser efficiency in Tm:$GdVO_4$ [13, 33, 41, 42]. Several additional energy transitions have been identified by various researchers which result in a reduced energy storage in the $^3F_4$ upper laser level, including the processes indicated in Figure 3.8.

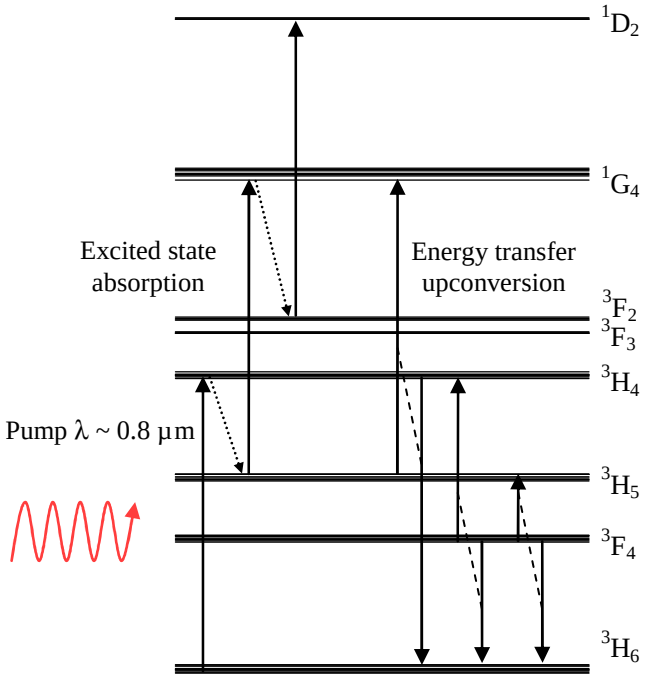

Figure 3.8: Energy transfer processes resulting in quenching of the laser action in Tm:$GdVO_4$ (references in text).

It has been argued that excited state absorption can take place in Tm:$GdVO_4$ due to the pump photon energy at 0.8 µm that corresponds to the energy transition from the $^3H_5$ to the $^1G_4$ level [13], as well as the transition from the $^3F_2$ level to the $^1D_2$ level [41]. In this parasitic process, the first pump photon excites a Tm^{3+} ion from the ground state

to the $^3H_4$ state, to subsequently decay to the $^3H_5$ state, from where the ion can absorb another pump photon to excite it to the $^1G_4$ state. This process has been confirmed by blue-green fluorescence from the $^1G_4$ state to the $^3H_6$ ground state [13]. The $^1G_4$ state can also decay non-radiatively to the $^3F_2$ state, which can absorb yet another pump photon to excite the Tm^{3+} ion to the high lying $^1D_2$ level, resulting in 440 nm blue fluorescence to the $^3F_4$ state and 361 nm UV fluorescence to the ground state [41].

The parasitic processes may not only be due to optical absorption, but can also include phonon assisted energy transfer upconversion processes, as indicated in Figure 3.8. The first possible energy transfer upconversion process involves an excited Tm^{3+} ion in the $^3H_4$ state exchanging energy with a close-lying Tm^{3+} ion in the $^3H_5$ state, which results in one ion being returned to the ground state and the other ion excited to the $^1G_4$ state, from where a $Tm:GdVO_4$ crystal can fluoresce blue-green to the ground state [13]. Alternatively, two ions in the long-lived $^3F_4$ upper laser level can exchange energy such that one ion returns to the ground state, and the other ion is excited to the $^3H_5$ level, or the $^3H_4$ level. Either way, this phenomenon depopulates the $^3F_4$ level, in an opposite effect of the original cross relaxation process populating the upper laser level, and has been shown to have a major detrimental influence on the laser performance of Tm:YLF and other crystals [40].

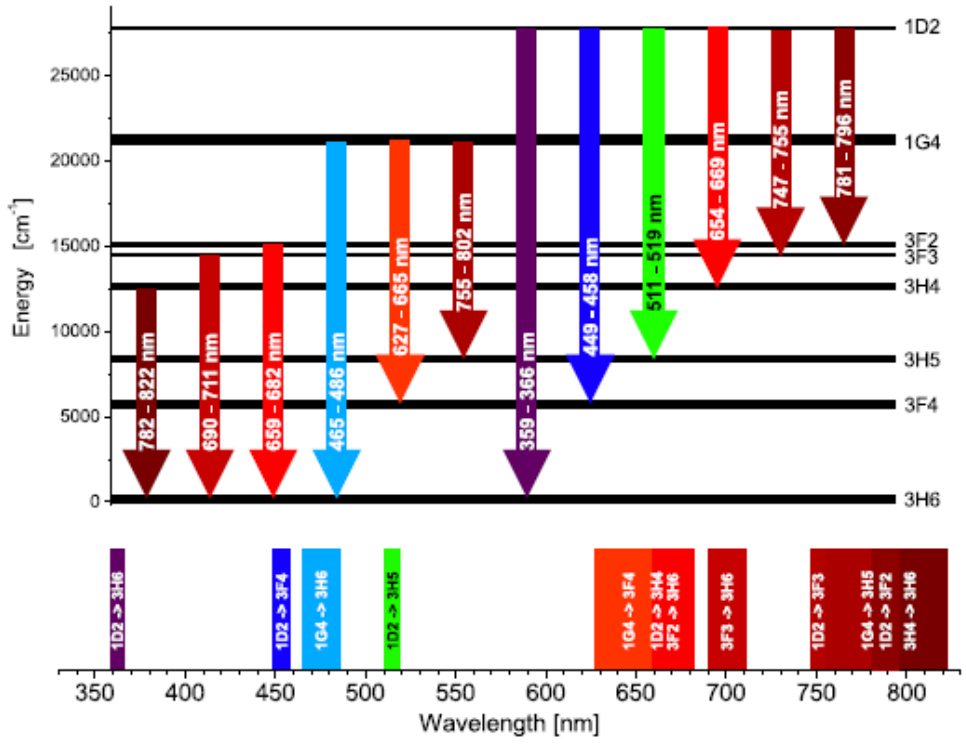

Figure 3.9: Energy level transitions responsible for the observed upconversion fluorescence in $Tm:GdVO_4$, $Tm:YVO_4$ and $Tm:LuVO_4$ laser crystals [33].

Energy transfer upconversion is pronounced at higher pump power densities, higher crystal temperatures and higher doping concentrations, in which case these parasitic processes increase in a non-linear way, as observed by the visible fluorescence from higher energy levels. The dependence of upconversion florescence on pump power or duty cycle and crystal temperature has recently been investigated for the Tm:$GdVO_4$, Tm:YVO_4 and Tm:$LuVO_4$ laser crystals [33]. During these experiments the upconversion fluorescence spectra were assigned to possible energy transitions in Tm^{3+}, as indicated in Figure 3.9.

3.2.5 Energy level lifetimes

Another parameter that influences the performance of a laser are the lifetimes of key energy levels. In Tm^{3+} doped lasers, the lifetime of the $^3F_4$ upper laser level is of primary importance, since this will determine the energy storage lifetime of the 1.9 µm laser transition. The lifetimes of the other energy levels involved in the population dynamics of the Tm^{3+} laser, such as the $^3H_4$ pump level, are also important.

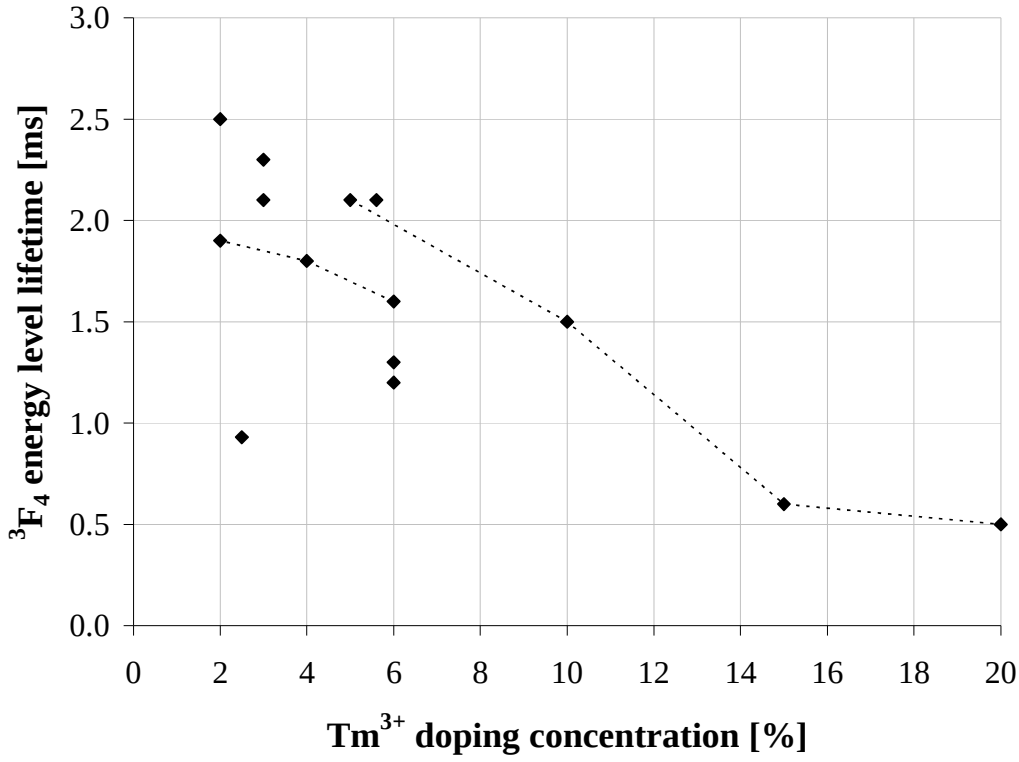

Figure 3.10: Reported lifetimes for the $^3F_4$ energy level of Tm:$GdVO_4$ at different doping concentrations. The connected data points originate from single sets of experiments.

The lifetime of the $^3F_4$ upper laser energy level of Tm:$GdVO_4$ that has been measured by numerous researchers, and is shown in Figure 3.10 [22, 23, 31, 32, 34, 42], with

some measurements conducted in single sets of experiments indicated by the connected data points [3, 24]. The reported $^3F_4$ lifetimes vary from 2.5 ms for a 2% doped crystal, down to 0.5 ms for a 20% doped Tm:$GdVO_4$ crystal.

The results of the lifetime fluorescence measurements strongly depend on the method used for measurement, as well as the doping concentration of the Tm^{3+} ions in $GdVO_4$. It is not evident from the Tm:$GdVO_4$ literature that an appropriate measurement technique was always used in order to minimise the effect of "self-trapping" that can occur when the fluorescence is reabsorbed by the crystal, which would typically result in a measured fluorescence lifetime longer than the real lifetime of a particular energy level. In addition, the energy lifetimes are influenced by the doping concentration due to the inter-ion processes such as cross relaxation, excited state absorption and energy transfer upconversion. Impurities in the crystal host can also serve as radiation traps, reducing the lifetime of excited Tm^{3+} ions [43].

3.2.6 Optical & mechanical properties of Tm:$GdVO_4$ laser crystals

Table 3.1: Comparison of Tm:YVO_4, Tm:$GdVO_4$, and Tm:$LuVO_4$ crystals properties [32].

Crystal			Tm:YVO_4	Tm:$GdVO_4$	Tm:$LuVO_4$
Refractive index		n_e	1.93[15]	1.96[16]	2.249[17]
($\lambda \sim 2\,\mu$m)		n_o	2.14[15]	2.17[16]	2.031[17]
Density	[g/cm^3]		4.22,[8] 4.33[15]	5.48[8]	6.06,[18] 6.2[19]
Thermal conductivity	[Wm^{-1}K^{-1}]	axis **a**	5.1,[20] 7.2,[21] 9.0[22]	8.6,[22] 9.7,[23] 10.1[21]	6.14,[18] 7.96[19]
		axis **c**	5.2,[20,24] 9.4,[21] 12.0[22]	10.4,[22] 11.4,[21] 12.3[24]	9.77[19]
Lattice constants	[nm]	axis **a**	0.712[20]	0.721[21,25]	0.703[17]
	[nm]	axis **b**, **c**	0.629[20]	0.635[21,25]	0.623[17]
Melting point	[°C]		1825, 1810[20]	1780[26]	1800
Thermal expansion	[10^{-6}K^{-1}]	axis **a**	1.69,[22] 4.43[20]	1.14[22]	1.5[19]
	[10^{-6}K^{-1}]	axis **c**	8.19,[22] 11.4[20]	7.89[22]	9.1[19]
Specific heat	[Jkg^{-1}K^{-1}]		560[22]	429[22]	390,[18] 442[19]
dn_o/dT	[10^{-6}K^{-1}]	axis **a**	7.92,[22] 8.5[8]	10.1[22]	—
dn_e/dT	[10^{-6}K^{-1}]	axis **c**	2.7,[27] 2.9[8]	4.7,[27] 13.8[22]	—
Absorption peak	[nm]	**E**||**c**	789.4	799.1	797.8
Abs. cross-section	[10^{-20}cm^2]	**E**||**c**	3.0	4.0	6.2
Eimss. cross-section peak	[nm]	**E**||**c**	1804	1807	1797
Eimss. cross-section	[10^{-20}cm^2]	**E**||**c**	2.7	2.0	3.1
Fluor. decay time (Tm^{3+})	[μs]		1400 (5 at.%)	2500 (2 at.%) 1300 (6 at.%)	560 (3 at.%)
Tm^{3+} density (1 at.%)	[10^{20} cm^{-3}]		1.25	1.21	1.29

A summary of the optical and physical properties of the Tm^{3+} doped vanadate laser crystals has been made by Jan Šulc and co-workers [32], which is reproduced in Table 3.1. It is, however, clear from the references used by the authors in the table that for

some of the parameter values the data for Tm:$GdVO_4$ is not available, but were taken from the data for Nd:$GdVO_4$.

3.3 Power scaling of diode-pumped Tm:$GdVO_4$ solid-state lasers

A summary of the most important literature results with respect to power scaling of diode-pumped Tm:$GdVO_4$ lasers is listed in Table 3.2 and discussed in detail below.

Table 3.2: Power scaling of diode-pumped Tm:$GdVO_4$ lasers.

Date	Mode	CW Power Peak Power Energy	Centre λ [nm]	Output coupler reflectivity	Pumping scheme	Tm^{3+} doping	Crystal Type	Crystal Temp.	Crystal Length	Ref.
1997	QCW	43 mW (PP)	1923	97.6%	Microchip	0.5-9%	Czochralski	un-cooled	1 mm	[11]
1998	QCW	1.4 W (PP) 4.1 mJ	1950	97.6%	Microchip	6.9%	Czochralski	5°C	1 mm	[16]
2001	CW	630 mW	1920	97.5%	Microchip	-	Czochralski	7°C	1 mm	[17]
2006	QCW	11 W (PP) 39 mJ	-	97%	Side-pumped	3%	Czochralski	-10°C	12 mm	[44]
2006	CW	2.6 W	1910	96%	Single end-pumped	2%	Floating Zone	Room temp.	3 mm	[5]
2007	CW	2.8 W	1912	95%	Double end-pumped	3%	Czochralski	18°C	5 mm	[34]
2009	Q-sw	2W, 48ns, 5kHz	1912	97%	Single end-pumped	3%	Czochralski	17°C	2 mm	[36]

The first diode-pumped Tm:$GdVO_4$ laser was demonstrated in 1997, using an un-cooled microchip laser crystal and a chopped pump beam, delivering 43 mW of QCW output power [11]. The QCW output power was subsequently increased to 1.4 W peak power by cooling the laser crystal to 5°C, and pumping with laser diode pump powers of 32 W at a low duty cycle of 1.9% with a pump on-time of 2.4 ms [16].

The extent to which the pump duty cycle and peak power could be increased, and therefore also the increase in average output power, were limited by the onset of laser damage on the mirror surfaces of the microchip laser crystal, and not due to thermal fracture of the crystal. In order to validate this statement and to verify that Tm:$GdVO_4$ has a high thermal conductivity, the researchers compared the output performance of the microchip laser for two different cooling configurations, namely cooling the

crystal from the sides only with a copper heat sink, or cooling the crystal from the sides and faces with sapphire plates mounted in the copper heat sink which provided better cooling. The mechanical setup and results for this experiment are reproduced in Figure 3.11, from which it can be seen that implementing the slightly more intricate face cooling of the microchip laser crystal with two sapphire plates did not lead to an improved QCW output performance as compared to the original side-cooling of the microchip laser.

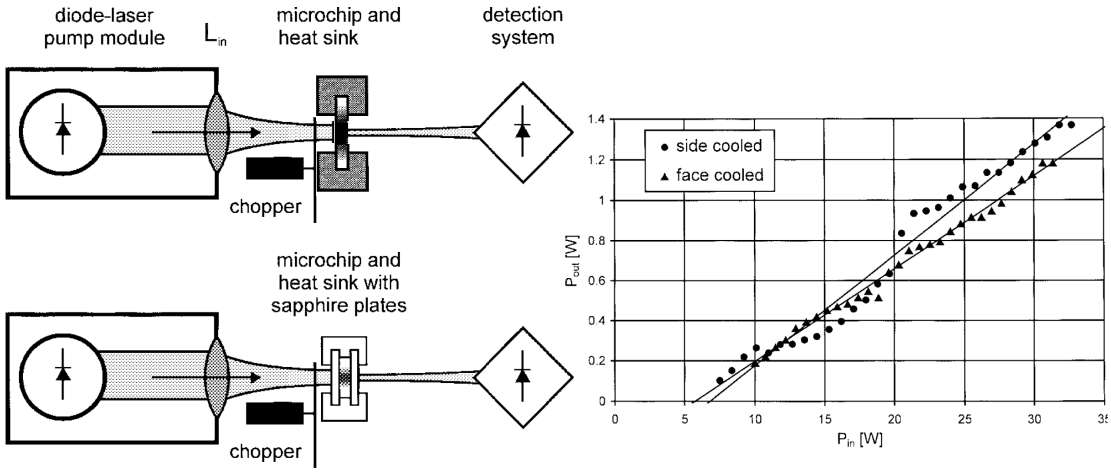

Figure 3.11: Comparison of the performance from a microchip Tm:$GdVO_4$ laser for two cooling configurations [16].

In order to operate the highly doped microchip Tm:$GdVO_4$ laser in CW mode and not only in QCW mode, it was necessary for the researchers from the same group to utilise a fibre-coupled laser diode with a fibre core diameter of only 115 µm, in order to focus the pump beam to a very small spot in the laser crystal. By implementing this key feature they were able to demonstrate 630 mW of CW output power from 3 W of pump power at 806 nm, seemingly only limited by the available power from this higher brightness pump source [17].

An attempt was made in 2006 by Atsushi Sato and co-workers from Japan to implement a diode-side-pumped Tm:$GdVO_4$ laser, as shown in Figure 3.12 [44]. Only QCW operation was reported, with a low laser slope efficiency of 2.2% as compared to previous diode-end-pumped microchip laser slope efficiencies of 33% and higher for Tm:$GdVO_4$ [17]. The total pump energy from six 2-bar diode stacks was 3 J in a 5 ms long pump pulse (total pump peak power of 600 W), which resulted in 39 mJ output (peak power 11 W) from the Tm:$GdVO_4$ laser when cooled to -10°C.

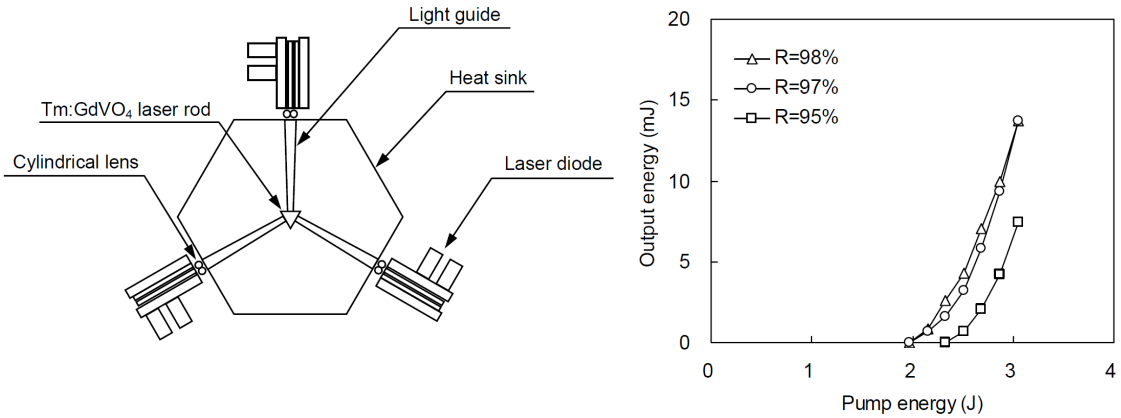

Figure 3.12: Design and performance of a diode-side-pumped Tm:$GdVO_4$ laser [44].

The limitation of the diode-side-pumped approach was the poor laser efficiency achieved, which was attributed to strong re-absorption of the laser light in the 12 mm long, 3% Tm^{3+} doped length of the crystal with 5 mm undoped end-caps, as well as the low pump power density in the side-pumped triangular-prism Tm:$GdVO_4$ laser rod.

As discussed in Section 3.1, the breakthrough in CW output power from a Tm:$GdVO_4$ laser to the multi-watt level was due to the implementation of high optical quality (Floating Zone grown) crystals in a diode-end-pumped laser architecture with a 2% doped crystal of length 3 mm, pumped by a fibre-coupled laser diode at 800-803 nm [5]. In the discussion of their results, the collaborators stated that the output power was solely limited by the available pump power of 20 W, and that thermal effects only slightly reduced the laser efficiency as compared to QCW operation of the same laser. In a subsequent experiment by the same researchers they also demonstrated 2.6 W of output power from a 4% doped crystal of length 3 mm pumped by a 17 W fibre-coupled laser diode at 805 nm with a pump spot diameter of 360 µm [3]. It was again stated that the output power was only limited by the available pump power, indicating that the fibre-coupled diode-end-pumped laser architecture is very attractive for power scaling Tm:$GdVO_4$ lasers.

A slight improvement in the performance of a diode-pumped Tm:$GdVO_4$ laser was achieved, with up to 2.8 W of CW output power from a double-end-pump laser design by Li *et al* from the Harbin Institute of Technology in China [34]. They implemented a 5 mm long, 3% doped Czochralski grown Tm:$GdVO_4$ crystal cooled to 18°C, pumped with an 18 W fibre-coupled laser diode at 795 nm, with a pump spot diameter estimated to be as small as 300 µm.

The researchers demonstrated in a previous experiment, (the setup and results of which are reproduced in Figure 3.13), that there is a significant advantage in using a double-end-pump setup as compared to a single-end-pump setup, especially for the 10 mm long, 2% Tm^{3+} doped, cryogenically cooled crystal used in the initial experiment [35]. This laser could not be operated at room temperature since thermal fracture occurred before CW laser threshold could be reached. Operating at 77 K, the threshold of the double-end-pumped laser was reduced down to 3.2 W with respect to the 13 W threshold of the single-end-pumped setup. The researchers stated that by pumping from both ends, the length of the gain region was increased, which subsequently reduced the quasi-three-level laser ground-state re-absorption effect; and also, the strong localised heating from the pump source that leads to a reduced laser performance when pumped from one end only, was reduced by distributing the heat load to both ends of the crystal.

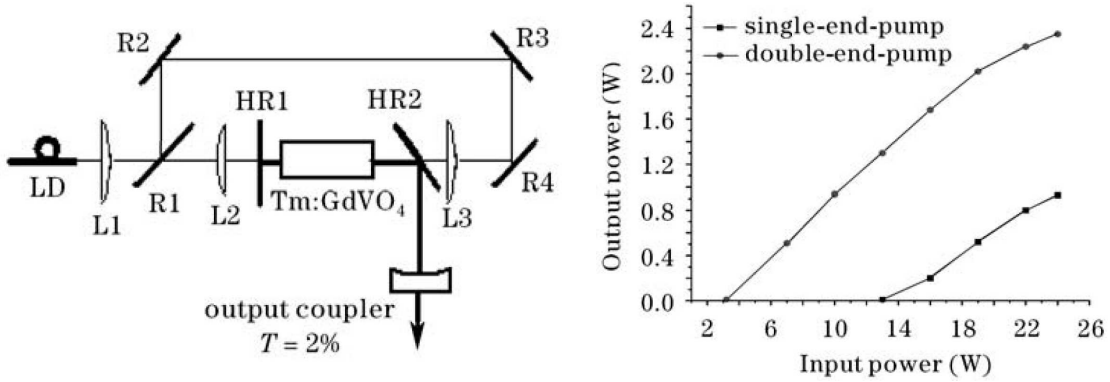

Figure 3.13: Experimental setup and results of a single-end-pumped or double-end-pumped Tm:$GdVO_4$ laser operated at 77 K [35].

Despite the advantage of a double-end-pumped arrangement, the researchers were forced to implement a single-end-pumped arrangement for the first demonstration of a *Q*-switched Tm:$GdVO_4$ laser due to the inclusion of a 22 mm wide air-cooled AOM in the compact linear laser resonator. Included in the resonator of length 35 mm was a 2 mm long 3% doped Czochralski Tm:$GdVO_4$ crystal pumped by a 15 W fibre-coupled laser diode at 805 nm with a pump spot diameter of 320 µm. The optical arrangement and results are reproduced in Figure 3.14 [36]. With this single-end-pumped setup the researchers also operated the laser in CW mode with the AOM *Q*-switch removed from the cavity, reportedly again producing 2.8 W of CW output

power, which demonstrated that by reducing the crystal length the same performance could be reached as with the double-end-pumped setup reported earlier [34].

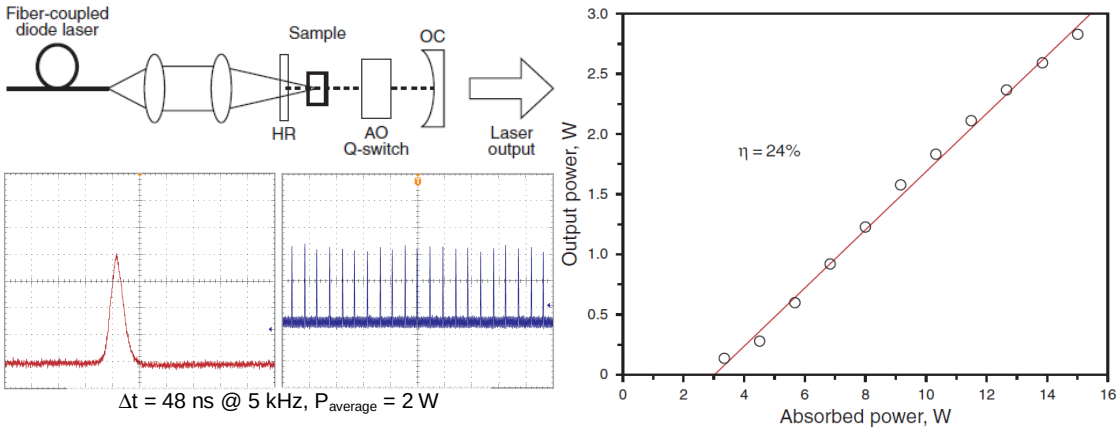

Figure 3.14: First demonstration of a *Q*-switched Tm:$GdVO_4$ laser, together with the CW slope efficiency [36].

3.4 Conclusion

The major conclusion to be drawn from an evaluation of the results of the lasers reported in the literature, as summarised here, is that the most promising approach to power scale a Tm:$GdVO_4$ laser is to implement a fibre-coupled diode-end-pumped setup from both ends with small pump beam diameters, utilising either Czochralski or Floating Zone grown crystals of Tm^{3+} doping concentration from 2% to 4%, and length 2 to 5 mm. A highly doped microchip Tm:$GdVO_4$ laser design seems not to be a viable approach to achieve multi-watt CW output at 1.9 µm, neither does a side-pumped laser architecture due to its low laser efficiency, even if hundreds of watts of pump power can be coupled into the laser crystal from the sides without inducing thermal fracture. The maximum absorbed diode pump power reported for a microchip laser setup was 33 W [15], and for a diode-end-pumped rod laser it was 18 W at 795 nm [34], seemingly limited by the available pump power and not by thermal fracture of the laser crystals. The laser diode wavelengths utilised in the literature, from 795 nm to 808 nm, covers the wide absorption band of Tm:$GdVO_4$.

This evaluation of the available literature on Tm:$GdVO_4$ was used to guide the design of a high-power diode-end-pumped Tm:$GdVO_4$ laser, as discussed in the next chapter.

3.5 References

[1] P. A. Studenikin, A. I. Zagumennyi, Yu. D. Zavartsv, P. A. Popov and I. A. Shcherbakov "$GdVO_4$ as a new medium for solid-state lasers- some optical and thermal properties of crystals doped with Nd^{3+}, Tm^{3+}, and Er^{3+} ions," Quantum Electronics **25** (12) 1162-1165 (1995).

[2] A. I. Zagumennyi, Yu. D. Zavartsv, P. A. Studenikin, I. A. Shcherbakov, A.F. Umyskov, P. A. Popov and V. B. Ufimtsev "$GdVO_4$ crystals with Nd^{3+}, Tm^{3+}, Ho^{3+}, and Er^{3+} ions for diode-pumped microchip laser," Proceedings of SPIE **2698** 182-192 (1996).

[3] R. Lisiecki, P. Solarz, G. Dominiak-Dzik, W. Ryba-Romanowski, M. Sobczyk, P. Černý, J. Šulc, H. Jelínková, Y. Urata, and M. Higuchi, "Comparative optical study of thulium-doped YVO_4, $GdVO_4$, and $LuVO_4$ single crystals" Phys. Rev. B **74**, 035103 (2006).

[4] E. Sorokin, A. N. Alpatiev, I. T. Sorokina, A. I. Zagumennyi, and I. A. Shcherbakov, "Tunable efficient continuous-wave room-temperature Tm^{3+}:$GdVO_4$ laser," OSA Trends Opt. Photonics Adv. Solid-State Lasers 68, 347–350 (Opt. Soc. Am., Washington, DC 2002).

[5] P. Černý, J. Oswald, J. Šulc, H. Jelínková, Y. Urata, and M. Higuchi, "Multi-watt and Tunable Diode-Pumped Operation of Tm:$GdVO_4$ Crystal Grown by a Floating Zone Method" Advanced Solid-State Photonics (ASSP), TuB6, (2006).

[6] A. I. Zagumennyi, Y. D. Zavartsev, P. A. Studenikin, V. I. Vlasov, I. A. Shcherbakov, C. P. Wyss, W. Lüthy, H. P. Weber, and P. A. Popov, "Thermal conductivity of a Tm^{3+}:$GdVO_4$ crystal and the operational characteristics of a microchip laser based on it," Quantum Electronics **29**, (4) 298-300 (1999).

[7] Y. Sato and T. Taira, "The studies of thermal conductivity in $GdVO_4$, YVO_4, and $Y_3Al_5O_{12}$ measured by quasi-one-dimensional flash method," Opt. Express **14**, 10528-10536 (2006).

[8] H. Saito, S. Chaddha, R. S. F. Chang, N. Djeu, "Efficient 1.94-µm Tm^{3+} laser in YVO_4, host," Optics Letters **17** (3), 189-191 (1992).

[9] P. J. Morris, W. Lüthy, H. P. Weber, Yu. D. Zavartsev, P. A. Studenikin, I. Shcherbakov, "Laser operation of Tm:Ho:$GdVO_4$," CLEO Europe CTuF5 (1994).

[10] P. J. Morris, W. Lüthy, H. P. Weber, Yu. D. Zavartsev, P. A. Studenikin, I. Shcherbakov, "Laser operation and spectroscopy of Tm:Ho:$GdVO_4$," Optics Communications **111** (5-6) 493-496 (1994).

[11] V. A. Mikhalov, Y. D. Zavartsev, A. I. Zagumenny, P. A. Studenikin, I. A. Shcherbakov, V. G. Ostroumov, E. Heumann, and G. Huber "Tm^{3+} : $GdVO_4$ – A new efficient medium for diode-pumped 2-µm lasers," Quantum Electronics **27**, (1) 13-14 (Jan 1997) (Translated from Kvantovaya Elektronika **24**, (1) 15-16 (1997)).

[12] A. I. Zagumenny, Y. D. Zavartsev, V. A. Mikhalov, P. A. Studenikin, I. A. Shcherbakov, V. G. Ostroumov, E. Heumann, and G. Huber, "New High Efficient Tm:$GdVO_4$ Diode Pumped Microchip Laser," OSA TOPS Vol. 10, Advanced Solid-State Lasers (ASSL), 205, (1997).

[13] Chr. P. Wyss, W. Lüthy, H. P. Weber, V. I. Vlasov, Yu. D. Zavartsev, P. A. Studenikin, A. I. Zagumenny, and I. A. Shcherbakov "Performance of a Tm^{3+}:$GdVO_4$ microchip laser at 1.9 µm," Optics Communications **153**, (1-3), 63-67 (15 Jul 1998).

[14] C. P. Wyss, W. Lüthy, H. P. Weber, V. I. Vlasov, Yu. D. Zavartsev, P. A. Studenikin, A. I. Zagumenny, and I. A. Shcherbakov, "Emission properties of a Tm^{3+}:$GdVO_4$ microchip laser at 1.9 µm," Applied Physics B **67**, (5), 545-548 (1998).

[15] Chr. P. Wyss, W. Lüthy, and H. P. Weber, "Performance of a Diode-Pumped 1.4 W Tm:$GdVO_4$ Microchip Laser at 1.9 µm," CLEO Europe **98**, CMC3, 11 (Sept 1998).

[16] Chr. P. Wyss, W. Lüthy, H. P. Weber, V. I. Vlasov, Yu. D. Zavartsev, A. Studenikin, A. I. Zagumenny, and I. A. Shcherbakov, "A diode-pumped 1.4-W Tm^{3+}:$GdVO_4$ microchip laser at 1.9 µm," IEEE Journal of Quantum Electronics **34**, (12), 2380-2382 (December 1998).

[17] A. I. Zagumenny, V. A. Mikhailov, Yu. D. Zavartsev, S. A. Koutovoi, F. Zerrouk, and I. A. Shcherbakov, "A diode pumped 0.6 W cw Tm:$GdVO_4$ microchip laser," CLEO Europe C-PSL 129 (2001).

[18] V. A. Mikhailov, A. I. Zagumenny, and I. A. Shcherbakov, "Diode-pumped lasers based on oxide crystals," Proceedings of SPIE **5147** 1-12 (November 2003).

[19] A. I. Zagumenny, V. A. Mikhailov, V. I. Vlasov, A. A. Soritkin, V. I. Podreshetnikov, Yu. L. Kalachev, Yu. D. Zavartsev, S. A. Kutovoi, and I. A. Shcherbakov, "Diode-pumped lasers based on $GdVO_4$ crystal" Laser Physics **13**, (3) 311-318 (March 2003).

[20] E. Sorokin, I. T. Sorokina, A. N. Alpatiev, A. I. Zagumenny, Yu. D. Zavartsev and I. A. Shcherbakov, "Spectroscopic and laser study of the tunable efficient continuous-wave Tm^{3+}:$GdVO_4$ laser," IQEC/LAT 2002 (Moscow) QSuR19 110 (2002).

[21] E. Sorokin, S. Naumov and I. T. Sorokina, "Ultrabroadband Infrared Solid-State Lasers" IEEE Selected Topics in Quantum Electronics **11**, (3) 690-712 (May/June 2005), p 693.

[22] Y. Urata, K. Akagawa, S. Wada, H. Tashiro, S.J. Suh, D. H. Yoon, and T. Fukuda, "Growth and optical properties of Tm:$GdVO_4$ single crystal," Crystal Research and Technology **34,** (1), 41-45 (1999).

[23] Y. Urata and S. Wada, “CW Tm:$GdVO_4$ laser pumped by 808-nm laser diodes operated at room temperature,” Proceedings of SPIE **5154** 179-186 (December 2003).

[24] Y. Urata, H. Machida, M. Higuchi, K. Kodaira, and S. Wada, “Thulium-doped gadolinium vanadate single crystals for efficient 2-μm source of practical use,” Proceedings of SPIE **4893** 422-431 (March 2003).

[25] M. Higuchi, K. Kodaira, Y. Urata, S. Wada, and H. Machida, “Float zone growth and spectroscopic characterization of Tm:$GdVO_4$ single crystals,” Journal of Crystal Growth **265**, (3-4), 487-493 (May 2004).

[26] Y. Urata, H. Machida, M. Higuchi, K. Kodaira, and S. Wada, “Improved performance of diode-pumped continuous-wave Tm:$GdVO_4$ laser using floating zone-grown crystals,” EPS-QEOD Europhoton Conference, Lausanne 2004, Sol10081 ThA4 (2004).

[27] Y. Urata, H. Machida, M. Higuchi, K. Kodaira, and S. Wada, “Diode-pumped CW Tm:$GdVO_4$ laser using floating zone-grown crystals” Proceedings of SPIE **5653** January 2005 (327-334).

[28] Y. Urata and S. Wada, “LD-pumped CW Tm-GdVO4 laser operated at room temperature,” Advanced Solid-State Photonics (ASSP) WB18 (2004).

[29] Y. Urata and S. Wada, “808-nm diode-pumped continuous-wave Tm:$GdVO_4$ laser at room temperature,” Applied Optics **44**, (15) 3087-3092 (2005).

[30] P. Černý, and H. Jelínková, “Developing thulium lasers for depth-selective scalpels,” SPIE Newsroom 2006070281 (2006), http://spie.org/x8689.xml?highlight=x2416.

[31] R. Lisiecki, P. Solarz, G. Dominiak-Dzik, W. Ryba-Romanowski, M. Sobczyk, P. Černý, J. Šulc, and H. Jelínková, Y. Urata, and M. Higuchi, “Spectroscopic

and laser characteristics of vanadate crystals doped with thulium," 2nd EPS-QEOD Europhoton Conference, Pisa, Italy 2006, SSL-50, (2006).

[32] J. Šulc, P. Koranda, P. Černý, H. Jelínková, Y. Urata, M. Higuchi, W. Ryba-Romanowski, R. Lisiecki, P. Solarz, G. Dominiak-Dzik, and M. Sobczyk, "Tunable lasers based on diode pumped Tm-doped vanadates Tm:YVO_4, Tm:$GdVO_4$, and Tm:$LuVO_4$," Proceedings of SPIE **6871**, 68711V, (2008).

[33] J. Šulc, P. Černý, H. Jelínková, W. Ryba-Romanowski, R. Lisiecki, P. Solarz, G. Dominiak-Dzik, Y. Urata, and M. Higuchic, "Tm-doped vanadates under pulsed pumping with variable duty cycle: impact on lasing and fluorescence," Proc. SPIE **6998**, 69980T, (2008).

[34] Y. Li, B. Yao, Y. Liu, Y. Wang, Y-L. Ju "Widely Tunable cw Diode-Pumped 1.9-um Tm:$GdVO_4$ Laser at Room Temperature," Chinese Physics Letters **24**, (3), 724 (2007).

[35] Y. Li, B. Yao, and Y. Wang, "Diode-pumped CW Tm:$GdVO_4$ laser at 1.9 μm," Chinese Optics Letters **4**, (3), 175-176 (March 2006).

[36] Z.G. Wang, C.W. Song, Y.F. Li, Y.L. Ju, and Y.Z. Wang, "CW and pulsed operation of a diode-end-pumped Tm:$GdVO_4$ laser at room temperature," Laser Physics Letters **6,** (2), 105–108 (2009).

[37] Y. Yang, B. Yao, B. Chen, C. Wang, G. Ren, and X. Wang, "Judd–Ofelt analysis of spectroscopic properties of Tm^{3+}, Ho^{3+} doped $GdVO_4$ crystals," Optical Materials **29**, (9), 1159-1165 (May 2007).

[38] Private Communication, Laboratory visit, R. Lisiecki, Institute of Low Temperature and Structure Research, Polish Academy of Sciences, Wrocław, Poland, May 2007.

[39] C. Bollig, "Single-Frequency Diode-Pumped Solid-State Lasers," PhD Thesis, Optoelectronics Research Centre, University of Southampton, (1997).

[40] S. So, J.I. Mackenzie, D.P. Shepherd, W.A. Clarkson, J.G. Betterton, and E.K. Gorton, “A power-scaling strategy for longitudinally diode-pumped Tm:YLF lasers,” Appl. Phys. B **84** (3) 389-393 (2006).

[41] Y. Li, Y. Ju, Y. Urata, and Y. Wang, “Experimental spectra study of Tm:$GdVO_4$ microchip laser at room temperature,” Chinese Optics Letters **5**, (6), 351-352, (2007).

[42] Y. F. Li, Y. Z. Wang, and B. Q. Yao, “Comparative optical study of thulium-doped $YAlO_3$ and $GdVO_4$ single crystals,” Laser Physics Letters **5**, (1), 37–40, (2008).

[43] R. Lisiecki, B. Macalik, G. Dominiak-Dzik, P. Solarz, B. Nowak, W. Ryba-Romanowski, J. K. Jabczyński, and T. Łukasiewicz “Influence of impurities and thermal treatment on spectroscopic properties and laser performance of Tm:YVO_4 laser crystals,” Applied Physics B **90**, (3-4), 477-483, (March 2008).

[44] A. Sato, K. Asai, S. Ishii, K. Mizutani, and T. Itabe, “Characteristics of pulsed / cw vanadate lasers operating at 2 μm,” Proceedings of SPIE **6409** 640916 (December 2006).

Chapter 4

Development of a diode-end-pumped $Tm:GdVO_4$ laser

Based on the evaluation of $Tm:GdVO_4$ lasers as presented in the previous chapter it was considered feasible that this laser material can be utilised to achieve the research goal of designing and demonstrating a diode-pumped solid-state 1.9 µm laser system that is compact and efficient with output power levels of 10 to 100 watt to pump a Ho^{3+} laser. Furthermore, the general availability of laser diode sources with higher output powers than used in the literature to pump $Tm:GdVO_4$ lasers suggests that power scaling experiments with this promising laser material may be fruitful. However, in order to scale the output power and wavelength range beyond the values that have already been demonstrated for $Tm:GdVO_4$, it was necessary to address the following main aspects:

- A theoretical analysis of the expected threshold and wavelength.
- The availability of $Tm:GdVO_4$ laser crystals and possible mounting methods.
- The identification of suitable laser diode pump sources.
- The laser resonator design and optical pump setup.
- Diagnostic instruments and other equipment required to perform the laser experiments.

It was considered likely that an improvement could be made on the state-of-the-art performance of $Tm:GdVO_4$ lasers by implementing laser experiments with laser diodes with more than 50 W output power as pump sources and by carefully designing a laser resonator based on quasi-three-level laser calculations. The development of an experimental high-power diode-end-pumped $Tm:GdVO_4$ laser is described in this chapter.

4.1 Theoretical evaluation of laser oscillation threshold

4.1.1 Absorption spectra

In order to optimise the design of a high-power diode-pumped Tm:$GdVO_4$ laser, detailed spectroscopic data of the laser material was required. However, in early trial calculations, it had been found that the spectral data available in the literature for Tm:$GdVO_4$ were not sufficiently precise to enable accurate predictions of the laser performance to be carried out, especially at longer wavelengths. Nevertheless, through a collaboration initiated with Professor Huber at the Institute of Laser-Physics of the University of Hamburg, the absorption spectra of the Tm:$GdVO_4$ laser crystals were measured at both 0.8 µm (pump band) and at 1.9 µm (emission band). The measurements were conducted with a Cary 5000 spectrometer with resolution set to 1 nm and an integration time of 0.1 seconds. The crystal used for the spectroscopic measurements was a 10 mm long Tm:$GdVO_4$ laser crystal.

The absorption cross section data (σ_{abs}) of Tm:$GdVO_4$, measured for the π-polarisation ($\boldsymbol{E}\|$c) and the σ-polarisation ($\boldsymbol{E}\perp$c) in the 1.9 µm wavelength region, are shown in Figure 4.1. A running average over 6 nm was applied in order to reduce the noise in the data. During the spectroscopic measurements the total transmission was less than 1% for the π-polarisation between 1735 and 1820 nm through the 10 mm crystal, which made the cross section data less reliable in this region. Also presented in Figure 4.1 are data for the emission cross sections, σ_{em} of the $^3F_4$-$^3H_6$ laser transition at 1.9 µm, which were calculated by the reciprocity method [1] from the smoothed and offset-corrected absorption cross section data, using the expression

$$\sigma_{em}(\lambda) = \sigma_{abs}(\lambda)\frac{Z_L}{Z_U}\exp\left[\frac{E_{ZL} - hc/\lambda}{k_B T}\right]. \qquad (5.1)$$

In order to perform the calculations the energy levels for Tm:$GdVO_4$ as reported by [2] were used to determine Z_L and Z_U, which are the partition functions of the lower and upper energy states, respectively. E_{ZL}, the energy separation between the lowest crystal field components of the upper and lower states, were also calculated based on the reported energy levels. T is the absolute temperature (293K), k_B is the Boltzmann constant and λ is the wavelength.

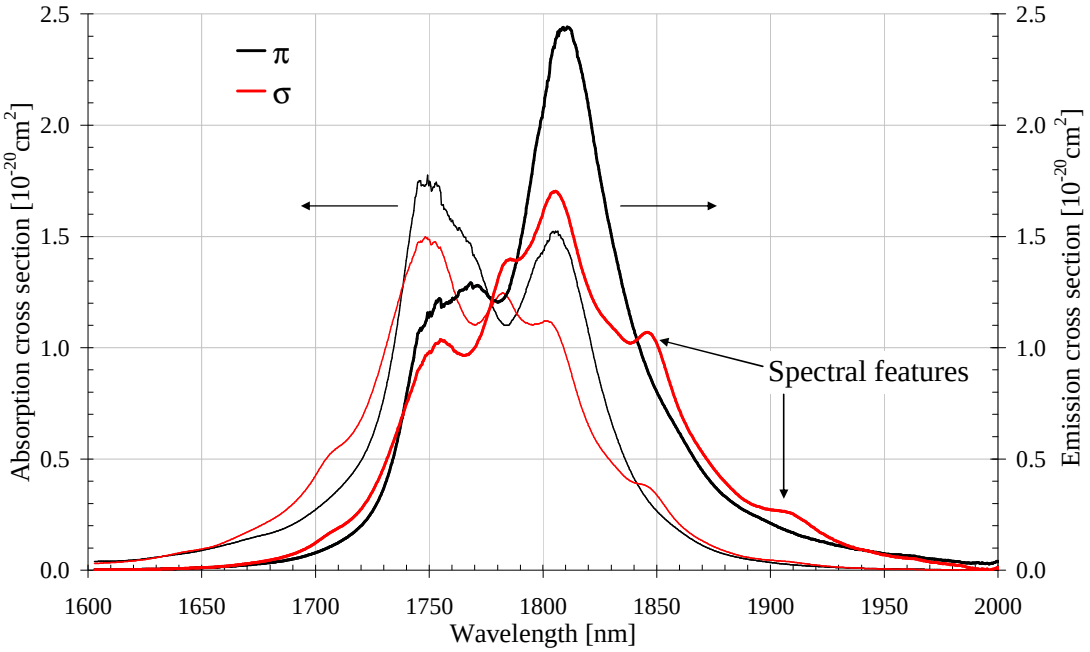

Figure 4.1: The measured absorption cross sections (thin) and the calculated emission cross sections (thick) of Tm:$GdVO_4$ for π-polarised and σ-polarised light between 1600 nm and 2000 nm.

The absorption and emission cross section data as depicted in Figure 4.1 were compared to previously reported data (Figure 3.4 in the previous chapter) and were found to be in good agreement. However, the smoothed and offset-corrected spectra highlighted the spectral features in the long-wavelength region of the spectra which were not distinguishable from the noise of the previously reported data.

From the measured data it was confirmed that on both polarisations the peak absorption is located around 1750 nm, and the peak emission occurs between 1810 – 1820 nm, with the peak cross sections of the π-polarisation always stronger. The π-polarisation emission cross section has a smooth decay towards longer wavelengths, while on the σ-polarisation the emission cross section has distinct spectral features located at 1850 nm and at 1910 nm. These accurately measured absorption spectra, and the calculated emission spectra, were found to be of crucial importance for the prediction of the expected threshold power and the operational wavelength of the Tm:$GdVO_4$ laser.

4.1.2 Laser threshold and wavelength analysis

The absorbed pump power required to achieve oscillation threshold for a diode-end-pumped Tm:$GdVO_4$ quasi-three-level laser can be calculated from the values of the absorption and emission cross section, σ_{abs} and σ_{em} using the approach developed in [3] and further extended in [4] to yield the expression,

$$P_{th}(\lambda) = \frac{\pi h \nu_p (w_l^2 + w_p^2)}{4\tau\eta_{p-q}\sigma_{em}(\lambda)}\left[L + T + 2Nl\sigma_{abs}(\lambda)\right] \tag{5.2}$$

where T is the transmission loss of the output coupler; L represents additional resonator losses, (1% is typical for a two-mirror resonator); w_l and w_p are the laser mode and pump beam radii in the laser crystal; N is the concentration of Tm^{3+} ions in the laser crystal (for 1% doping N = 1.21x10^{22} cm^{-3} [5]); ν_p is the frequency of the pump light; η_{p-q} is the pump quantum efficiency, assumed to be 1.5 as discussed in Section 3.2.3; τ is the lifetime of the $^3F_4$ upper laser manifold, taken as 1.85 ms [2]); and l is the length of the laser crystal.

The laser was designed for end-pumping with the pump beam and the laser mode arranged to be of equal size ($w_l \approx w_p \approx w$) in the crystal. The expression for the threshold power can then easily be converted to an expression for the threshold power density, namely:

$$P_{th\_density}(\lambda) = \frac{P_{th}}{\pi w^2} = \frac{h\nu_p\left[L + T + 2Nl\sigma_{abs}(\lambda)\right]}{2\tau\eta_{p-q}\sigma_{em}(\lambda)} \tag{5.3}$$

By plotting $P_{th\_density}$ against wavelength for different values of output coupling T, the threshold power density required to establish lasing can be determined, an example of which is shown in Figure 4.2. Furthermore, it can be assumed that for a particular output coupling value T, continuous-wave laser oscillation will occur at the wavelength and polarisation for which the threshold power density is a minimum [4].

This method of analysing a laser material for laser performance is valid for the case of a quasi-three-level laser where the population in the upper laser manifold is small compared to the total doping level, and is derived using a low loss approximation [3]. It is complementary to the "effective emission cross section" method used by other researchers [2, 6]. However, the threshold analysis used here provides the laser designer with a clear indication of the expected laser threshold pump power density, wavelength and polarisation of the laser.

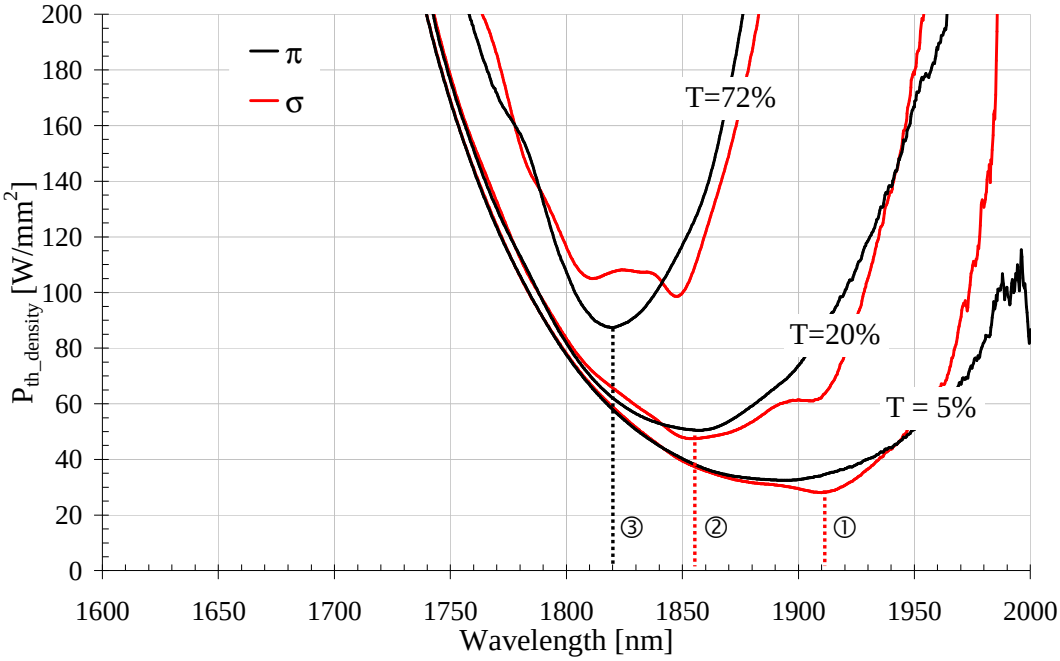

Figure 4.2: The calculated Tm:$GdVO_4$ laser threshold power density at output coupling values *T*, as a function of wavelength for a 3.0% doped, 3 mm length crystal and 1% resonator loss.

The calculations presented in Figure 4.2 were made for a 3.0% doped, 3 mm long Tm:$GdVO_4$ crystal pumped at 803 nm. It was concluded from the graph in Figure 4.2 that laser threshold can be reached with realistic values of resonator output coupling and pump beam focussing.

The predicted threshold power density for a 5% transmission output coupler was ~28 W/mm^2 at 1912 nm, and the Tm:$GdVO_4$ laser is predicted to lase on σ-polarisation as indicated by line ① in the graph. Similarly, the oscillation wavelength for the case of 20% output coupler transmission was predicted to be approximately 1855 nm with a threshold power density of ~47 W/mm^2, also on σ-polarisation as indicated by line ② in the graph. At a high output coupler transmission of 72%, the expected threshold power density was ~87 W/mm^2 while the predicted wavelength was 1820 nm on π-polarisation as indicated by line ③.

It was concluded that the slight features at 1850 nm and 1910 nm, as observed in the emission spectra of Figure 4.1, did play a major role in the predictions of oscillation wavelength, polarisation and threshold values for the Tm:$GdVO_4$ laser at typical output coupler values. Based on these calculations, the desired pump beam sizes and laser resonator configuration were designed, as described in the next sections.

4.2 Tm:$GdVO_4$ laser crystals and their mounting design

Several suppliers who could possibly produce high-quality Tm:$GdVO_4$ laser crystals were approached. However, it was found that the crystals are not readily available on the commercial market, although some manufactures indicated that they would be able to custom produce Tm:$GdVO_4$. Fortunately one supplier was able to offer a selection of laser crystals suited for end-pumping with 800 nm laser diodes. The Czochralski grown crystals listed in Table 4.1 were available as stock items from Crystech Inc, China. The crystals were a-cut, such that the laser could operate on either the π-polarisation ($\boldsymbol{E}$||c) or on the σ-polarisation ($\boldsymbol{E}\perp$c) of the Tm:$GdVO_4$ crystal.

Table 4.1: Tm:$GdVO_4$ laser crystals available for the laser experiments.

Tm^{3+} doping	Dimensions [mm] Width	Height	Length	Coating specification	Quantity
3.0%	2.5	2.5	2	AR/AR800+1920nm	4pcs
3.0%	2.5	2.5	3	AR/AR800+1920nm	5pcs
3.0%	2.5	2.5	4	AR/AR800+1920nm	7pcs
3.0%	2.5	2.5	5	AR/AR800+1920nm	2pcs
3.0%	4	4	10	AR/AR801+2048nm	3pcs
3.0%	4	4	10	AR/AR801+1935nm	3pcs
2.5%	4	4	10	AR/AR801+1935nm	3pcs
2.0%	4	4	10	AR/AR801+1935nm	2pcs

Initial laser threshold calculations were performed using the relevant data for the available crystals. It was concluded from these calculations and literature results which utilised similar crystals [7, 8, 9], that the available Tm:$GdVO_4$ crystals are suitable for diode-end-pumped laser experiments and the crystal samples were subsequently procured. All the crystals had the same broad-band anti-reflection coating produced in the same coating run.

4.2.1 Design of cooling mounts

Upon receiving the laser crystals they were inspected and their dimensions were measured accurately to sub-mm accuracy. This was necessary in order to check the uniformity of the large number of Tm:$GdVO_4$ crystals. Furthermore, the precise width & height dimensions were necessary inputs to the crystal cooling design. Photos of a 2.5 x 2.5 x 2 mm^3 crystal and a 4 x 4 x 10 mm^3 crystal are shown in Figure 4.3. The orientation of the crystalline c-axis was indicated on each crystal by the manufacturer.

Figure 4.3: Two of the Tm:$GdVO_4$ laser crystals received from Crystech Inc, China.

Two mounts of similar design were fabricated (for the 2.5 x 2.5 mm^2 and 4 x 4 mm^2 cross-section crystals) each capable of accommodating all the crystal dimensions listed in Table 4.6 in the appendix of this chapter.

The design drawings are shown in Figure 4.4 and the assembly drawing in Figure 4.5. The mounts consisted of the following components:

1. Cooling block (copper), providing the exchange of heat between the copper parts and circulating water which was kept at 20°C.
2. Isolating plate (plastic), preventing heat flow between the water-cooled parts and the base.
3. Base (stainless steel), used to secure the mount to the optical table.
4. Tm:$GdVO_4$ crystal, either with 2.5 x 2.5 mm^2 or 4 x 4 mm^2 cross section.

5. Crystal base plate (copper), providing cooling of the crystal from the bottom. Thicker base plates were used for the 2.5 x 2.5 mm^2 crystals, and thinner base plates were used for the 4 x 4 mm^2 crystals to ensure that the centre of either type of crystal would be on the designed optical height of the laser.

6 & 7. Crystal side plates (copper), providing cooling of the crystal from the sides. The contact area of the side-plates were designed to accommodate the crystals up to 5 mm in length for the 2.5 x 2.5 mm^2 design, whereas the contact area for the 4 x 4 mm^2 crystals were all 10 mm in length. The height of the side plates were machined to the tolerance listed in Table 4.6 in the appendix of this chapter, to match the variance in crystal side dimensions.

8. Crystal top plate (copper), providing cooling of the crystal from the top.

9. Water connections (plastic), connecting water pipes from a circulating chiller to the cooling block.

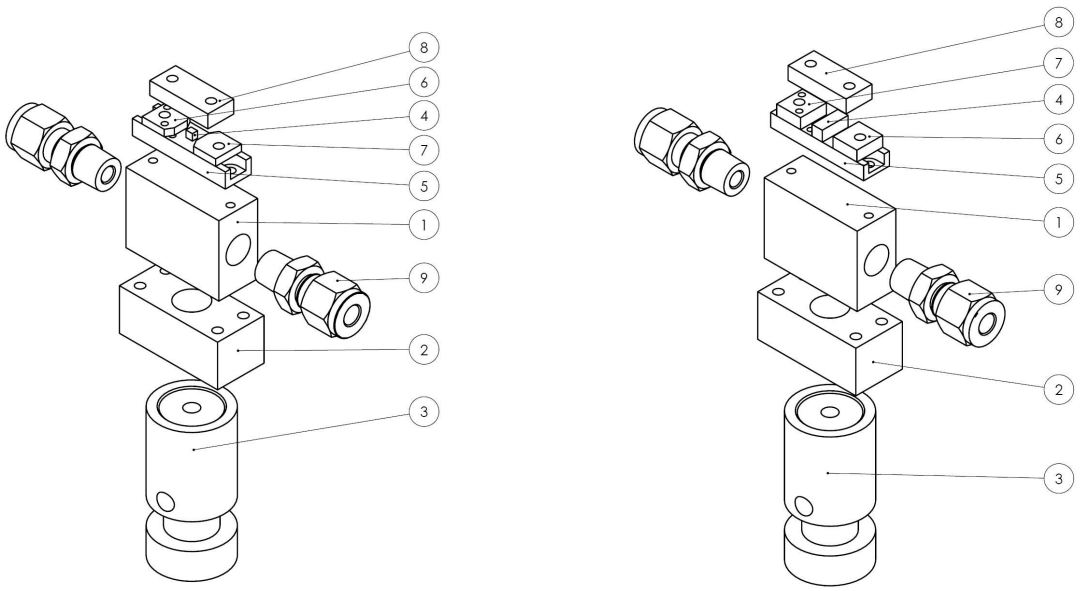

Figure 4.4: Design drawings for the 2.5 x 2.5 mm^2 (left) and 4 x 4 mm^2 (right) Tm:$GdVO_4$ crystals.

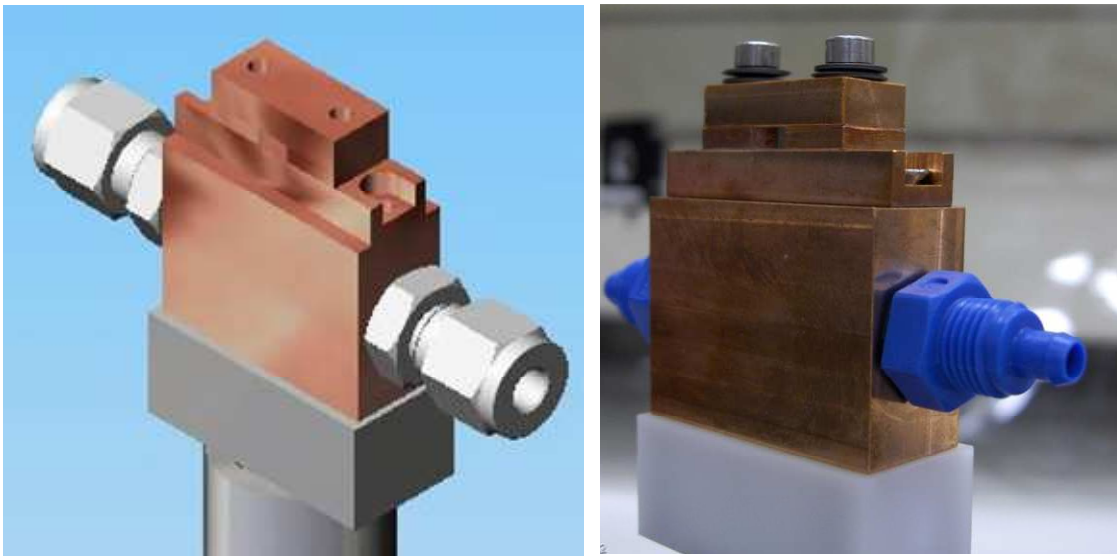

Figure 4.5: Assembly drawing (left) and photo (right) of a Tm:$GdVO_4$ crystal mount.

4.2.2 Crystal mounting method

A mounting jig was also designed and constructed as shown in Figure 4.6, which was used to mount the crystals. Figure 4.7 shows a photo of the mounting jig, part of the crystal mount and a Tm:$GdVO_4$ crystal during the mounting process. The main requirement of the crystal cooling mount was that the copper cooling plates of the mount should make good, uniform thermal contact with the crystal by applying some force to the crystal sides. Indium foil served as a soft and pliable contact medium between the copper cooling plates and the crystal, which assured that the contact was uniform. It was essential that the mechanical pressure applied to the crystal did not induce non-uniform stress in the crystal.

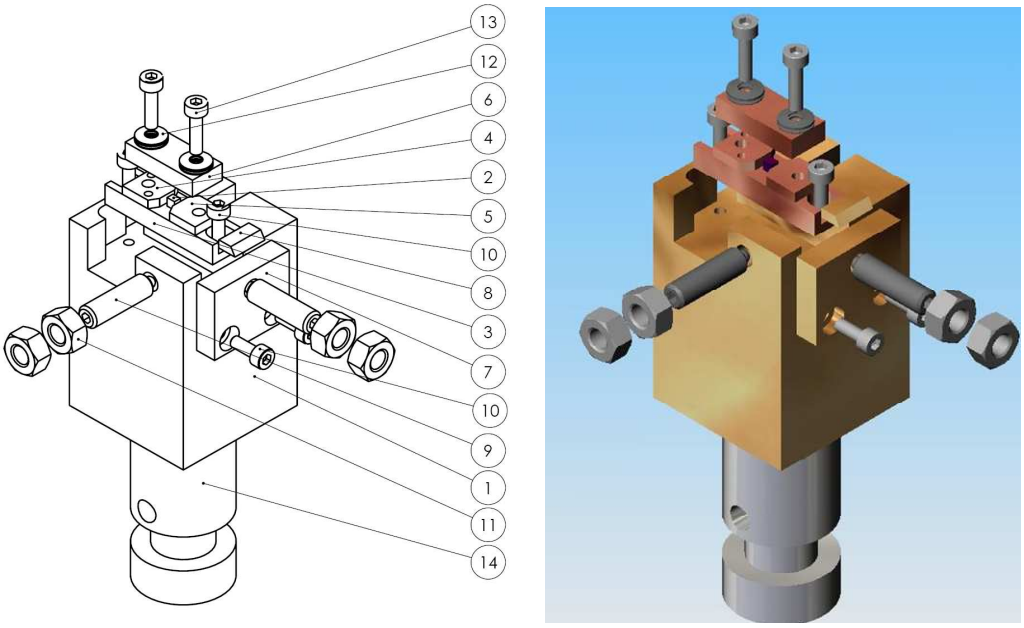

Figure 4.6: Design drawing and assembly of the mounting jig for the Tm:$GdVO_4$ crystal mounts.

A mounting procedure was compiled to document the process by which the crystals were mounted. To mount a particular crystal, the associated crystal mount with the correct height crystal side plates were chosen, as listed in Table 4.6 in the appendix of this chapter. Upon placing the crystal base plate in the mounting jig, a 50 µm thick indium foil layer was placed below the crystal side plates and the crystal itself, as well as between the crystal and the two side plates. One of the crystal side plates was locked in position by precision dowel pins. The spring-loaded plungers (item 9 in Figure 4.6) were used to push the second crystal side plate with a known force against the crystal side, as shown in Figure 4.7. The top layer of indium foil and the crystal top plate was subsequently placed in position and clamped down with two screws and disk springs. The torque applied to the clamping screws was controlled such that the force by which the top plate pressed down on the crystal was roughly equal to the force applied to the sides of the crystal by the spring-loaded plunger. The assembled crystal mount was placed in a vacuum oven for 12 hours and heated to 80°C where the indium foil became very soft, which further reduced the non-uniform contact between the copper, the indium layer and the crystal.

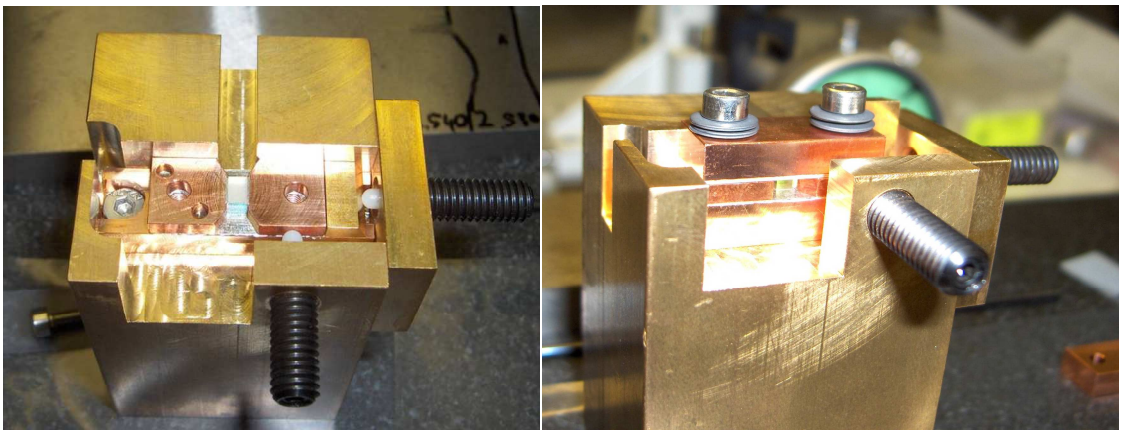

Figure 4.7: Mounting jig in the process of mounting a 2.5 x 2.5 mm^2 Tm:$GdVO_4$ crystal (left), and the crystal completely mounted (right).

The above-mentioned procedure was implemented to mount the Tm:$GdVO_4$ crystals used in the laser experiments with the goal to provide uniform thermal cooling from all four sides.

4.3 Pump laser diode modules

The most suitable pump source for end-pumping laser crystals with a traditional square cross section is the fibre-coupled laser diode module. Such modules were preferred due to their ease of operation, favourable beam properties from the delivery fibres and their availability from numerous laser diode suppliers. With this approach, the pump light can be delivered to the laser crystal through the fibre, producing pump beams with circular transverse intensity profiles. Furthermore, the fibre homogenises the pump light intensity distribution and polarisation. The disadvantages of fibre-coupled laser diode modules are the higher cost per watt and the fact that they are more limited in power than diode laser stacks, neither of which were limitations during the execution of the Tm:$GdVO_4$ laser experiments.

For the development of the Tm:$GdVO_4$ laser, four fibre-coupled laser diode modules were obtained from Jenoptik Laserdiode GmbH, Germany. The selected modules (JOLD-75-CPXF-2P iTEC, design no 15529224) delivered 75 W from a 400 µm diameter, 0.22 NA fibre. Figure 4.8 shows a photo of two of the modules mounted on a water cooled heat sink which was custom designed for the laser diode modules.

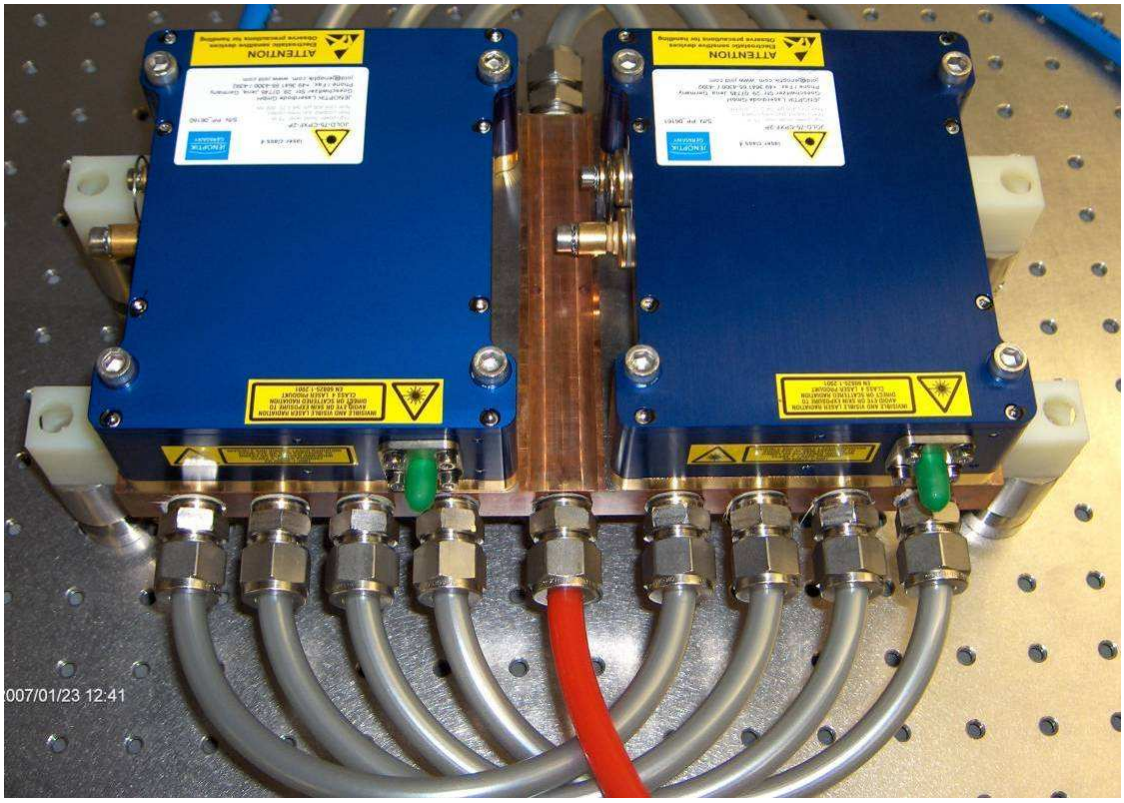

Figure 4.8: Photo of two 75 W Jenoptik Laserdiode GmbH laser diode modules on a water-cooled heat sink.

4.3.1 Operational mode

The laser diode module power supplies were slaved to a pulse generator such that they could be operated either in CW mode, or in QCW mode with an adjustable duty cycle, as indicated in Figure 4.9.

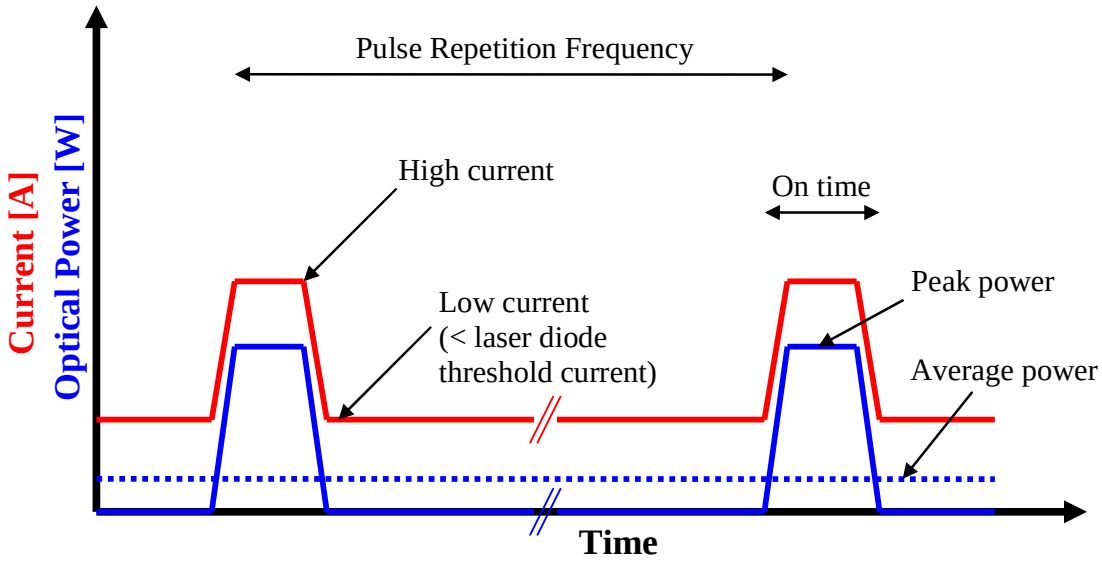

Figure 4.9: Modulation of the input current and the optical output power for QCW operation of the laser diodes.

In QCW mode, the laser diode modules were operated up to 75 W maximum peak power by adjusting the laser diode current from just below the laser diode threshold at 8.8 A (low current) up to 55 A (high current) during the on-time of the pump pulse, which was initially set to 20 ms at 5 Hz pulse repetition frequency (PRF). By implementing QCW pumping, a low average pump power could be maintained to reduce the likelihood that thermal damage would occur in the Tm:$GdVO_4$ laser crystal.

4.3.2 Laser diode module wavelength

The Jenoptik laser diode modules had a specified full power wavelength of 803 nm at 25°C diode temperature which could be tuned with the internal Thermo-Electric Coolers (TECs) at a rate of ~0.3 nm/°C.

At the full CW power of 75 W, the modules could be tuned from approximately 800 nm at 15°C, up to 804.5 nm at the maximum operational temperature of 30°C. This tuning range was well within the absorption band of Tm:$GdVO_4$, as discussed in Chapter 3. Furthermore, the available pump power was significantly more than reported in the literature, making it possible to scale the output power of diode-end-pumped Tm:$GdVO_4$ lasers.

4.3.3 Pump beam size

The initial pump beam radius in the Tm:$GdVO_4$ crystal was chosen to be 220 µm with a resultant pump area of 0.152 mm^2. This pump beam was easily realizable from the fibre-coupled laser diode module using conventional spherical lenses as described below. Furthermore, the confocal length of the pump waist was approximately 2.6 mm which was in the same order of magnitude as the effective crystal length, but more importantly, it was longer than the absorption length of 1.7 mm at 803 nm of the 3.0% doped Tm:$GdVO_4$. The pump beam was therefore sufficiently collimated along the crystal length where the pump light was absorbed.

To further evaluate the suitability of the chosen pump beam size, the threshold values that were predicted for a 220 µm radius pump beam were deduced from the calculations presented in Figure 4.2 and are listed in Table 4.2. The expected threshold powers of a few watts were acceptable since each of the laser diode modules could deliver up to 75 W of pump power.

Table 4.2: Calculated threshold powers of a Tm:$GdVO_4$ laser based on a 3 mm long, 3.0% doped crystal, end-pumped with a beam radius of 220 µm.

	***σ*-polarisation**		***π*-polarisation**	
Output coupler	**Threshold [W]**	**$P_{th\_density}$ [W/mm^2]**	**Threshold [W]**	**$P_{th\_density}$ [W/mm^2]**
T = 5%	**4.3**	28	4.9	32
T = 20%	**7.2**	47	7.7	50
T = 45%	**10.1**	66	10.5	69
T = 72%	15.0	99	**13.3**	87

4.3.4 Pump beam optical setup

For the initial laser experiments a single end-pumped setup was designed, using a two-lens arrangement in such a way that the transverse intensity distribution in the focus was roughly bell-shaped [10].

Figure 4.10 shows a schematic diagram of the setup. L_1, L_2 and L_3 are the distances from the optical fibre (OF) to the first lens f_1, the first to the second lens f_2, and from the second lens to the laser crystal, respectively.

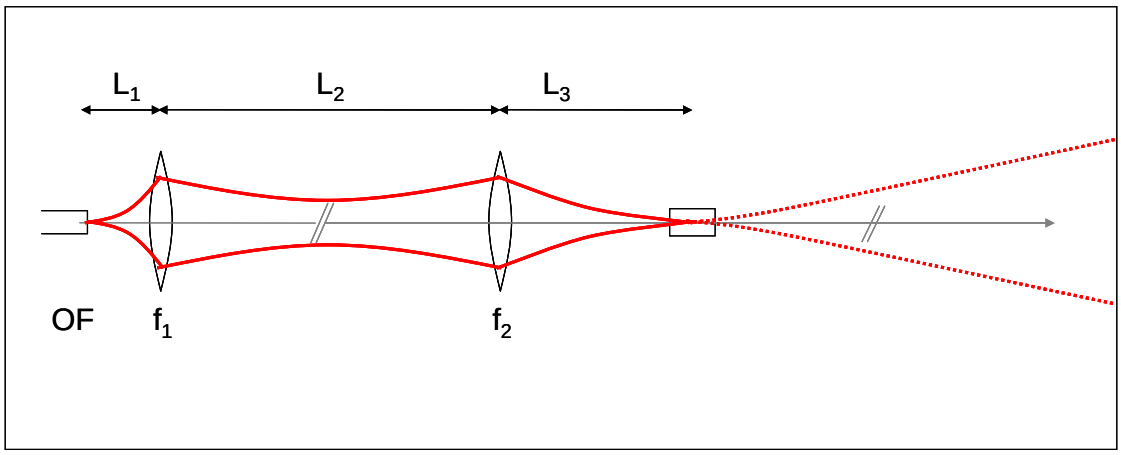

Figure 4.10: Diagram of the pump setup (OF: optical fibre, f: lens, L: length).

To produce the desired pump beam size in the crystal of 220 µm, the appropriate distances L_1, L_2 and L_3 for the available combinations of lenses f_1 and f_2 were calculated using the laser and optics design software Paraxia Plus. Table 4.3 lists the parameter values for the combinations that were investigated. Standard spherical lenses from Thorlabs Inc. with broadband anti-reflection coatings were used, the specified damage threshold of which were 100 W/cm^2. It was, however, confirmed by the supplier that this relatively low value is very conservative, and that higher real damage threshold values could be expected.

Table 4.3: The parameter values for several available combinations of lens focal lengths f1 and f2 to produce a pump beam radius of 220 µm in the Tm:$GdVO_4$ crystal.

f1 [mm]	f2 [mm]	L1 [mm]	L2 [mm]	L3 [mm]	w1 [mm]	w2 [mm]	I-peak 1 [W/cm^2]	I-peak 2 [W/cm^2]
15	25.4	15.62	380.0	27.2	3.49	4.87	392	201
15	40	15.39	589	43.0	3.44	7.65	403	82
15	50	15.31	733	53.7	3.42	9.57	408	52
15	60	15.26	878	64.4	3.41	11.51	411	36
20	25.4	20.84	498	26.8	4.65	4.78	221	209
20	40	20.53	772	42.2	4.58	7.52	228	84
20	50	20.42	960	52.8	4.55	9.40	231	54
20	60	20.35	1150	63.3	4.54	11.30	232	37
25.4	25.4	26.48	625.0	26.45	5.86	4.72	139	214
25.4	40	26.08	970.0	41.7	5.82	7.44	141	86
25.4	50	25.94	1205.0	52.2	5.78	9.29	143	55
25.4	60	25.85	1445.0	62.6	5.76	11.18	144	38

In the table, w_1 and w_2 show the calculated radius of the pump beam on lens f_1 and lens f_2, while I-peak$_1$ and I-peak$_2$ show the peak intensity on lens f_1 and lens f_2, respectively. The combinations with the f_1 = 25.4 mm lens had a peak intensity of ~140 W/cm^2 on the first lens, which was higher than the specification, but was deemed acceptable. Combinations with shorter focal lengths had a correspondingly higher intensity on the first lens.

The combination which was selected for the initial pump setup is marked in green in the table. It was decided to choose $f_2 = 50$ mm for the second lens, to ensure a long working distance L_3 between the second lens and the pump focus in the laser crystal, while L_2 was also a length easily manageable on the optical table.

The above-mentioned optical setup was implemented to pump the Tm:$GdVO_4$ crystal from one end only. An appropriate laser resonator was designed to ensure that the resonator mode overlapped with the pump beam inside the laser crystal as described in Section 4.4.

4.4 Resonator design

The resonator was designed with the assistance of the Paraxia Plus software, an example of which is shown in Figure 4.11. The design was based on an elementary plano-concave resonator with a plane high-reflector (HR) end-mirror, which was also coated for high transmission (HT) at the pump wavelength. The length of the resonator was approximately 26 mm which, together with the radius of curvature of the output coupler mirror, defined a fundamental laser mode size in the crystal that closely matched the pump beam size, as shown in Figure 4.12. The resonator length could be adjusted by a few millimetres under lasing conditions to compensate for the change in resonator mode size by the thermal lens generated in the laser crystal, represented as a variable thin lens in the resonator design.

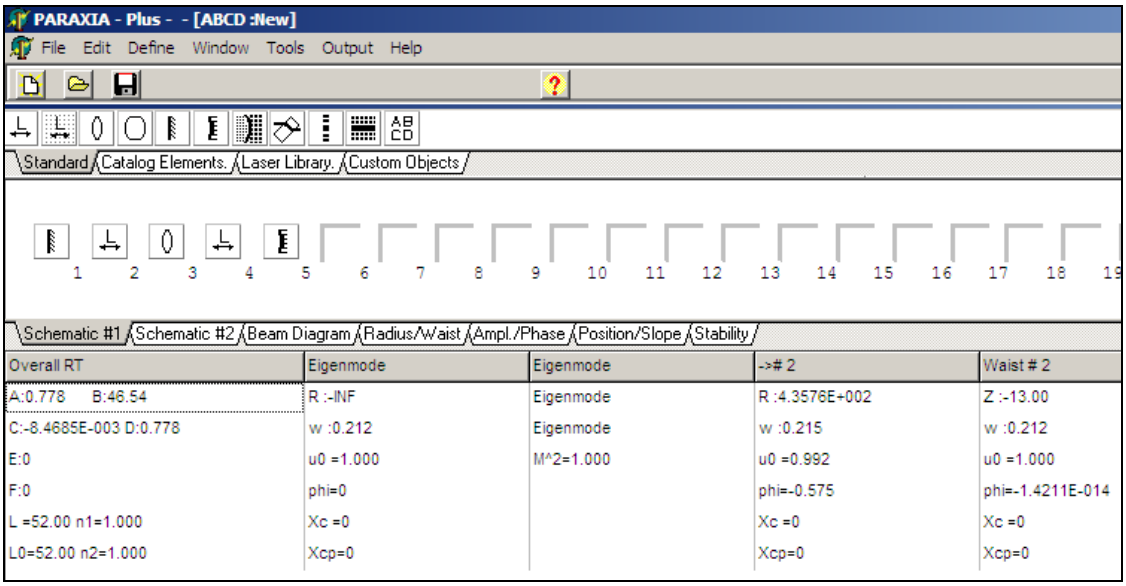

Figure 4.11: Tm:$GdVO_4$ resonator design in Paraxia Plus for a 300 mm radius of curvature output coupler mirror.

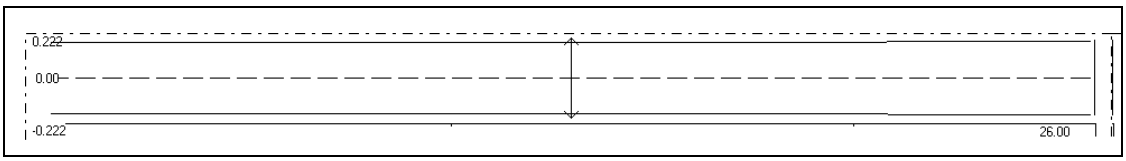

Figure 4.12: Resonator mode size of the Tm:$GdVO_4$ resonator design with a 300 mm radius of curvature output coupler mirror and a weak thermal lens.

Two output coupler mirrors were available for the experiments. The output coupler employed in the first set of experiments had 95% reflectivity at 1.9 µm with 300 mm radius of curvature. The second output coupler had 55% reflectivity at 1.9 µm dropping to 28% at 1.82 µm. The radius of curvature of the second output coupler was 250 mm.

4.5 Experimental arrangement

A schematic outlay of the experimental arrangement is shown in Figure 4.13. The opto-mechanical layout of the constructed Tm:$GdVO_4$ laser is shown in Figure 4.14 and the complete arrangement, including the pump optics, is shown in Figure 4.15.

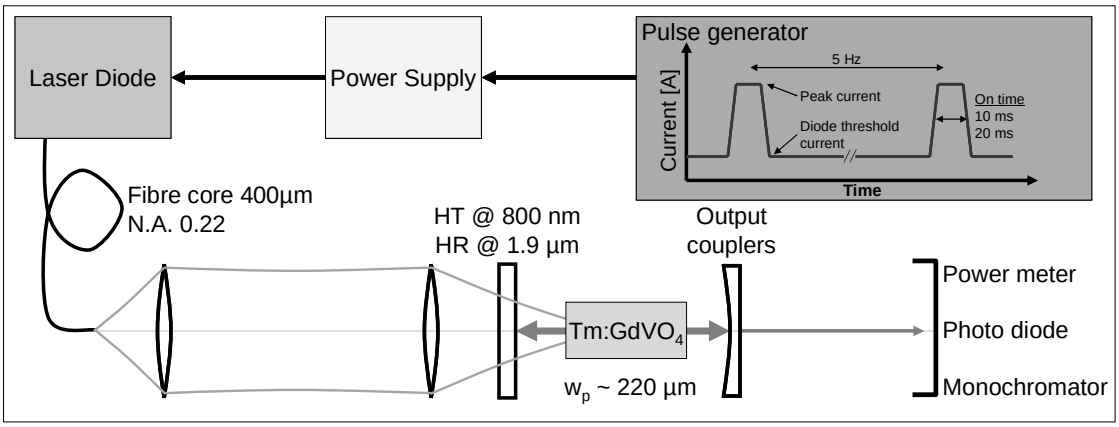

Figure 4.13: The experimental arrangement of the quasi-continuous-wave Tm:$GdVO_4$ laser.

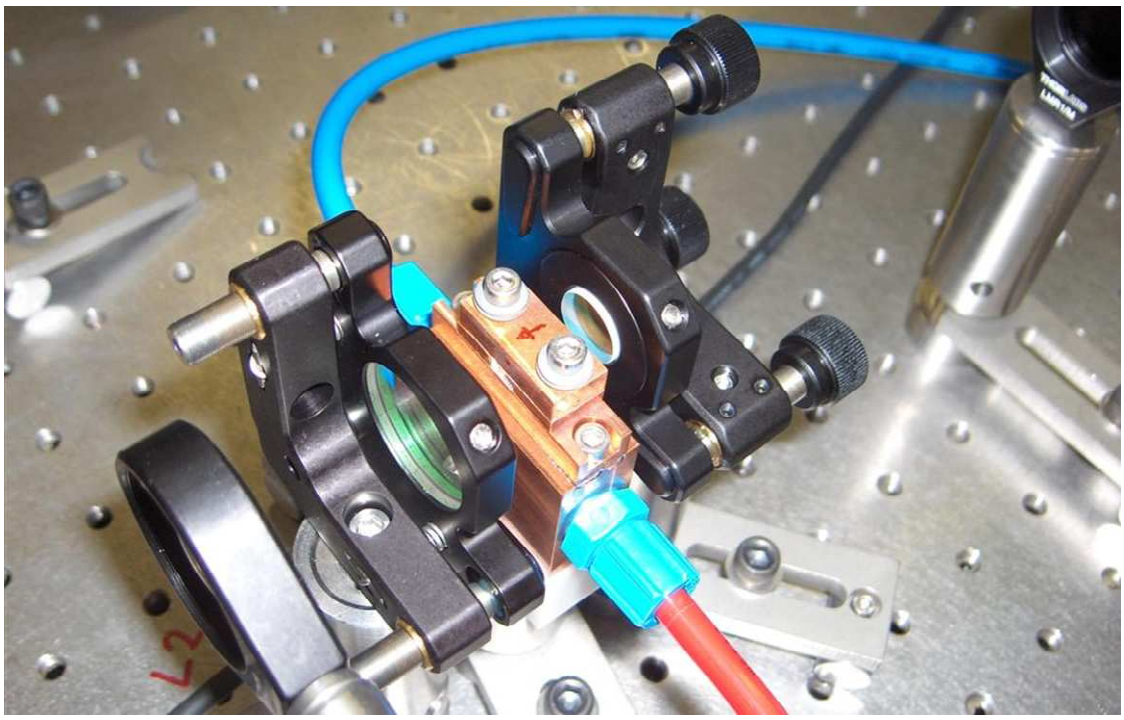

Figure 4.14: The Tm:$GdVO_4$ laser resonator. The pump radiation was incident from the left side.

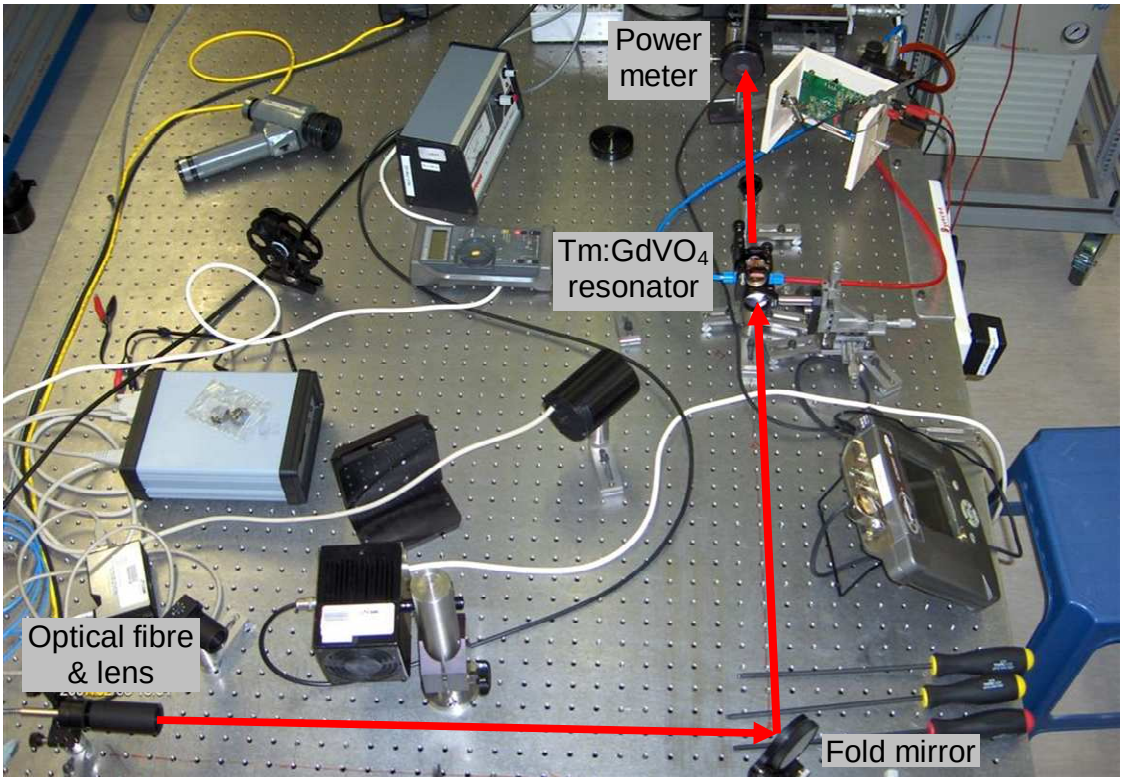

Figure 4.15: The opto-mechanical layout of the experimental Tm:$GdVO_4$ laser.

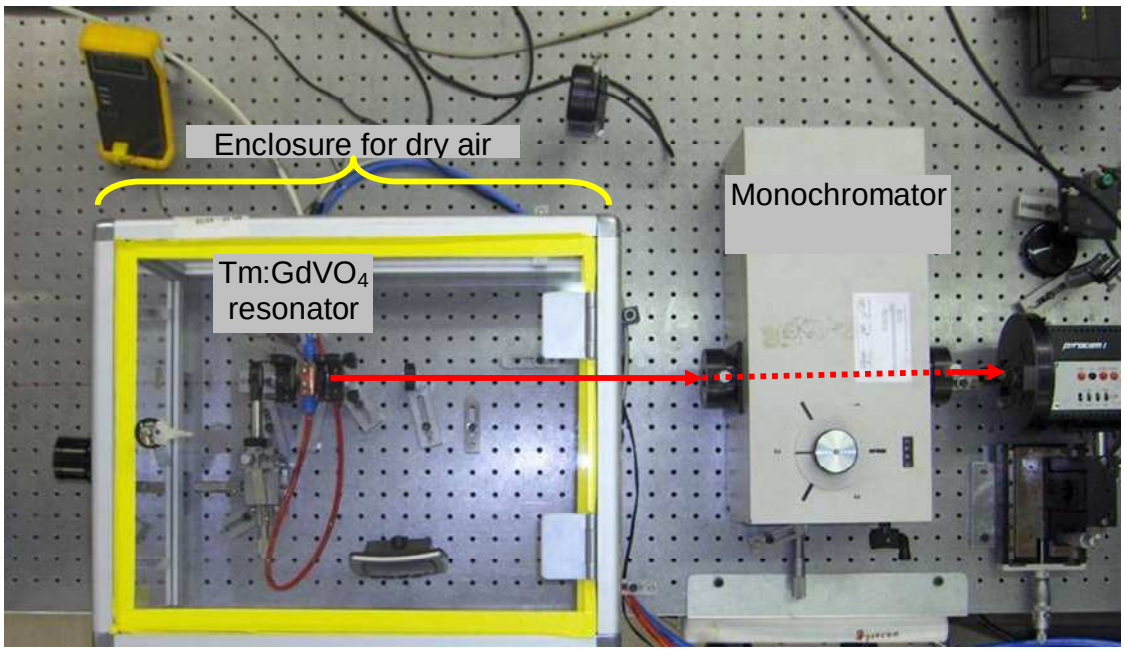

Figure 4.16: Top view of the experimental arrangement to measure the Tm:$GdVO_4$ laser wavelength.

The average pump power incident on the Tm:$GdVO_4$ laser crystal was measured with a power meter, from which the peak pump power during the on-time of the pulse was calculated using the pump duty cycle. Similarly, the average output power of the Tm:$GdVO_4$ laser was measured with a power meter, and together with a photodiode sensitive at 1.9 µm, the peak output power and energy of the QCW laser output pulse were determined. The beam profile was captured with a Pyrocam-I camera connected to a Spiricon Laser Beam Analyser. The wavelength was measured with a monochromator which has a ± 2.5 nm measurement uncertainty with the Pyrocam-I camera as detector, a photo of which is shown in Figure 4.16.

4.6 Tm:$GdVO_4$ Laser – Experimental Results

In the first set of experiments laser action was achieved with QCW pumping using the 95% reflectivity output coupler mirror for the Tm:$GdVO_4$ laser. CW lasing was also achieved but with limited success due to the onset of thermal fracture of the laser crystal. Subsequent to the first experiments, QCW lasing was also achieved with the second output coupler which had nominal 55% reflectivity. The laser wavelength, power, temporal response and beam profiles were analysed in all cases, as discussed below.

4.6.1 95% reflectivity output coupler – QCW operation

The centre wavelength of the Tm:$GdVO_4$ laser with the 95% reflectivity output coupler was measured to be 1915 nm. The laser output was polarised and it was established that the polarisation corresponded to the σ-polarisation of the Tm:$GdVO_4$ laser crystal, both of which are in agreement with the calculated predictions. The QCW laser output was observed with the 1.9 µm photo detector to follow the pump pulse, which had an on-time of 20 ms at 5 Hz repetition rate. The threshold peak pump power was measured to be 5.6 W, which corresponded to a power density of 37 W/mm^2 compared to the predicted value of 28 W/mm^2.

The graph of the Tm:$GdVO_4$ laser output power against the diode pump power incident on the crystal is shown in Figure 4.17. The maximum sustainable laser peak output power during the pulse was 8.7 W for 37.3 W of incident pump power on the laser crystal, corresponding to an output energy of 175 mJ per pulse which is plotted in Figure 4.19. Unfortunately, increasing the pump power beyond this point resulted in optical damage to the exit face of the crystal, characterised by the drop in QCW output power and output energy, at 38.6 W of incident pump power. The measured slope efficiency was 28% and the optical-to-optical efficiency was 23%.

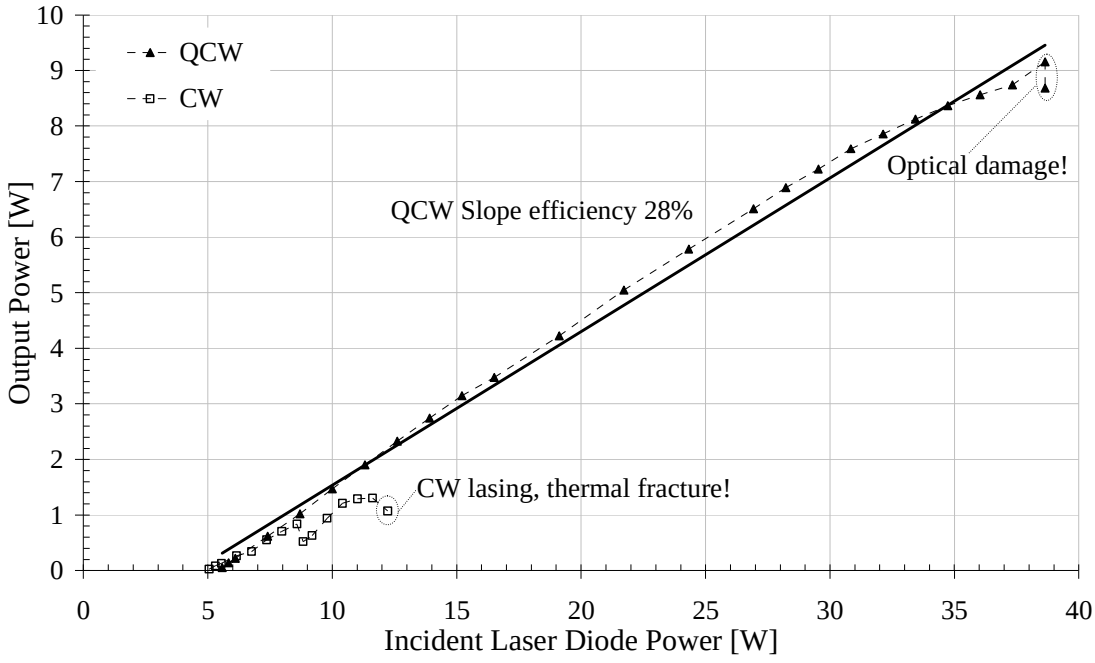

Figure 4.17: The QCW and CW output power of the Tm:$GdVO_4$ laser with the R = 95% output coupler.

The intensity beam profile was measured throughout all the experiments, which indicated a circular beam with a Gaussian intensity profile.

4.6.2 95% reflectivity output coupler – continuous wave operation

Continuous wave laser operation was also achieved with the laser-damaged crystal with the R = 95% output coupler, the result of which is shown in Figure 4.17. The crystal was moved by 0.5 mm before the CW experiments were conducted such that the damaged spot was not in the centre of the optical path.

The CW threshold power density was very similar to the QCW case, as well as the slope efficiency at pump powers below 8.6 W. Increasing the pump power further resulted in a drop in output power followed by a steep increase again. This behaviour was reproducible and could perhaps be ascribed to a strong thermal lens in the Tm:$GdVO_4$ crystal influencing the stability of the resonator. However, increasing the pump power beyond 11.6 W incident on the crystal where the CW laser produced 1.5 W, resulted in a permanent drop in output power and a sudden deterioration of the beam quality, as shown in Table 4.4. Upon visual inspection it was confirmed that this was due to thermal fracture of the laser crystal. Further analysis of the CW laser could not be conducted.

Table 4.4: Output beam profiles of the CW Tm:$GdVO_4$ laser at different input powers.

Laser diode		Tm:$GdVO_4$		Laser diode		Tm:$GdVO_4$	
current [A]	**power [W]**	**power [W]**	**Intensity beam profile**	**current [A]**	**power [W]**	**power [W]**	**Intensity beam profile**
14.0	5.5	0.15	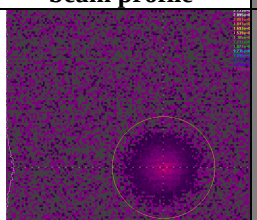	17.0	9.2	0.74	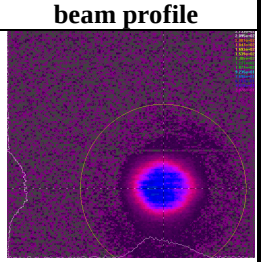
14.5	6.2	0.31	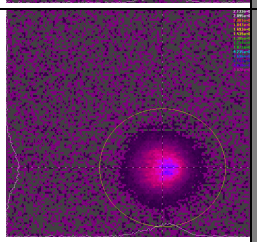	17.5	9.8	1.10	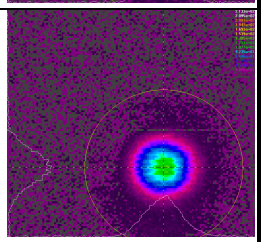
15.0	6.8	0.40	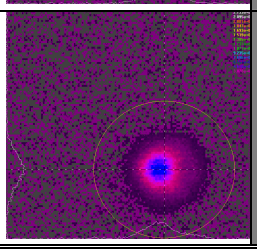	18.0	10.4	1.42	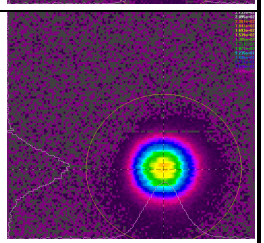

Laser diode		Tm:$GdVO_4$		Laser diode		Tm:$GdVO_4$	
current [A]	**power [W]**	**power [W]**	**Intensity beam profile**	**current [A]**	**power [W]**	**power [W]**	**Intensity beam profile**
15.5	7.4	0.65	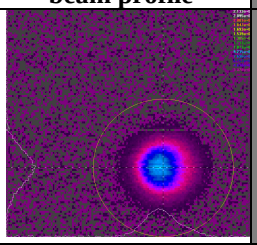	18.5	11.0	1.51	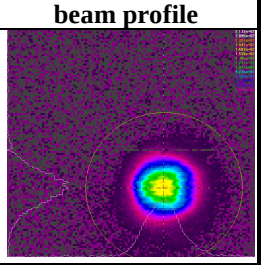
16.0	8.0	0.83	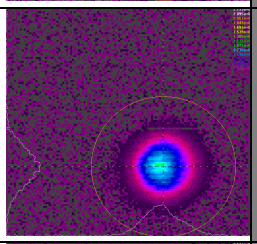	19.0	11.6	1.53	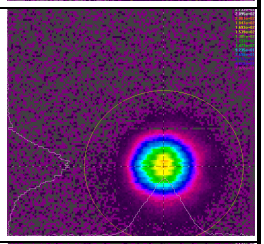
16.5	8.6	0.98	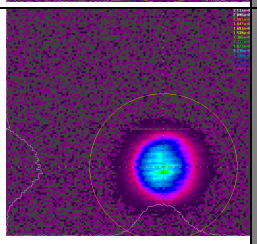	19.5	12.2	1.26	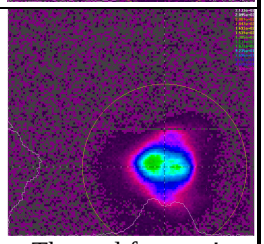 Thermal fracture!

4.6.3 28% reflectivity output coupler

In the next series of experiments only QCW operation was implemented and the output coupler with low reflectivity (55% at 1.9 µm and 28% at 1.82 µm) was used in an effort to reduce the intra-cavity power density to avoid laser-induced damage on the crystal faces. Furthermore, the on-time of the QCW pump pulse was shortened to 10 ms (5% duty cycle) to reduce the thermal load in the laser crystal. The damaged crystal was replaced with one of the other Tm:$GdVO_4$ crystals of similar doping concentration and dimensions.

The centre wavelength of the second Tm:$GdVO_4$ laser was measured to be 1818 nm whereas the threshold peak pump power was much higher, at 21.9 W, corresponding to a threshold power density of 144 W/mm^2 compared to the predicted value of 87 W/mm^2. It was also observed that the laser polarisation was perpendicular to the Tm:$GdVO_4$ laser with the 95% output coupler, therefore operating on π-polarisation.

The peak output power (energy) versus incident pump peak power (energy) of the Tm:$GdVO_4$ laser for the 95% reflectivity output coupler and 28% reflectivity output coupler for two pump pulse durations are plotted in Figure 4.18 (Figure 4.19).

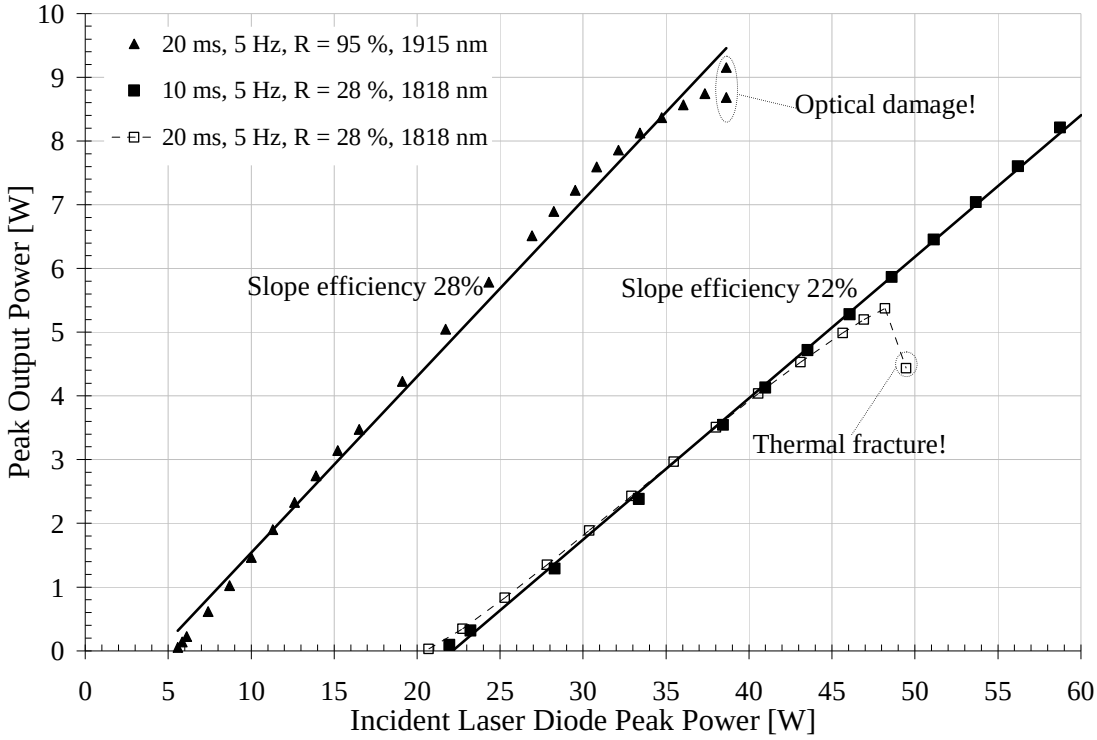

Figure 4.18: The QCW output power of the Tm:$GdVO_4$ laser with the R = 95% output coupler and with the R = 28% output coupler.

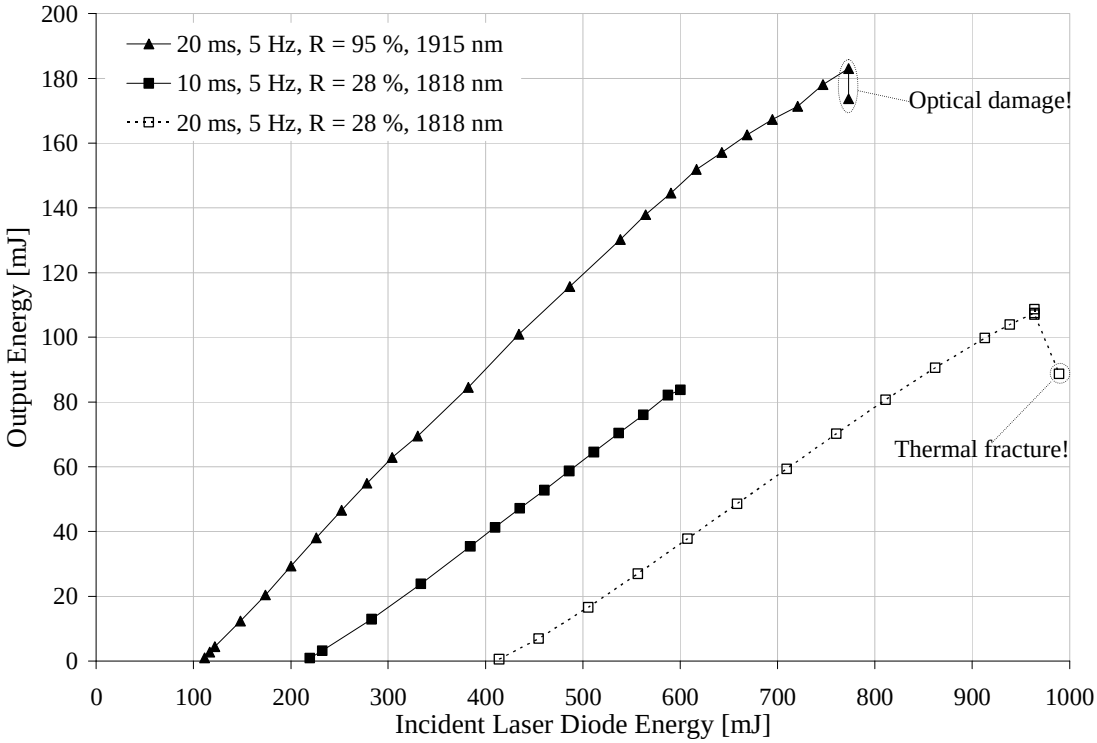

Figure 4.19: The output energy of the Tm:$GdVO_4$ laser with the R = 95% output coupler and with the R = 28% output coupler.

The maximum QCW output power of the Tm:$GdVO_4$ laser with the 28% reflectivity output coupler and 5% duty cycle was observed to be 8.4 W at full diode pump power, corresponding to 84 mJ per pulse. At this wavelength of 1818 nm, the slope efficiency was 22% and the overall laser efficiency was 14% of the incident laser diode power. With the low duty cycle of 5% on-time, the output energy was limited by the available pump energy.

The pump pulse on-time was again set to 20 ms (duty cycle of 10%) to increase the input pump energy. The maximum output energy was 104 mJ corresponding to 5.2 W peak output power at a peak incident power of 46.9 W. However, the thermal fracture limit was reached at 989 J input energy, or alternatively, 49.5 W of peak incident power due to the increased thermal load on the crystal. Up to the point of fracture, the slope efficiency was comparable to the 5% duty cycle case with no noticeable roll-off prior to thermal fracture. The peak pump power to reach laser threshold was also approximately the same for the different duty cycles, but for the 10% duty cycle, the threshold pump energy was twice that of the 5 % duty cycle case, as expected.

The temporal response and the intensity beam profile of the Tm:$GdVO_4$ laser with the 28% reflectivity output coupler are shown in Table 4.5. A quantitative measurement of the laser beam quality could not be made but the measured intensity beam profiles were used as an indication of the laser beam quality during the experiments.

Table 4.5: The peak output power, energy, temporal response and beam profile of the Tm:$GdVO_4$ laser with the R = 28% output coupler with a 10% pump duty cycle.

Peak pump power [W]	**Peak output power [W]**	**Output Energy [mJ]**	**Temporal response** Ch1: Pump pulse Ch2: Laser pulse	**Intensity beam profile**
22.7	0.35	6.92	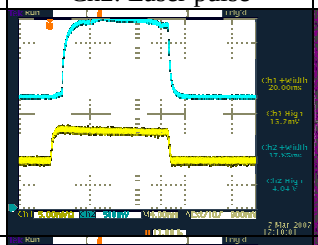	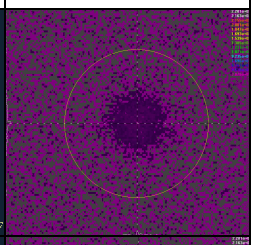
27.8	1.35	27.0	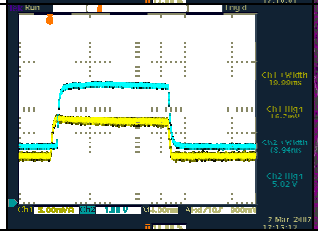	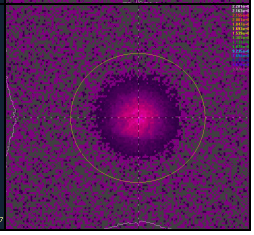

Peak pump power [W]	**Peak output power [W]**	**Output Energy [mJ]**	**Temporal response** Ch1: Pump pulse Ch2: Laser pulse	**Intensity beam profile**
30.4	1.89	37.8	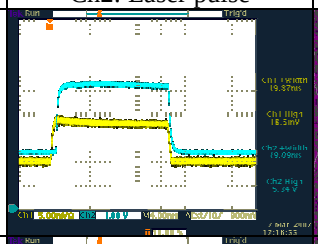	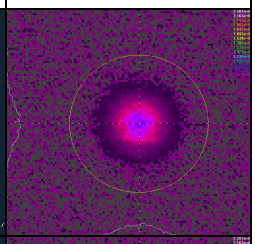
32.9	2.43	48.6	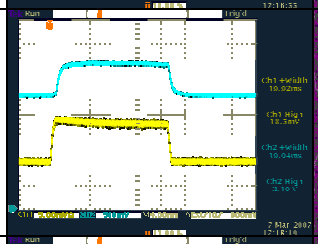	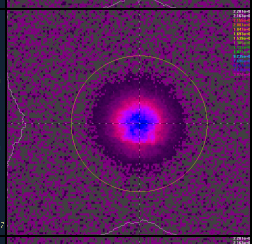
35.5	2.97	59.4	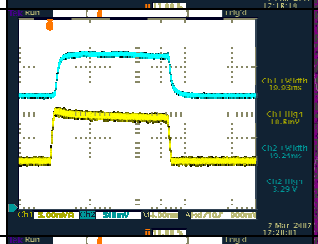	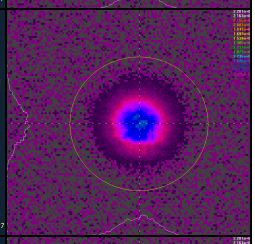
38.0	3.51	70.2		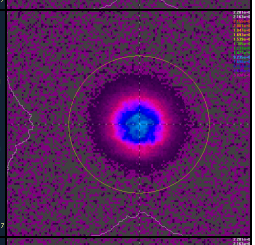
40.6	4.04	80.7	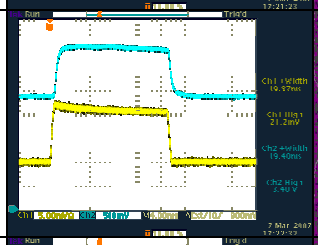	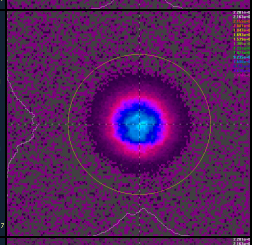
43.1	4.53	90.6	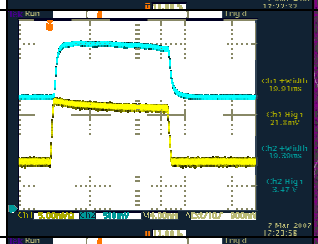	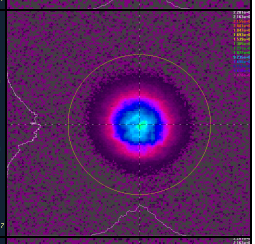
46.9	5.20	104.0		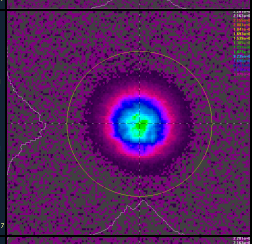
49.5	4.44	88.7 Thermal fracture!		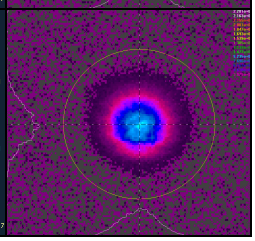

In the table it can be seen that the intensity of the laser steadily increased with increased peak pump power. Even at the point of thermal fracture, at 49.5W of peak pump power, it could not be deduced from the intensity profile that thermal damage had occurred, which was primarily indicated by the sudden drop in output energy.

From the measured temporal responses listed in the table, it was clear that the Tm:$GdVO_4$ output pulses followed the pump pulse, with approximately a 2 ms delay of the laser pulse. However, at the point of thermal fracture some instability was observed in the output temporal response, the resolution of which might be limited by the speed of the 1.9 µm photo detector.

4.7 Discussion of experimental results

4.7.1 Comparison of experimental results with theoretical predictions

The results achieved experimentally for the diode-end-pumped Tm:$GdVO_4$ laser compared well with the theoretical predictions of Section 4.1 as indicated in Figure 4.20.

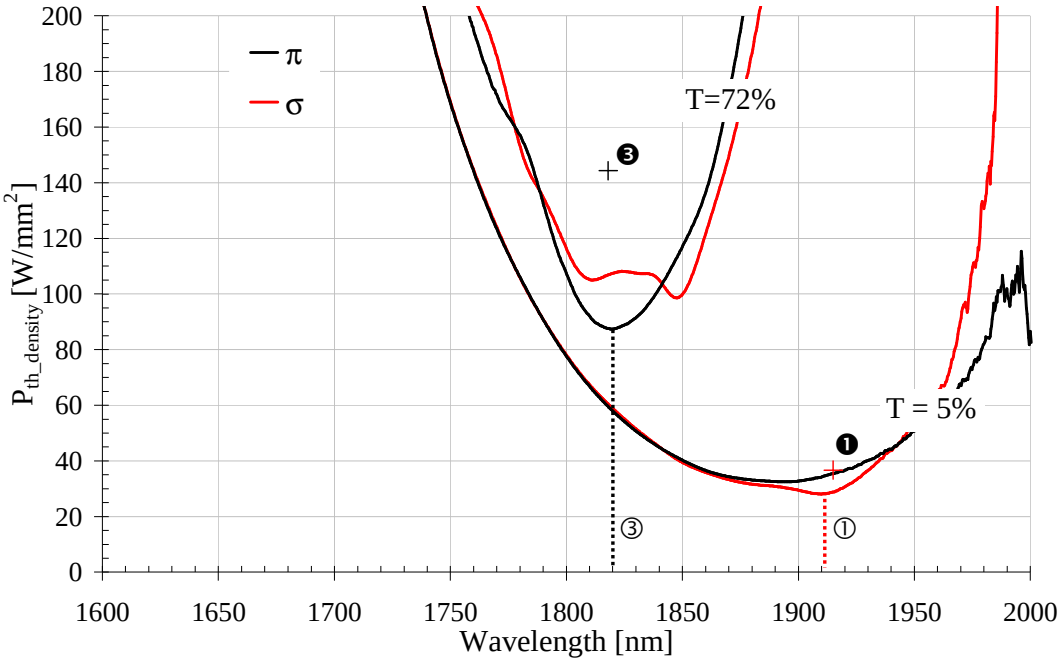

Figure 4.20: Comparison of the experimental results with theoretical predictions. The two crosses on the graph indicate the experimentally measured wavelength, polarisation and incident threshold power density of the two QCW Tm:$GdVO_4$ lasers.

The wavelength, polarisation and incident threshold power density of the QCW laser with 95% reflectivity output coupler mirror are indicated by a red cross (data point ❶) in Figure 4.20. The laser wavelength was 1915 nm on σ-polarisation which was within experimental error the same as the predicted output wavelength of 1912 nm, also on σ-polarisation. The experimental threshold of the Tm:$GdVO_4$ laser was 5.6 W of peak pump power, or alternatively, a power density of 37 W/mm^2 with a pump beam size of 220 µm. This is close to the predicted value of 28 W/mm^2. The small discrepancy between the calculated and measured threshold power density values is most probably caused by additional losses induced in the laser cavity by thermal effects in the laser crystal before threshold is reached.

The output parameters of the QCW Tm:$GdVO_4$ laser with the 28% reflectivity output coupler are indicated as a black cross (data point ❸) in Figure 4.20. The centre wavelength was 1818 nm and the threshold peak pump power was 21.9 W, corresponding to a threshold power density of 144 W/mm^2 compared to the predicted value of 87 W/mm^2. The wavelength was close to the predicted wavelength of 1820 nm and the laser was operating on π-polarisation, as predicted by theory.

The larger discrepancy between the calculated and measured threshold power density values for the laser with the 28% reflectivity output coupler is most probably caused by additional losses induced in the laser cavity by thermal effects in the laser crystal before the high threshold is reached. The higher population inversion needed to overcome the high threshold also increased the upconversion losses, which are not incorporated in the threshold calculations. The thermal lens, which is pump-power dependent, most likely also influenced the laser mode size thereby invalidating the assumption that $w_l \approx w_p \approx w$. Furthermore, the increased heat load with stronger pumping caused a higher crystal temperature which subsequently increased the quasi-three-level nature of the Tm^{3+} laser.

It was, however, concluded that the calculations did provide adequate predictions of the experimentally-observed laser wavelength and polarisation, even for the 28% reflectivity output coupler. This is an important result since it is the first time that the operational wavelength and polarisation of Tm:$GdVO_4$ lasers are correctly predicted.

4.7.2 Comparison of experimental results with literature

The experimental results were compared to the literature results for power scaling Tm:$GdVO_4$ lasers, as listed in Table 3.2 of Section 3.3.

The result of the Tm:$GdVO_4$ laser with the 95% reflectivity output coupler mirror is significant since the maximum laser peak output power of 8.7 W, or alternatively, the output energy of 175 mJ per pulse, is the highest reported output from a diode-end-pumped QCW Tm:$GdVO_4$ laser. Further power scaling was limited by the onset of optical damage of the crystal coating due to the high intra-cavity power density. The highest energy previously reported in the literature was 39 mJ from a diode-side-pumped Tm:$GdVO_4$ laser which had a very low optical-to-optical efficiency [11].

During the set of laser experiments using the output coupler with 55% reflectivity at 1.9 µm which dropped to 28% at 1.82 µm, the wavelength of the Tm:$GdVO_4$ laser was measured to be at 1818 nm on π-polarisation at a QCW output power of 8.4 W. This was the first demonstration of a multi-watt Tm:$GdVO_4$ laser operating at a central wavelength shorter than 1910 nm without the use of intra-cavity tuning elements. The shortest wavelength from a Tm:$GdVO_4$ laser reported in the literature was demonstrated using an intra-cavity birefringent plate to produce a full wavelength tuning range from 1820 – 1946 nm, but the continuous-wave power level at 1820 nm was only 0.2 W compared to 2.5 W at 1912 nm [9]. Furthermore, the 1818 nm output from the QCW Tm:$GdVO_4$ laser was also the shortest wavelength produced by any diode-pumped Tm^{3+} laser without intra-cavity tuning elements, which is an important contribution to the experimental development of diode-pumped Tm^{3+} lasers.

In continuous-wave laser operation an output power above 1.5 W could not be obtained experimentally due to thermal fracture of the Tm:$GdVO_4$ laser crystal when pumping with more than 11.6 W at 803 nm with a 220 µm radius pump beam. This experimental result is in contrast with previous literature results of CW Tm:$GdVO_4$ lasers producing up to 2.8 W with similar crystal dimensions and doping concentration which were reportedly limited only by the available pump power [e.g. 5, 8, 12]. The only major difference is that the lasers in the literature had smaller pump beam sizes, in the order of 130 – 180 µm radius. For the experimental results presented here the higher pump power required to reach laser threshold most likely produced significantly higher heat load in the crystal, which led to thermal fracture. Another

reason for the disparity might be the mechanical strength of the particular batch of crystals used during the experiments, which could not be verified to be of the highest standard. It is also very likely that the Czochralski grown crystals had some impurities which would add to excessive heat load and thermal fracture.

Since there are only limited reports of thermal fracture of Tm:$GdVO_4$ in the literature, the data obtained during the continuous-wave experiment is valuable. The second new data point for thermal fracture was obtained in QCW operation of the Tm:$GdVO_4$ laser with the 28% reflectivity output coupler. Thermal fracture occurred at 989 J input energy with a pump pulse on-time of 20 ms (duty cycle of 10%) corresponding to 49.5 W of peak incident power on the Tm:$GdVO_4$ crystal. These new results will aid in the future development of high-power diode-end-pumped Tm:$GdVO_4$ lasers.

4.8 Summary

The results of the experiments described above indicate clearly that a multi-watt diode-end-pumped Tm:$GdVO_4$ laser can be operated at 1818 nm or at 1915 nm. In order to demonstrate this, it was necessary to consider an number of important issues.

Predictions were made with quasi-three-level laser threshold calculations for the expected threshold pump power, wavelength and polarisation of the Tm:$GdVO_4$ laser with different output coupler reflectivity values. These calculations were based on detailed spectroscopic measurements of the Tm:$GdVO_4$ laser crystals, as discussed in Section 4.1. It was concluded from the calculations that for a 3 mm long, 3.0% doped Tm:$GdVO_4$ crystal pumped at 805 nm with a pump spot radius of 220 µm, lasing can be achieved with reasonable threshold pump powers. Furthermore, it was predicted that a laser with 95% reflection output coupler will lase on σ-polarisation at 1912 nm, and a laser with 28% reflection output coupler will lase on π-polarisation at 1820 nm.

A supplier of Tm:$GdVO_4$ laser crystals was identified, from whom a large number of Czochralski grown crystals were obtained with different lengths and doping concentrations. Cooling mounts were designed for these particular crystals as described in Section 4.2.1, including a mounting jig and procedure which ensured that the crystals were adequately cooled from all four sides. The laser experiments described above were performed only on 3 mm long, 2.5 x 2.5 mm^2 crystals with 3.0% Tm^{3+} doping concentration.

Fibre-coupled laser diode modules were acquired as suitable pump sources for the Tm:$GdVO_4$ laser. The modules, which could deliver up to 75 W centred at 803 nm, were operated both in CW and QCW mode, with an external pulse generator controlling the peak power during the on-time of the QCW pulse with 5% or 10% duty cycle at 5 Hz. The wavelength and output power of the laser diode modules were characterised under different experimental conditions. An optical setup was designed to focus the light from the optical fibre of one of the laser diode modules into the Tm:$GdVO_4$ laser crystal from one side only with the desired pump spot of 220 µm, as described in Section 4.3.3.

A suitable laser resonator was designed and implemented such that the resonator mode matched the pump beam size inside the laser crystal. The resonator consisted of a plane high-reflector end-mirror and a curved output coupler mirror. The length of the resonator of approximately 26 mm was adjustable by a few millimetres to compensate for resonator mode size changes due to a thermal lens generated in the laser crystal. The two output coupler mirrors that were available for the experiments either had 95% reflectivity at 1.9 µm with 300 mm radius of curvature, or had 55% reflectivity at 1.9 µm dropping to 28% at 1.82 µm with a radius of curvature of 250 mm. The experimental arrangement included a power meter, photodiode, beam profiler and a monochromator as diagnostic instruments to characterise the Tm:$GdVO_4$ laser output.

The first laser experiments were conducted in QCW mode with the 95% reflectivity output coupler. The laser wavelength was 1915 nm on σ-polarisation, which agreed very well with the predicted output. The maximum laser peak output power, prior to experiencing laser-induced damage, was 8.7 W for 37.3 W of incident pump power on the laser crystal, which was an output energy of 175 mJ per pulse. The laser slope efficiency was 28% and the optical-to-optical efficiency was 23%. This is the highest reported output energy from a diode-end-pumped QCW Tm:$GdVO_4$ laser. Continuous-wave laser operation was also achieved but were limited to 1.5 W of output power due to thermal fracture of the Tm:$GdVO_4$ laser crystal. The highest sustainable CW incident pump power was 11.6 W at 803 nm for a 220 µm pump beam radius.

During the next set of QCW laser experiments with a replacement laser crystal, the risk of laser-induced damage was reduced by using the output coupler with 55% reflectivity at 1.9 µm which dropped to 28% at 1.82 µm. Also, the thermal load in the laser crystal was reduced by initially operating the QCW laser only at 5% duty cycle at 5 Hz. With this arrangement, the wavelength of the Tm:$GdVO_4$ laser was at 1818 nm on π-polarisation, which is the shortest wavelength produced by a diode-pumped Tm^{3+} laser without intra-cavity tuning elements reported to date. The results compared well with the threshold analysis predictions for this output coupler mirror. The maximum QCW output power of the laser was 8.4 W, corresponding to 84 mJ per pulse, which was limited by the available pump energy. The slope efficiency was 22% and the overall laser efficiency was 14%. By increasing the pump duty cycle to 10%, thermal fracture was observed at 49.5 W of peak pump power, or 4.95 W average pump power incident on the Tm:$GdVO_4$ laser crystal.

It was therefore experimentally verified that a Tm:$GdVO_4$ laser can be efficiently operated with multi-watt output over a wavelength range that is suitable for pumping Ho^{3+} doped solid-state lasers. It was shown that the laser threshold analysis based on the measured spectroscopic data for Tm:$GdVO_4$ can be used with confidence to predict the threshold powers, output wavelength and polarisation of a particular laser setup.

However, it was identified that the scaling of the Tm:$GdVO_4$ laser output power is limited by thermal fracture of the available Tm:$GdVO_4$ crystals when pumped from one end only with a pump beam size of 220 µm. It was unclear why thermal fracture occurred at relatively low pump powers but possible reasons could be material quality and impurities in the laser crystals, or fundamental processes such as upconversion and cross relaxation leading to excessive heat load and thermal fracture. To scale the output further with the existing Tm:$GdVO_4$ crystals will require an alternative approach, for example pumping from both ends.

4.9 References

[1] S. A. Payne, L. L. Chase, L. K. Smith, W. L. Kway and W. F. Krupke, "Infrared cross-section measurements for crystals doped with Er^{3+}, Tm^{3+}, and Ho^{3+}," IEEE Journal of Quantum Electronics, **28**, (11) 2619 -2630 (1992).

[2] R. Lisiecki, P. Solarz, G. Dominiak-Dzik, W. Ryba-Romanowski, M. Sobczyk, P. Černý, J. Šulc, H. Jelínková, Y. Urata, and M. Higuchi, "Comparative optical study of thulium-doped YVO_4, $GdVO_4$, and $LuVO_4$ single crystals" Physical Review B **74**, 035103 (2006).

[3] T.Y. Fan, and R.L. Byer, "Modeling and CW operation of a quasi-three-level 946 nm Nd:YAG laser," IEEE Journal of Quantum Electronics, **23,** (5) 605–612 (1987).

[4] R. C. Stoneman and L. Esterowitz, "Efficient 1.94-μm Tm:YALO laser," IEEE Journal of Selected Topics in Quantum Electronics, **1,** (1) 78-81 (1995).

[5] J. Šulc, P. Koranda, P. Černý, H. Jelínková, Y. Urata, M. Higuchic, W. Ryba-Romanowski, R. Lisiecki, P. Solarz, G. Dominiak-Dzik, and M. Sobczyk, "Tunable lasers based on diode pumped Tm-doped vanadates Tm:YVO_4, Tm:$GdVO_4$, and Tm:$LuVO_4$," in *Solid State Lasers XVII: Technology and Devices*, W. A. Clarkson, N. Hodgson, and R. K. Shori, eds., Proceedings of SPIE **6871**, 68711V (2008).

[6] A.A. Lagatsky, N.V. Kuleshov, and V.P. Mikhailov, "Diode-pumped CW lasing of Yb:KYW and Yb:KGW," Optics Communications **165**, 71–75 (1999).

[7] Y. Li, B. Yao, and Y. Wang, "Diode-pumped CW Tm:$GdVO_4$ laser at 1.9 μm," Chinese Optics Letters **4**, (3), 175-176 (March 2006).

[8] Y. Li, B. Yao, Y. Liu, Y. Wang, Y-L. Ju "Widely Tunable cw Diode-Pumped 1.9-um Tm:$GdVO_4$ Laser at Room Temperature," Chinese Physics Letters **24**, (3), 724 (2007).

[9] Y. F. Li, Y. Z. Wang, and B. Q. Yao, “Comparative optical study of thulium-doped $YAlO_3$ and $GdVO_4$ single crystals,” Laser Physics Letters **5**, (1), 37–40, (2008).

[10] C. Bollig, C. Jacobs, M. J. D. Esser, and H. M. von Bergmann “Power and energy scaling of a diode-end-pumped Nd:YLF laser through gain optimization” *Optics Express* **18** (13), 13993-14003 (Jun 2010).

[11] A. Sato, K. Asai, S. Ishii, K. Mizutani, and T. Itabe, “Characteristics of pulsed / cw vanadate lasers operating at 2 μm,” Proceedings of SPIE **6409** 640916 (December 2006).

[12] P. Černý, J. Oswald, J. Šulc, H. Jelínková, Y. Urata, and M. Higuchi, “Multi-watt and Tunable Diode-Pumped Operation of Tm:$GdVO_4$ Crystal Grown by a Floating Zone Method” Advanced Solid-State Photonics (ASSP), TuB6, (2006).

Appendix: Dimensions of the Tm:$GdVO_4$ laser crystals and cooling mounts

Table 4.6: Dimensions of the Tm:$GdVO_4$ laser crystals and cooling mounts.

Tm:$GdVO_4$		Dimensions [mm]					Mounts		
Serial number	Doping	X	Y	a-c	b-d	Z	Height [mm]	Qty	
06-1516-h-1	3.0%	2.5	2.5	2.512	2.510	2	2.515	3	6
06-1516-h-2	3.0%	2.5	2.5	2.515	2.505	2			
06-1516-h-3	3.0%	2.5	2.5	2.518	2.508	2			
06-1516-h-4	3.0%	2.5	2.5	2.514	2.512	2			
06-1516-g-1	3.0%	2.5	2.5	2.511	2.511	3			
06-1516-g-2	3.0%	2.5	2.5	2.515	2.511	3			
06-1516-g-3	3.0%	2.5	2.5	2.511	2.511	3			
06-1516-g-4	3.0%	2.5	2.5	2.519	2.506	3			
06-1516-g-5	3.0%	2.5	2.5	2.519	2.510	3			
06-1516-f-1	3.0%	2.5	2.5	2.520	2.515	4	2.520	3	
06-1516-f-2	3.0%	2.5	2.5	2.520	2.515	4			
06-1516-f-3	3.0%	2.5	2.5	2.520	2.515	4			
06-1516-f-4	3.0%	2.5	2.5	2.520	2.512	4			
06-1516-f-5	3.0%	2.5	2.5	2.520	2.511	4			
06-1516-f-6	3.0%	2.5	2.5	2.520	2.511	4			
06-1516-f-7	3.0%	2.5	2.5	2.520	2.511	4			
06-1516-e-1	3.0%	2.5	2.5	2.520	2.515	5			
06-1516-e-2	3.0%	2.5	2.5	2.520	2.519	5			
06-1516-d-1	3.0%	4	4	4.000	4.000	10	4.010	1	4
06-1516-d-2	3.0%	4	4	4.000	4.000	10			
06-1516-d-3	3.0%	4	4	4.010	3.990	10			
06-1516-c-1	3.0%	4	4	4.010	3.991	10			
06-1516-c-2	3.0%	4	4	4.000	4.000	10			
06-1516-c-3	3.0%	4	4	4.010	3.991	10			
06-1516-b-1	2.5%	4	4	4.000	4.010	10	4.110	2	
06-1516-b-2	2.5%	4	4	4.010	4.011	10			
06-1516-b-3	2.5%	4	4	4.000	4.010	10			
06-1516-a-1	2.0%	4	4	4.050	4.050	10			
06-1516-a-2	2.0%	4	4	4.200	4.160	10	4.200	1	

The four sides of each crystal were labelled a, b, c, and d, and the measurements were made at three points along the length of each crystal between sides a-c, and between sides b-d. The width & height dimensions of the 2.5 x 2.5 x 2 mm^3 and 2.5 x 2.5 x 3 mm^3 crystals did not vary significantly, and it was decided to produce three mounts for these types of crystals with a height of 2.515 mm. Furthermore, the height chosen for the 2.5 x 2.5 x 4 mm^3 and 2.5 x 2.5 x 5 mm^3 crystals was 2.520 mm, of which also three mounts were made. The 4 x 4 mm^2 crystals all had a length of 10 mm but had Tm^{3+} doping concentrations of 2.0%, 2.5% and 3.0%, for which one mount was made with height 4.010 mm, two of height 4.110 mm, and one of height 4.200 mm to accommodate the variance in crystal dimensions. A total of 10 mounts were therefore made, six for the 2.5 x 2.5 mm^2 cross section crystals, and four for the 4 x 4 mm^2 cross section crystals.

Chapter 5

$Tm:GdVO_4$ laser as pump source for Ho:YLF

In the previous chapters it was argued that a $Tm:GdVO_4$ laser can be used to pump a Ho^{3+} laser at 1.9 µm. The experimental results of the diode-end-pumped $Tm:GdVO_4$ laser confirmed that the output wavelength of this laser could be chosen to lie between 1818 nm and 1910 nm by selecting the appropriate output coupler mirror, as calculated from thee-level laser threshold analyses.

A number of additional laser configurations were experimentally evaluated in an effort to further increase the output power of the $Tm:GdVO_4$ laser. This included an investigation of the influence of the resonator mode size, pump beam size, different crystal lengths and dual end-pumping on the $Tm:GdVO_4$ laser output power and wavelength. However, the previous result of the single-end-pumped $Tm:GdVO_4$ laser as presented in Chapter 4 was the highest quasi-continuous-wave power obtained from a diode-end-pumped $Tm:GdVO_4$ laser. Subsequent to these additional laser experiments, a $Tm:GdVO_4$ laser was specifically designed and constructed as the pump source for a Ho:YLF laser on one of its absorption peaks located at 1892 nm as will be described in this chapter.

5.1 Ho:YLF absorption spectra

To select the appropriate wavelength for the diode-pumped $Tm:GdVO_4$ laser for pumping a Ho:YLF laser, an analysis of the spectroscopic data of Ho:YLF was required. The absorption cross section data (σ_{abs}) of Ho:YLF for the $^5I_8 - {}^5I_7$ transition is shown in Figure 5.1 [1].

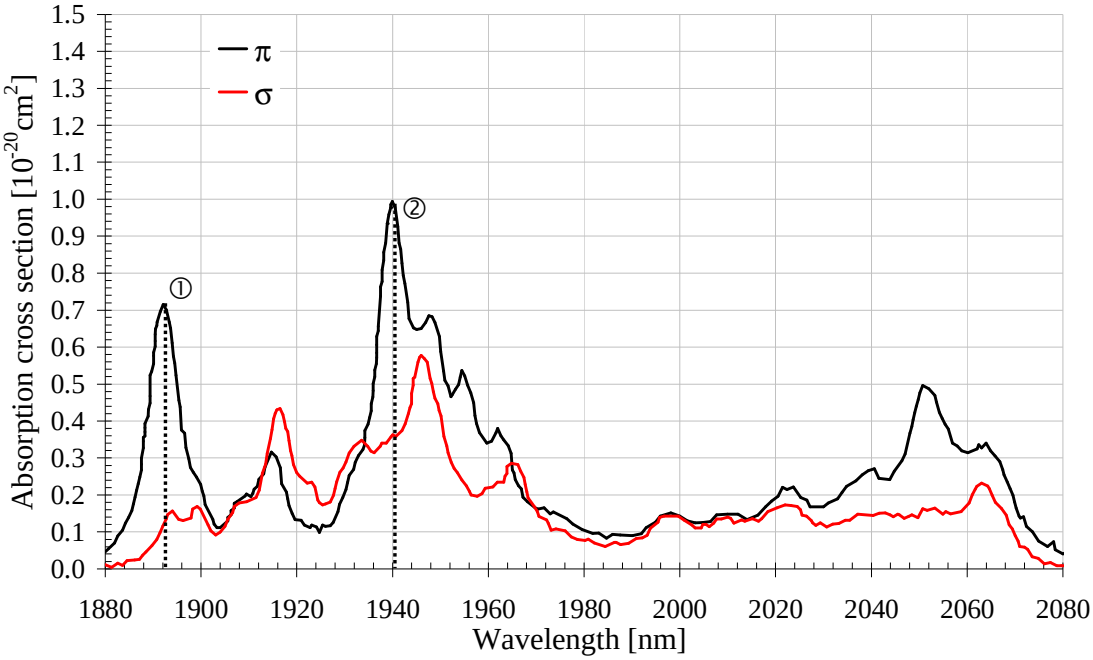

Figure 5.1: The measured absorption cross sections of Ho:YLF for π-polarised and σ-polarised light between 1880 nm and 2080 nm [1].

The Ho:YLF absorption in the wavelength range from 1.880 µm to 1.980 µm is polarised and it would be highly preferential to pump on either of the two absorption peaks of the π-polarisation (***E***||*c*), located at 1892 nm (0.72×10^{-20} cm^2), and at 1940 nm (0.99×10^{-20} cm^2), as indicated by the dotted lines ① and ② respectively in Figure 5.1

Since the demonstrated Tm:$GdVO_4$ output wavelengths reported in Chapter 4 were observed to lie between 1818 nm and 1910 nm, it is apparent that the 1892 nm absorption peak could be used as pump wavelength for Ho:YLF. It is furthermore concluded that the linearly polarised Tm:$GdVO_4$ laser output can be utilised effectively by orientating it along the π-polarisation of Ho:YLF to ensure efficient absorption of the pump light.

5.2 Selection of the Tm:$GdVO_4$ output wavelength

The threshold analysis on Tm:$GdVO_4$ presented in Chapter 4 was subsequently revisited to establish the optimum output coupling and desired laser polarisation of the Tm:$GdVO_4$ laser to provide the optimum conditions for pumping the 1892 nm transition in Ho:YLF.

It was determined through these subsequent calculations that by selecting an output coupler transmission T = 5% (reflectivity 95%), the Tm:$GdVO_4$ laser will naturally oscillate the on σ-polarisation, and that the oscillation wavelength will be approximately 1910 nm as indicated by the red dotted line ❶ in Figure 5.2. However, this is not the desired optimum wavelength to pump the Ho:YLF laser.

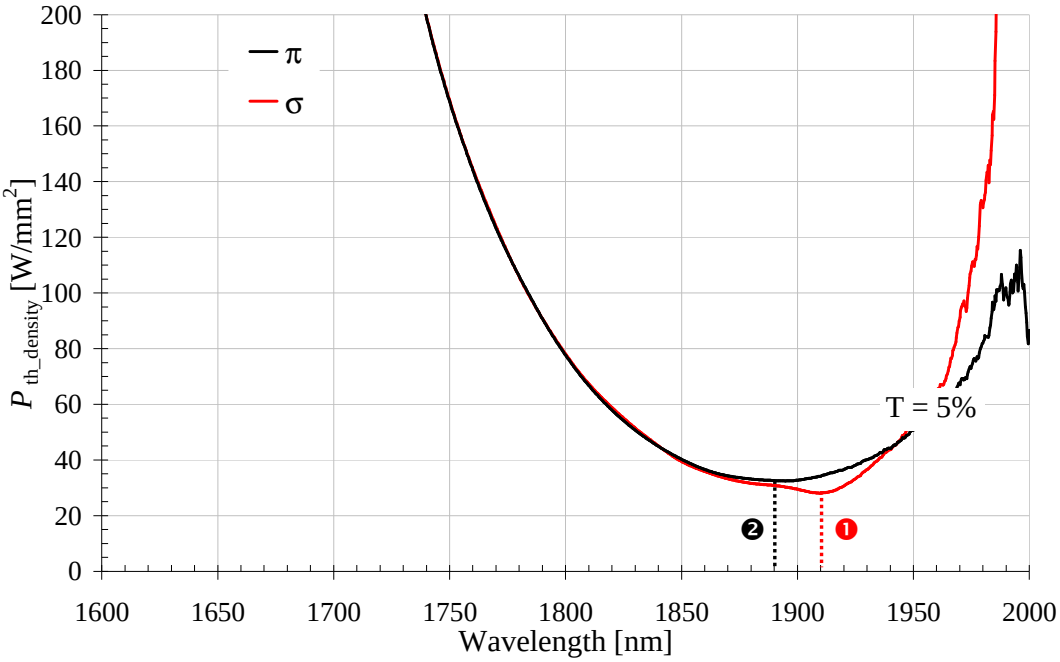

Figure 5.2: Calculated threshold power density of a Tm:$GdVO_4$ laser with a 5% transmission output coupler.

Nevertheless, the Tm:$GdVO_4$ laser oscillation wavelength can be changed to a value of approximately 1890 nm by inserting a Brewster plate inside the laser resonator to force oscillation on the π-polarisation, as indicated in Figure 5.2 by the black dotted line ❷. Furthermore, if an uncoated fused-silica etalon of thickness 100 µm is inserted within the Tm:$GdVO_4$ laser resonator operating on π-polarisation, the output wavelength of the Tm:$GdVO_4$ laser can be fine-tuned onto the absorption peak of Ho:YLF at 1892 nm.

The conceptual design of the corresponding Tm:$GdVO_4$ laser with an intra-cavity Brewster plate, as well as a tuneable etalon, is shown in Figure 5.3.

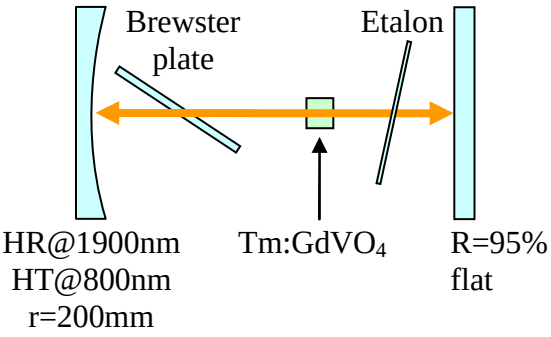

Figure 5.3: Conceptual design of the Tm:$GdVO_4$ laser with a 95% reflectivity output coupler, Brewster plate and etalon to select the output wavelength 1892 nm.

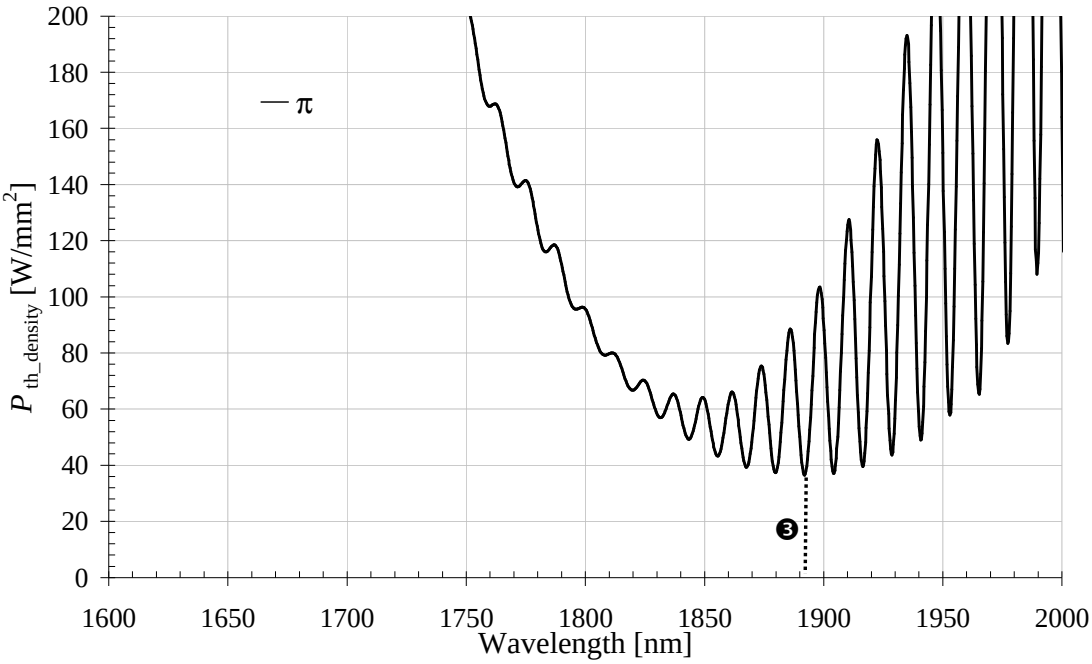

Figure 5.4: The threshold power density required to operate the Tm:$GdVO_4$ laser with a R95% output coupler, Brewster plate and 100 µm etalon, at a wavelength of 1892 nm.

The etalon loss was included in the laser threshold density calculations for the Tm:$GdVO_4$ laser with a 95% reflectivity output mirror and the Brewster plate, the result of which is shown in Figure 5.4. It is clear from this analysis that the minimum threshold will be at 1892 nm as indicated by the dotted line ❸, such that the Tm:$GdVO_4$ can be used to pump a Ho:YLF laser. Furthermore, by adjusting the etalon tilt inside the laser cavity while operating the Tm:$GdVO_4$ laser, it is possible to slightly adjust the output wavelength to ensure maximum absorption of the pump light in the Ho:YLF laser crystal.

It was concluded that according to the laser threshold calculations the wavelength of the Tm:$GdVO_4$ laser can be selected to optimally pump a Ho:YLF laser. However, the

practical challenge to ensure reliable operation of the Tm:$GdVO_4$ laser with a 95% reflectivity output coupler mirror without inducing optical damage or thermal fracture needed to be evaluated, as discussed in the next section.

5.3 The dual-end-pumped Tm:$GdVO_4$ laser as pump for the Ho:YLF laser

The new Tm:$GdVO_4$ laser design incorporated a number of key improvements identified during the first Tm:$GdVO_4$ laser experiments. A dual-end-pump geometry was implemented with a slightly larger pump beam radius as compared to the original design. Furthermore, a laser resonator was implemented which could accommodate a strongly varying thermal lens, and, from the available selection of crystals, a 3 mm long Tm:$GdVO_4$ crystal was chosen for the laser to pump the Ho:YLF laser. These aspects are discussed below.

5.3.1 Pumping from both ends

A dual-end-pump approach was implemented with two of the Jenoptik laser diode modules in order to increase the available pump power. Furthermore, it was shown in the literature that a dual-end-pump design could result in a lower laser threshold as compared to a single-end-pumped arrangement for the same pump beam size [2], as was discussed in Chapter 3. The optical layout of the dual-end-pumped laser design is shown in Figure 5.5 and a photo of the arrangement is shown in Figure 5.6.

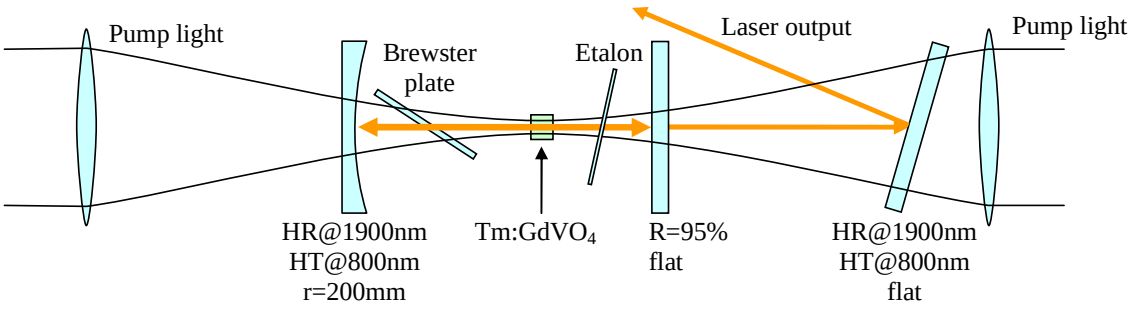

Figure 5.5: Schematic of the dual-end-pumped Tm:$GdVO_4$ laser, including a Brewster plate and etalon to operate at 1892nm.

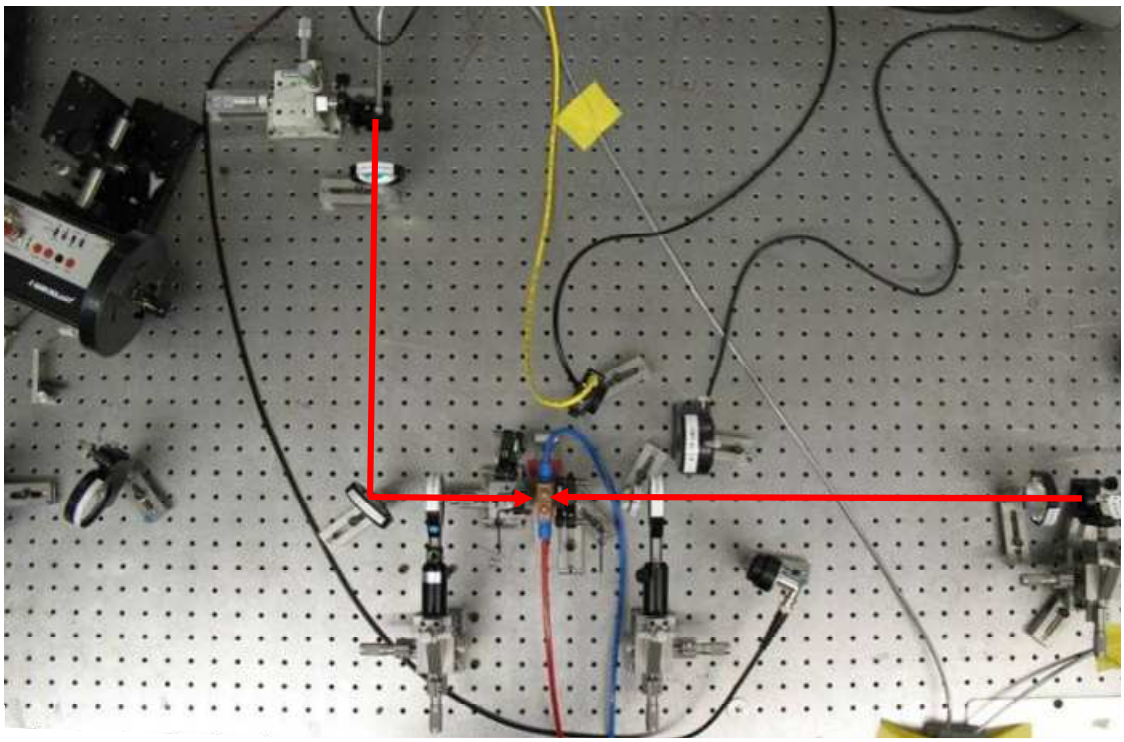

Figure 5.6: Top-view of the dual-end-pumped Tm:$GdVO_4$ laser.

The main concept of the pump arrangement operated in QCW mode, remained the same as in the first laser, except that it was set up with two fibre-coupled laser diode modules pumping the laser crystal from each end. Care was taken to ensure that the two pump beam foci overlapped exactly in the position of the laser crystal, and that they were co-linear with the optical axis of the laser resonator.

5.3.2 Combined pump power

The QCW pump power incident from each laser diode onto the Tm:$GdVO_4$ laser crystal was measured for the case of operating at 5 Hz and 20 ms on-time (10% duty cycle), as shown in Figure 5.7. The calculated energy from the left and right, as well as the total incident energy, are shown in Figure 5.8.

The pump light incident from the left had only minor reflection losses as it propagated from the fibre output to the Tm:$GdVO_4$ laser crystal. In contrast, the pump light incident from the right had high reflection losses due to the optical layout of the dual-end-pumped design, as it is shown in Figure 5.5. In this arrangement the pump light propagating from the right passed through the resonator output coupler mirror which was not specified at the 0.8 µm pump wavelength, resulting in a measured 54% lower incident energy on the crystal from the right, as compared to the energy incident from the left. It was in practice not feasible to produce equal energy values incident on the

$Tm:GdVO_4$ crystal from each end because the two pump laser diodes were simultaneously powered from a single power supply which was slaved to the QCW pulse generator.

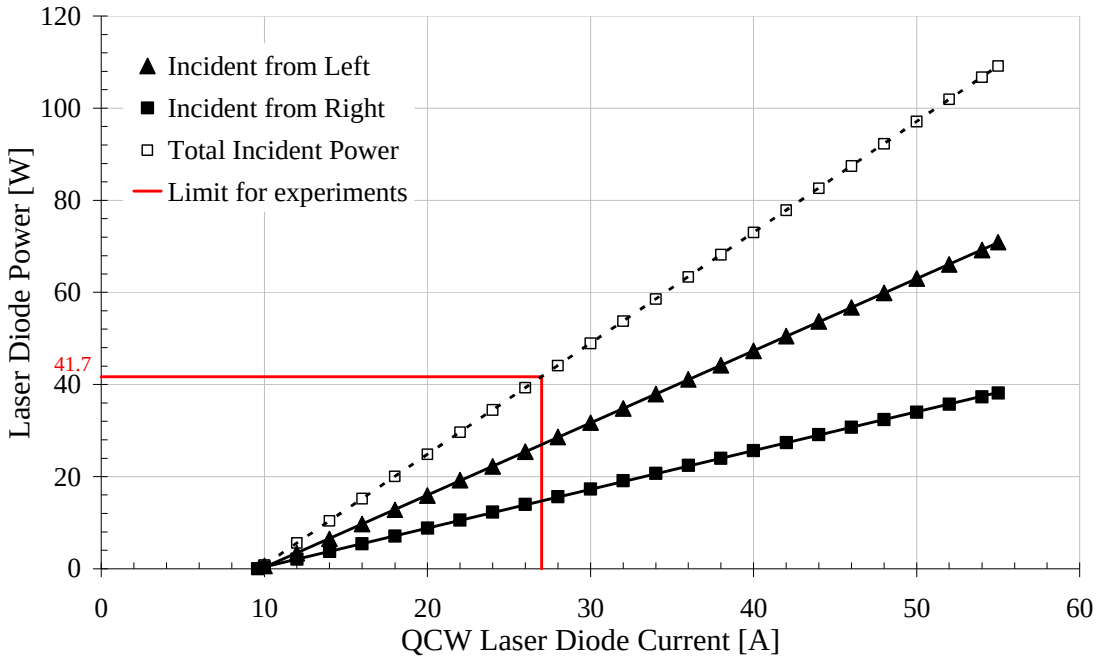

Figure 5.7: Laser diode QCW pump power incident from the left and right onto the $Tm:GdVO_4$ laser crystal. The total incident peak (average) power was limited to 41.7 W (4.17 W) to avoid crystal damage.

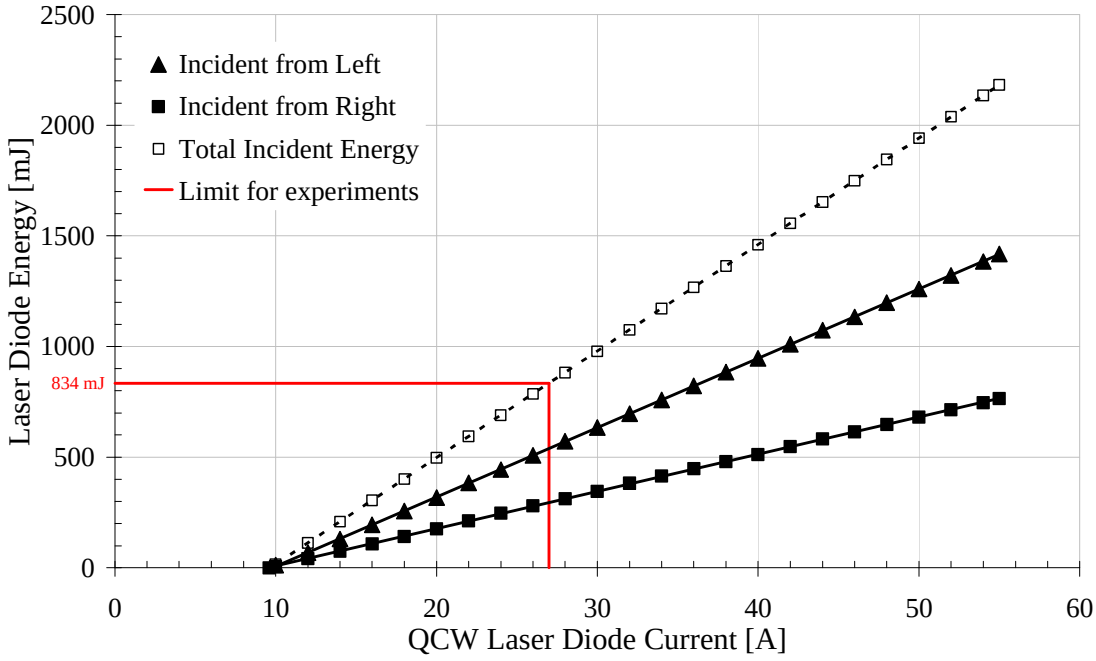

Figure 5.8: Laser diode pump energy incident from the left and right onto the $Tm:GdVO_4$ laser crystal. The total incident energy was limited to 834 mJ to avoid crystal damage.

Even though more than 100 W QCW power and 2 J of total energy was available from the laser diodes when operated at maximum drive current during the 20 ms on-time of the QCW pulse (and significantly more energy if the on-time was longer), the total incident energy was deliberately limited to 834 mJ, or alternatively, 41.7 W of peak power during the 20 ms pump pulse to reduce the risk of laser induced optical damage, which was observed in the single-end-pumped laser to occur at 180 mJ output energy. Furthermore, the pump energy was kept well below the thermal fracture limit of the Tm:$GdVO_4$ crystal, which was estimated to be 960 mJ for the single-end-pumped configuration with 220 µm pump beam radius. This is further discussed in Section 5.5 below.

5.3.3 Pump beam size

In an initial set of experiments it was determined that a large pump beam radius of 330 µm resulted in very poor laser efficiency due to an increased laser threshold power. The stronger thermal lens associated with the higher pump power also resulted in higher resonator losses and even caused several crystals to fracture at moderate output powers.

It was subsequently decided during the the new Tm:$GdVO_4$ laser design that a pump beam radius of 265 µm should be utilised, compared to the original value of 220 µm in the single-end-pump design. The rationale was that the larger pump beam, and the correspondingly larger resonator mode size, will result in lower intra-cavity power densities to avoid laser-induced damage, as experienced in the first Tm:$GdVO_4$ laser which utilised a 95% reflectivity output coupler mirror.

Table 5.1: Calculated threshold powers of a Tm:$GdVO_4$ laser based on a 3 mm long, 3.0% doped crystal with a 95% output coupler mirror.

Pump beam	Calculated threshold [W] σ-polarisation	π-polarisation	Observation
220 µm	4.3	4.9	Laser damage on coatings
265 µm	5.8	6.7	-
330 µm	9.6	11.1	Crystal fracture

The calculated pump power required for obtaining laser threshold for the three different pump beam sizes are shown in Table 5.1 using the same method and data as previously presented in Chapter 4. For this calculation the threshold power density for a Tm:$GdVO_4$ laser based on a 3 mm long, 3.0% doped crystal with a 95% output coupler mirror operating on σ-polarisation was again taken as 28 W/mm^2, and for π-

polarisation it was 32 W/mm^2. The chosen pump beam radius of 265 µm implemented in the final Tm:$GdVO_4$ laser to pump the Ho:YLF laser was considered a good compromise between the original 220 µm radius and the tested 330 µm radius.

5.3.4 Tm:$GdVO_4$ resonator design

A flexible laser resonator design was implemented where the positions of the laser mirrors were changed in a controlled manner with respect to each other and with respect to the crystal position using micrometer-controlled translation stages, a photo of which is shown in Figure 5.9.

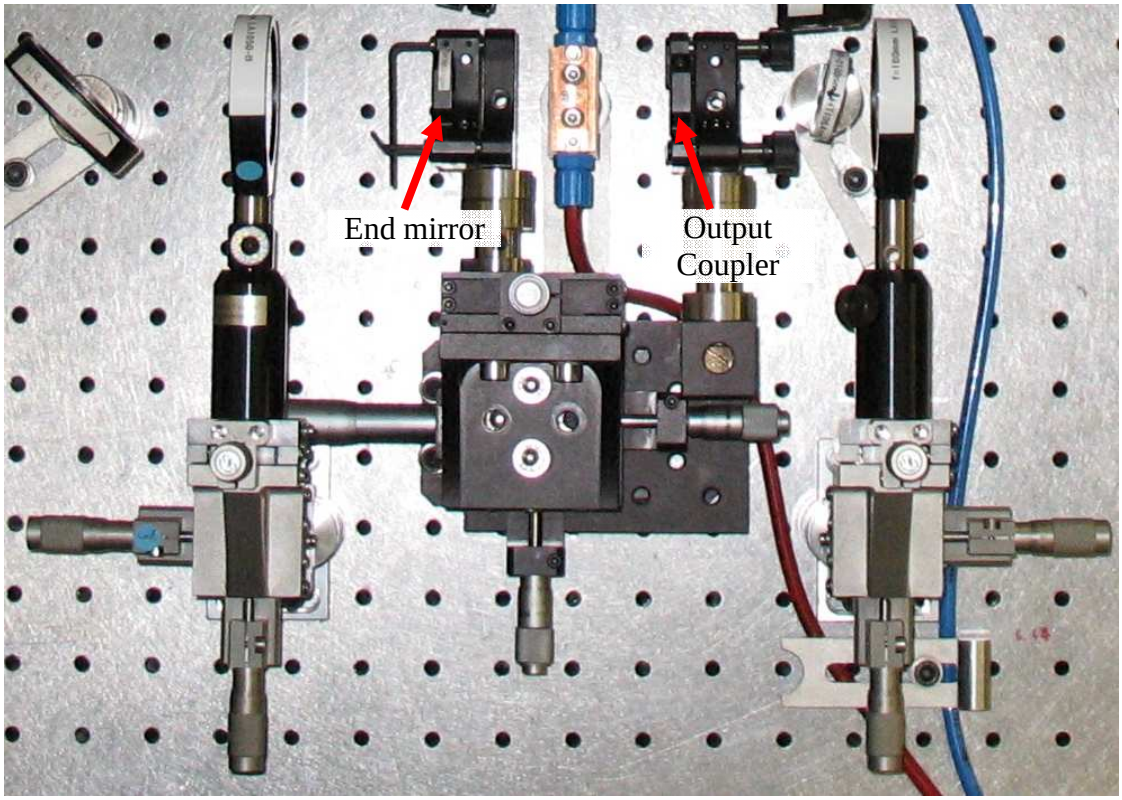

Figure 5.9: Top-view photo of the Tm:$GdVO_4$ laser resonator with adjustable resonator length and mirror positions.

The above-mentioned laser design was introduced because it had been found that the thermal lens generated inside the resonator varied significantly during the on-time of the QCW pump pulse, and that this induced major detrimental effects on the resonator stability and efficiency.

In order to address this issue, resonator mode size calculations were performed for strongly varying thermal lenses inside the laser cavity. Both in the calculations and during the experimental verification it was found that if the laser crystal, and hence the thermal lens, was placed in a specific (optimum) position within the resonator, that the

laser performance remained stable over a very large range of thermal lens strengths. In such a configuration the laser could therefore accommodate the time-varying thermal lens associated with a QCW pump pulse.

After performing resonator calculations, the optimum resonator length, mirror radii and mirror positions were confirmed experimentally. The optimum distance from the curved high-reflective mirror to the centre of the crystal was 40 mm, and 33 mm from the centre of the crystal to the flat output coupler mirror, resulting in a total optical resonator length of 73 mm. The experimental criterion for determining these values was observation of the maximum energy output of the Tm:$GdVO_4$ laser for a given pump energy. A plane output coupler with 95% reflectivity at 1900-2100 nm and a curved high-reflector mirror with radius of curvature r = 200 mm were used in the Tm:$GdVO_4$ laser which operated at 1892 nm.

5.3.5 Crystal length

During the experimental evaluation of different laser configurations with the pump beam size set to 330 µm, a selection of 3% Tm^{3+} doped crystals was used which had lengths 2 mm, 3 mm, 4 mm and 10 mm. It was found that the Tm:$GdVO_4$ laser with 2 mm long crystal had inferior performance compared to that of the 3 mm crystal, due to the lower total absorption of pump light. The 4 mm crystals suffered from thermal fracture, while lasing could not be achieved with the 10 mm long Tm:$GdVO_4$ laser crystals. It was therefore decided to use the 3 mm long crystals for the Tm:$GdVO_4$ laser to pump the Ho:YLF laser.

5.3.6 Diagnostic equipment

The diagnostic arrangement used to monitor the performance of the new dual-end-pumped Tm:$GdVO_4$ laser is shown in Figure 5.10 and Figure 5.11.

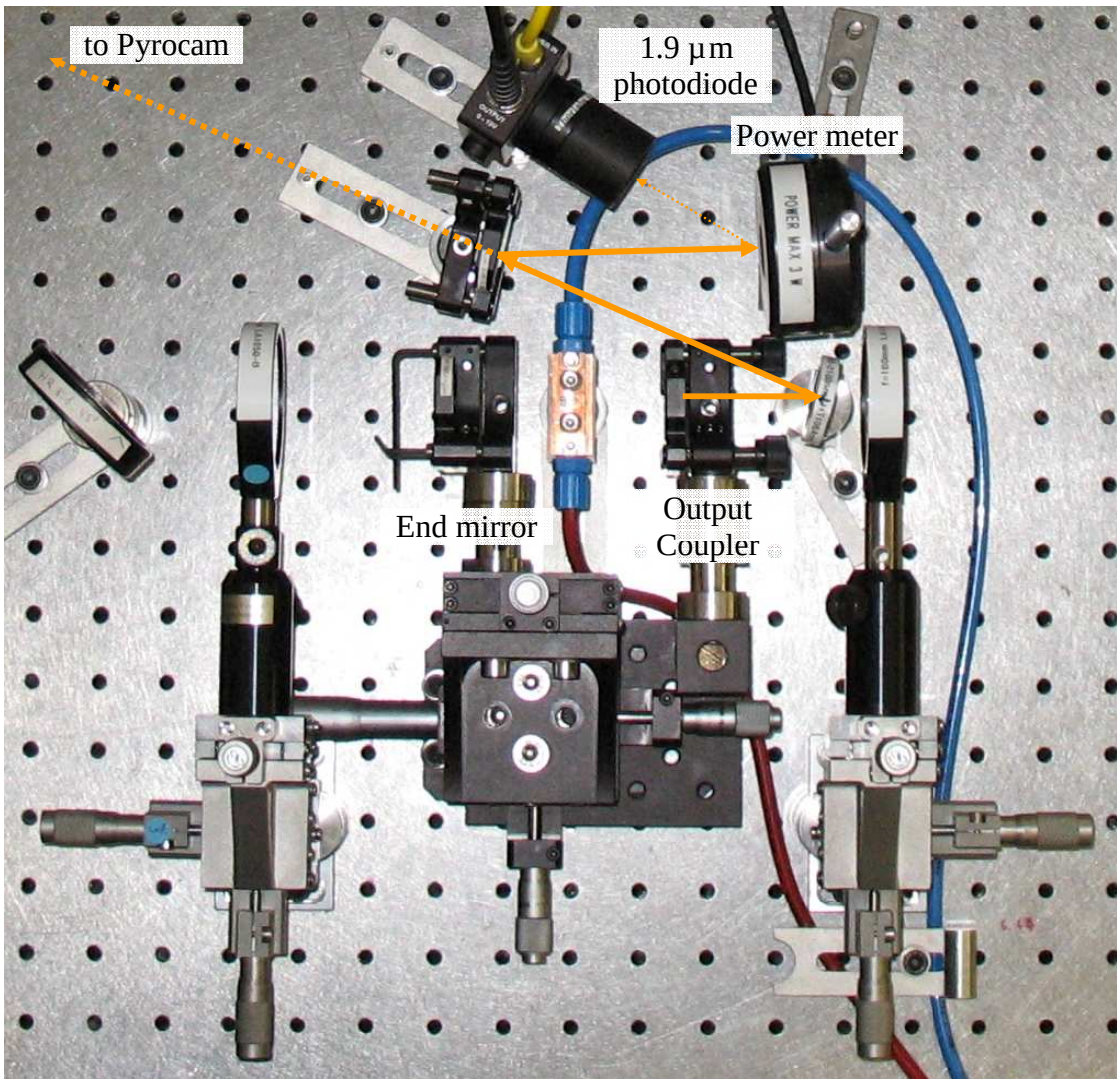

Figure 5.10: Top-view photo of the Tm:$GdVO_4$ laser resonator with some of the diagnostic equipment used during the Tm:$GdVO_4$ laser characterisation.

The laser fold mirror separated the generated Tm:$GdVO_4$ laser light at 1.9 µm from the pump light at 0.8 µm. The average output power of the laser was measured with a power meter while a commercial fast InGaAs photodiode sensitive at 1.9 µm (Thorlabs Inc. model PDA10D, 1.2-2.6 µm fixed gain detector, 15 MHz bandwidth) was used to capture the temporal profile of the laser output. From these two measurements the laser energy during the QCW pulse was calculated. Furthermore, the diagnostic fold mirror transmitted 2% of the laser beam onto a Spricon Pyrocam I to measure the intensity beam profile of the Tm:$GdVO_4$ laser.

An additional photodiode, sensitive only at 0.8 µm, was used to monitor the incident QCW pump pulse, a small percentage of which was scattered off the pump lens as indicated by the red arrows in Figure 5.11. Also shown is the monochromator that was used together with a photodiode sensitive over a wide wavelength range (1.5 to

4.0 µm) to measure the Tm:$GdVO_4$ laser central wavelength λ_c and the full spectral width Δ.

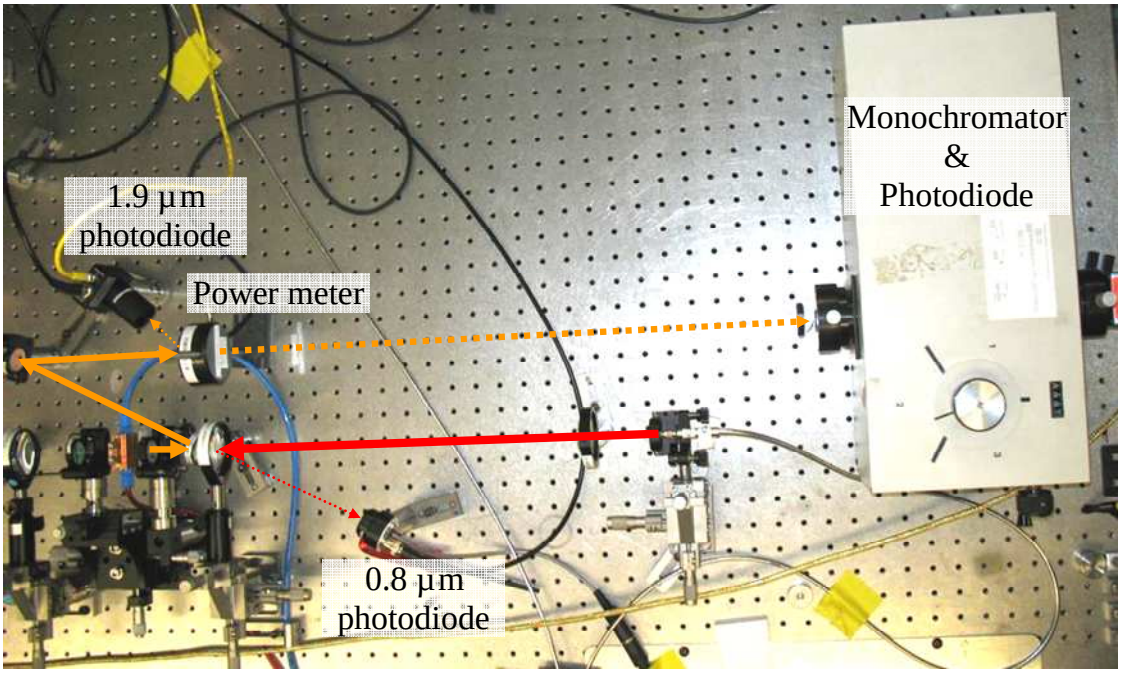

Figure 5.11: Top-view photo of the diagnostic arrangement used to characterise the Tm:$GdVO_4$ laser output.

5.4 Experimental characterisation of the Tm:$GdVO_4$ laser

The dual-end-pumped Tm:$GdVO_4$ laser for which the optimum resonator length, mirror radii and mirror positions were determined experimentally, as described in Section 5.3.4 above, was operated in three configurations with a 95% reflectivity output coupler mirror. Initially, the laser performance was measured with only the plano-concave resonator, then the Brewster plate was added to the cavity, and ultimately the etalon was also inserted in the laser.

The output energy of the Tm:$GdVO_4$ laser as a function of QCW pump energy for the three configurations are presented in Figure 5.12. Also indicated on the graph is the central wavelength λ_c and the full spectral width Δ measured for each configuration.

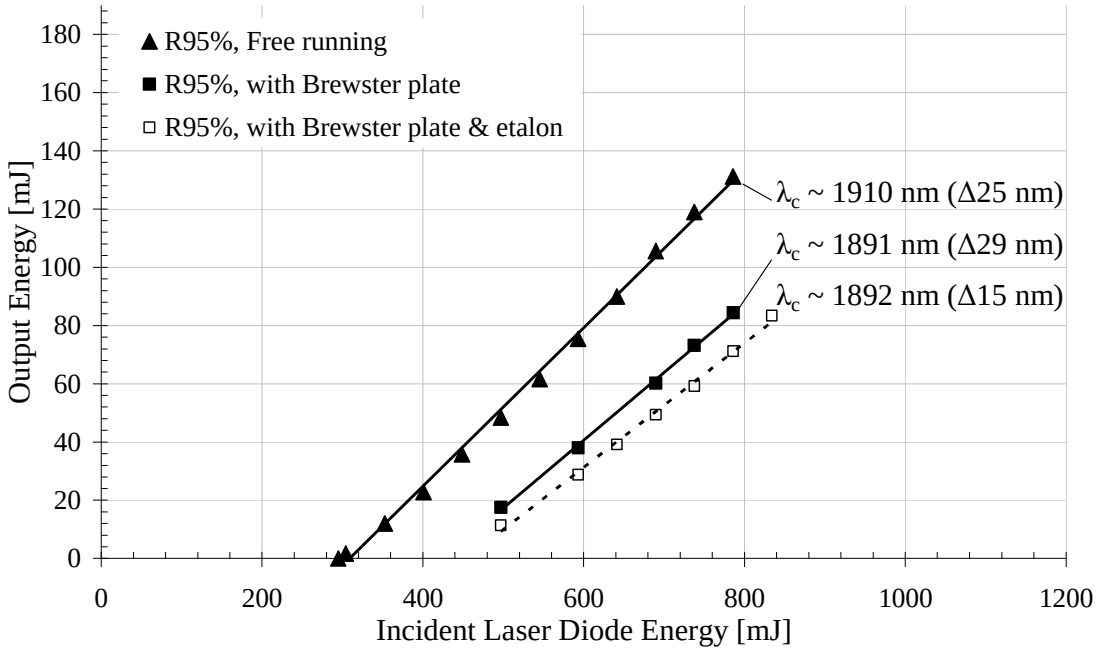

Figure 5.12: Output energy of the dual-end-pumped QCW Tm:$GdVO_4$ laser with the 95% output coupler, operating free running, with the Brewster plate, and with the Brewster plate and etalon in the laser cavity.

The Tm:$GdVO_4$ laser with only the 95% output coupler mirror had a slope efficiency of 26% and a threshold pump power of 14.8 W during the on-time of the pump pulse. The calculated threshold power density was 67 W/mm^2. The laser operated on σ-polarisation and the central wavelength λ_c was at 1910 nm with a full spectral width Δ of 25 nm.

By inserting the Brewster plate into the cavity at a tilt angle which introduced losses for σ-polarisation, the Tm:$GdVO_4$ laser was forced to operate on π-polarisation. The measured slope efficiency was 22% and the estimated threshold pump power was 21.5 W, which was equivalent to a pump power density of 97 W/mm^2. The measured central wavelength λ_c shifted towards 1891 nm, while the full spectral bandwidth Δ increased slightly to 29 nm.

The uncoated fused-silica etalon of thickness 100 μm was introduced to the cavity to narrow the spectral bandwidth Δ of the Tm:$GdVO_4$ laser to 15 nm, and to be able to slightly tune the λ_c wavelength around the central 1892 nm output. The etalon tilt was adjusted to maximise the transmission through the monochromator which was set to 1892 nm, thereby ensuring that the output wavelength was tuned to the absorption peak of Ho:YLF. The measured slope efficiency was 20% and the pump power

required to reach laser threshold was 23.9 W while the threshold power density was 108 W/mm^2.

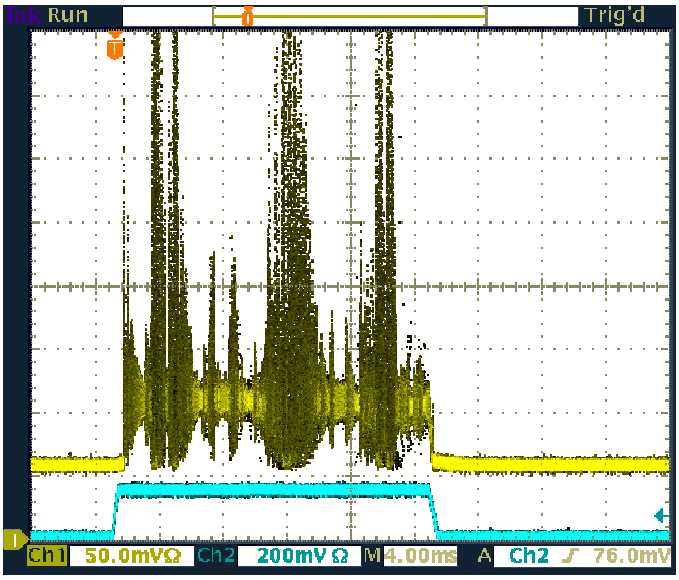

Figure 5.13: The temporal response of the Tm:$GdVO_4$ laser (channel 1, yellow) in relation to the QCW pump pulse (channel 2, blue).

Shown in Figure 5.13 is the captured oscilloscope screenshot for the first configuration, namely with only the R95% output coupler in the laser cavity. The laser output pulse had an approximate duration of 19 ms measured with the InGaAs detector (channel 1 of the oscilloscope screenshot - yellow). The observed spiking of the Tm:$GdVO_4$ laser was therefore considered a real feature of the output. The incident laser diode QCW pump pulse of 20 ms on-time was measured with the fast photodiode sensitive only at 0.8 µm (channel 2 of the oscilloscope screenshot - blue).

In order to avoid laser damage or crystal fracture, the total pump energy was limited to a maximum of 835 mJ during the 20 ms on-time of the pulse. The maximum measured average output power of the Tm:$GdVO_4$ laser was 656 mW during the configuration when only the 95% output coupler was in place. Based on this average power measurement, the output energy was calculated to be 131 mJ. Similarly, the output energy of the configuration with the Brewster plate, and the configuration with both the Brewster plate and etalon, was calculated to be 84 mJ and 83 mJ respectively. The maximum output energy for each configuration is summarised in Table 5.2.

Table 5.2: Summary of results of the dual-end-pumped Tm:$GdVO_4$ laser in the three laser configurations.

Laser configuration	**Maximum Output Energy for 20 ms pump**	**Polarisation, Wavelength, Full width**	**Temporal response** Ch1 (yellow): Tm:$GdVO_4$ pulse Ch2 (blue): transmission through monochromator	**Intensity beam profile**
R95% output coupler	131 mJ	σ-polarisation λ_c 1910 nm Δ 25 nm	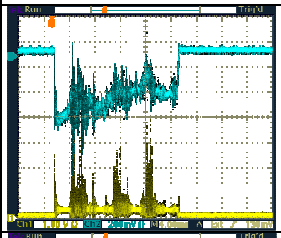	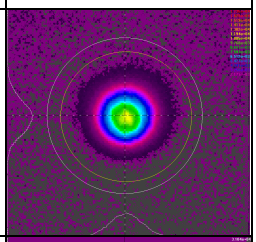
R95% output coupler, Brewster plate	84 mJ	π-polarisation λ_c 1891 nm Δ 29 nm	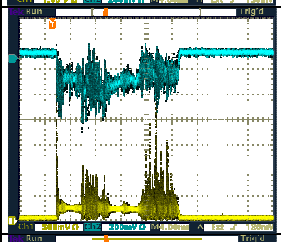	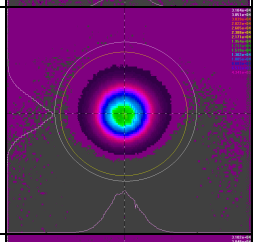
R95% output coupler, Brewster plate & etalon	83 mJ	π-polarisation λ_c 1892 nm Δ 15 nm	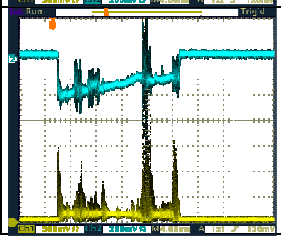	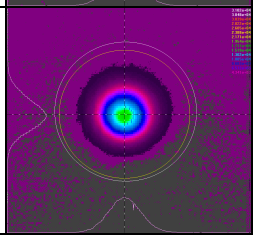

The polarisation orientation of the laser output and the output wavelength properties are also listed in Table 5.2, together with the measured temporal response and the intensity beam profiles for the different Tm:$GdVO_4$ laser configurations. A quantitative measurement of the laser beam quality was not made but the measured intensity beam profiles were used as an indication of the laser beam quality during the experiments.

The captured oscilloscope screenshots show the measured Tm:$GdVO_4$ output pulse (channel 1 of the oscilloscope screenshot - yellow), while the broadband photodiode measured the transmission through the monochromator (channel 2 of the oscilloscope screenshot - blue), which was set to the central output wavelength of the particular laser configuration.

The measured laser output transmitted through the monochromator followed the spiking behaviour of the Tm:$GdVO_4$ output pulse. During several measurements where the monochromator transmission wavelength was adjusted, it was found that different temporal parts of the Tm:$GdVO_4$ laser output pulse had different wavelength

contributions. This most likely also contributed to an increase in the measured full spectral width of the laser output and a reduction in the accuracy of the measurement.

The temporal spiking behaviour of the laser was prominent for the configuration with only the 95% output coupler mirror in place, as well as for the configuration with the Brewster plate also in the laser cavity. The temporal response of the laser with both the Brewster plate and etalon in the cavity indicated a slightly more stable laser output, which also manifested in the measured pulse transmitted through the monochromator which was set to 1892 nm.

The intensity beam profiles measured for the three laser configurations indicated circular beams with Gaussian intensity profiles. No deterioration in beam quality was observed upon the insertion of the Brewster plate and the etalon in the laser cavity, but a reduction in peak intensity was observed which was associated with the lower output energy.

5.5 Discussion of experimental results

It was confirmed by the experimental results that the Tm:$GdVO_4$ laser with the 95% output coupler mirror, Brewster plate and etalon in the cavity, which utilised a 3% Tm^{3+} doped crystal of length 3 mm pumped from both ends with a pump spot radius of 265 µm, produced the desired wavelength of 1892 nm at a suitable output energy and beam profile to pump a Ho:YLF laser. The following observations were made during the experimental evaluation of the three laser configurations used.

5.5.1 Threshold power densities

It was noted that the pump powers required to achieve laser operation on σ-polarisation and on π-polarisation was higher than the theoretically predicted values. The first Tm:$GdVO_4$ laser reported in Chapter 4 also had higher threshold power densities, but the discrepancy was not as large as in these experiments.

The lower emission cross section of Tm:$GdVO_4$ on the π-polarisation at 1892 nm, as compared to the σ-polarisation at 1910 nm, could only partially account for the high threshold values measured for these two laser configurations since the laser threshold calculations indicated an increase in threshold power density by a factor of 1.16 only.

Since the etalon and Brewster plate were both uncoated fused silica elements, it was reasonable to assume losses for the pump light which passed through these elements. The etalon was mounted at near-normal incidence and would have resulted in an approximate 8% loss for the pump light incident from the right of the cavity, with reference to the experimental arrangement as depicted in Figure 5.5 and Figure 5.14. Similarly, the unpolarised pump light from the left would have experienced approximately 7.5% loss on the Brewster plate, thereby reducing the incident pump power into the Tm:$GdVO_4$ laser crystal. Taking these additional losses for the pump light into account, the total incident pump power was lower than originally calculated. The experimental threshold power density for the final laser was most likely closer to 100 W/mm^2, which was still higher than the predicted 78 W/mm^2. This discrepancy could only be attributed to higher-than-intended losses in the laser cavity for the laser light.

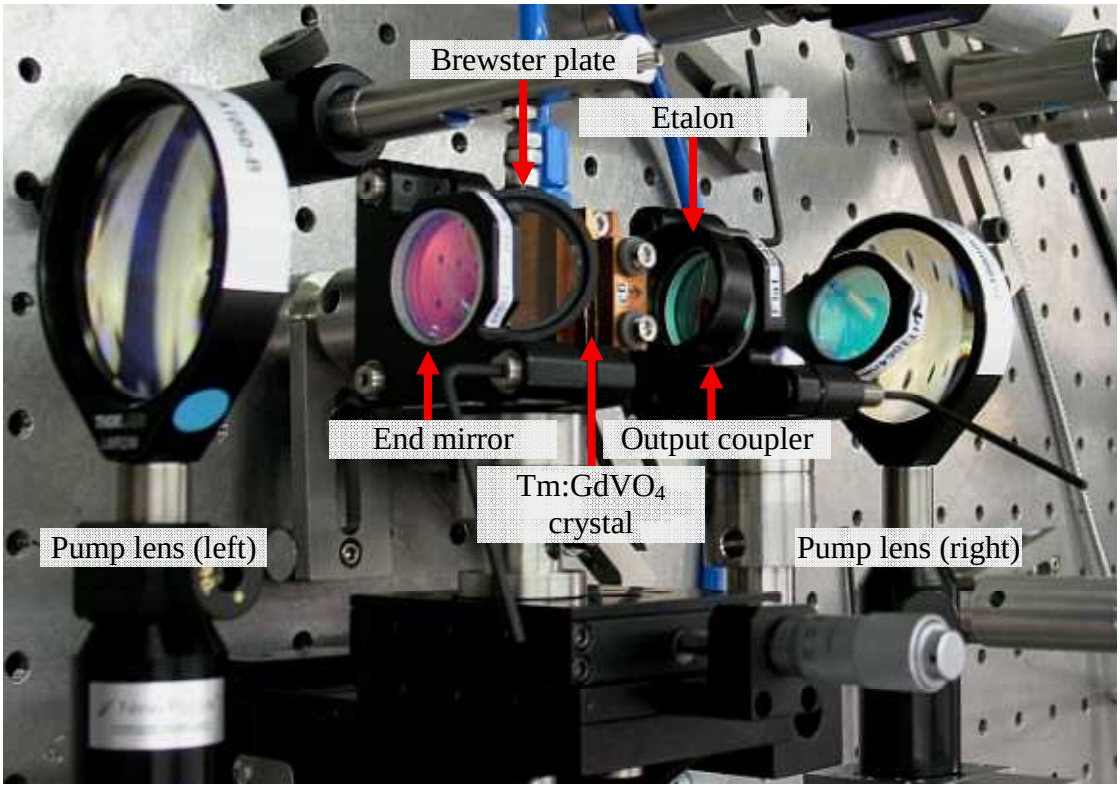

Figure 5.14: Photo of the Tm:$GdVO_4$ laser resonator with the Brewster plate and etalon in the cavity.

An additional factor which is a likely source of added higher cavity loss is the fact that the resonator mirrors used in this set of experiments were unfortunately not the same set of mirrors as used in the first laser experiments reported in Chapter 4. In particular, the 200 mm radius of curvature mirror was specified for high reflectance at 1900-2100 nm, and most likely had a slight increase in transmission when the laser

operated at 1892 nm, resulting in additional resonator losses. Similarly, the output coupler mirror reflectivity was not constant over the wavelength range between 1892 nm and 1910 nm, which may contribute to explaining the discrepancies between the calculated and experimentally observed threshold power density values.

5.5.2 Slope efficiency and output energy

The existence of higher losses in the resonator is also evident in Figure 5.15 which is a comparison of the output energy of the new dual-end-pumped laser compared to the output energy of the original single-end-pumped configuration with only the 95% output coupler mirror in the cavity. As discussed above, the threshold was higher than the expected increase due to the larger pump beam used in the dual-end-pumped configuration, namely 265 µm compared to the original 220 µm in the single-end-pump configuration. However, the slope efficiencies of 28% and 26%, respectively, was very similar for the two pump configurations.

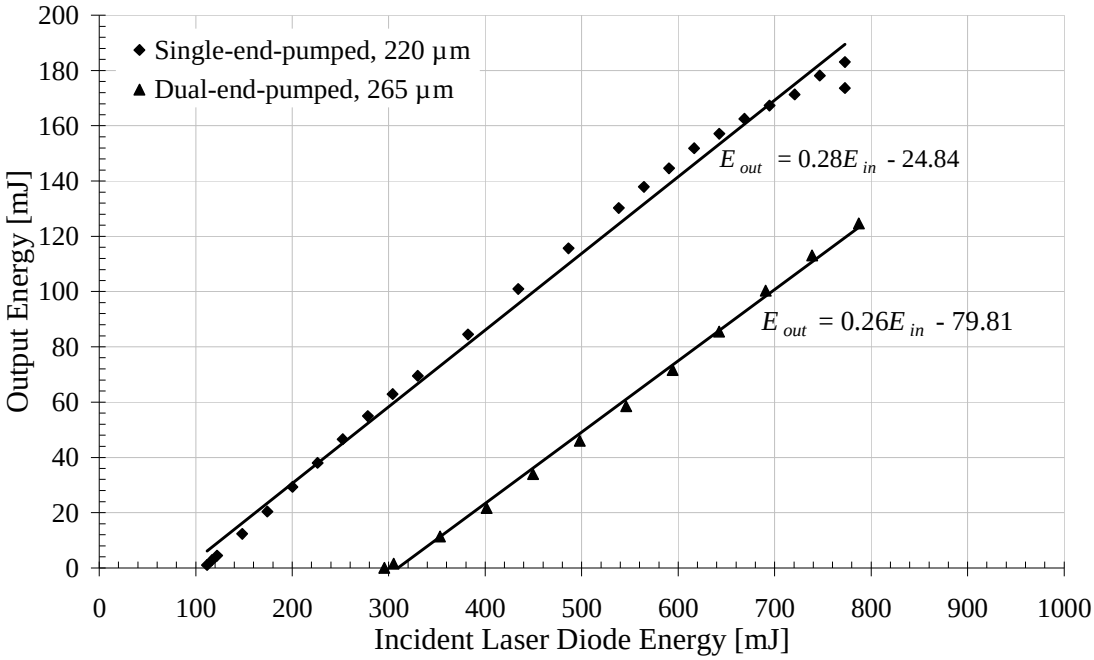

Figure 5.15: Difference in output energy for the Tm:$GdVO_4$ laser with a 95% output coupler mirror in the original single-end-pumped configuration with a pump spot radius of 220 µm, and in the dual-end-pump configuration a pump spot radius of 265 µm.

The output energy of the dual-end-pumped laser was deliberately kept low to avoid optical damage to the Tm:$GdVO_4$ crystal faces, as had been experienced in the single-end-pumped laser at 180 mJ output energy. Furthermore, the pump energy was kept well below the thermal fracture limit of the Tm:$GdVO_4$ crystal, which was estimated

to be 960 mJ for the single-end-pumped configuration with 220 µm pump beam radius.

5.5.3 Temporal behaviour and atmospheric water absorption

During the measurements of the temporal output of the first single-end-pumped Tm:$GdVO_4$ laser, its fast dynamic behaviour could not observed because the detector used in the diagnostic arrangement had a response time of a few ms only. However, with the new diagnostic instrument in place, the temporal behaviour of the dual-end-pumped Tm:$GdVO_4$ laser output was adequately resolved and evaluated.

The spiking behaviour of the Tm:$GdVO_4$ laser was evident in all three laser configurations, namely with the 95% output coupler mirror in place, with the Brewster plate also in the laser cavity, and the final configuration which also included the etalon. As described above, the spiking was reduced for the latter case.

Even though spiking was expected in the form of relaxation oscillations due to the QCW pump pulse, the observed chaotic spiking could not be attributed to this effect. In a separate set of experiments it was attempted to identify the relaxation frequency and cavity decay time in the temporal output of the Tm:$GdVO_4$ laser, but a conclusive assessment could not be made.

However, the spiking behaviour was most likely caused by the additional dynamic losses due to water absorption in the atmosphere inside the laser cavity, which is a typical problem for Tm^{3+} doped solid-state lasers operating in this wavelength region [3]. The atmospheric water absorption over 1 m distance in 50% relative humidity is shown in Figure 5.16 for the wavelength region of interest [4]. Superimposed on the graph is an indication of the measured emission central wavelengths and bandwidths of the Tm:$GdVO_4$ laser for the instances with only the 95% output coupler mirror in place (shaded red), with the Brewster plate also in the laser cavity (shaded green), and with both the Brewster plate and etalon in the laser (shaded blue). It is clear from this graph that in all thee cases the emission bandwidth included a number of prominent atmospheric water absorption features, which could have influenced the dynamics of the laser operation.

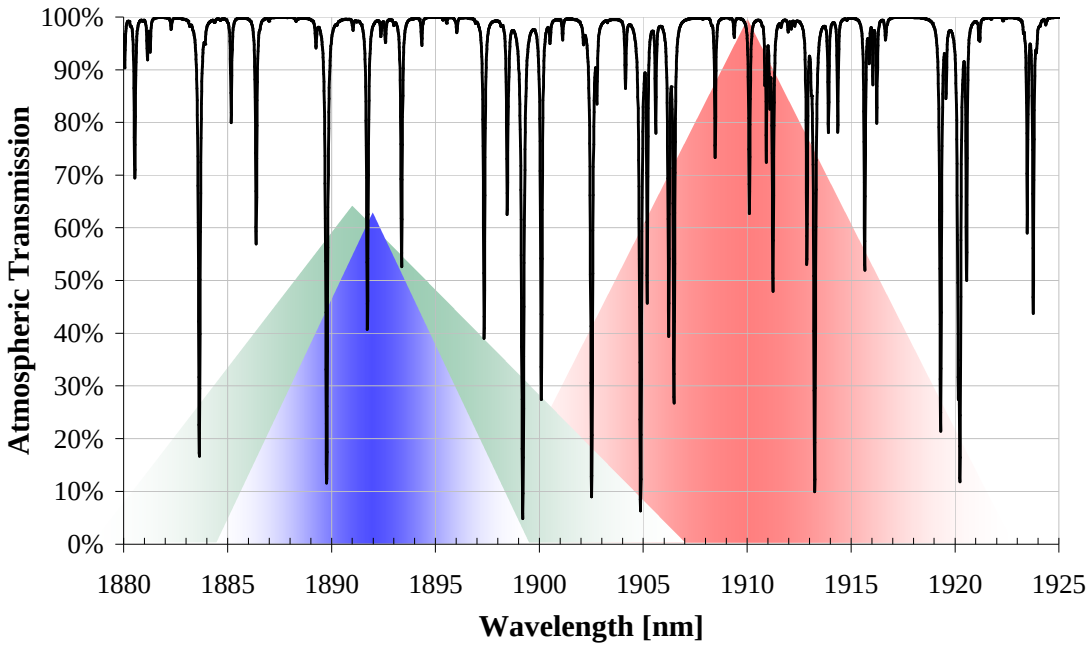

Figure 5.16: Atmospheric transmission through 1 m of air at 50% relative humidity in the wavelength region where the Tm:$GdVO_4$ laser operated [4]. The shaded triangles indicate the width of the measured emission bandwidth (base of triangle) and central wavelength (apex of triangle) normalised to the maximum output energy for the three resonator configurations.

The 100 µm etalon which has a free spectral range of 12 to 13 nm, limited the emission band of the Tm:$GdVO_4$ laser over a smaller number of atmospheric water absorption lines, as compared to the other two laser configurations. It was concluded that this reduced the influence of the atmospheric water absorption on the laser operation, which resulted in the slightly more stable operation.

5.5.4 Laser parameters

The characteristics of the final Tm:$GdVO_4$ laser configuration were the following:

- Operational mode: QCW
- Pulse repetition frequency: 5 Hz
- Output pulse duration: 19 ms (with spiking behaviour)
- Central wavelength: 1892 nm, slightly tuneable
- Wavelength bandwidth: 15 nm
- Output energy: 83 mJ
- Average output power during the QCW pulse: 4.17 W (estimated)
- Average output power: 417 mW
- Intensity beam profile: circular Gaussian distribution

The constructed Tm:$GdVO_4$ laser was unique in its design and output parameters since it was specifically developed as pump source for a Ho:YLF laser. No such laser has been reported before in the literature, and neither has a Tm:$GdVO_4$ laser been developed to be a pump source for another laser system, although its potential has been described.

5.6 Conclusions

In conclusion, it can be stated that the Tm:$GdVO_4$ laser, designed and constructed as described above, has most of the attributes necessary to make it a suitable pump source for the proposed Ho:YLF laser. As described, the Tm:$GdVO_4$ laser was diode-end-pumped from both ends in QCW mode with a 20 ms pump on-time at 5 Hz, which resulted in a 19 ms long laser output pulse. Strong spiking behaviour was observed in the output laser pulse waveform, which is attributed to the dynamic influence of intra-cavity water vapour absorption. It was expected that the spiking behaviour could influence the operation of the Ho:YLF laser.

The absorption spectra of Ho:YLF dictated that the polarised Tm:$GdVO_4$ laser wavelength must be centred at 1892 nm. To realise this, a resonator was designed using the quasi-three-level threshold analysis for the available 3 mm long, 3% doped Tm:$GdVO_4$ laser crystal. The calculations indicated that a 95% reflectivity mirror should be used as output coupler and that the laser should be forced to operate on the slightly weaker π-polarisation with a Brewster plate to reach the desired wavelength range. Furthermore, it was calculated that a 100 µm etalon was required to fine-tune the laser wavelength onto 1892 nm.

It was demonstrated experimentally that the insertion of an intra-cavity fused silica etalon was essential to select the output wavelength of 1892 nm. It was also shown that the etalon reduced the wavelength bandwidth to 15 nm, compared to 29 nm without the etalon in the cavity. An added benefit of the etalon was that the temporal spiking behaviour was slightly suppressed due to a reduced influence of atmospheric water absorption in the Tm:$GdVO_4$ laser cavity.

The influence of the Brewster plate and the etalon on the laser threshold and slope efficiency was evaluated in detail. It was found that their inclusion in the resonator resulted in additional intra-cavity losses for the pump light and laser light, with a

magnitude which was slightly larger than that which could be attributed to Fresnel reflection losses or due to the lower emission cross section associated with the π-polarisation. A additional source of resonator loss was the lower-than-expected reflectivity of the resonator mirrors employed the relevant wavelengths of 1892 nm and 1910 nm.

The objective of using a dual-end-pump configuration in conjunction with slightly larger pump beam radii of 265 µm was to reduce the risk of optical damage due to high intra-cavity power densities associated with the use of a 95% reflectivity output coupler. Furthermore, the Tm:$GdVO_4$ pump energy was deliberately maintained at a low value to minimise the prospect of thermal fracture of the laser crystal. The combined effect of this conservative approach, together with the inclusion of a Brewster plate and etalon in the laser cavity, was that in practice the Tm:$GdVO_4$ laser output could not safely be scaled to higher average power or higher energy than the value demonstrated earlier using the single-end-pump geometry with a pump beam radius of 220 µm.

Nevertheless, a Tm:$GdVO_4$ laser was successfully designed and constructed that delivered 83 mJ in a 19 ms QCW pulse at the desired wavelength of 1892 nm to pump a Ho:YLF laser. This corresponded to a measured average output power of 417 mW, or alternatively, an estimated 4.17 W average output during the QCW pulse. This pump laser was unique and offered the opportunity to construct an all-solid-state 2 µm laser system, as will be described in the next chapter.

5.7 References

[1] Brian M. Walsh, Norman P. Barnes, Baldassare Di Bartolo, "Branching ratios, cross sections, and radiative lifetimes of rare earth ions in solids: Application to Tm3+ and Ho3+ ions in $LiYF^4$", *Journal of Applied Physics*, vol. 83, no 5, pp. 2772-2787, 1 March 1998.

[2] Y. Li, B. Yao, and Y. Wang, "Diode-pumped CW Tm:$GdVO_4$ laser at 1.9 μm," Chinese Optics Letters **4**, (3), 175-176 (March 2006).

[3] M. Shellhorn, "High-power diode-pumped Tm:YLF laser," Applied Physics B **91**, (1) 71–74 (2008).

[4] Data from HITRAN, compiled by Martin Schellhorn, French-German Research Institute, Saint Louis, France, (11 March 2009).

Chapter 6

Ho:YLF laser pumped by a $Tm:GdVO_4$ laser

The performance of the $Tm:GdVO_4$ laser, which was developed as a pump source for a Ho:YLF laser, was summarised in the previous chapter. There it was shown that the Tm laser met the pump requirements for a Ho:YLF laser of linearly polarised output at a wavelength of 1892 nm in a QCW pulse of suitable duration and multi-watt peak output power with a good quality beam. As described in this chapter, the $Tm:GdVO_4$ laser was subsequently used to pump a Ho:YLF 2 µm laser oscillator, operated both in free-running mode and in *Q*-switched mode. This chapter describes the pump arrangement as well as the design and performance of the Ho:YLF oscillator which ultimately produced a *Q*-switched output energy of 2 mJ per pulse.

6.1 Arrangement to pump the Ho:YLF laser with the $Tm:GdVO_4$ laser

A number of beam steering mirrors, a lens, an optical isolator, as well as a half-wave plate for 1892 nm were required to deliver the laser output from the $Tm:GdVO_4$ laser to the Ho:YLF laser, as indicated in the schematic of Figure 6.1.

The optical isolator was aligned for maximum transmission at 1.892 µm in the forward direction, while it eliminated back reflections from the Ho:YLF laser mirrors which would otherwise give rise to instabilities within the $Tm:GdVO_4$ pump laser. The half-wave plate orientated the pump light polarisation with respect to the π-polarisation of the Ho:YLF laser crystal. A partially reflective mirror was used to monitor the output energy and beam profile of the $Tm:GdVO_4$ laser during the Ho:YLF laser experiments.

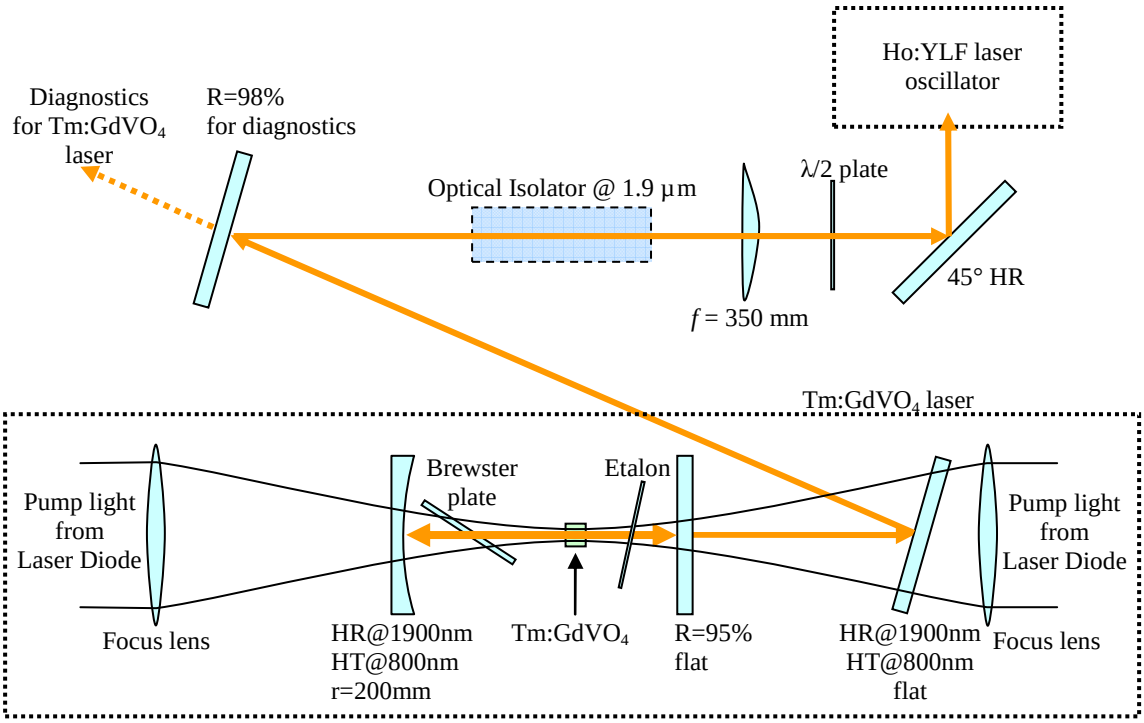

Figure 6.1: The optical layout of the Tm:GdVO$_4$ laser with beam delivery optics to pump the Ho:YLF laser oscillator.

A plano-convex lens with focal length f = 350 mm was placed an approximate distance 2f away from the Tm:GdVO$_4$ crystal to image the pump beam into the Ho:YLF crystal, which was also placed a distance 2f from the focussing lens.

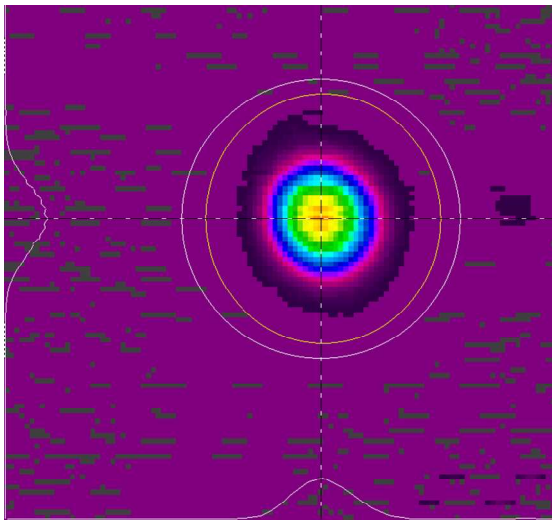

Figure 6.2: Intensity beam profile of the Tm:GdVO$_4$ pump beam measured at the position of the Ho:YLF crystal.

The pump beam focus in the position of the Ho:YLF was measured to have a radius of between 240 and 250 µm. The intensity beam profile of the pump beam is shown in Figure 6.2. Due to the losses of the pump optics, in particular the optical isolator, the

maximum pump energy incident on the Ho:YLF resonator was 73 mJ, reduced from 83 mJ at the output of the Tm:$GdVO_4$ laser.

6.2 The design of the Ho:YLF laser

The overall design of the Ho:YLF laser is described here in terms of the chosen gain medium, the laser resonator which included an Acousto-Optic Modulator (AOM) which was used as *Q*-switch, and the pump optical layout.

6.2.1 The Ho:YLF laser crystal and its mounting

A Ho:YLF laser crystal rod of length 40 mm was available for the experiments. The rod diameter was 6.0 mm and the atomic doping concentration of Ho^{3+} was 0.5%. The end-faces of the crystal were anti-reflection coated for both the pump light (1850-1950 nm) and for the Ho:YLF laser wavelength (2050-2064 nm).

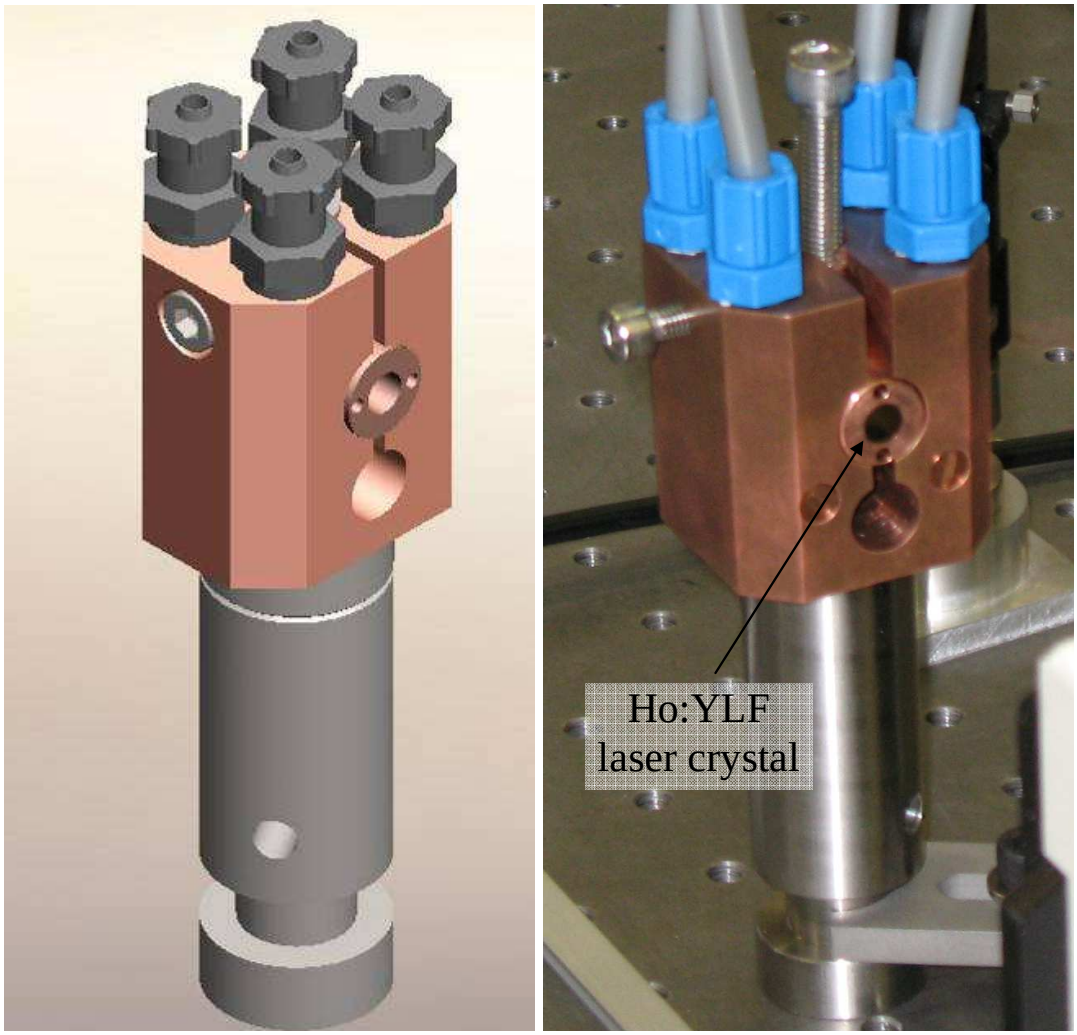

Figure 6.3: The assembly drawing (left) and photo (right) of the custom-designed copper cooling rod for the Ho:YLF laser crystal, mounted in a water-cooled block.

The Ho:YLF laser crystal rod was mounted in a custom-designed cylindrical copper cooling rod of which the inside diameter was reamed to high tolerance to match the outside diameter of the laser rod. The length of the copper rod was also accurately matched to the length of the laser rod. The copper cooling rod was designed to fit into a water-cooled block, the temperature of which could be maintained with a circulating temperature-controlled water cooler. An assembly drawing of the copper cooling block and the cooling rod is shown in Figure 6.3.

The Ho:YLF laser rod was inspected for quality and subsequently mounted in the copper cooling rod using UV-curing glue as an interface between the crystal and the copper. Also shown in Figure 6.3 is a photo of the mounted 40 mm long Ho:YLF laser crystal which was used for the laser experiments.

6.2.2 Linear Ho:YLF laser resonator

Two different resonator configurations were implemented during the experiments on the Ho:YLF laser. The first resonator was based on a simple linear cavity consisting of two resonator mirrors, the Ho:YLF laser crystal and, optionally, the AOM *Q*-switch. The schematic of this resonator is shown in Figure 6.4.

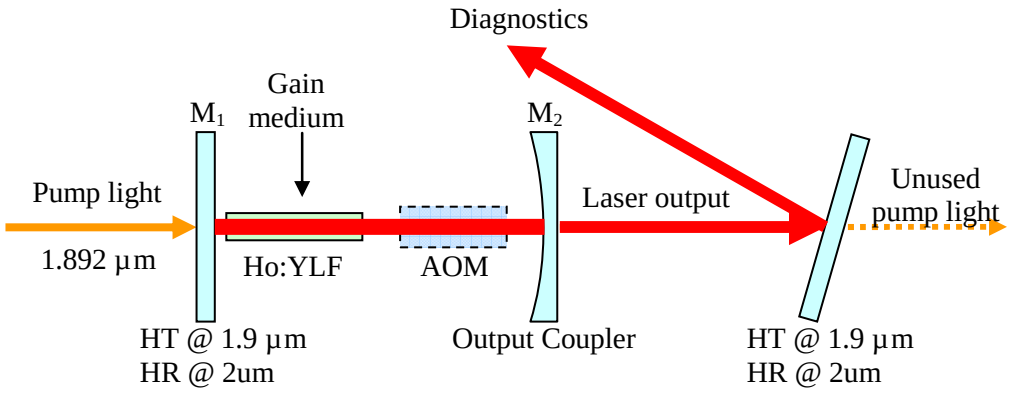

Figure 6.4: Schematic diagram of the linear 2 µm Ho:YLF laser oscillator.

The input coupler (M_1) was a plane mirror with high transmission (HT) at the pump light, and high reflection (HR) at the laser light. The reflectivity of the curved output coupler (M_2) was initially 90% at both the laser light and the pump light, although other output couplers were also evaluated. This arrangement ensured efficient output coupling for the Ho:YLF laser, but also reflected the pump light back into the crystal for double-passing the partially reflected pump light.

Different radii of curvature were selected for the output coupler during the laser experiments, namely r = 100, 200 and 300 mm. The radius of curvature of the output coupler mirror, together with the resonator length of approximately 80 mm, determined the fundamental laser mode size inside the Ho:YLF laser crystal. The calculated laser mode radii in the crystal for each of these output coupler mirrors were as follows:

- w = 190 µm for r = 100 mm
- w = 254 µm for r = 200 mm
- w = 290 µm for r = 300 mm.

Neglecting the influence of the choice of output coupler on the back-reflected pump light, it was expected that the highest laser efficiency would be achieved with an output coupler mirror with radius of r = 100 mm which produced a calculated laser mode size of w = 190 µm, which is slightly smaller than the pump beam size of 240 – 250 µm in the Ho:YLF laser crystal. With this design, the highest efficiency operation was anticipated because it was expected that the re-absorption losses due to the quasi-three-level nature of the Ho:YLF laser would be minimised in the wings of the Gaussian laser beam. A photo of the constructed 2 µm laser resonator is shown in Figure 6.5.

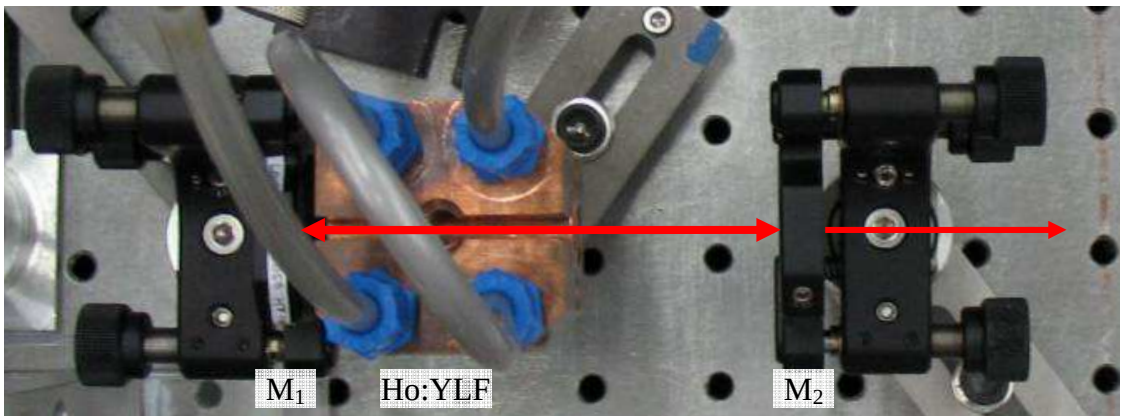

Figure 6.5: Top view photo of the linear Ho:YLF laser.

To operate the Ho:YLF laser in *Q*-switched mode, the AOM (Gooch & Housego, model QS027-10M-NL5) was inserted between the Ho:YLF laser crystal and the output coupler mirror M_2. In doing so, the resonator length was changed slightly to fit the AOM. The AOM was orientated such that it introduced a loss for the π-polarisation on which the Ho:YLF laser will naturally operate due its stronger emission cross section, as compared to the σ-polarisation. A close-up photo of the Ho:YLF resonator including the AOM is shown in Figure 6.6.

Figure 6.6: **Close-up view of the Ho:YLF laser oscillator input coupler, crystal mount and acousto-optic modulator.**

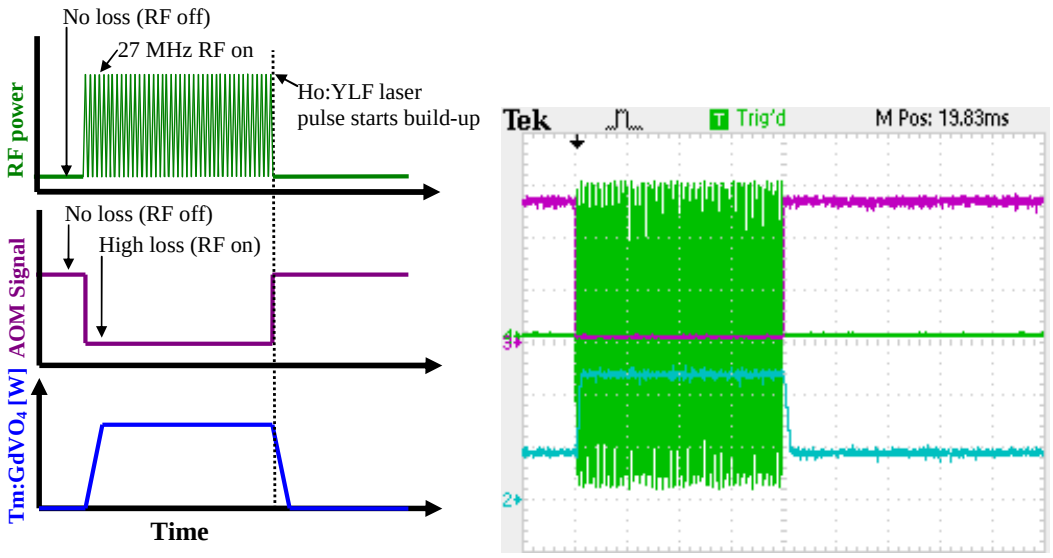

Figure 6.7: **The timing of the AOM drive signal synchronised to the Tm:$GdVO_4$ pump pulse (left). An oscilloscope screenshot (right) of the RF power from the AOM driver (channel 4, green) which followed the control signal (channel 3, purple) synchronised to the pump pulse of the Tm:$GdVO_4$ laser (channel 2, blue).**

The timing of the AOM drive signal was synchronised to the quasi-continuous-wave Tm:$GdVO_4$ pulse. The AOM was switched to high loss during the on-time of the pump pulse, as shown in Figure 6.7. The AOM loss (channel 4, green) was switched off by the control signal (channel 3, purple) at the end of the Tm:$GdVO_4$ laser pump pulse (channel 2, blue) to allow the Ho:YLF laser pulse to build up.

6.2.3 Ho:YLF laser diagnostic arrangement

An example of the diagnostic arrangement used for the Ho:YLF laser experiments is shown in Figure 6.8.

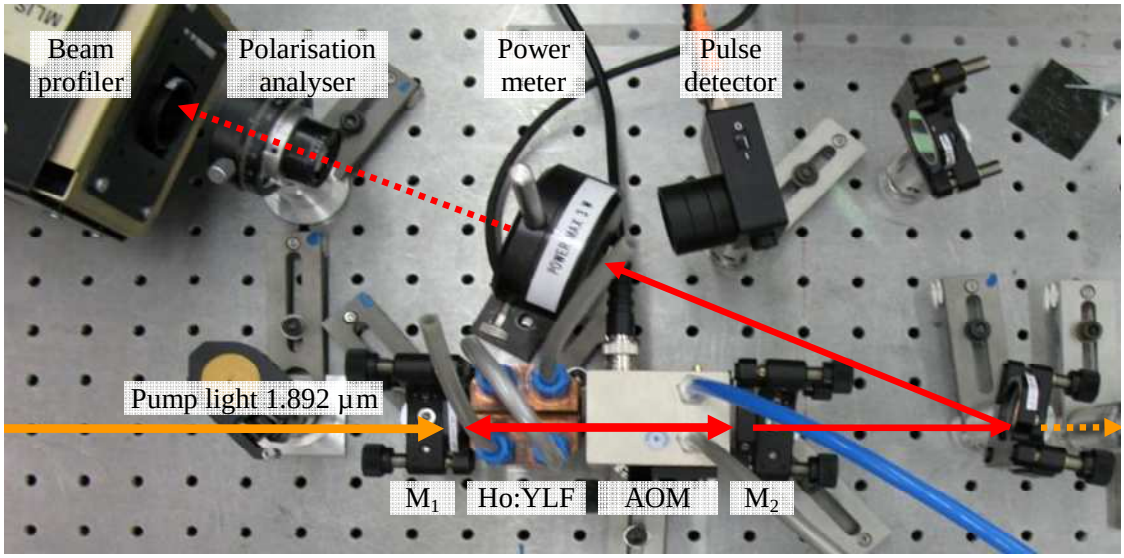

Figure 6.8: Top view of the constructed linear resonator Ho:YLF laser, indicating the laser components and diagnostic equipment used in the experiments.

The following diagnostic instruments were used to evaluate the performance of the Ho:YLF laser pumped by the Tm:$GdVO_4$ laser. The average laser output power was measured with a Gentec PS-310 power meter from which the energy per pulse was calculated using the pulse repetition frequency of 5 Hz produced by the Tm:$GdVO_4$ pump laser. The time resolved behaviour of the Ho:YLF laser was captured with a commercial amplified PbSe pulse detector (Thorlabs Inc., PDA20H, 1.5-4.8 µm Fixed Gain, AC Coupled Amplifier, 10 kHz bandwidth). To measure the shape of the fast *Q*-switched pulses, the output of an un-amplified InAs photodiode was recorded on a fast oscilloscope. The intensity beam profile of the linear resonator Ho:YLF laser was measured with a Pyrocam-I camera connected to a Spiricon Laser Beam Analyser. A polarising beam splitter cube for 2 µm wavelength was used to analyse the polarisation orientation of the Ho:YLF laser output.

6.3 Experimental evaluation of the linear resonator Ho:YLF laser

The performance of the Ho:YLF laser was evaluated for the linear resonator design in free-running mode and then in pulsed *Q*-switched mode, as described below.

6.3.1 Influence of output coupler radius of curvature

The first experiments were conducted on the linear resonator Ho:YLF laser operated in free-running mode with the Ho:YLF crystalline c-axis orientated horizontally. As expected, the output polarisation was horizontal and on the π-polarisation, which has a higher emission cross section in Ho:YLF.

The output energy of the Ho:YLF laser was measured as a function of incident pump energy for three different output coupler mirrors with radius of curvature r = 100, 200 and 300 mm with 90% reflectivity, as shown in Figure 6.9.

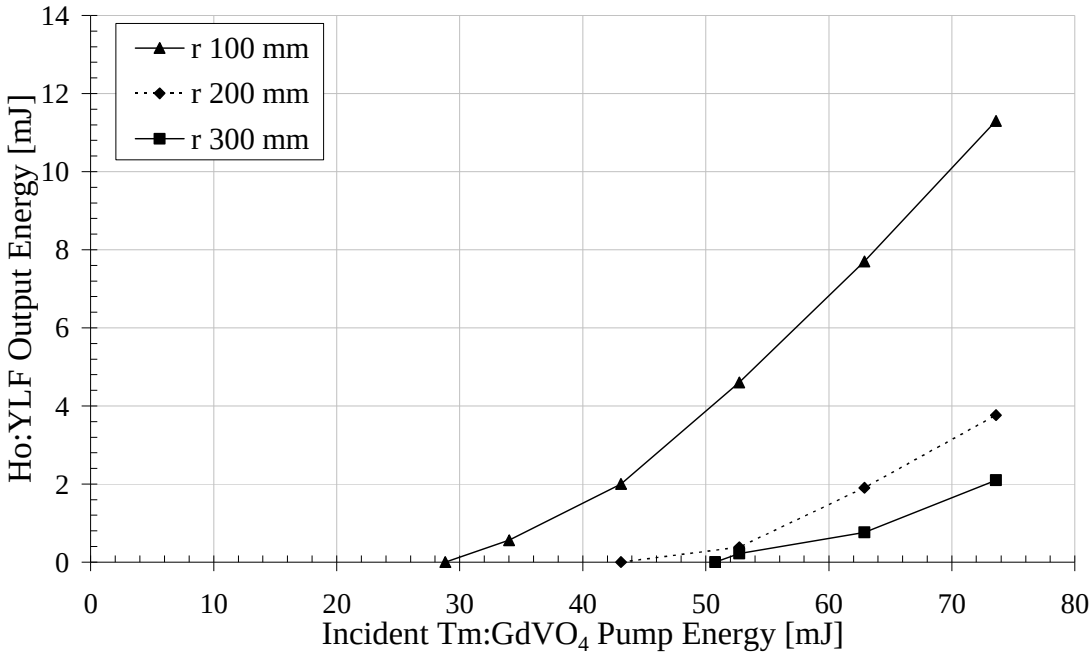

Figure 6.9: Output energy of the free-running Ho:YLF laser with a 90% reflectivity output coupler with *r* = 100, 200 and 300 mm radius of curvature.

The free-running Ho:YLF laser pulse energy had the highest value for the case when the 100 mm radius of curvature mirror was used. In this case, the threshold pump energy was only 28.8 mJ compared to 43.1 mJ and 50.8 mJ respectively for the r = 200 mm and r = 300 mm radii of curvature mirrors. Similarly, the maximum output energy for the r = 100 mm mirror was 11.3 mJ compared to 3.7 mJ and 2.1 mJ for the other two curvatures, and it had a superior slope efficiency of 30% (measured above 40 mJ of pump energy).

The difference in performance for the laser with output coupler mirrors of equal reflectivity (90%) but different radii of curvature can be attributed to the better matching of the fundamental laser resonator mode size to the pump beam size in the Ho:YLF crystal in the case of the r = 100 mm mirror. The improved performance was most likely also due to the back reflected pump light being strongly focussed by the *r* = 100 mm mirror causing a high pump energy density. However, a negative effect of this arrangement was that the Ho:YLF laser produced a sub-optimum output beam intensity profile, as discussed below.

6.3.2 Influence of output coupler reflectivity

The performance of the linear Ho:YLF resonator operated in free-running mode was also analysed for different output coupler transmissions but with equal radius of curvature (*r* = 100 mm). The results of this experiment are shown in Figure 6.10.

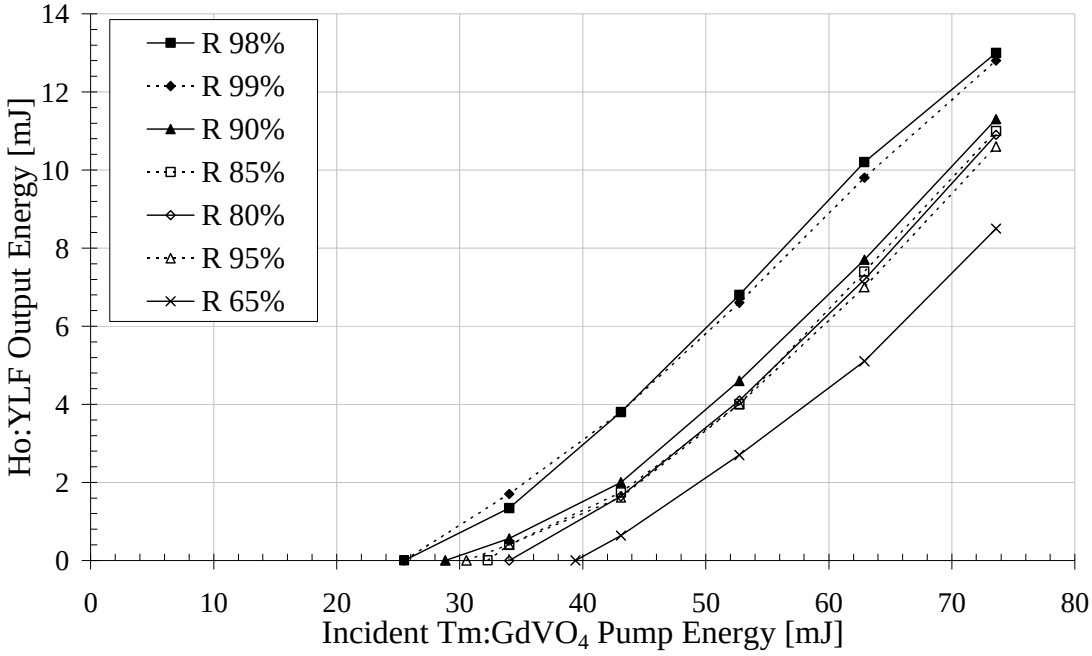

Figure 6.10: Output energy of the free-running linear resonator Ho:YLF laser for different output coupler reflectivity values.

In all the configurations the measured laser slope efficiency above 40 mJ pump energy was 30% - 31%, except for the case with the 65% reflectivity output coupler, which showed a 26% slope efficiency and the lowest output energy of 8.5 mJ at the maximum pump energy. The highest free-running output energy was 13 mJ for the 98% reflectivity output coupler mirror.

From these results it was concluded that the linear resonator Ho:YLF laser operated in free-running mode had very low internal loss. This conclusion is based on the observation that the measured slope efficiency was the same high value of 30% even at 99% and 98% output coupler reflectivity.

6.3.3 Intensity beam profile of the linear Ho:YLF resonator

Shown in Figure 6.11 is a typical intensity beam profile measured with the Pyrocam-I camera for the linear resonator Ho:YLF laser with a r = 100 mm output coupler mirror without the AOM in the cavity.

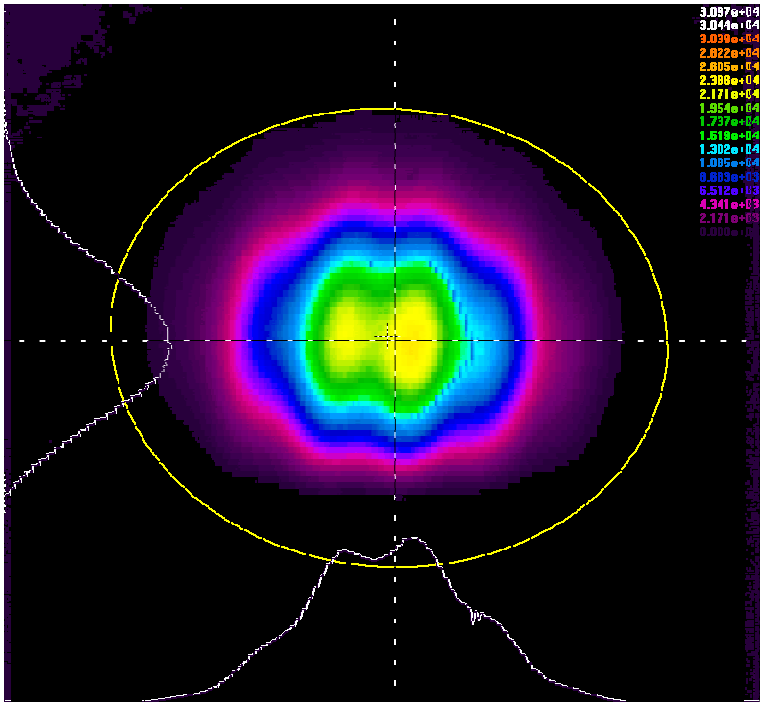

Figure 6.11: Intensity beam profile of the Ho:YLF laser with the linear resonator design.

The distortion in the intensity beam profile producing a non-Gaussian distribution in the horizontal plane was an indication that the resonator configuration was not optimally set up. The calculated fundamental mode radius in the crystal was 190 µm, which is slightly smaller than the pump beam size of 240 – 250 µm which could have also resulted in higher order modes being produced by the Ho:YLF laser. Another factor was that the r = 100 mm output coupler mirror reflected the pump light back with a small focus in the crystal, most likely causing a non-uniform gain distribution, which further distorted the output beam profile. An M^2 analysis of the output beam was not conducted.

6.3.4 *Temporal response of the free-running linear resonator Ho:YLF laser*

Figure 6.12 shows the temporal behaviour of the free-running Ho:YLF laser (channel 2, blue) as a response to the QCW pump pulse produced by the Tm:$GdVO_4$ laser (channel 1, yellow).

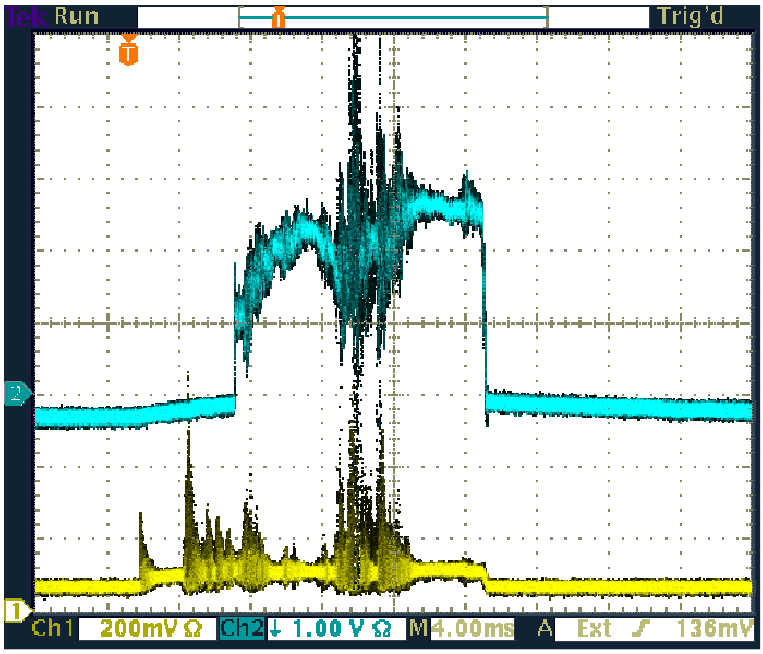

Figure 6.12: The temporal response of the Ho:YLF laser (channel 2, blue) in relation to the Tm:$GdVO_4$ pump laser pulse (channel 1, yellow).

It was observed that for the Ho:YLF laser in free-running mode pumped at maximum incident pump energy, the output pulse started operating approximately 5.6 ms after the start of the Tm:$GdVO_4$ pump laser pulse. The duration of the output pulse was slightly longer than 12 ms and demonstrated spiking behaviour which followed the spiking of the Tm:$GdVO_4$ laser pump pulse.

It was assumed that the spiking will not have a negative impact on *Q*-switched operation, in which case all the pump light would be integrated by the Ho:YLF gain medium to produce a single *Q*-switched output pulse.

6.3.5 *Q-switched operation of the linear resonator Ho:YLF laser*

The second set of experiments performed on the linear resonator Ho:YLF laser was in *Q*-switched mode with the AOM inserted in the linear resonator. For these experiments an output coupler reflectivity of 80% was selected to avoid high intra-cavity energy densities which may have led to optical damage to the resonator mirrors or the Ho:YLF laser crystal faces.

An example of the *Q*-switched output pulse measured with the fast InAs photodiode is shown in Figure 6.13. The measured full-width half-maximum pulse length was approximately 45 ns. Also shown in Figure 6.13 is an oscilloscope trace with a time scale which is 5 orders of magnitude slower showing the Ho:YLF laser output measured with the amplified PbSe detector which revealed the presence of pre-pulse laser oscillation. It is clear from the measurement that the laser already oscillated before the *Q*-switched pulse for approximately 12 ms, extracting the energy stored in the Ho:YLF crystal. Upon further investigation it was found that that the laser output changed from horizontal to vertical polarisation, i.e. from σ-polarisation of the Ho:YLF laser during pre-pulse oscillation to π-polarisation during the *Q*-switched pulse.

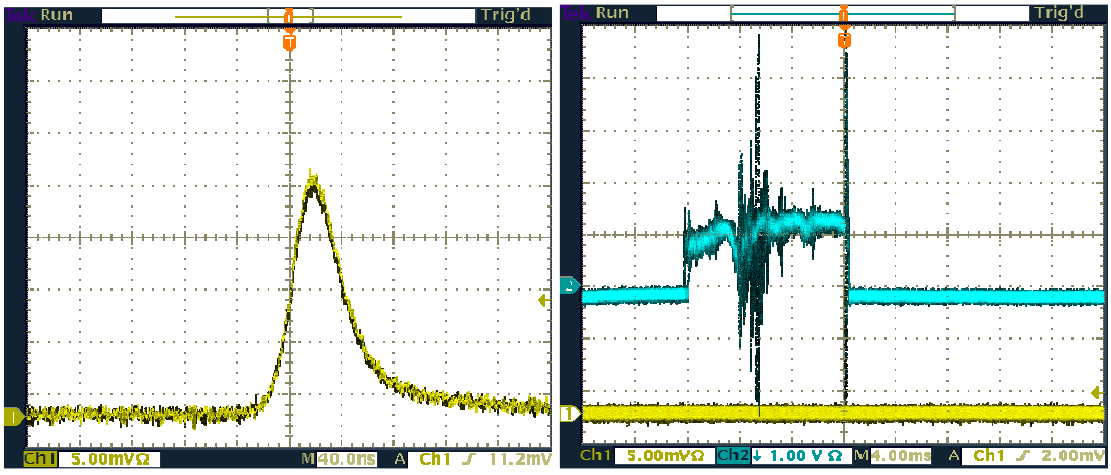

Figure 6.13: The Ho:YLF *Q*-switched output pulse of 45 ns (left, channel 1, yellow, 40 ns/div) which followed a 12 ms period of pre-pulse oscillation (right, channel 2, blue, 4 ms/div).

The observed behaviour was ascribed to the AOM not introducing sufficient loss to ensure complete hold-off before the intended *Q*-switch pulse is produced. The change in laser output polarisation also confirmed that the AOM had a lower diffraction loss in the vertical plane than in the horizontal plane, resulting in pre-pulse oscillation on the σ-polarisation followed by a *Q*-switched pulse with reduced energy on the π-polarisation when the AOM loss is switched off.

6.3.6 Conclusion on the linear resonator Ho:YLF laser

The linear resonator configuration performed very well in free-running mode but had limited performance when *Q*-switched.

The analysis of the free-running Ho:YLF laser indicated that the intra-cavity loss for this simple linear resonator design was very low. Furthermore, it was demonstrated that at the maximum available pump energy, an output energy of up to 13 mJ can be extracted from the Ho:YLF laser in free-running mode with the r = 100 mm output coupler mirrors. A 30% slope efficiency was recorded for output couplers with 80% and higher reflectivity.

Sub-optimum performance was, however, noted for the free-running linear resonator with respect to spiking in the temporal output of the Ho:YLF laser (which was expected due to the spiking of the Tm:$GdVO_4$ pump laser), and a non-Gaussian intensity beam profile which could have been caused by the strongly focussed back-reflected pump light from the r = 100 mm radius of curvature output coupler mirror.

The major limitations of the linear resonator Ho:YLF laser were observed when operated in *Q*-switched mode with the AOM in the cavity. It was demonstrated that the laser changed its output polarisation during the output pulse to avoid the polarised AOM loss, which resulted in pre-pulse extraction of energy. It was also subsequently observed that the AOM diffracted the pump beam transmitted through the Ho:YLF crystal, and in so doing prevented double-passing of the pump light and reducing the efficiency of the system.

6.4 Improved Ho:YLF laser resonator

The analysis of the linear resonator configuration led to the design of the three-mirror folded resonator as described below. The improved design was implemented to address the limitations of the first Ho:YLF laser.

6.4.1 Design of the folded three-mirror Ho:YLF laser resonator

The schematic diagram of the second Ho:YLF resonator configuration, which was a folded three-mirror resonator, is shown in Figure 6.14.

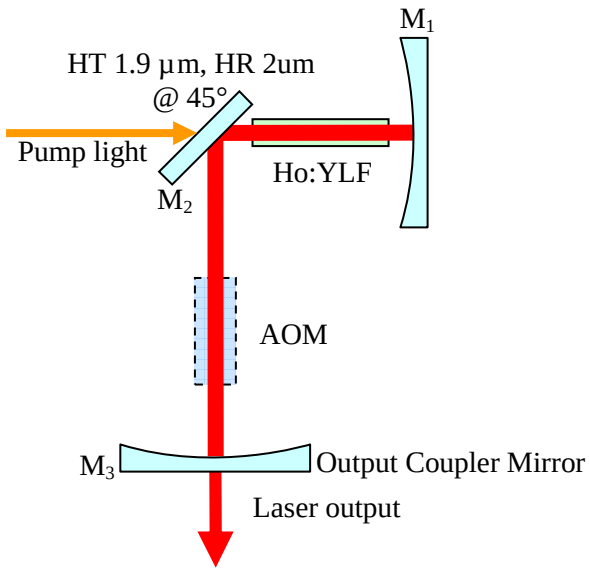

Figure 6.14: Schematic diagram of the folded three-mirror Ho:YLF laser resonator.

Mirror M_1 was a high reflector for both the laser and pump wavelength. The radius of curvature of 500 mm as well as its distance from the Ho:YLF crystal were chosen such that the curved mirror reflected the pump light back into the crystal to the same size and focus position as the incident pump light, enabling a double-pass pump design.

The 45° mirror M_2 had a high transmission for the pump wavelength on both s-polarisation and p-polarisation while for the laser light it had a high reflectivity for s-polarisation and 30% transmission for p-polarisation. This arrangement was used to suppress laser oscillation in the plane of the resonator. By orientating the Ho:YLF crystal c-axis either parallel or perpendicular to the resonator plane, it was possible to force oscillation of the Ho:YLF laser on either the σ-polarisation or π-polarisation, respectively.

For *Q*-switched operation of the folded three-mirror Ho:YLF resonator the AOM was placed between M_2 and the output coupler mirror M_3. The benefit of this arrangement was that the AOM neither influenced the incident nor the back-reflected pump light, in contrast to the linear Ho:YLF resonator described previously. The AOM was orientated such that it introduced a loss for the s-polarisation (vertical) of the resonator.

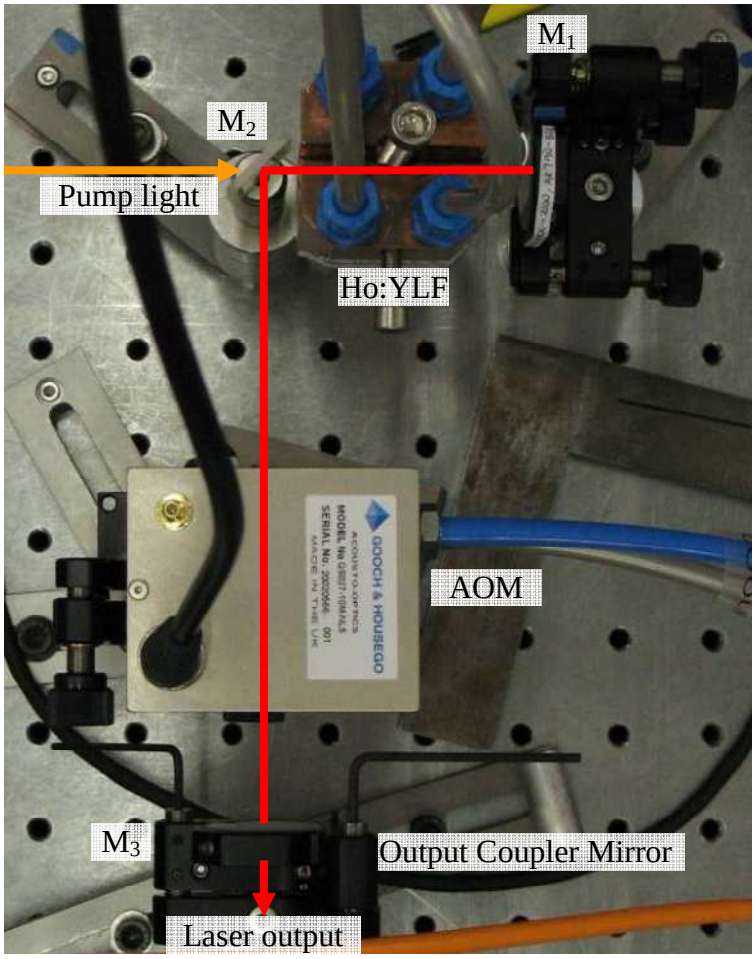

Figure 6.15: Top view photo of the three-mirror folded Ho:YLF laser resonator.

A photo of the three-mirror resonator is shown in Figure 6.15. The optical resonator was chosen to be 200 mm in length in order to establish, together with the 500 mm radius of curvature high reflector M_1 and 200 mm radius of curvature output coupler M_3, a fundamental laser mode radius of approximately 200 µm in the crystal. When the AOM was inserted in the resonator, the change in optical length resulted in a calculated fundamental mode radius of 220 µm in the laser crystal. This mode size was the desired size to match the pump beam size of 240-250 µm in the Ho:YLF laser crystal.

It was expected that the folded three-mirror Ho:YLF laser would perform better than the linear resonator, since the following were incorporated in the design:

- The back reflected pump light could be optimally utilised by implementing a 100% reflectivity mirror with 500 mm radius of curvature to reproduce the same size focus in the Ho:YLF crystal for the second pass of the pump light.

- The polarisation of the folded three-mirror resonator could be controlled by the 30% loss introduced by the 45° fold mirror for the p-polarisation of the resonator.
- The AOM was placed in the resonator where it could not negatively influence the pump beam, but only interacted on the Ho:YLF resonator beam.
- The fundamental resonator mode size could be chosen to be slightly smaller than the pump beam size by selecting a 200 mm radius of curvature output coupler.

The experiments discussed below were executed to evaluate the performance of the folded three-mirror resonator Ho:YLF laser.

6.4.2 Analysis of the free-running folded three-mirror Ho:YLF laser

As described above, the Ho:YLF laser was first investigated and analysed in free running mode. Initially the Ho:YLF crystal c-axis was orientated along the s-polarisation of the resonator (vertical) so that the laser can operate on the strong π-polarisation of Ho:YLF while oscillation on the σ-polarisation was suppressed.

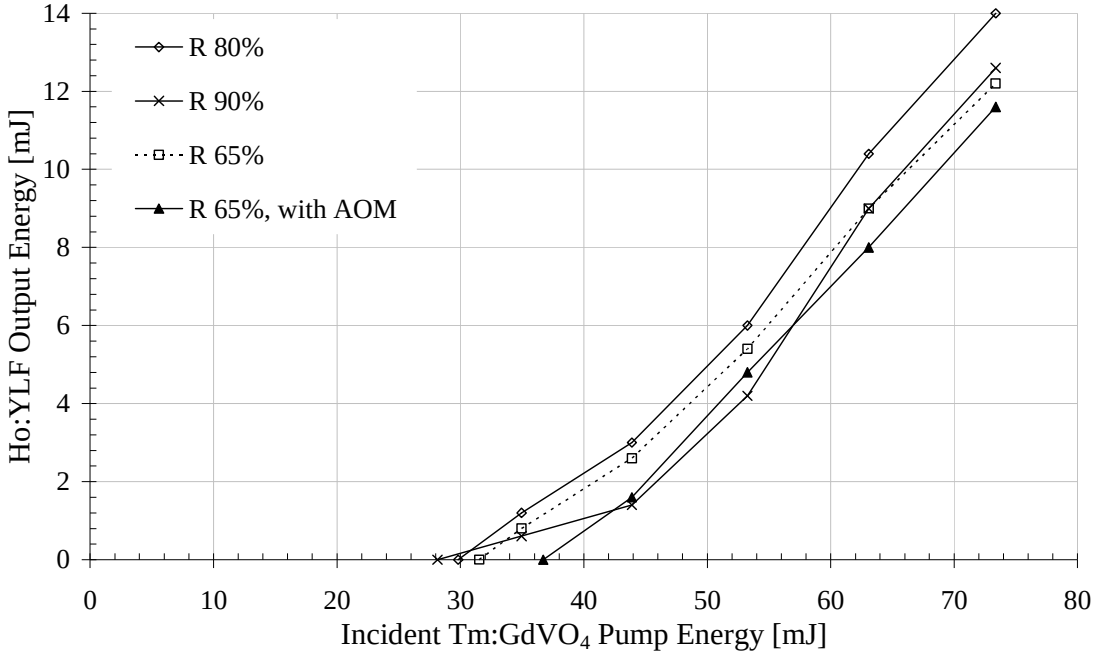

Figure 6.16: Output energy of the free-running folded three-mirror Ho:YLF laser for three output coupler reflectivity values and with the AOM placed in the cavity.

For the chosen output coupler radius of curvature of 200 mm there were only three reflectivity values available, namely 65%, 80% and 90%. Figure 6.16 shows the output energy of the free-running Ho:YLF laser for the three available output couplers as a

function of incident pump energy, as well as for the case where the AOM was inserted in the R 65% cavity (without the AOM being operated).

The measurements indicated that the folded three-mirror resonator performed slightly better in terms of pulse energy and efficiency compared to the original linear Ho:YLF cavity. The slope efficiencies, measured above 40 mJ of pump energy, were higher with values of 38% and 39% respectively for the R 80% and R 90% reflectivity output couplers. The slope efficiency of the Ho:YLF laser with the R 65% output coupler reflectivity was 32%, also when the AOM (with no RF applied) was inserted in the cavity, albeit with a slightly higher threshold pump energy. The maximum output energy for the free-running laser was 14 mJ with the R 80% mirror while the Ho:YLF laser with the R 65% mirror and AOM in the cavity (with no RF applied) produced 11.6 mJ in a 13.9 ms long output pulse.

Table 6.1: Temporal response of the free-running Ho:YLF laser with the R 90% output coupler mirror at increasing incident pump energy.

Pump energy [mJ]	**Ho:YLF output energy [mJ]**	**Temporal response** Ch1 (yellow): $Tm:GdVO_4$ pulse Ch2 (blue): Ho:YLF output pulse	**Pump energy [mJ]**	**Ho:YLF output energy [mJ]**	**Temporal response** Ch1 (yellow): $Tm:GdVO_4$ pulse Ch2 (blue): Ho:YLF output pulse
28.1	Threshold	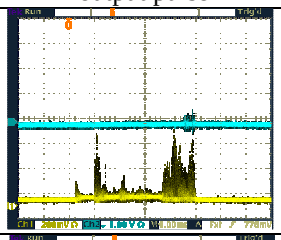	53.3	4.2	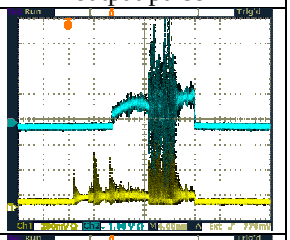
35	0.6 mJ	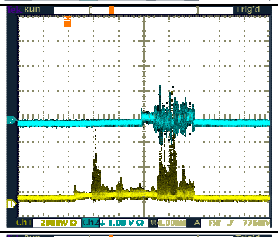	63.1	9.0	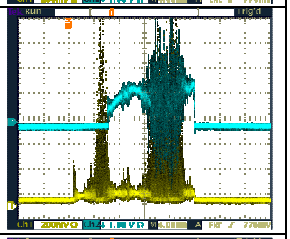
43.9	1.4	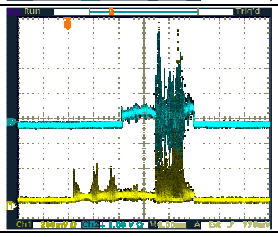	73.4	12.6	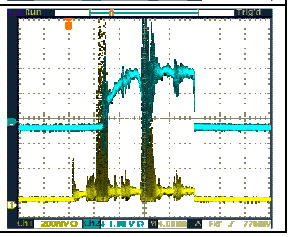

The output pulses produced by the free-running Ho:YLF laser were evaluated at different incident pump energies. For example, Table 6.1 shows oscilloscope traces for the laser with the R 90% output coupler at six measured data points. It can be seen

from this table that the time delay between the pump pulse and the Ho:YLF output pulse depended on the incident pump energy. At maximum incident pump energy the build-up time was approximately 4.8 ms and the output pulse duration was 14.6 ms.

Furthermore, it can be seen in Table 6.1 that the Ho:YLF also produced spiked output when the Tm:$GdVO_4$ pump laser spiked. It was once again assumed that the spiking will not have a negative impact on *Q*-switched operation, since, if pre-pulse oscillation can be avoided, all the pump light will integrated by the Ho:YLF gain medium to produce a single *Q*-switched output pulse.

Table 6.2: Intensity beam profile at maximum output energy of the folded three-mirror Ho:YLF laser for three different output coupler reflectivity values, operated in free-running mode.

Resonator output coupler reflectivity	Maximum free-running output energy [mJ]	Intensity beam profile
R 65%	12.2	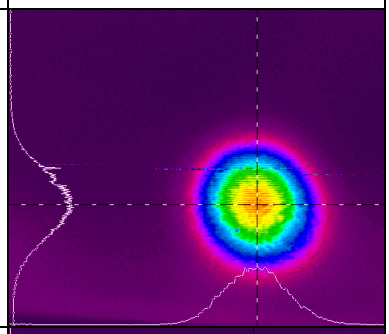
R 80%	14.0	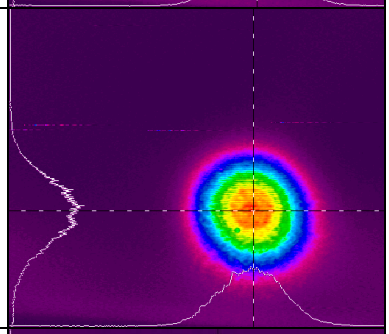
R 90%	12.6	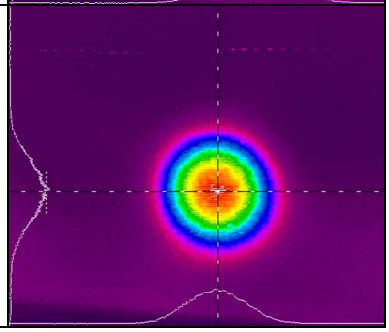

The intensity beam profile of the Ho:YLF laser was recorded at maximum output energy for each of the output coupler reflectivity values R 65%, R 80% and R 90%, as

listed in Table 6.2. It can be seen that in each case the beam was circular with a Gaussian distribution in both planes. Even though M^2 measurements were not conducted, it was concluded from the good quality beam profiles that the folded three-mirror Ho:YLF resonator was optimally designed and set up, in contrast to the first linear Ho:YLF resonator.

Since the performance of the folded three-mirror resonator was similar with all three available output coupler reflectivity values, it was decided to use the 65% reflectivity output coupler for the *Q*-switched experiments to minimise the risk of laser damage due to possible high intra-cavity energy densities. It was also demonstrated that the insertion of the AOM increased the threshold pump energy only slightly from 31.5 mJ to 36.7 mJ while the slope efficiency remained approximately 32%.

6.4.3 Output energy of the Q-switched folded three-mirror Ho:YLF laser

In the next set of experiments the folded three-mirror Ho:YLF laser was operated in *Q*-switched mode. In order to do so, the AOM modulator was aligned for maximum diffraction loss on the vertical polarisation of the resonator mode. This arrangement, together with the initial vertical orientation of the Ho:YLF crystal c-axis, allowed *Q*-switched operation on the π-polarisation of the Ho:YLF laser. The output energy and pulse length of the *Q*-switched Ho:YLF laser is shown in Figure 6.17.

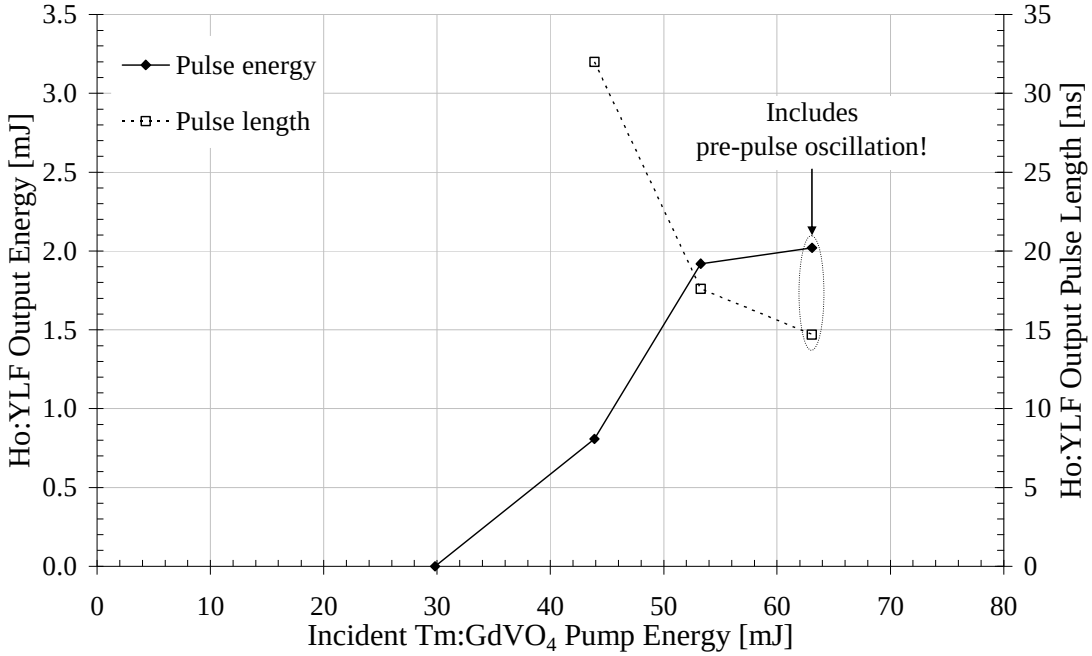

Figure 6.17: Output energy and pulse length of the *Q*-switched Ho:YLF laser based on the folded three-mirror resonator.

The folded three-mirror Ho:YLF laser operated in *Q*-switched mode extracting the stored energy in a short laser pulse. At 53.3 mJ of incident pump energy the Ho:YLF laser produced 1.92 mJ in a 17.6 ns pulse with a calculated peak power of 109 kW. Pumping with more energy resulted in the Ho:YLF laser exhibiting double pulsing and pre-pulse oscillation, which is described below.

6.4.4 Output pulses of the Q-switched folded three-mirror Ho:YLF laser

The recorded *Q*-switched output pulses of the folded three-mirror Ho:YLF laser are shown in Figure 6.18 and Figure 6.19 when pumped with 53.3 mJ and 63.1 mJ, respectively. Also shown in the figures are oscilloscope traces of the Ho:YLF laser output with a time scale which is significantly slower, measured with the amplified PbSe photodiode to detect the presence of pre-pulse oscillation output.

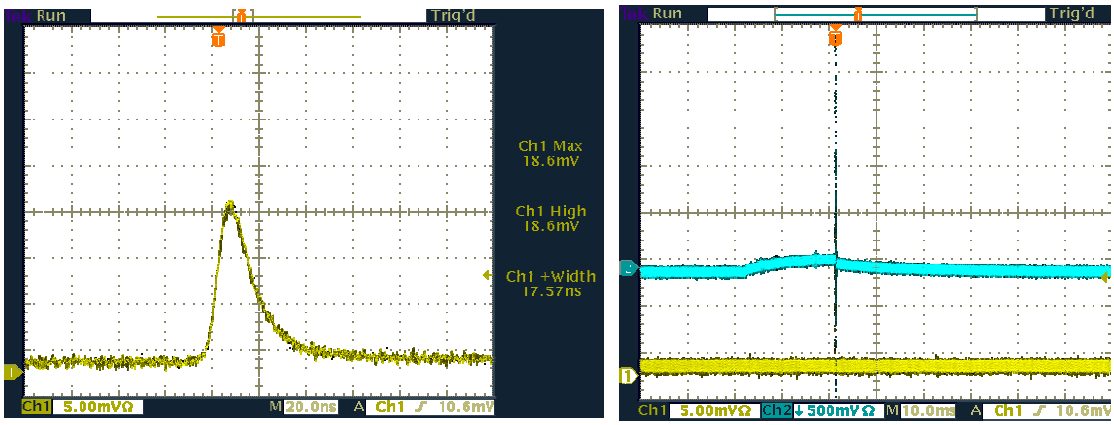

Figure 6.18: Temporal response over a short (left, 20 ns/div) and long (right, 10 ms/div) time scale of the *Q*-switched three-mirror folded Ho:YLF laser pumped with 53.3 mJ. No pre-pulse oscillation was observed.

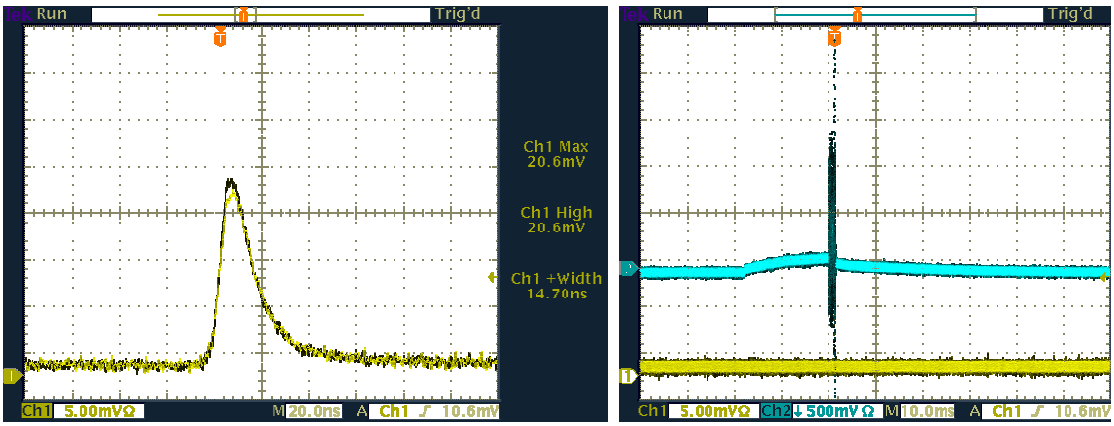

Figure 6.19: Temporal response over a short (left, 20 ns/div) and long (right, 10 ms/div) time scale of the *Q*-switched folded three-mirror Ho:YLF laser pumped with 63.1 mJ, showing the presence of pre-pulse oscillation.

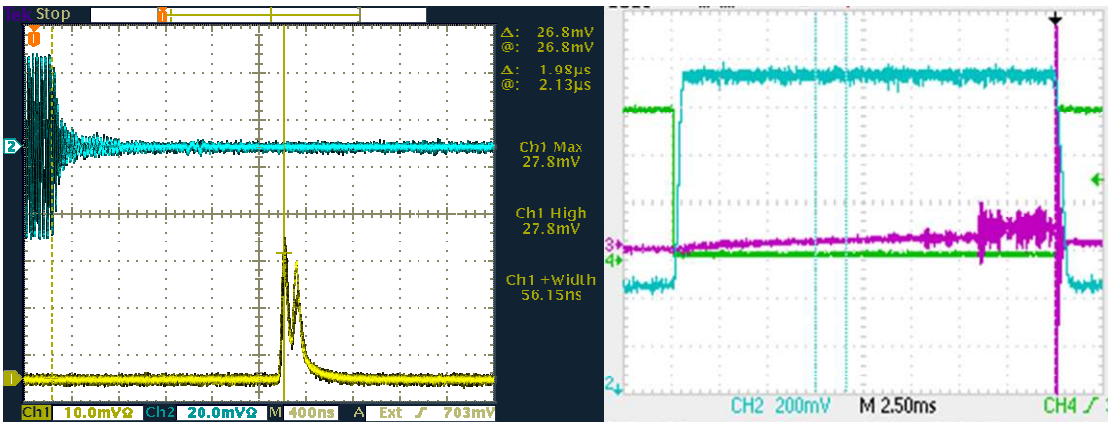

Figure 6.20: Temporal response over a short (left, 400 ns/div) and long (right, 2.5 ms/div) time scale of the *Q*-switched folded three-mirror Ho:YLF laser pumped with 63.1 mJ, showing the presence of double pulsing and pre-pulse oscillation.

It is seen in Figure 6.18 that pre-pulse oscillation was not present when the laser produced 1.9 mJ output energy at 53.3 mJ pump energy. However in Figure 6.19 it is seen that at 63.1 mJ of pump energy the Ho:YLF laser definitely exhibited pre-pulse oscillation and in Figure 6.20 it is seen that the laser intermittently produced double pulses at the same pump energy. These parasitic phenomena caused a reduction in laser efficiency at high incident pump energy.

Upon further investigation it was found that the pre-pulse oscillation occurred due to the limited diffraction loss introduced by the AOM. At high incident pump energy the AOM could not induce oscillation hold-off. Unfortunately the RF input driver for the AOM *Q*-switch could not produce more than 60 W of RF power, even though the AOM was rated for 100 W. If more RF power was available it would have been possible to increase the diffraction loss of the AOM to prevent pre-pulse oscillation at higher incident pump energies.

6.4.5 Q-switched folded three-mirror Ho:YLF laser on σ-polarisation

It was attempted to scale the output energy of the Ho:YLF laser by operating it on the σ-polarisation which has a lower emission cross section in Ho:YLF [1]. This was achieved by rotating the Ho:YLF crystal c-axis by 90° to orientate it parallel to the resonator p-polarisation (horizontal) which had a 30% loss on the 45° resonator fold mirror. The high loss (horizontal) forced the laser to operate on the σ-polarisation (vertical) of the Ho:YLF laser.

The Tm:$GdVO_4$ pump beam polarisation orientation was also rotated by 90° with the half-wave plate to ensure that the Ho:YLF crystal absorbed the pump light along the π-polarisation which has a higher absorption cross section than the σ-polarisation in Ho:YLF at the 1.892 µm pump wavelength.

The maximum output energy achieved with the folded three-mirror Ho:YLF laser operated in *Q*-switch mode on σ-polarisation, while producing stable output pulses, was 2.1 mJ in a 47.7 ns pulse which was a calculated peak output power of 44 kW. Increasing the pump energy beyond 53.3 mJ again caused pre-pulse oscillation and double pulsing, as was the case for the laser operating on π-polarisation. The temporal response of the Ho:YLF laser on σ-polarisation at 53.3 mJ and at 63.1 mJ of pump energy is shown in Figure 6.21 and Figure 6.22, respectively.

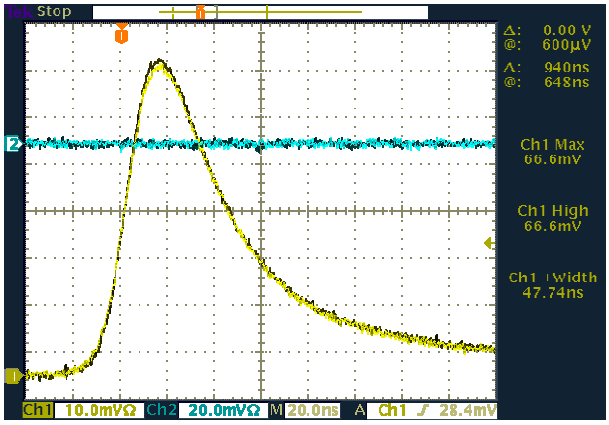

Figure 6.21: *Q*-switch pulse (channel 1, yellow) of the Ho:YLF laser operating on σ-polarisation, at 53.3 mJ of pump energy.

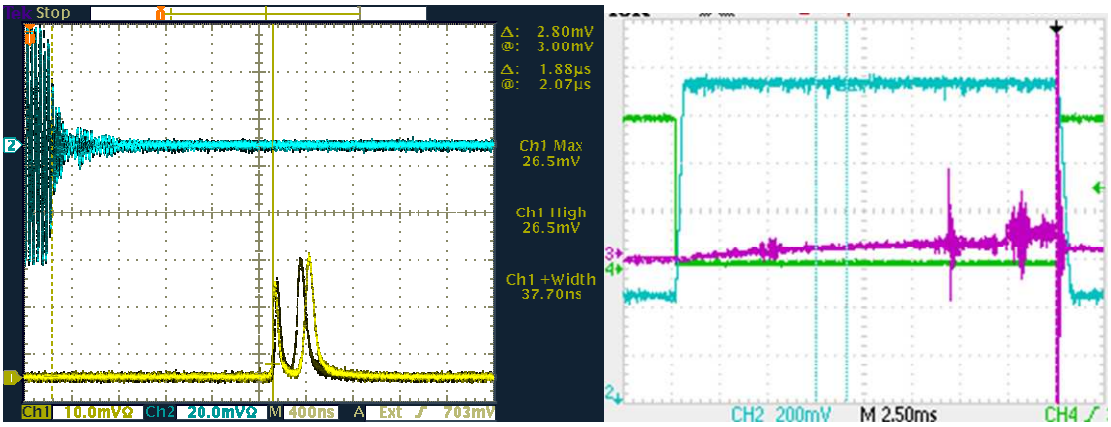

Figure 6.22: Double pulsed output (left, channel 1, yellow, 400 ns/div) and pre-pulse oscillation (right, channel 3, purple, 2.5 ms/div) of the Ho:YLF laser operating on σ-polarisation, at 63.1 mJ incident pump energy.

It was concluded from these experiments that the output energy of the Ho:YLF laser cannot be scaled significantly by operating on σ-polarisation, since the available AOM and RF driver could not induce oscillation hold-off at high incident pump energy, not even on the σ-polarisation which has a weaker emission cross section.

6.4.6 Intensity beam profile of the Q-switched folded three-mirror Ho:YLF laser

The measured intensity beam profiles of the *Q*-switched Ho:YLF laser operating on π-polarisation and on σ-polarisation are shown in Figure 6.23 at maximum stable output energy.

For both laser configurations the output beam was circular with a near-Gaussian distribution in both planes. A secondary beam was observed just next to the main Ho:YLF laser beam. It was confirmed through experiments that the secondary beam was a small fraction of the double-passed pump light, reflected off the 45° resonator fold mirror, which was also incident on the beam profile camera. M^2 measurements were not conducted on the Ho:YLF output beam. However, it was estimated from the intensity beam profiles that the *Q*-switched folded three-mirror Ho:YLF laser had a good beam quality.

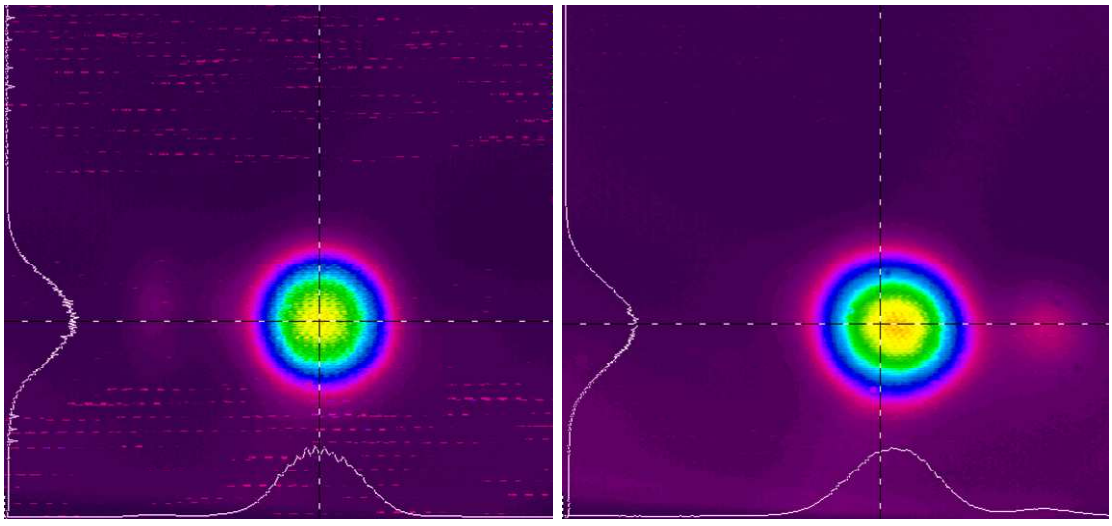

Figure 6.23: Intensity beam profile of the *Q*-switched Ho:YLF laser on π-polarisation (left) and σ-polarisation (right) at maximum stable output energy. A small fraction of the back reflected pump beam is also visible next to the main Ho:YLF laser beam.

6.4.7 Wavelength of the Q-switched folded three-mirror Ho:YLF laser

The central wavelength λ_c of the Ho:YLF laser was measured with a monochromator together with a photodiode sensitive over a wide wavelength range (1.5 – 4 µm). The

measured Ho:YLF laser wavelength is indicated in Figure 6.24 as line ❶ on the graph of the emission cross section (σ_{em}) of Ho:YLF for the $^5I_7 - {}^5I_8$ transition [1].

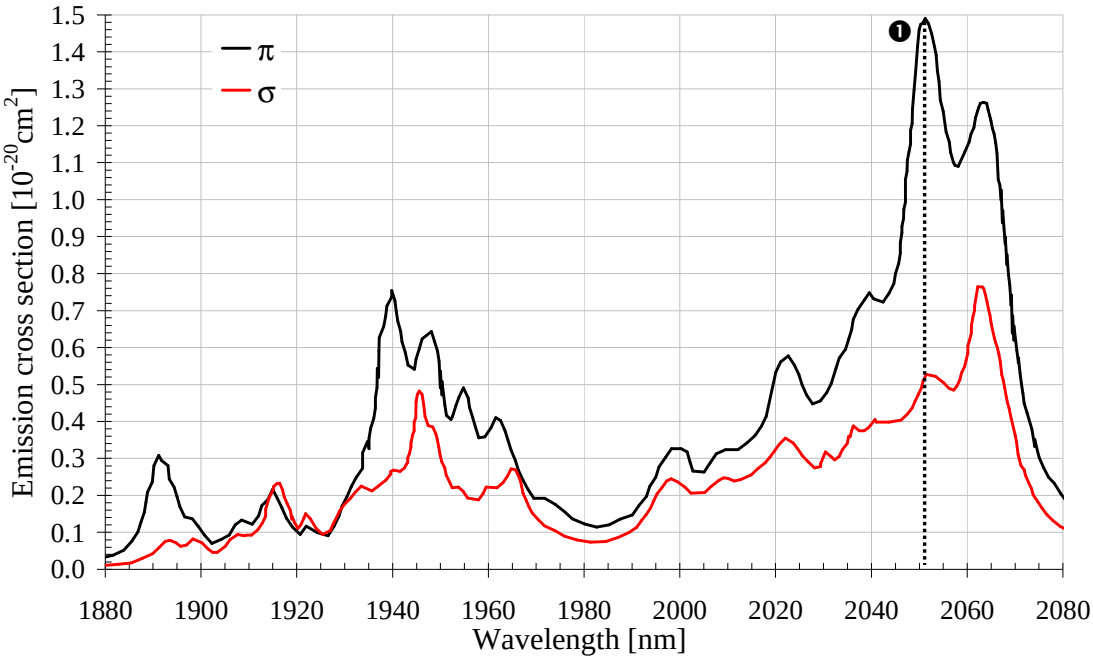

Figure 6.24: The polarisation resolved emission cross section of Ho:YLF [1] and the measured output wavelength (line ❶) of the *Q*-switched Ho:YLF laser.

The *Q*-switched Ho:YLF centre wavelength when operated on π-polarisation was confirmed to be on the strong emission peak at 2051 nm. The wavelength was not measured when the laser was operated on σ-polarisation but it was assumed to be on the σ-polarisation emission peak located at 2064 nm.

6.4.8 Conclusion on the folded three-mirror resonator Ho:YLF laser

The folded three-mirror resonator was judged to be a well-designed Ho:YLF laser which could be operated in free-running mode as well as in *Q*-switched mode.

In free-running mode the Ho:YLF laser exhibited spiking behaviour which was directly correlated to the temporal spiking of the Tm:$GdVO_4$ pump laser. Up to 14 mJ output energy was demonstrated for the free-running laser with the 80% reflectivity output coupler at the maximum pump energy of 73 mJ. With the 65% reflectivity output coupler and with the AOM in the cavity, the output energy was 11.6 mJ while the measured intensity beam profiles indicated a good beam quality. This experiment demonstrated that the folded three-mirror resonator, with a designed resonator mode size that matched the pump beam size, was optimally aligned and efficiently utilised

the back-reflected pump light without introducing distortions in the circular Ho:YLF output beam with Gaussian intensity profiles.

The implementation of the 45° resonator fold mirror was essential to efficiently operate the Ho:YLF laser in *Q*-switched mode. The mirror introduced a 30% loss on the horizontal polarisation, which, at limited pump energy, prevented the laser from operating on the "wrong" polarisation during the pump pulse while the acousto-optic modulator induced oscillation hold-off on the vertical polarisation. Upon switching off the AOM diffraction loss right after the pump pulse, the Ho:YLF laser produced a vertically polarised, short duration, *Q*-switched pulse on either the π-polarisation or σ-polarisation of Ho:YLF, depending on the orientation of the Ho:YLF crystal c-axis with respect to the resonator plane.

The folded three-mirror resonator with a 65% reflectivity output coupler produced up to 1.9 mJ output energy in a stable *Q*-switched pulse of duration 17.6 ns when operating on π-polarisation at 2051 nm wavelength. When operating on σ-polarisation the Ho:YLF laser produced 2.1 mJ in a 47.7 ns pulse. In both configurations the output beams were circular with near-Gaussian intensity beam profiles.

Pumping with more than 53.3 mJ of energy from the QCW Tm:$GdVO_4$ laser at 5 Hz in a 20 ms pulse resulted in double pulsing and pre-pulse oscillation of the *Q*-switched Ho:YLF laser, when operated either on π-polarisation or on σ-polarisation. The maximum pump energy of 73.4 mJ available form the Tm:$GdVO_4$ laser could therefore not be utilised in this resonator configuration.

6.5 Discussion of experimental results

A quasi-continuous-wave Tm:$GdVO_4$ laser was developed to specifically pump a Ho:YLF laser on the 1.892 µm wavelength absorption peak of the π-polarisation, as described in Chapter 5.

To execute the experiments described in this chapter, an optical layout was designed and implemented to deliver the Tm:$GdVO_4$ laser output as a pump beam of radius 240 - 250 µm in the available, 40 mm long, 0.5% doped Ho:YLF crystal. An optical isolator was used to prevent back reflected pump light, originating from the double-pump-pass design of the Ho:YLF laser, to cause further instabilities in the Tm:$GdVO_4$

laser output. It was demonstrated during the experiments that this pump arrangement worked well, but at the cost of reducing the available incident pump energy for the Ho:YLF laser up to a maximum of 73 mJ. Scaling the pump energy to higher values would have increased the risk of optical damage or thermal fracture in the Tm:$GdVO_4$ laser.

A mount was designed for the Ho:YLF crystal which could be water cooled. However, during the experiments the average pump power into the Ho:YLF crystal was less than 400 mW due to the low duty cycle of 5% of the Tm:$GdVO_4$ laser. Because of the low average pump power, it was not required to actively cool the crystal mount. The crystal mount design was however used with great effect in subsequent developments of high average power and high-energy YLF lasers [2, 3, 4], which are also discussed in Chapter 8.

Two different resonator configurations were implemented during the experiments. The first resonator was based on a simple linear design while the second Ho:YLF resonator configuration was a right-angle folded three-mirror resonator.

The linear resonator configuration was not ideal for scaling the output energy in *Q*-switched mode with the acousto-optic modulator in the cavity. Firstly, the AOM also diffracted the transmitted pump light, which prevented efficient double-pass pumping of the Ho:YLF crystal. This, together with the short radius of curvature of the output coupler mirror that defined a fundamental mode size to be smaller than the pump beam, which also acted as pump back reflector, negatively influenced the output beam quality of the Ho:YLF laser. However, the most important limitation of the linear resonator design was that there was no additional polarisation control of the Ho:YLF laser which led to pre-pulse oscillation on the σ-polarisation while the AOM induced oscillation hold-off on the π-polarisation. This limited the energy that could be extracted as a short *Q*-switched pulse on π-polarisation. It was argued that the resonator design should be improvement taking these observations into account. This resulted in the folded three-mirror resonator design.

In free-running mode the folded three-mirror Ho:YLF laser had slightly better performance than the initial linear resonator. The demonstration of 14 mJ of output energy at maximum available pump energy from the QCW Tm:$GdVO_4$ laser, while

maintaining a circular Gaussian intensity beam profile, was evidence that the resonator mode size was well matched to the pump beam size, that the resonator was optimally aligned and that it efficiently utilised the back-reflected pump light.

It was demonstrated that the resonator 45° fold mirror which had a high loss on the p-polarisation of the laser light was essential to obtain *Q*-switched pulses from the Ho:YLF laser without pre-pulse oscillation, up to a pump energy of 53.3 mJ. With this improved laser configuration, 1.9 mJ output energy in a 17.6 ns pulse was achieved on the Ho:YLF π-polarisation, and on σ-polarisation 2.1 mJ was demonstrated in a 47.7 ns pulse.

Unfortunately, the good performance of the three-mirror resonator could however not be scaled to higher energies due to the onset of double-pulsing and pre-pulse oscillation. It was concluded that these parasitic processes occurred due to the limited diffraction loss introduced by the acousto-optic modulator. It would have been beneficial in this laser configuration if more RF power was available to drive the acousto-optic modulator harder to increase the diffraction loss which would have led to laser hold-off at the values of incident pump energy which were available from the Tm:$GdVO_4$ laser. Recommendations for improving the performance of the system are discussed in Chapter 7.

6.6 Conclusion

The experiments described in this chapter are significant since it is the first demonstration of a Tm:$GdVO_4$ laser pumping a Ho:YLF laser. It is believed to be the only demonstration of a Ho^{3+} laser pumped by Tm:$GdVO_4$ despite the fact that this possible approach has been proposed in the literature. A photo of the arrangement on the optical table that culminated the demonstration of the Tm:$GdVO_4$ laser pumping the Ho:YLF laser is shown in Figure 6.25.

In order to demonstrate the 2 µm laser system, it was required to firstly develop the Tm:$GdVO_4$ laser and design it such that it operated on 1.892 µm, an absorption peak of Ho:YLF. Furthermore, an optical arrangement was implemented to couple the Tm:$GdVO_4$ pump light into the Ho:YLF resonator.

Two Ho:YLF resonator designs were evaluated in free-running mode and in *Q*-switched mode, the first being a simple linear resonator with limited performance, which subsequently led to the development of a folded three-mirror Ho:YLF laser. The highest energy produced by the *Q*-switched Ho:YLF laser operating on π-polarisation was 1.9 mJ in a 17.6 ns pulse and on σ-polarisation it was 2.1 mJ in a 47.7 ns pulse.

Figure 6.25: The laboratory demonstration of the 2 µm laser system based on the Ho:YLF oscillator pumped by the Tm:$GdVO_4$ laser, also showing the diagnostic equipment.

Even though the performance of the Ho:YLF laser was somewhat improved with the second resonator design, it was still limited by the onset of double-pulsing and pre-pulse oscillation at higher pump energies. The cause of this was identified. It would have been beneficial if the acousto-optic modulator produced higher diffraction losses to induce oscillation hold-off during the high energy pump pulse from the Tm:$GdVO_4$ laser.

Despite the limitations of the Ho:YLF laser end-pumped by the custom-developed Tm:$GdVO_4$ laser, the research goal of developing an all-solid-state 2 µm laser system has been accomplished with the experimental demonstration of the system described here. This initial research work directed the way towards the development of high-energy Ho:YLF lasers pumped with alternative high average power Tm^{3+} doped lasers, as described in Chapter 8.

6.7 References

[1] Brian M. Walsh, Norman P. Barnes, Baldassare Di Bartolo, "Branching ratios, cross sections, and radiative lifetimes of rare earth ions in solids: Application to Tm3+ and Ho3+ ions in $LiYF^4$", *Journal of Applied Physics*, vol. 83, no 5, pp. 2772-2787, 1 March 1998.

[2] W. Koen, C. Bollig, H. Strauss, M. Schellhorn, C. Jacobs and M. J. D. Esser, "Compact Fibre-Laser-Pumped Ho:YLF Oscillator-Amplifier System," *Applied Physics B* **99** (1-2) 101-106 (April 2010).

[3] C. Bollig, M. J. D. Esser, C. Jacobs, W. Koen, D. Preussler, K. Nyangaza and M. Schellhorn, "70 mJ Single-Frequency *Q*-Switched Ho:YLF Ring Laser – Amplifier System Pumped by a Single 82-W Tm Fibre Laser," *Middle-Infrared Coherent Sources*, Trouville, France, 8-12 June 2009, Mo3 ***(invited)*** (2009).

[4] C. Bollig, C. Jacobs, M. J. D. Esser, and H. M. von Bergmann "Power and energy scaling of a diode-end-pumped Nd:YLF laser through gain optimization" *Optics Express* **18** (13), 13993-14003 (Jun 2010).

Chapter 7

Conclusions and Recommendations

To fulfil the goal of the research project a diode-end-pumped Tm:$GdVO_4$ laser was developed as a suitable pump source for a *Q*-switched Ho:YLF laser. In this chapter, a review of the significant experimental results achieved is presented. The review is placed in context with the results that have been demonstrated prior to this work and reported in the literature for this promising laser material. One significant conclusion is that there remains scope for further scaling of the output power of the Tm:$GdVO_4$ laser and the output energy of the *Q*-switched Ho:YLF laser. A number of recommendations are made to achieve high-energy output utilising the concept of a Tm^{3+} doped solid-state laser pumping a Ho^{3+} 2 µm laser.

7.1 Summary of significant results

7.1.1 Diode-end-pumped Tm:$GdVO_4$ laser operated over a 100 nm spectral range

It was shown that by using detailed spectroscopic data which was measured for Tm:$GdVO_4$, quite accurate calculations can be made of the expected output parameters of a diode-end-pumped Tm:$GdVO_4$ laser. The measured values of laser threshold, polarisation and wavelength were very close to the theoretically predicted values for the laser with a 5% transmission output coupler. Also with a 72% transmission output coupler, the oscillation wavelength and polarisation of the Tm:$GdVO_4$ laser were accurately predicted.

It was shown and experimentally verified that this Tm:$GdVO_4$ laser can be efficiently operated with multi-watt output at the short wavelength of 1818 nm merely through the selection of a high output coupling value, making it the first time that multi-watt

operation at 1818 nm is achieved with a Tm:$GdVO_4$ laser. With reference to the reported wavelength ranges of diode-pumped Tm^{3+} doped solid-state lasers in Section 2.3.2, this Tm:$GdVO_4$ laser produced the shortest wavelength without the use of intra-cavity tuning elements. The maximum QCW output power was 8.7 W and the energy of 175 mJ in a 20 ms pulse produced by the laser operating at 1915 nm is the highest reported output energy from a diode-end-pumped QCW Tm:$GdVO_4$ laser.

It is unclear why thermal fracture of the Tm:$GdVO_4$ laser crystal occurred at relatively low continuous-wave pump power of 11.6 W at 803 nm for a pump beam radius of 220 µm. The maximum CW output power of 1.5 W is less than values which have been reported in the literature for high quality Floating Zone grown Tm:$GdVO_4$ crystals. A possible reason for the limitation observed here could be the material quality of the commercial Czochralski grown crystals used during the experiments. Alternatively, fundamental processes such as upconversion and cross relaxation, which have not been studied extensively in Tm:$GdVO_4$, could have led to excessive heat load and ultimate thermal fracture at high pump powers.

7.1.2 Development of a dual-end-pumped Tm:$GdVO_4$ laser at 1892 nm

The theoretical laser threshold calculations, which were verified experimentally, were used to design a Tm:$GdVO_4$ laser to operate at 1892 nm as pump source for a Ho:YLF laser. A 95% reflectivity mirror was used as resonator output coupler and an intra-cavity Brewster plate was inserted to operate the Tm:$GdVO_4$ laser on the π-polarisation to achieve the desired wavelength range. An additional intra-cavity 100 µm etalon was required to fine-tune the laser wavelength onto the 1892 nm absorption peak of Ho:YLF.

The dual-end-pumped Tm:$GdVO_4$ laser was designed, implemented and analysed in detail with respect to the oscillation threshold values, output energy, temporal output and intensity beam profiles. At 5 Hz repetition rate the laser produced 83 mJ in a QCW pulse of 19 ms duration, which was a unique laser system capable of pumping a Ho:YLF laser.

7.1.3 First demonstration of a Tm:$GdVO_4$ laser pumped Ho:YLF laser

The climax of the research was the first demonstration of a Ho^{3+} laser pumped by Tm:$GdVO_4$ in the form of the free-running and *Q*-switched Ho:YLF laser.

To demonstrate the 2 µm laser system, it was required to couple the 1892 nm Tm:$GdVO_4$ pump light into the Ho:YLF resonator, the optical arrangement of which was described in detail. The first Ho:YLF resonator investigated was a simple linear resonator with low internal losses, but with limited performance when operated in *Q*-switched mode. An improved three-mirror resonator was subsequently designed which led to the successful demonstration of the Tm:$GdVO_4$ pumped Ho:YLF laser system. It was experimentally verified that the 2 µm wavelength *Q*-switched Ho:YLF laser could be operated either on the π-polarisation or on the σ-polarisation, which produced 1.9 mJ in a 17.6 ns pulse and 2.1 mJ in a 47.7 ns pulse, respectively.

7.2 Recommendations for future work

Based on the thorough experimental evaluation of several Tm:$GdVO_4$ laser configurations, as well as the Ho:YLF laser pumped by a 1892 nm Tm:$GdVO_4$ laser, a number of potential improvements were identified that could be implemented to scale the performance of both laser systems. These recommendations are discussed for both the Tm:$GdVO_4$ laser material and the Ho:YLF laser system.

7.2.1 Tm:$GdVO_4$

The output power of the demonstrated Tm:$GdVO_4$ lasers were mainly limited by high intra-cavity power densities leading to optical damage and by the onset of thermal fracture of the laser crystal. Since this material is still relatively unknown in the literature, it is difficult to calculate the limit imposed by thermal fracture. Although new mathematical models have been developed to explain thermal stress and fracture during QCW operation of end-pumped solid-state lasers [1], it remains uncertain what is the major contributor to thermal loading in this laser material. If possible, the fundamental properties of Tm:$GdVO_4$ material should be further explored and experimentally verified before a laser design can be finalised to scale the output power of lasers based on Tm:$GdVO_4$.

In addition to the need to determine and verify all relevant thermal, mechanical and optical properties of Tm:$GdVO_4$, there are several practical solutions that can be explored that could produce higher output powers. These options include the following:

- **Crystals of higher quality.** It is doubtful and difficult to determine if crystals of the highest optical quality were used during the experimental evaluation,

since only one supplier (Crystech, China) was able to provide this type of laser material on a commercial basis. Higher quality crystals, including Floating Zone grown crystals, could potentially be obtained through research collaborations, which might result in substantial improvements in damage threshold and output power performance.

- **Crystals with lower doping concentration.** In general the doping concentration of a diode-pumped Tm^{3+} laser should be high for the "2-for-1" cross relaxation process to be efficient. However, the typical values of 2% to 3% might not be optimal for Tm:$GdVO_4$, which should be determined through laser material studies. Lower doping could lead to lower thermal load while maintaining adequate absorption and cross relaxation coefficients for efficient laser diode pumping.
- **Crystals in slab geometry.** It is well known that better thermal management can be achieved by using a laser crystal which has a slab geometry (i.e. crystal width >> height) which has been demonstrated to be applicable to Tm^{3+} doped lasers [2, 3, 4, 5, Chapter 8]. This method facilitates good thermal extraction, in contrast to the square crystal rods (i.e. crystal width = height) used during the experiments, which could increase the thermal fracture limit sufficiently to produce high power continuous-wave Tm:$GdVO_4$ lasers.
- **Optimum pump wavelength**. From the literature discussed in Chapter 3 it is unclear as to what is the ideal pump wavelength since the reported Tm:$GdVO_4$ lasers have used laser diode pump wavelengths ranging from 795 nm to 808 nm. However, to determine experimentally the optimum pump wavelength for the available Tm:$GdVO_4$ crystals requires a number of different laser diode modules, which are generally not available or expensive to implement.
- **Optimum pump beam size**. It is also unclear as to what is the optimum pump beam size for a particular Tm^{3+} doping concentration, crystal length and total pump power. The approach followed in the literature of utilising small pump beams to reduce the laser threshold is limited by high intra-cavity power densities which lead to optical damage when scaling to high powers, as demonstrated in the first set of Tm:$GdVO_4$ laser experiments reported in Chapter 4 and in Chapter 5. Increasing the pump beam size to eliminate optical damage causes a significant increase in threshold power and thermal load inside the Tm:$GdVO_4$ crystal. The optimum pump beam size should be determined experimentally and through a study of the thermo-optical properties

of Tm:$GdVO_4$, but might be strongly influenced by the optical quality of the laser crystals.

- **Master oscillator power amplifier** (MOPA) scheme. If the above mentioned suggestions are implemented, and the achievable output power from the Tm:$GdVO_4$ laser is still limited, an amplifier scheme for the 1.9 µm pump light should be considered to scale the output power.

To implement the above-mentioned suggestions would have required substantial additional investment for the procurement of laser crystals and laser diode modules, which was not considered worth pursuing within the scope of the initial research project.

It was concluded that data on the Tm:$GdVO_4$ laser material is not known well enough, and the commercial material is not of high enough quality to consider this material as main contender as pump source for 2 µm Ho:YLF laser system with high output energy. An alternative Tm^{3+} pump source was developed and a commercial source was implemented, as discussed in Chapter 8. The option of using the Tm:$GdVO_4$ laser material should however not be discarded, since by implementing some of the above mentioned schemes, it could be a good alternative pump source at 1.9 µm.

7.2.2 Ho:YLF laser

The performance of the Ho:YLF laser was limited by the onset of double-pulsing and pre-lase oscillation at higher pump energies. As was discussed in Chapter 6, it is likely that the performance would have been improved if higher diffraction losses could have been achieved with the acousto-optic modulator to increase the oscillation hold-off during the pump pulse from the Tm:$GdVO_4$ laser.

Alternative methods to improve the Ho:YLF laser performance would have been to simultaneously:

- reduce the gain in the Ho:YLF resonator to a level where the AOM can hold off laser oscillation by increasing the fundamental resonator mode size together with the pump beam size inside the Ho:YLF crystal.
- increase the available energy (and peak power) from the Tm:$GdVO_4$ laser to overcome the higher Ho:YLF laser threshold associated with a larger pump beam.

or alternatively,

- operate the Tm:$GdVO_4$ laser in continuous-wave mode and operate the *Q*-switched Ho:YLF laser at high pulse repetition rates to produce a high average output power at 2 µm.

The above-mentioned steps were not implemented due to the risk of optical damage to the Tm:$GdVO_4$ laser optical components, and of crystal thermal fracture when scaling to higher output energy and when operating the laser in continuous-wave mode.

Increasing the Ho:YLF resonator mode size and the Tm:$GdVO_4$ pump beam size inside the Ho:YLF crystal, while limiting the pump energy to 73.4 mJ, was not practical since the Ho:YLF laser threshold would have increased significantly. In the demonstrated system the Ho:YLF laser threshold of 29.8 mJ was already at 41% of the total available energy from the Tm:$GdVO_4$ laser, leaving little scope for improving the performance of the *Q*-switched Ho:YLF laser.

Although the custom-developed Tm:$GdVO_4$ laser represents a unique and efficient pump source at 1892 nm for Ho:YLF, it is limited in the magnitude of the output power that can be achieved. Alternative pump sources, including a 200 W Tm:YLF laser and a commercial 80 W Tm:fibre laser (with the potential to scale the output energy of the Ho:YLF laser system to unprecedented values) only became available subsequent to this initial research work.

7.3 Conclusion

The key research question posed at the outset of this research project has been answered in that a solid-state 2 µm laser system can indeed be designed to be compact and efficient, using the approach of a diode-pumped Tm^{3+} laser pumping a Ho^{3+} laser. This has been demonstrated in the form of a unique multi-watt diode-end-pumped QCW Tm:$GdVO_4$ laser operated on 1892 nm through careful design, pumping a *Q*-switched Ho:YLF laser in a folded three-mirror resonator producing 2 mJ energy pulses.

The challenge of scaling to high powers has not been fully addressed, although the 175 mJ output energy demonstrated for the QCW Tm:$GdVO_4$ is the highest reported for this material to date, as is the multi-watt laser output at 1818 nm. The limitations of

scaling the output power from the continuous-wave Tm:$GdVO_4$ laser, of increasing the average pump power into the QCW Tm:$GdVO_4$ laser and scaling the output energy of the Ho:YLF laser pumped by the Tm:$GdVO_4$ laser have been identified, upon which a number of recommendations were made.

The research presented in this work is the most comprehensive analysis of the Tm:$GdVO_4$ laser material and the lasers constructed with this material as reported in the literature. The thorough experimental evaluation of the various Tm:$GdVO_4$ laser configurations, as presented here, is a significant contribution to the knowledgebase of this relatively new laser material, which still holds promise as an efficient laser source in the 1.8 – 1.9 µm wavelength range. The demonstration of a Tm:$GdVO_4$ laser as pump source for a Ho^{3+} laser is also an important landmark result, which has prior to this work only been postulated in the literature as an attractive solution for 2 µm laser generation.

A major outcome of the 2 µm laser development project was a clear understanding of the way forward in developing high average power Tm^{3+} lasers and for developing high power and high-energy Ho^{3+} lasers. The experimental analysis techniques and diagnostic arrangements that were developed during this initial research project were applied in subsequent laser development work. Of high importance were the theoretical analysis methods and the crystal mounting techniques that were described in detail in this work, which were directly applied in the development of world-leading high power and high energy 2 µm laser devices, as summarised in Chapter 8.

7.4 References

[1] E. H. Bernhardi, A. Forbes, C. Bollig, and M. J. D. Esser, "Estimation of thermal fracture limits in quasi-continuous-wave end-pumped lasers through a time-dependent analytical model," *Optics Express*, vol. 16 (15), pp. 11115–11123 (2008).

[2] R. Paschotta, J. Aus der Au, U. Keller, "Thermal Effects in High-Power End-Pumped Lasers with Elliptical-Mode Geometry" IEEE *Journal of Selected Topics in Quantum Electronics* **6** (4) 636-642 (2000).

[3] S. So, J.I. Mackenzie, D.P. Shepherd, W.A. Clarkson, J.G. Betterton, E.K. Gorton, "A power-scaling strategy for longitudinally diode-pumped Tm:YLF lasers", *Appl. Phys. B* 84, pp.389-393 (2006).

[4] M. Shellhorn, S. Ngcobo, and C. Bollig, "High-power diode-pumped Tm:YLF slab laser" *Applied Physics B* **94** (2) 195-198 (2008).

[5] M. Schellhorn, S. Ngcobo, C. Bollig, M. J. D. Esser, D. Preussler, K. Nyangaza, "High-power diode-pumped Tm:YLF slab laser," *CLEO Europe*, Munich, Germany, 14-19 June 2009, CA1.3 (2009).

Chapter 8

Additional *Collaborative* Laser Device Research

In addition to the research work described in Chapters 1 – 7 of this thesis, for which he was solely responsible, the author has been closely engaged collaboratively in a number of additional research projects also on mid-infrared laser systems. As project leader of the mid-infrared research team at the National Laser Centre, the author played a significant role in the research on these laser systems, with specific roles as described in more detail below.

The main additional projects in this category have been as follows:

- Tm:fibre laser pumped Ho:YLF laser and amplifier
- Single-frequency *Q*-switched Ho:YLF ring oscillator-amplifier
- High power Tm:YLF slab laser
- Ho:YLF Ho:LuLF slab amplifier
- Hybrid Ho:YLF Ho:LuLF slab laser

In this Chapter, each of these research projects is briefly *summarised* and the specific contributions made by the author indicated. Where appropriate, reference is made to relevant journal papers derived from the work.

The publication list also includes reference to a comprehensive series of monthly Technical Reports which were prepared for the principal (external) sponsor of the research. In practice, these Reports were typically accompanied by detailed oral presentations describing technical progress.

8.1 Tm:fibre laser pumped Ho:YLF laser & amplifier

8.1.1 Introduction

It was argued in Chapter 2 that an alternative approach to obtain a high average power pump source for Ho:YLF at 1.9 µm is to utilise the new Tm:fibre laser technology. Subsequent to the initial research project, a commercial Tm:fibre laser was procured from IPG photonics (Model TLR-80-1940) to scale the output at 2 µm by utilising a Ho:YLF oscillator and amplifier pumped by the single fibre laser.

Initially it had been intended to follow the traditional approach when pumping a Ho^{3+} oscillator-amplifier system with one Tm:fibre laser pump source wherein the unpolarised pump beam is split into two polarised beams in order to pump the oscillator and amplifier crystals separately [1]. However, an alternative novel approach was developed by utilising the full unpolarised beam from the Tm:fibre laser to pump the oscillator, and then use the partially polarised transmitted pump light through the oscillator crystal to pump the amplifier with its crystal rotated by 90° around the laser beam axis. This led to a small system footprint and kept the path length of the pump light short, reducing adverse effects of atmospheric water absorption at the 1.9 µm pump wavelength.

This approach required the Ho:YLF resonator as presented in Chapter 6 to be redesigned to optimally utilise this concept and to accommodate an oscillator-amplifier design, as discussed below.

8.1.2 The fibre pump laser

The IPG fibre laser had a measured output power of 85 W at 1938.7 nm with a specified near-diffraction limited beam quality ($M^2 < 1.1$). A collimator was attached to the delivery fibre to produce a collimated output beam of 4 mm diameter.

It was found when operating the Tm:fibre laser at full power that a small fraction of the laser power was absorbed by atmospheric water vapour which resulted in localised heating of the air and subsequent distortion of the beam profile and direction. Several experiments were performed prior to the design of the 2 µm Ho:YLF oscillator and amplifier to quantify the influence of water absorption at the Tm:fibre laser wavelength.

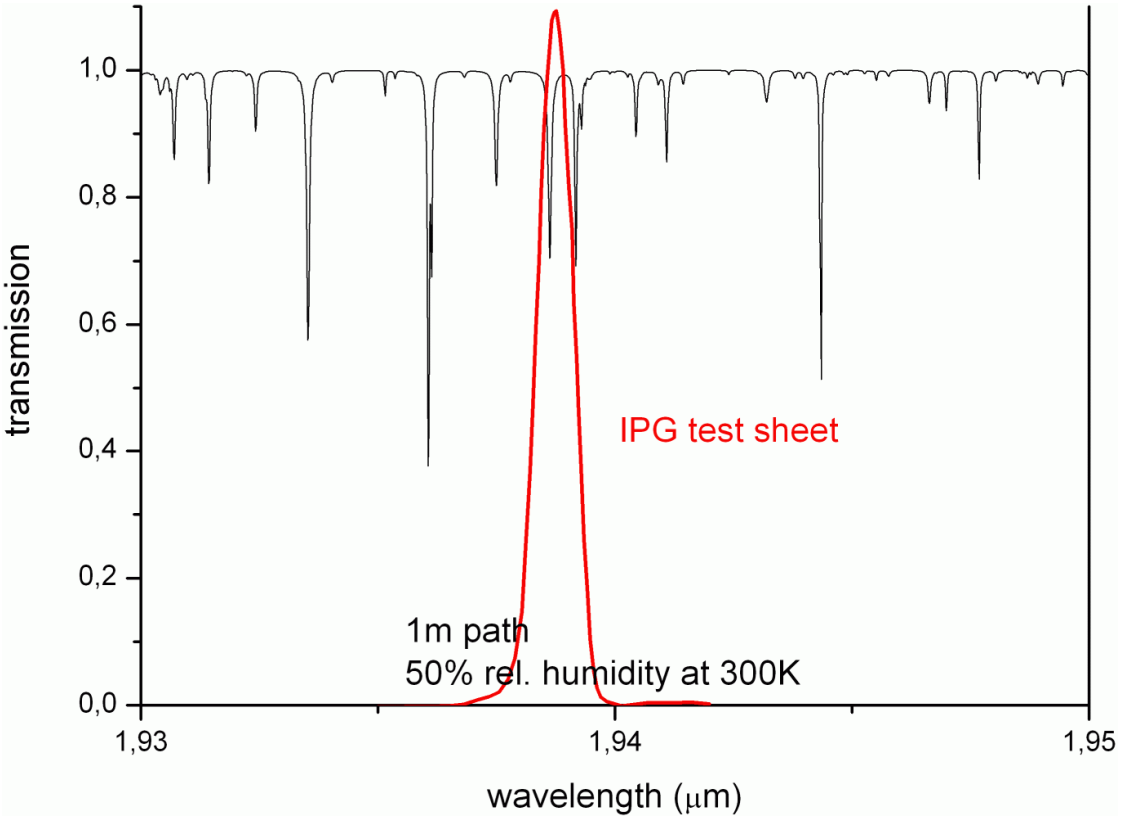

Figure 8.1: Transmission in air as a function of wavelength close to 1940 nm (1 m path, 50% relative humidity). The Tm:fibre laser output wavelength at full power is shown in red.

The measured wavelength of the Tm:fibre laser, as provided by the supplier, is shown in Figure 8.1 together with the transmission of air over 1 m path length at 50% relative humidity [2]. It was found that the Tm:fibre wavelength shifts slightly from a shorter wavelength at low power up to 1938.7 nm at full power. At the 50% set point of the Tm:fibre laser power, the absorption in air was the strongest with a significant beam distortion measured over a 1.85 m path length with a Pyrocam I beam profiler, which is shown in Figure 8.2. Also shown in Figure 8.2 is the intensity beam profile at full Tm:fibre power which indicated less distortion.

At the 50% set point of the Tm:fibre laser power, 4% of the power was absorbed over 1.5 m distance. However, at the 100% set point, the absorption was not measurable even though significant beam wander was still observed.

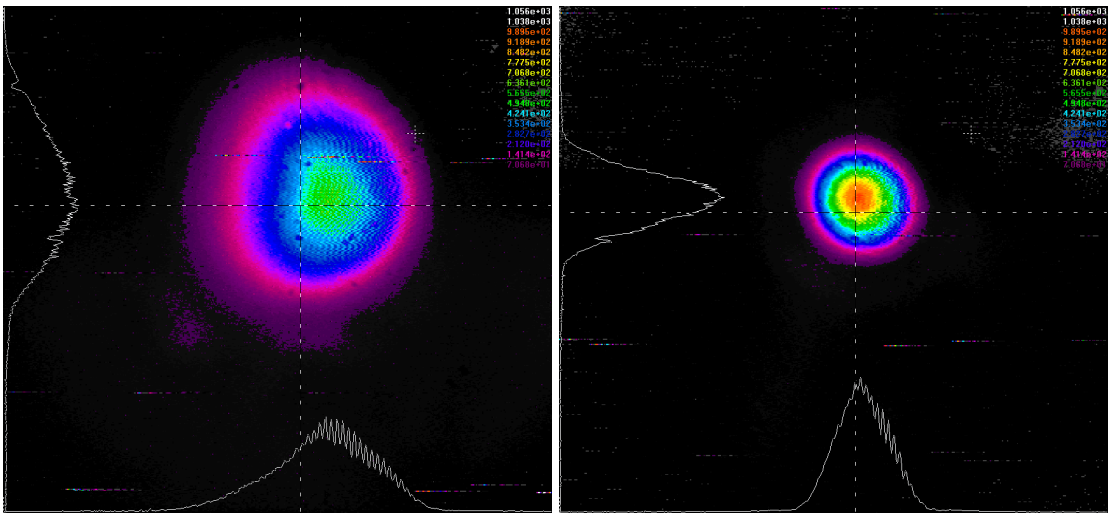

Figure 8.2: Intensity beam profile of the Tm:fibre laser measured after a distance of 1.85 m at 50% power (left) and at 100% power (right).

It was concluded that the Ho:YLF laser and amplifier must either be in a sealed box filled with dry air, or the distances between the Tm:fibre laser output collimator and the Ho:YLF crystals must be kept as short as possible. It was considered that the distortion and beam wander effects due to water absorption would be pronounced when the Tm:fibre output beam is reduced to the beam diameters required for efficient pumping of the Ho:YLF crystals.

8.1.3 The Ho:YLF oscillator-amplifier design

Numerical rate-equation simulations of the Ho:YLF oscillator-amplifier system showed that a good performance with respect to output power and energy would be obtained for both continuous-wave and *Q*-switched operation if the system is designed for a fundamental laser mode radius of ~1 mm in the Ho:YLF oscillator crystal with the pump beam closely matching this beam size [3].

The optical layout of the newly designed 2 µm Ho:YLF oscillator is shown in Figure 8.3 and a photo of the assembled system is shown in Figure 8.4. The collimated Tm:fibre pump light first encountered a beam reducing telescope consisting of two lenses with respective focal lengths of 100 mm and -50 mm such that the pump beam radius in the position of the Ho:YLF crystal was reduced to a measured ~600 µm.

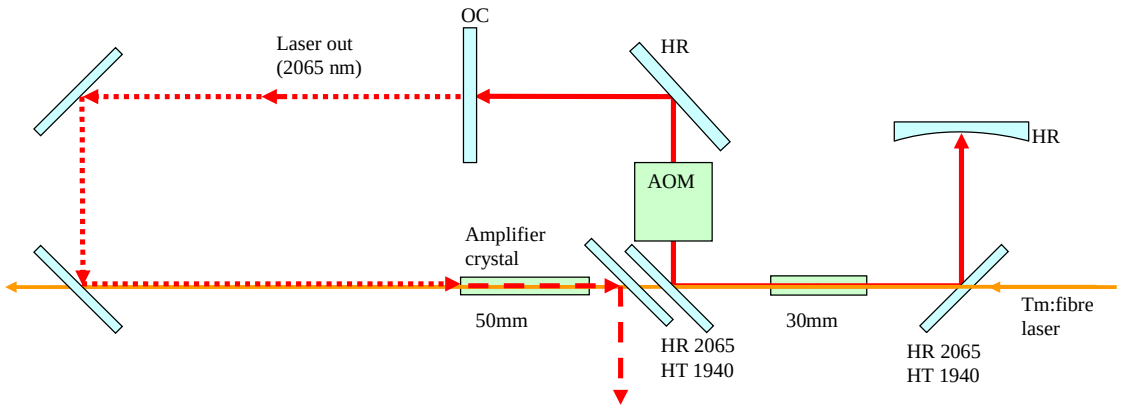

Figure 8.3: Optical layout of the 2 µm Ho:YLF oscillator-amplifier. The pump light of the fibre laser is shown in orange (1940 nm) and the laser light in red (2064 nm).

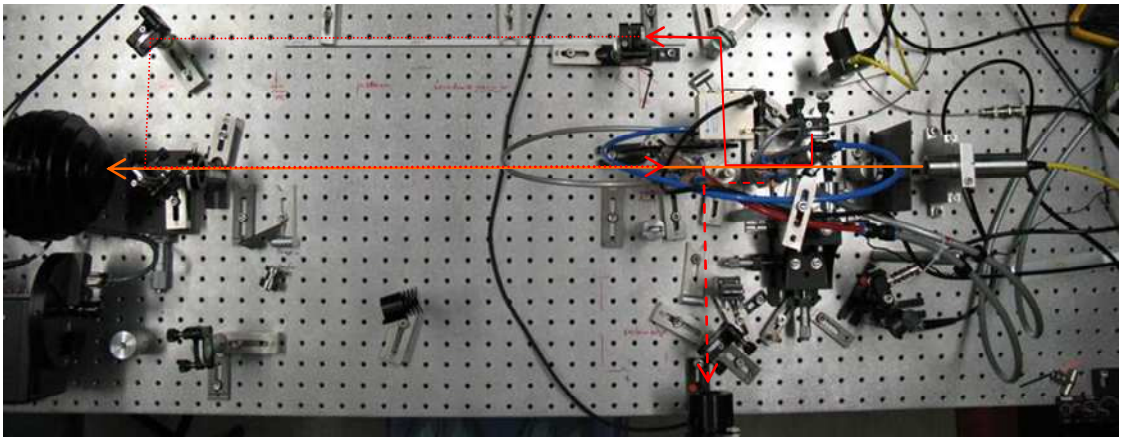

Figure 8.4: Photo of the 2 µm Ho:YLF oscillator-amplifier. The pump light of the fibre laser is shown in orange (1940 nm) and the laser light in red (2065 nm).

The full unpolarised pump beam from the Tm:fibre laser was used to pump the oscillator crystal, which was a 0.5% doped, a-cut Ho:YLF crystal with a length of 30 mm and a diameter of 6 mm. The crystal was mounted in a water cooled copper mount, the design of which was described in Chapter 6. In this experiment the crystal was actively cooled by keeping the water temperature constant at 20°C.

The resonator design was based on a plano-concave resonator with three 45° fold mirrors, a plane output coupler mirror and a curved high-reflector mirror with 500 mm radius of curvature. The resonator was 370 mm long and the output coupler reflectivity was 50%. The calculated TEM_{00} beam radius in the Ho:YLF crystal was 580 µm, which was assumed to increase at higher pump power due to the effect of the weak negative thermal lens in Ho:YLF.

The objective of using the 45° dichroic mirrors was to keep the optical path length of the Tm:fibre pump light to the amplifier crystal a minimum. The 45° dichroic mirrors had a high transmission for the pump light (s- and p-polarisation), high reflection for s-polarised laser light, and 20 % transmission for p-polarised laser light, forcing the oscillator to operate vertically polarised. The Ho:YLF crystal c-axis was orientated horizontal such that the laser was forced to operate on the σ-polarisation of Ho:YLF which has a weak thermal lens.

The same AR coated acousto-optic modulator (Gooch & Housego, model QS027-10M-NL5) that was used in the initial Ho:YLF experiments (Chapter 6) was inserted in the newly designed oscillator for *Q*-switched operation. A new RF driver was available for these experiments such that the AOM delivered a loss modulation of approximately 80% at the maximum recommended RF power of 100 W.

The Tm:fibre pump power transmitted through the Ho:YLF oscillator crystal was used to pump the Ho:YLF amplifier crystal which was 50 mm long, also 0.5% doped. The amplifier crystal, mounted in a water-cooled copper mount similar to the oscillator crystal, was placed as close to the resonator as possible to minimise atmospheric water absorption of the 1940 nm pump light to avoid heating of the air and subsequent thermal turbulence. This negated the need for any enclosure or dry-air flushing typically used for such setups to prevent pump-beam distortions and optical damage [4].

In order to achieve maximum absorption of the pump light in the amplifier crystal, it was orientated with its c-axis rotated by 90° with respect to the c-axis of the oscillator crystal. This effectively rotated the polarisations for the amplifier crystal. Thus, the π-polarisation, with the higher emission cross section but stronger thermal lens was used for amplification while the σ-polarisation, with the very weak thermal lens but lower cross section, was used in the oscillator. The laser output was coupled into the amplifier crystal using a lens with a focal length of 350 mm.

The Ho:YLF oscillator-amplifier was set up according to the optical layout presented above which adhered to the design criteria. The resonator length was adjustable such that the optimum length could be determined experimentally by evaluating the output beam profile and output power. A photo of the system is shown in Figure 8.5.

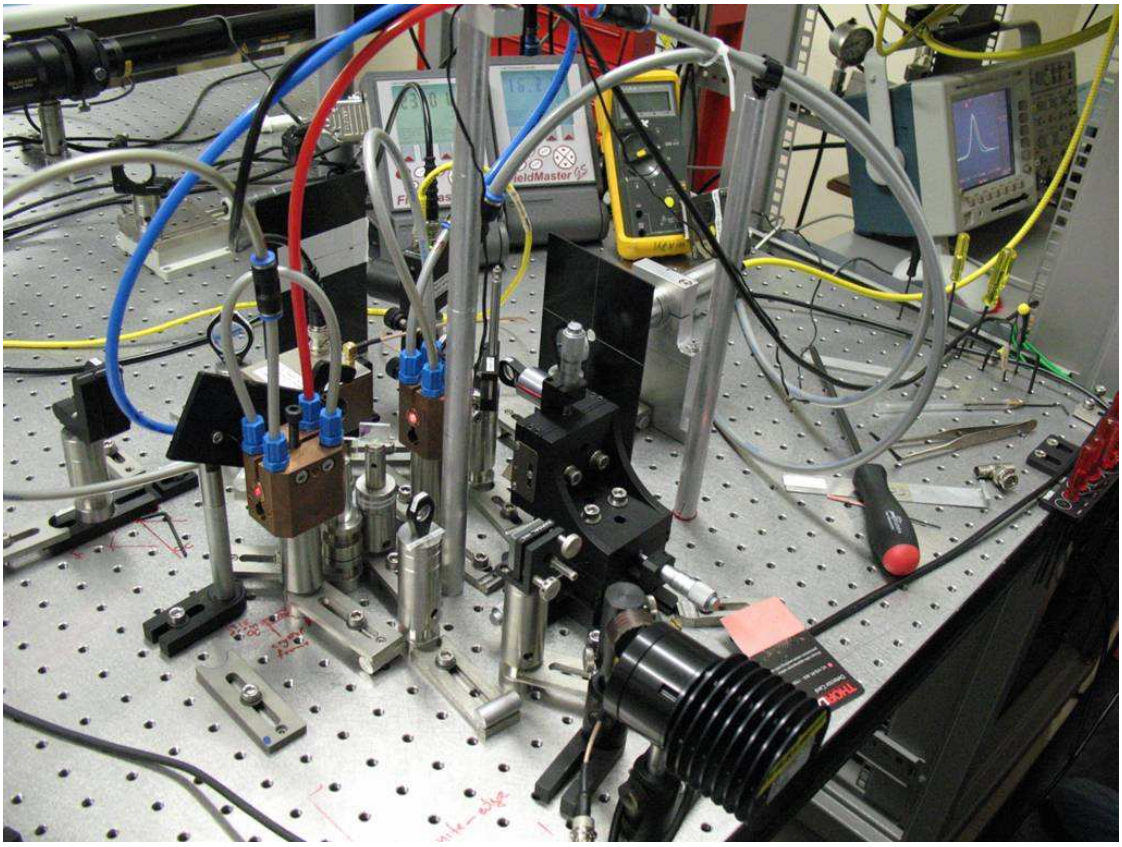

Figure 8.5: Photo of the 2 µm Ho:YLF oscillator-amplifier. The two Ho:YLF crystals can be seen in the water-cooled copper mounts (left: amplifier; right: oscillator crystal).

8.1.4 Experimental results

The Ho:YLF oscillator-amplifier system was first operated in CW mode. The output power of the system as a function of the incident Tm:fibre laser pump power is shown in Figure 8.6. The measured output wavelength of the Ho:YLF oscillator-amplifier system was 2064 nm. The oscillator had a threshold of 31 W (17 W absorbed) of incident pump power, with an overall slope efficiency of 25 % (47 % vs. absorbed power). At full pump power (82 W), the Ho:YLF oscillator output power was 12.4 W and the power after the amplifier was 23.7 W. The measured gain of the amplifier at full pump power was a factor of 1.9. The total pump power transmitted through the oscillator crystal was 47 W (57 % of the pump power) at full power. The amplifier crystal absorbed 62 % (29 W) of this transmitted pump light, with 22 % (18 W) of the total pump power unused. The slope efficiency of the amplified output power as a function of total *incident* Tm:fibre laser pump power was 47%, with an overall optical-to-optical efficiency of 29%. With respect to the total *absorbed* power (35 + 29 W), the slope efficiency was 60 % and the optical-to-optical efficiency was 37 %.

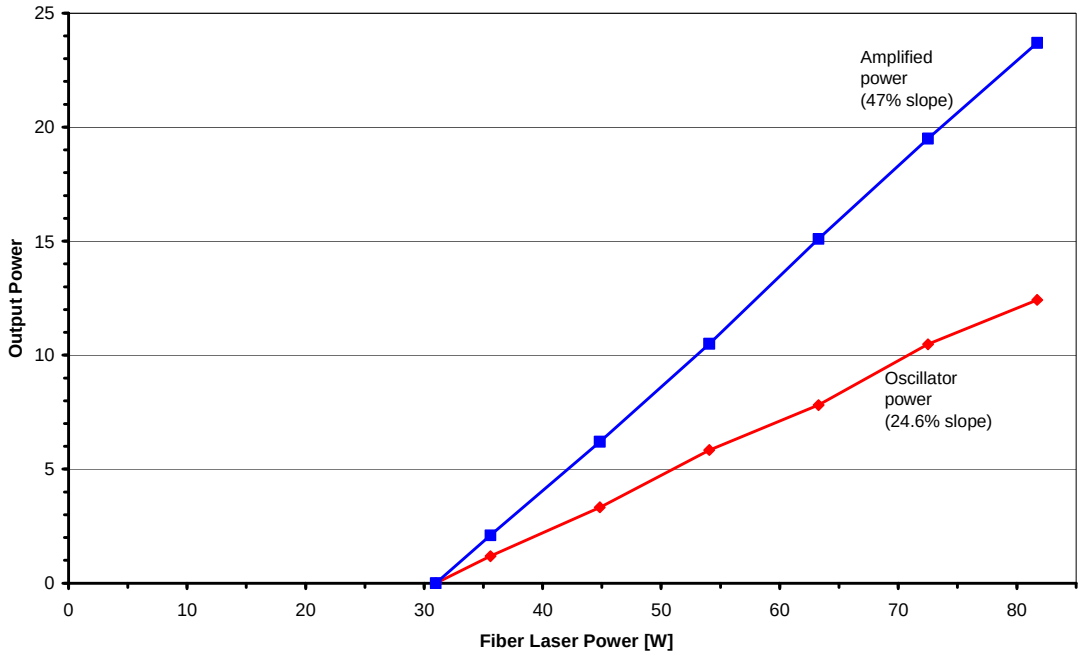

Figure 8.6: The continuous-wave Ho:YLF oscillator-amplifier output power as a function of incident Tm:fibre laser pump power.

The Ho:YLF oscillator was subsequently *Q*-switched at repetition rates between 5 kHz and 1 kHz. The output pulse energy at full pump power of the Ho:YLF oscillator-amplifier system as a function of the repetition rate is shown in Figure 8.7. Also shown in the figure is the duration of the output pulse at each repetition rate set point.

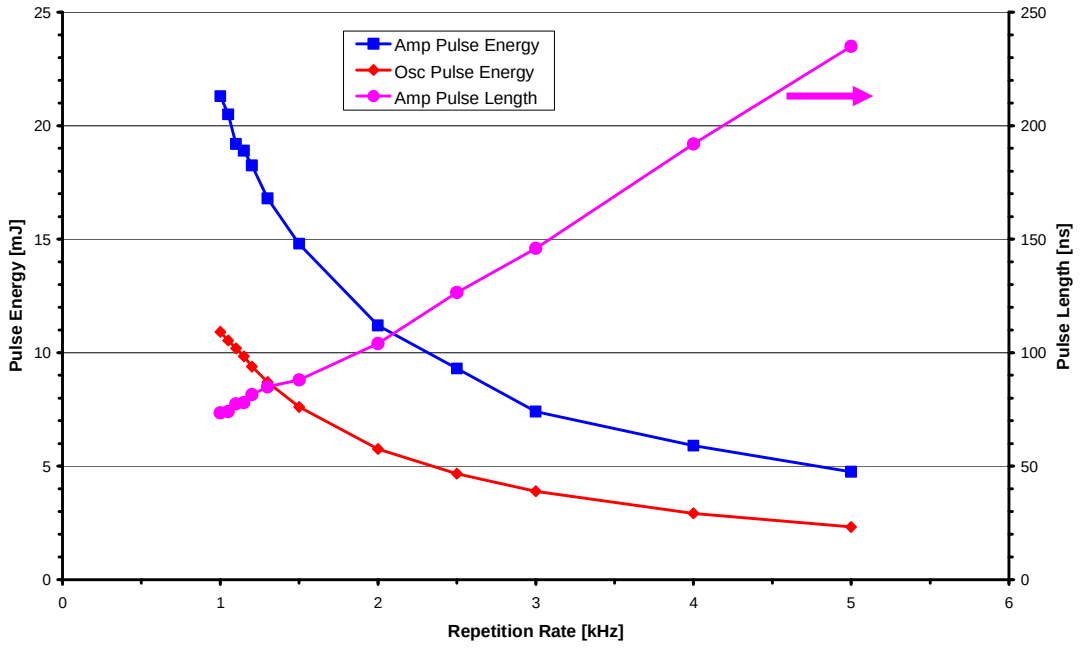

Figure 8.7: The output energy and output pulse duration of the *Q*-switched Ho:YLF oscillator-amplifier system at 1 – 5 kHz pulse repetition rate.

The highest output pulse energy of the Ho:YLF oscillator-amplifier system was at a repetition rate of 1 kHz where the oscillator produced 10.9 mJ per pulse which was amplified to 21.3 mJ. The measured amplifier gain factor was 1.95. No attempt was made to operate the Ho:YLF oscillator at lower repetition rates to avoid the risk of optical damage to the 45° dichroic mirrors at higher output energy. (These mirrors had been damaged in a prior experiment at the point where the *Q*-switched oscillator, which utilised a 50 mm long Ho:YLF crystal to absorb more pump power, produced 18.8 mJ at 700 Hz repetition rate.)

An oscilloscope screenshot of the Ho:YLF oscillator-amplifier system output pulse at maximum output energy is shown in Figure 8.8. This was measured with both a PEM detector (VIGO System S.A., Photoelectromagnetic IR detector, 2 – 11 μm spectral range, time constant of 1 ns or less) and a fast InGaAs photo diode (Thorlabs Inc. model PDA10D, 1.2-2.6 μm fixed gain detector, 15 MHz bandwidth). The InGaAs photo diode had a response time of a few ns, which resulted in a slightly longer measured pulse duration as compared to the PEM detector, which had a sub-ns response time. The measured full-width half-maximum pulse length at maximum output energy of the Ho:YLF oscillator-amplifier system was 73.4 ns.

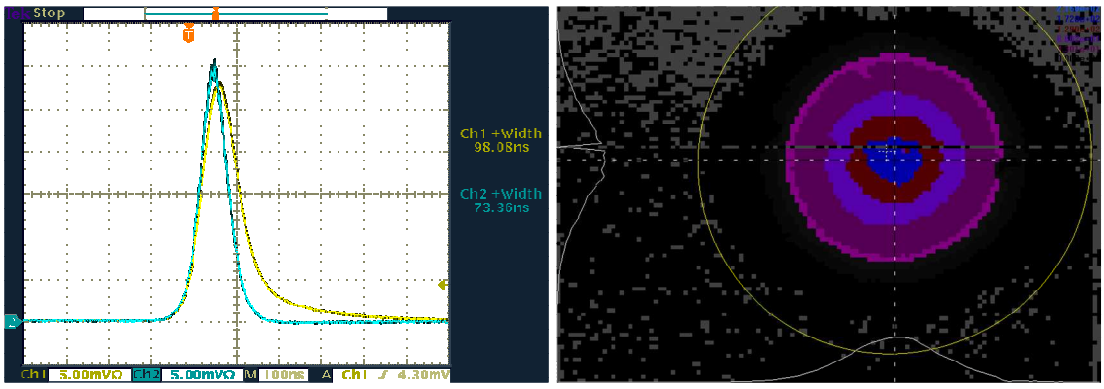

Figure 8.8: Oscilloscope screenshot (left) of the Ho:YLF oscillator-amplifier output pulse at maximum output energy, as well as the intensity beam profile (right).

Also shown in Figure 8.8 is the intensity beam profile at maximum output energy of the Ho:YLF oscillator-amplifier system, measured with a Pyrocam I camera and displayed on the Spiricon Laser Beam Analyser software. The intensity profile indicated a circular beam with a Gaussian profile. The M^2 beam quality of the amplified beam was also measured and found to be better than 1.1.

8.1.5 Conclusions

A novel Ho:YLF oscillator-amplifier scheme pumped by a single randomly-polarised Tm:fibre laser was developed, where the pump light transmitted by the Ho:YLF oscillator crystal was utilised to pump a Ho:YLF amplifier crystal. For this purpose a 2 µm Ho:YLF oscillator was designed to accommodate an amplifier crystal in close proximity of the oscillator crystal. This design was an improvement on the first 2 µm Ho:YLF oscillator pumped by the Tm:$GdVO_4$ laser as reported in Chapter 6. The Tm:fibre laser procured from IPG Photonics delivered a maximum output power of 82 W at 1939 nm.

The Ho:YLF oscillator utilised a 30 mm long Ho:YLF crystal and produced 10.9 mJ output energy at 1 kHz repetition rate for 35 W absorbed pump power. The transmitted pump power of 47 W was incident on the 50 mm long Ho:YLF amplifier crystal which absorbed 29 W, transmitting 18 W of total pump power which was not utilised in the Ho:YLF oscillator-amplifier system. The amplifier increased the output energy to a maximum of 21.3 mJ, which was a gain factor of 1.95. In continuous-wave mode the Ho:YLF oscillator-amplifier system had a slope efficiency of 47% and an optical-to-optical efficiency of 29%. With respect to the total absorbed power of 64 W the slope efficiency was 60 % and the optical-to-optical efficiency was 37 %.

No attempt was made to increase the efficiency of the system by reflecting the 18 W of unutilised pump power back into the Ho:YLF amplifier and oscillator crystals, due to the potential risk of damage to the Tm:fibre laser. If an optical isolator capable of withstanding the high average power had been available this potential improvement could have been investigated without risk to the Tm:fibre laser. The novel scheme employed as described above demonstrated a unique solution to scaling the output energy of a Ho:YLF system pumped by a Tm:fibre laser in a compact and efficient 2 µm laser device.

8.1.6 Contribution

The author contributed to the Ho:YLF oscillator-amplifier system in the following way:

- Jointly specified the Tm:fibre laser parameters, including the selection of operational wavelength suitable for pumping Ho:YLF.

- Implemented and experimentally evaluated the first Ho:YLF oscillator pumped by the Tm:fibre laser producing 18.8 mJ at 700 Hz, limited by optical damage.
- Jointly developed the novel concept of pumping the Ho:YLF amplifier crystal with the partially polarised pump light transmitted through the oscillator crystal.
- Implemented the folded Ho:YLF oscillator and experiential evaluation of its performance.
- Oversaw the implementation and experimental evaluation of the Ho:YLF oscillator-amplifier system.
- Jointly oversaw the data analysis and publication of results.

8.1.7 References

[1] Dergachev, D. Armstrong, A, Smith, T. Drake and M. Dubois, "3.4-µm ZGP RISTRA nanosecond optical parametric oscillator pumped by a 2.05-µm Ho:YLF MOPA system," *Opt. Express,* vol. **15**, p. 14404 (2007).

[2] L.S. Rothman, *et al* "The HITRAN Molecular Spectroscopic Database: Edition of 2000 Including Updates through 2001," *J. Quant. Spectrosc. and Radiat. Transfer,* vol. **82**, pp. 5-44 (2003).

[3] W. Koen, C. Bollig, H. Strauss, M. Schellhorn, C. Jacobs and M. J. D. Esser, "Compact Fibre-Laser-Pumped Ho:YLF Oscillator-Amplifier System," *Applied Physics B* **99** (1-2) 101-106 (April 2010).

[4] M. Shellhorn, "High-power diode-pumped Tm:YLF laser" *Applied Physics B* **91** (1) 71-74 (2008).

8.2 Single-frequency *Q*-switched Ho:YLF ring oscillator-amplifier system

The demonstration the Tm:fibre laser pumped Ho:YLF oscillator-amplifier system formed the basis for the development of a singe-frequency 2 µm system which was used as source for an optically pumped molecular laser. At low pressure the active HBr molecule absorbs 2 µm light on one of its narrow absorption lines and emits at 4 µm. To ensure efficient absorption it was necessary to operate the Ho:YLF oscillator on a single longitudinal mode of the resonator, seeded with the exact wavelength of an absorption line of the HBr molecule. Once the oscillator was locked to the seed wavelength, the pulsed output was amplified by Ho:YLF amplifier crystals. Alternative applications of the single-frequency 2-µm laser system include remote trace gas monitoring and wind detection using coherent lidar.

Prior to this work a single-frequency *Q*-switched fibre-laser-pumped Ho laser has not been reported. To this purpose an injection-seeded single-frequency *Q*-switched Ho:YLF oscillator-amplifier system was developed, pumped by a single 82-W Tm:fibre laser, which delivered 70 mJ per pulse at 50 Hz repetition rate at 2064.12 nm, as described below.

8.2.1 Pump scheme

For the development of the single-frequency *Q*-switched Ho:YLF oscillator-amplifier system the same concept as presented in Section 8.1 was used, namely by pumping the amplifier crystal with the partially polarised Tm:fibre pump light transmitted through the oscillator crystal. In addition to designing a single-frequency ring laser as the oscillator, a number of additional improvements for the system were implemented such that the system could be operated at high energy output at low pulse repetition rates, as described below.

8.2.2 Single-frequency ring Ho:YLF oscillator design

The achievable energy at low repetition rates is often limited by either a too-high gain, an example of which is the Ho:YLF laser pumped by the Tm:$GdVO_4$ laser (Chapter 6), or damage to optical components, which was the case for the first Tm:fibre laser pumped Ho:YLF oscillator (Section 8.1). These limitations can be avoided by increasing the laser mode size in the gain medium and on the optical components. However, a large mode size in the gain crystal leads to an increased laser threshold and reduced efficiency. Therefore, a careful trade-off between these two effects is

required. Since the oscillation threshold depends only on the mode size in the crystal, the resonator design can be made such that the laser mode size in the oscillator crystal is optimum for the available pump power, and that the beam sizes on the other optical components is just as large or larger than the resonator mode size in the crystal.

For the design of the high energy single-frequency Ho:YLF oscillator the pump beam size and laser mode radius was selected to be w = ~1 mm in the 40 mm long, 0.5% doped Ho:YLF crystal. A 2.4 m long ring resonator was used to achieve relatively long *Q*-switched pulses. The optical layout of the ring oscillator, which had the minimum mode size in the gain crystal, is presented in Figure 8.9. The near-normal incidence dichroic mirrors M1 and M2 had a higher damage threshold value than the 45° dichroic mirrors used previously. The ~125 mm distance between the convex mirror M6 (500 mm radius of curvature) and the concave mirror M5 (-300 mm radius of curvature) could be adjusted to fine tune the resonator mode size in the Ho:YLF crystal and to compensate for the weak negative thermal lens on σ-polarisation. The output coupler reflectivity of 80% was experimentally determined to provide efficient operation while maintaining a low intra-cavity fluence. The transmitted pump power through the oscillator crystal was approximately 40 W at full pump power.

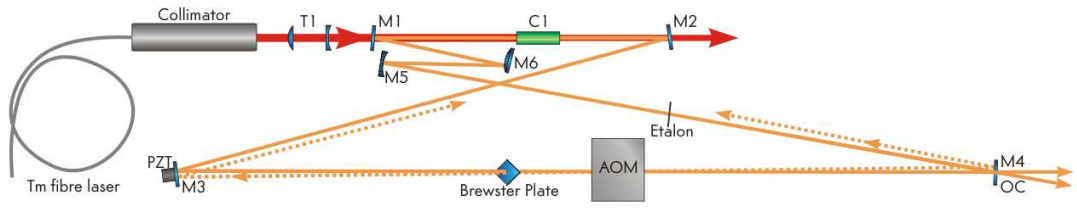

Figure 8.9: Optical layout of the Ho:YLF ring laser.

To force the laser to operate on the σ-polarisation, which was vertical to the resonator plane due to the Ho:YLF oscillator crystal orientation, a 4-mm thick crystalline quartz plate was inserted as intra-cavity Brewster plate and orientated for minimum loss. A 400-µm thick fused-silica etalon was used to fine-tune the oscillator wavelength to be close to the 2064 nm seeding wavelength.

8.2.3 Injection seeding

A commercial single frequency diode laser was utilised to seed the ring oscillator through the first diffraction order of the acousto-optic modulator (AOM). The laser diode emitted 13 mW continuous-wave power at 2064 nm in a circular-symmetric

beam. Seeding of the Ho:YLF ring oscillator was implemented by using a number of beam steering mirrors (M7 – M11), an optical isolator, a half-wave plate and a telescope (T2), as indicated in Figure 8.10

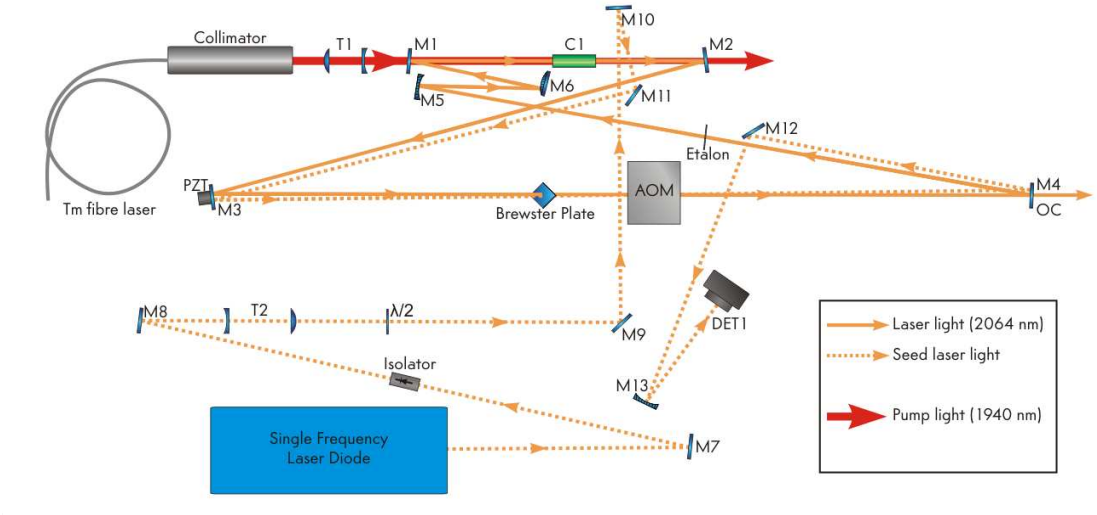

Figure 8.10: Optical layout to seed the Ho:YLF oscillator with a single-frequency diode laser.

The diode laser wavelength was locked to an HBr molecule absorption line by utilising electronic feedback and a multi-pass absorption cell which was placed behind the 95% reflecting mirror M7. The diode laser current was modulated with a 20 MHz RF signal so that the Pound-Drever-Hall technique could be used for locking the Ho:YLF ring resonator [1]. The detector DET1 was used to detect the oscillator resonance of the seed laser on the forward-propagating first order diffracted beam of the AOM, with electronic feedback to the piezo-controlled mirror M3. Once the resonator length was locked, the seeding was stable and in resonance, ensuring reliable unidirectional, single-frequency operation with its wavelength locked to an absorption line of HBr.

8.2.4 Amplifier setup

The optical layout of the system including the amplifier arrangement is shown in Figure 8.11. Initially, the partially polarised Tm:fibre pump light transmitted through the oscillator crystal was used to pump a single 50 mm long Ho:YLF crystal (C2) inserted with its c-axis vertical, to amplify on the π-polarisation. However the remaining transmitted pump power was measured to be 16.5 W, which was consequently used to pump a third, 30 mm long, Ho:YLF crystal (C3) with its c-axis horizontal to amplify on the σ-polarisation. During the amplification experiments it was found that the output energy was nearly independent of the orientation of the last amplifier crystal C3 but the beam quality was significantly better in this configuration.

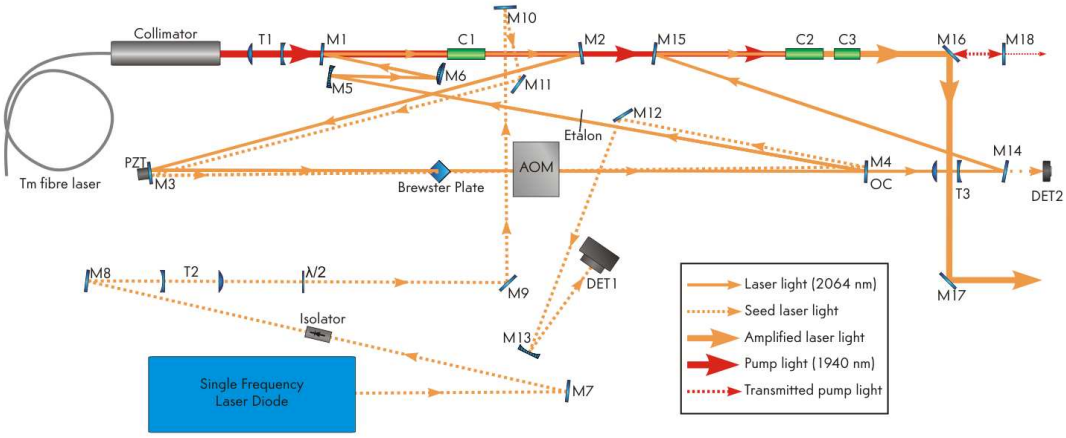

Figure 8.11: Optical layout of the single-frequency Ho:YLF oscillator-amplifier system.

With all three crystals inserted the transmitted pump power was measured to be 6 W, which was deemed low enough to reflect 99% of it back with mirror M18 to the amplifier and oscillator crystals to implement a double-pump-pass configuration. It was estimated that the back-reflected pump light reaching the Tm:fibre laser collimator was significantly less than the maximum permissible 5% of the total power.

The amplifier crystals were seeded in a single-pass configuration, with the output beam of the Ho:YLF oscillator guided with mirrors M14 and M15 into the amplifier crystals. The telescope T3 was used to match the beam size of the Ho:YLF oscillator output with the transmitted Tm:fibre laser pump beam in the position of the amplifier crystals, which was measured to be approximately 1 mm radius. The reflectivity of mirror M14 was 98% such that the Ho:YLF oscillator energy could be monitored, and the output pulse shape and duration be measured with a PEM detector (DET2).

8.2.5 Single-frequency Ho:YLF oscillator-amplifier experimental results

The output energy of the single-frequency Ho:YLF oscillator-amplifier system operated at 50 Hz pulse repetition rate is shown in Figure 8.12 as a function of Tm:fibre laser power. The oscillation threshold was above 60 W pump power which was a consequence of implementing a large pump beam size and resonator mode size to avoid optical damage. The maximum output energy was 72 mJ at 82 W of Tm:fibre pump power.

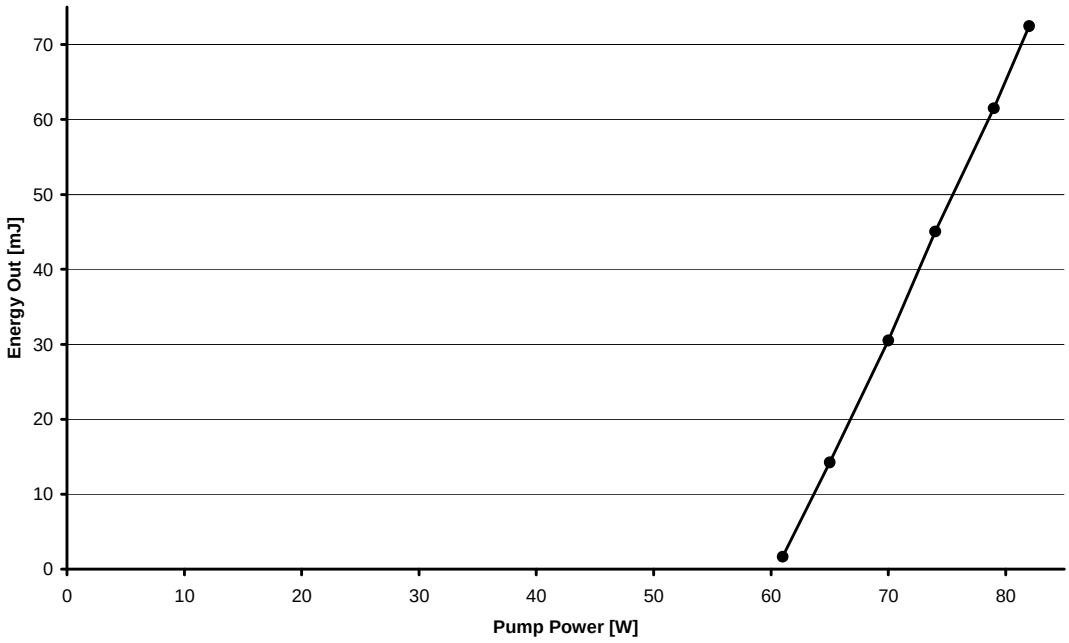

Figure 8.12: Output energy of the single-frequency Ho:YLF oscillator-amplifier system as a function of Tm:fibre laser pump power

The output energy of the single-frequency Ho:YLF system for different configurations are listed in Table 8.1. Roughly 40 W of the 82 W Tm fibre laser pump power was absorbed in the Ho:YLF oscillator crystal in a single pump pass. At this pump power level, the oscillator delivered 31 mJ of single-frequency energy per pulse at 50 Hz repetition rate. This increased to 35 mJ when the double-pass pumping scheme was implemented, despite the fact that it added less than 1 W of absorbed pump power to the oscillator crystal.

Table 8.1: Output energy of the single-frequency Ho:YLF system in different oscillator-amplifier configurations.

Configuration	Output energy @ 50 Hz	Tm:fibre laser pump power
Single pass pump, oscillator only (40 mm Ho:YLF)	31 mJ	42 W absorbed 40 W transmitted
Double pass pump, oscillator only (40 mm Ho:YLF)	35 mJ	~43 W absorbed in oscillator
Single pass pump, oscillator & 1 amplifier crystal (40 mm + 50 mm Ho:YLF)	52 mJ	16.5 W transmitted
Single pass pump, oscillator & two amplifier crystals (40 mm + 50 mm + 30 mm Ho:YLF)	54 mJ	6 W transmitted
Double pass pump, oscillator & two amplifier crystals (40 mm + 50 mm + 30 mm Ho:YLF)	72 mJ	All pump power utilised

At 50 Hz, the output of a single 50 mm amplifier crystal with single-pass pump was 52 mJ. With both 50 and 30 mm amplifier crystals in place, but with single-pass

pumping the output energy was 54 mJ while with double-pass pumping the output energy was 72 mJ per pulse.

The big increase in output energy was most likely due to an increased energy of both the oscillator and the amplifier during double-pass pumping. It was possible that the Tm:fibre pump laser also increased in performance due to the low level of back reflected light entering the fibre collimator. The feedback could have increased the Tm:fibre laser power or it could have introduced some polarisation preference for the Tm:fibre laser output [2], resulting in a increased absorption on the first pass through the Ho:YLF oscillator and amplifier crystals. The effects of the back reflected pump light on the Tm:fibre laser could however not be verified experimentally.

The output energy of the single-frequency Ho:YLF oscillator and the oscillator-amplifier as a function of pulse repetition frequency are shown in Figure 8.13. There was an increase in output energy with a decrease in pulse repetition rate, which levelled off at 40 – 50 Hz, which was well below the inverse lifetime of Ho:YLF. The resonator alignment was optimised at the typical operating PRF of 50 Hz.

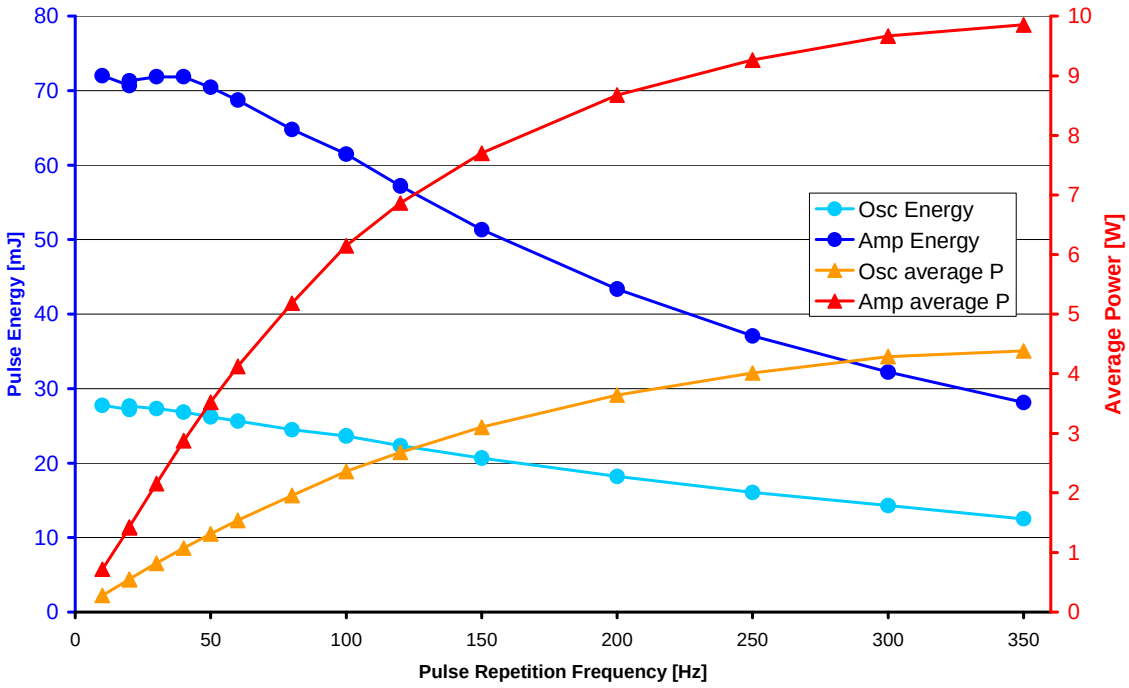

Figure 8.13: Output energy of the single-frequency Ho:YLF oscillator-amplifier system between 10 Hz and 350 Hz pulse repetition frequency.

It is important to note that the achievable energy at decreasing repetition rate was not limited by optical damage nor by effects such as double pulsing or pre-lase *Q*-

switching which are symptoms of too high gain. This confirmed that the system was optimally designed for high-energy operation. Decreasing the PRF below 20 Hz did not result in an increase in output energy. Increasing the PRF above 350 Hz resulted in difficulty for the feedback system to maintain stable locking of the Ho:YLF oscillator to the single-frequency diode laser seed.

The full width at half maximum (FWHM) pulse length of the *Q*-switched Ho:YLF oscillator output increased from ~320 ns at 10 Hz repetition rate up to 600 ns at 350 Hz. The pulse shape was captured on an oscilloscope, an example of which is the green trace in Figure 8.14. The long pulse lengths were a deliberate consequence of the long resonator length and contributed to reducing the risk of optical damage to the Ho:YLF oscillator components. In addition, the long pulse lengths were preferred for the optically pumped molecular laser.

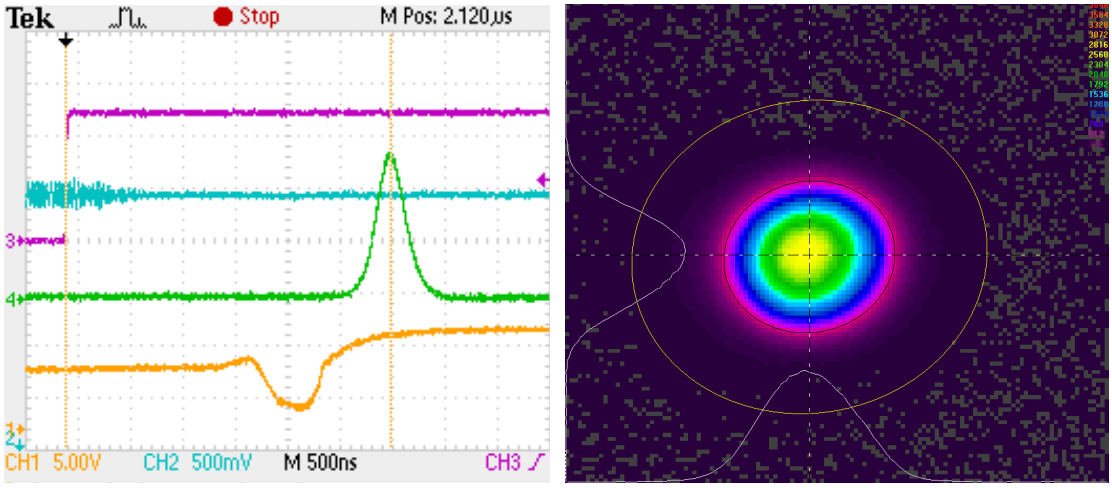

Figure 8.14: Oscilloscope screenshot (left) and intensity beam profile (right) of the single-frequency Ho:YLF oscillator-amplifier system at maximum output energy.

An M^2-measurement at full pump power at 50 Hz repetition rate revealed that the Ho:YLF oscillator-amplifier system produced a near perfect beam, with an $M^2 < 1.05$. The intensity beam profile of the amplified beam is shown in Figure 8.14.

The output energy of the Ho:YLF oscillator-amplifier system was measured for different diode laser seed wavelengths over a 1.1 nm scan range, as indicated in Figure 8.15. The tilt angle of the 400-µm thick fused-silica etalon in the cavity was not adjusted during these experiments, but was optimised for operation on the 2064.12 nm absorption line of the HBr molecule used in the optically pumped molecular laser.

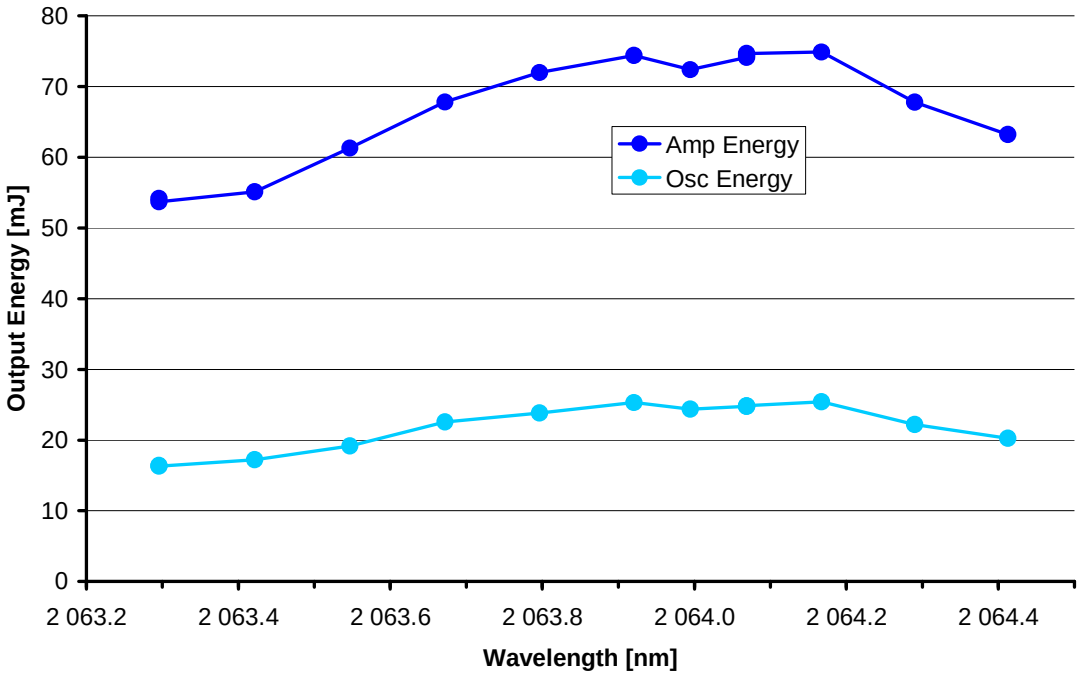

Figure 8.15: Output energy of the single-frequency Ho:YLF oscillator-amplifier system as a function of diode laser seed wavelength in the range 2063.3 – 2064.4 nm.

8.2.6 Conclusion

A single-frequency *Q*-switched oscillator-amplifier system was designed and developed with more than 70 mJ output energy at 50 Hz pulse repetition rate. The laser system was operated daily over several months with robust locking at all times. During the time, the output energy varied between 60 and 80 mJ due to fluctuations in the Tm:fibre laser power and ambient temperature and humidity. This is the first report of a fibre-laser pumped single-frequency *Q*-switched Ho^{3+} laser. Furthermore, it is the highest energy ever reported of any Ho oscillator-amplifier system pumped by a single Tm:fibre laser.

The single-frequency Ho:YLF oscillator-amplifier system was subsequently used to pump an HBr molecular laser [3]. The 1.2 m long resonator contained an HBr cell of length 91 cm which was operated at 60 mBar pressure. The 80% reflectivity output coupler at 4 µm also reflected the 2 µm pump light back for a double-pass pump configuration, albeit at a small angle to avoid optical feedback into the Ho:YLF ring oscillator. The maximum output energy of 2.5 mJ at 60 mJ incident pump energy was three times more than what was previously demonstrated with an optically pumped HBr laser [4]. The HBr laser simultaneously produced 4.17 µm and 4.19 µm in a 238 ns pulse which had a very sharp rise time of 14 ns. These results matched very well with predictions made with the numerical model developed for the HBr laser.

8.2.7 Contribution

The author contributed to the single-frequency *Q*-switched Ho:YLF oscillator-amplifier system in the following way:

- Jointly designed the Ho:YLF oscillator for high energy operation.
- Jointly specified the single-frequency diode seed laser, including the selection of operational wavelength suitable for pumping HBr.
- Jointly designed the optical layout for seeding the Ho:YLF oscillator.
- Jointly implemented the seeded Ho:YLF oscillator-amplifier system, including setting up diagnostics to evaluate the performance during intermediate steps.
- Jointly executed the experimental evaluation of the single-frequency *Q*-switched Ho:YLF oscillator-amplifier system.
- Led the implementation and experimental evaluation of the HBr molecular laser pumped by the single-frequency Ho:YLF oscillator-amplifier system.
- Presented an international *invited talk* on this research work [5].

8.2.8 References

[1] E. D. Black, "An introduction to Pound-Drever-Hall laser frequency stabilization," Am. J. Phys. **69** (1) pp 79-87 (2001).

[2] Y. Bai, J. Yui, M. Petros, P.Petzar, P. Trieu, H. Lee and U. Singh, "Highly efficient *Q*-switched Ho:YLF laser pumped by Tm:fiber laser." CLEO/QELS Conference, paper CtuN5, Baltimore, Maryland, USA (May 2007).

[3] L. R. Botha, C. Bollig, M. J. D. Esser, R. N. Campbell, C. Jacobs and D. R. Preussler "Ho:YLF pumped HBr Laser," *Optics Express*, **17** (22) 20615–20622 (Oct 2009).

[4] Miller *et al*, "An optically pumped mid-infrared HBr laser," *IEEE Journal of Quantum Electronics* **30** (10) 2395-2400 (Oct 1994).

[5] C. Bollig, M. J. D. Esser, C. Jacobs, W. Koen, D. Preussler, K. Nyangaza and M. Schellhorn, "70 mJ Single-Frequency *Q*-Switched Ho:YLF Ring Laser – Amplifier System Pumped by a Single 82-W Tm Fibre Laser," *Middle-Infrared Coherent Sources*, Trouville, France, 8-12 June 2009, Mo3 **(*invited*)** (2009).

8.3 Development of a high power Tm:YLF slab laser

Tm:YLF is an attractive alternative material for laser operation at 1.9 µm and as a pump source for Ho^{3+} doped laser systems [1, 2, 3, 4, 5, 6, 7, 8]. However, scaling to high average powers is challenging since the host material, YLF, has a low fracture limit [9]. The highest reported output power of a Tm:YLF laser in a rod geometry is 55 W [10] but further power scaling has been demonstrated using an end-pumped slab geometry [7], which is an attractive approach also considering the natural geometric match to the elongated beam profile of high average power laser diode stacks. The previous maximum continuous-wave power reported of a single slab Tm:YLF laser is 68 W for an absorbed pump-power of 218 W [7]. According to their scaling calculations, the authors expected ~ 200 W for an optimised two-slab laser.

8.3.1 Introduction

The objective of the research work reported in this section was to develop a high power Tm:YLF slab laser end-pumped by two high power laser diode stacks from each end such that the Tm:YLF laser could be used as pump source for a Ho:YLF slab amplifier. The available Ho:YLF amplifier crystal had Brewster cut entrance and exit faces in order to avoid the need of anti-reflection coatings. At very high energy densities anti-reflection coatings can be damaged, whereas the damage threshold of Brewster angled faces is significantly higher. However, the Brewster cut faces only allow low-loss transmission on one polarisation, in this case the horizontal polarisation. The Ho:YLF amplifier crystal was cut such that the crystalline c-axis was horizontal, making the π-polarisation the only accessible polarisation on which the Ho:YLF crystal could be pumped with the Tm:YLF slab laser.

Figure 8.16 shows the π-polarisation absorption spectrum of Ho:YLF. Ideally, Ho:YLF would be pumped on the π-polarisation either at 1890 nm or at 1940 nm. However, neither of these two wavelengths was easily accessible with the high-power Tm:YLF laser which typically operated on the σ-polarisation of Tm:YLF. The wavelengths at which the initial high-power Tm:YLF laser operated are indicated on the graph of Figure 8.16.

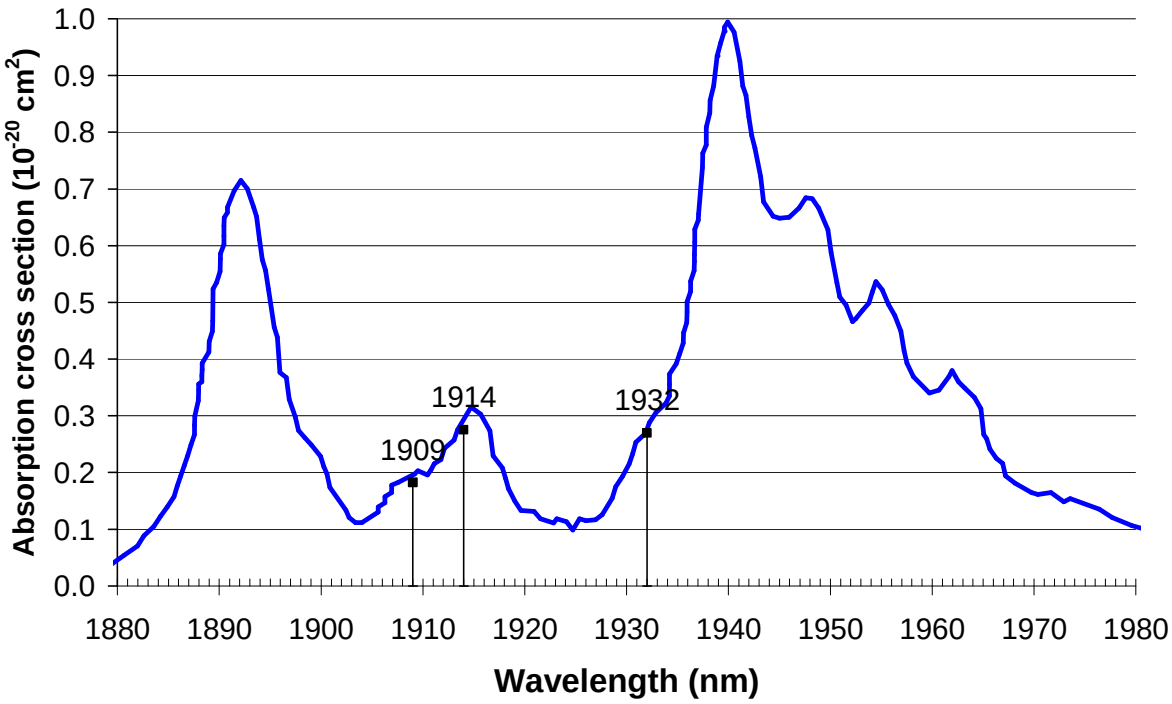

Figure 8.16: Ho:YLF absorption spectra on π-polarisation and the achieved wavelengths of the high-power Tm:YLF laser operated on σ-polarisation.

8.3.2 Tm:YLF slab laser design

It was concluded from the literature and numerical calculations that a 2.5% doped Tm:YLF slab with dimensions 11 mm-wide (c-axis), 1.5 mm-thick (a-axis) and 19 mm-long (a-axis) should be utilised when pumped with two laser diode stacks (nLIGHT, NL-VSA-05-300-792-F900D), each producing 300 W at 792.5 nm.

The Tm:YLF slab crystal was mounted in a custom-designed water-cooled copper heat sink using 200 µm thick indium foil as interface layer. The water temperature was kept between 10 °C and 20 °C during the experiments. An assembly drawing of the custom-designed cooling mount is shown in Figure 8.17. The novel design ensured sufficient cooling of the Tm:YLF crystal even under intense laser diode pump radiation.

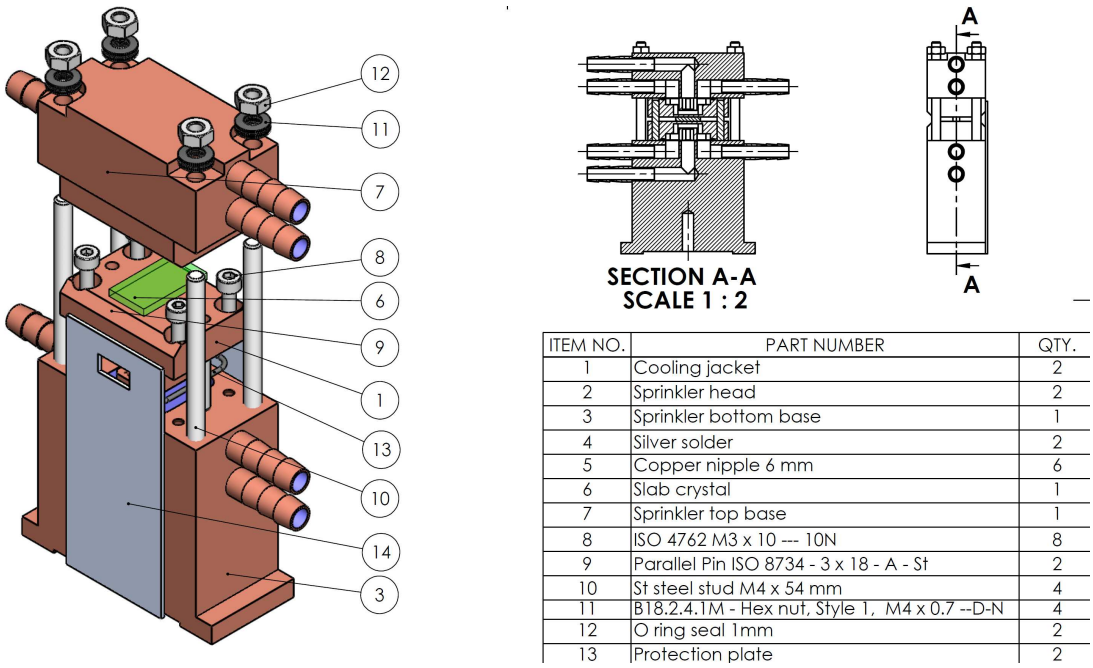

ITEM NO.	PART NUMBER	QTY.
1	Cooling jacket	2
2	Sprinkler head	2
3	Sprinkler bottom base	1
4	Silver solder	2
5	Copper nipple 6 mm	6
6	Slab crystal	1
7	Sprinkler top base	1
8	ISO 4762 M3 x 10 --- 10N	8
9	Parallel Pin ISO 8734 - 3 x 18 - A - St	2
10	St steel stud M4 x 54 mm	4
11	B18.2.4.1M - Hex nut, Style 1, M4 x 0.7 --D-N	4
12	O ring seal 1mm	2
13	Protection plate	2

Figure 8.17: Assembly drawing of the custom-designed water-cooled copper mount for the Tm:YLF slab crystal.

The optical layout of the dual-end-pumped Tm:YLF slab laser is shown in Figure 8.18. Two cylindrical lenses were used for each stack to produce a line focus inside the slab of ~900 µm in height and ~10 mm in width. Half-wave plates at 792 nm (not indicated in Figure 8.18) were used to orientate the output polarisation of the laser diode stacks for maximum absorption in the Tm:YLF crystal. Approximately 80% – 90% of the polarized pump radiation was absorbed in a single pass from each side. The transmitted pump power was spatially separated from the counter-propagating incident pump beam and measured on a power meter (not indicated in Figure 8.18). The resonator length was between 160 mm and 210 mm for different configurations.

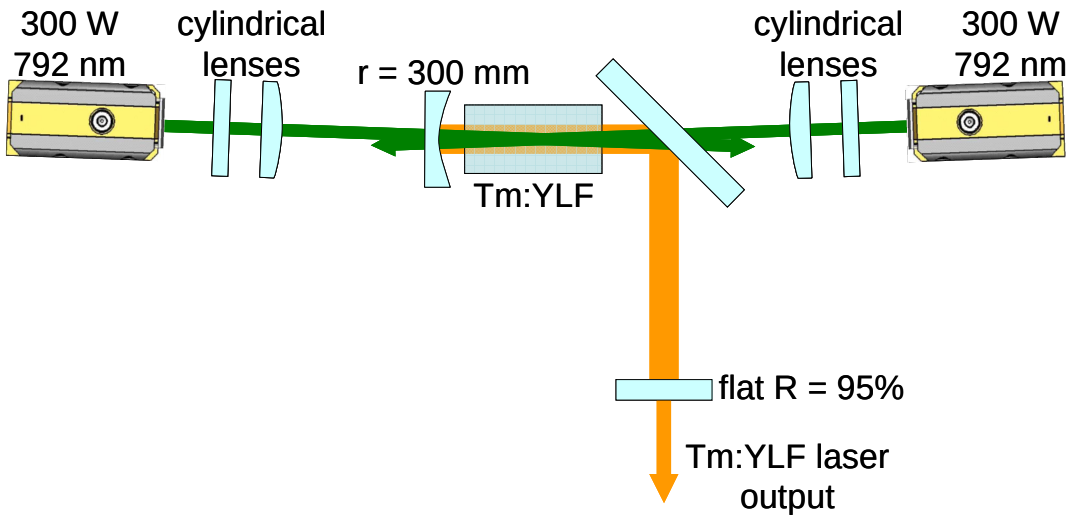

Figure 8.18: Optical layout of the dual-end-pumped Tm:YLF slab laser.

The folded resonator consisted of a concave end-mirror with 300 mm radius of curvature with high reflectivity (R > 99.8%) in the wavelength range 1.9 – 2.1 µm and high transmission (T > 95%) at the pump wavelength, one flat 45° dichroic mirror with high reflectivity (R > 99.9%) at the s-polarised and p-polarised components in the wavelength range 1.9 – 1.95 µm and high transmission at the pump wavelength (T > 95%), as well as a flat output coupler mirror.

Several output coupler reflectivity values were tested during the experiments with the Tm:YLF laser operating on the σ-polarisation. In the final configuration a 95% reflectivity output coupler was used. The complete optical layout was enclosed in a box which was flushed with dry synthetic air to avoid atmospheric water absorption of the generated 1.9 µm laser light which could have led to instabilities and optical damage to the laser components.

8.3.3 Experimental results on σ-polarisation

During the implementation of the high-power Tm:YLF laser the following laser configurations were analysed:

- With an R = 90% output coupler and no etalon, operating at 1909 nm.
- With an R = 90% output coupler and a 55 µm etalon, operating at 1914 nm.
- With an R = 95% output coupler and no etalon, operating at 1932 nm.

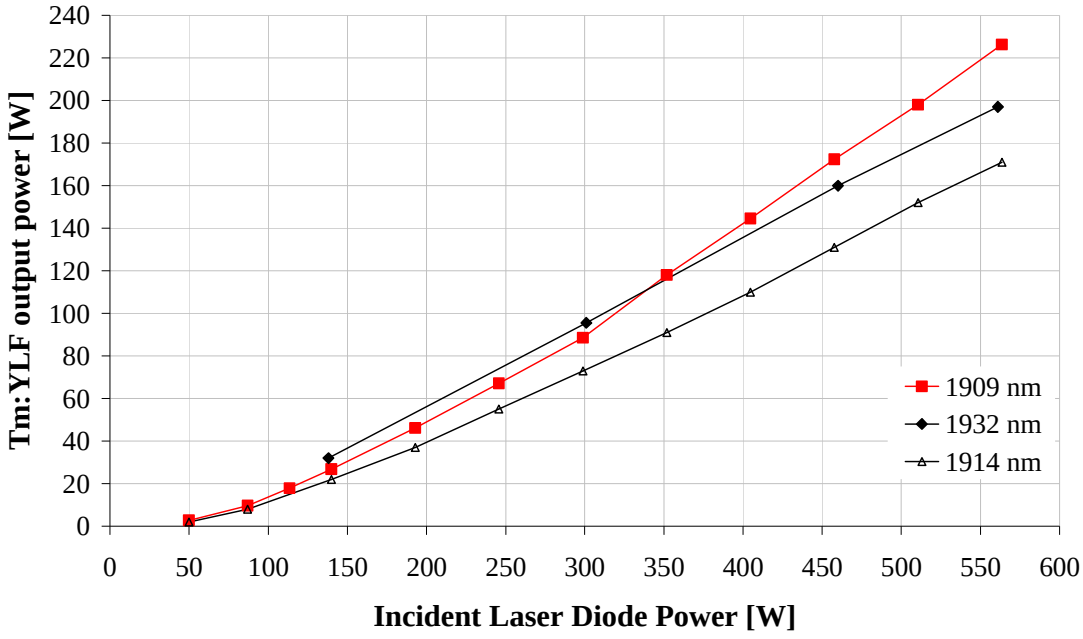

Figure 8.19: Output power of the Tm:YLF laser as a function of laser diode pump power.

The output power of the Tm:YLF laser as a function of laser diode pump power is shown in Figure 8.19. The first Tm:YLF slab laser yielded 225 W of output power, which is the highest reported power ever achieved from a Tm:YLF laser. The slope efficiency of the laser was 52% over the pump power range 300 W – 560 W. The optical-to-optical efficiency at full pump power was 40%. The drawback of this laser was that it operated on 1909 nm, which is not ideal for pumping a Ho:YLF amplifier due to the low absorption on the π-polarisation at 1909 nm.

A theoretical analysis of the expected laser threshold and wavelength of the Tm:YLF laser was conducted, similar to that reported in Chapter 4 for the Tm:$GdVO_4$ laser. It was concluded that operation at the 1915 nm peak of the Ho:YLF absorption ought to be achievable with the Tm:YLF laser by inserting an etalon into the cavity with a 90% reflectivity output coupler.

With the etalon inserted in the Tm:YLF laser cavity it was determined that laser oscillation at 1914 nm is feasible, but with a reduced output power of 171 W as indicated in Figure 8.19. Even more critical was the fact that both the output power and the wavelength fluctuated quite strongly over a short time scale. This was attributed to temperature changes of the etalon which was also influenced by stray pump light heating up elements in the closed laser box.

After an initial evaluation of the high-energy Ho:YLF amplifier pumped with the second version of the Tm:YLF laser, it was concluded that the performance was not repeatable due to the power and wavelength fluctuations. A third approach was implemented to force the laser to longer wavelengths by using the quasi-three-level nature of Tm:YLF and an output coupler with higher reflectivity. With a 95% reflectivity output coupler the third version of the Tm:YLF laser reached a wavelength of 1932 nm with a maximum output power of 197 W, without the need of an etalon in the laser cavity. As can be seen in Figure 8.16, 1932 nm is on the slope of the strong 1940 nm absorption line but has a similar cross section as the peak of the weaker 1914 nm line. The intensity beam profile at maximum output power output power of the third Tm:YLF laser operated at 1932 nm is shown in Figure 8.20.

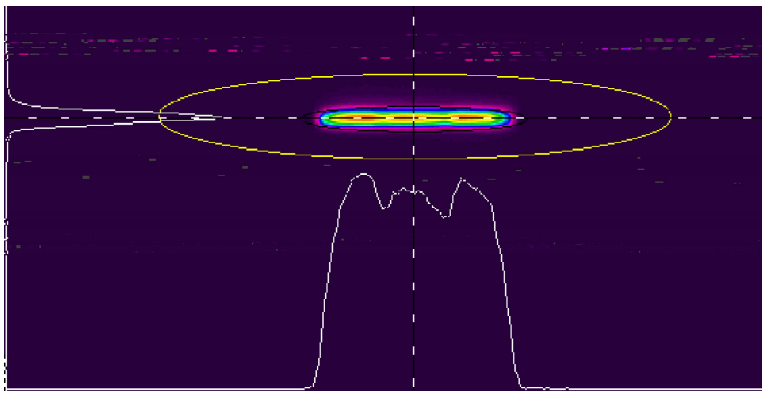

Figure 8.20: Intensity beam profile of the high-power Tm:YLF slab laser.

During the experimentation it was found that this Tm:YLF laser design was, in general, much more stable than the second version. Unfortunately, optical damage occurred on the 45° resonator mirror during the experiments due to the extremely high intra-cavity circulating power at this 95% reflectivity output coupler. The damage resulted in obtaining only 100 W output power and the output wavelength changed to 1928 nm. The Tm:YLF laser with the optical damage was not suitable for pumping a Ho:YLF amplifier.

8.3.4 Final experimental results

Using the Tm:YLF lasers described above (prior to obtaining optical damage) only between 50% and 70% of the Tm:YLF power was absorbed in the Ho:YLF amplifier crystal. This was mainly due to the fact that the wavelengths 1914 nm and 1932 nm of the Tm:YLF lasers were not optimum. To improve the performance of the Ho:YLF amplifier setup it was therefore required to change the Tm:YLF output wavelength to better overlap with one of the Ho:YLF absorption peaks, either at 1940 nm or at 1890 nm.

High power operation of the Tm:YLF laser at the 200 W level on 1940 nm might be possible by using a Volume Bragg Mirror (VBM) although this has not been demonstrated above 40 W of output power [6, 11]. Furthermore, such a specialised mirror was not available for these experiments. The alternative solution was to operate the Tm:YLF laser on π-polarisation which was previously not preferred due to the stronger negative thermal lens as compared to the σ-polarisation. The new resonator design described below therefore had to accommodate this strong negative thermal lens generated under intense laser diode end-pumping. The optical layout of the high power Tm:YLF laser operated on π-polarisation is shown in Figure 8.21.

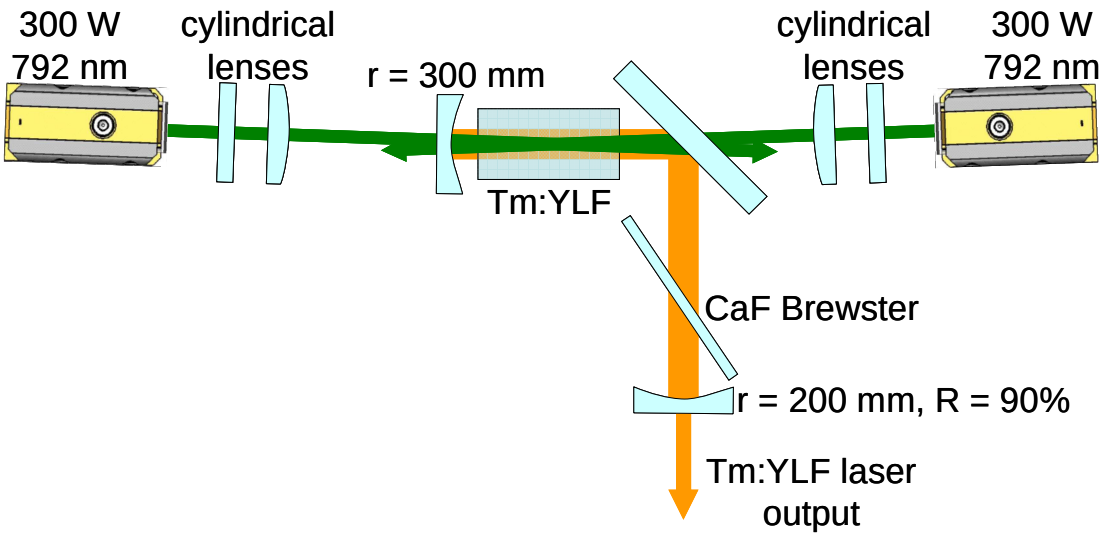

Figure 8.21: Optical layout of the high power Tm:YLF slab laser operated on π-polarisation.

In this arrangement the output coupler reflectivity was decreased from 95 % to 90 % in order to decrease the intra-cavity power in the resonator, thus preventing optical damage of the laser components. Furthermore, the flat output coupler was changed to a concave output coupler mirror with a curvature of 200 mm in order for the resonator to be stable for lasing on the π-polarisation which had a strong negative thermal lens. Finally, a CaF Brewster plate was inserted into the resonator to induce losses for the σ-polarisation, thus ensuring that the laser only operated on the π-polarisation. This resulted in stable output of the Tm:YLF laser with a wavelength in the range 1888 – 1890 nm. The new laser resonator design resulted in a more divergent output beam due to the curved output coupler mirror and strong negative thermal lens, which was corrected outside the cavity with a plano-convex lens with a focal length of 100 mm, placed just behind the output coupler.

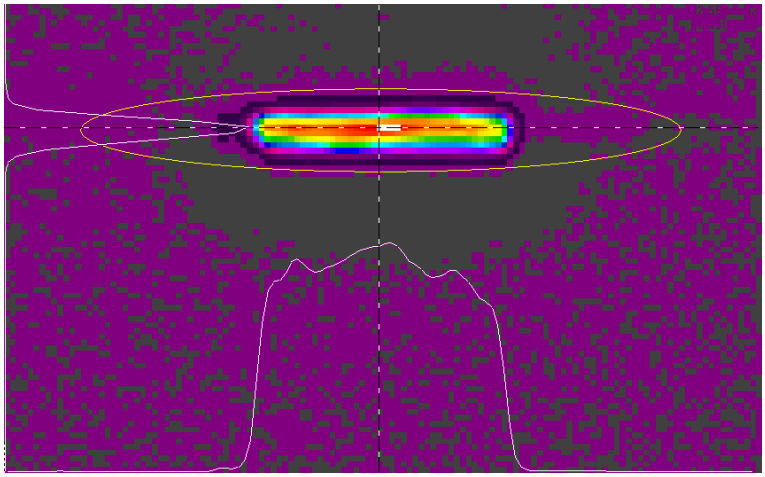

Figure 8.22: Intensity beam profile of the Tm:YLF slab laser operated on π-polarisation.

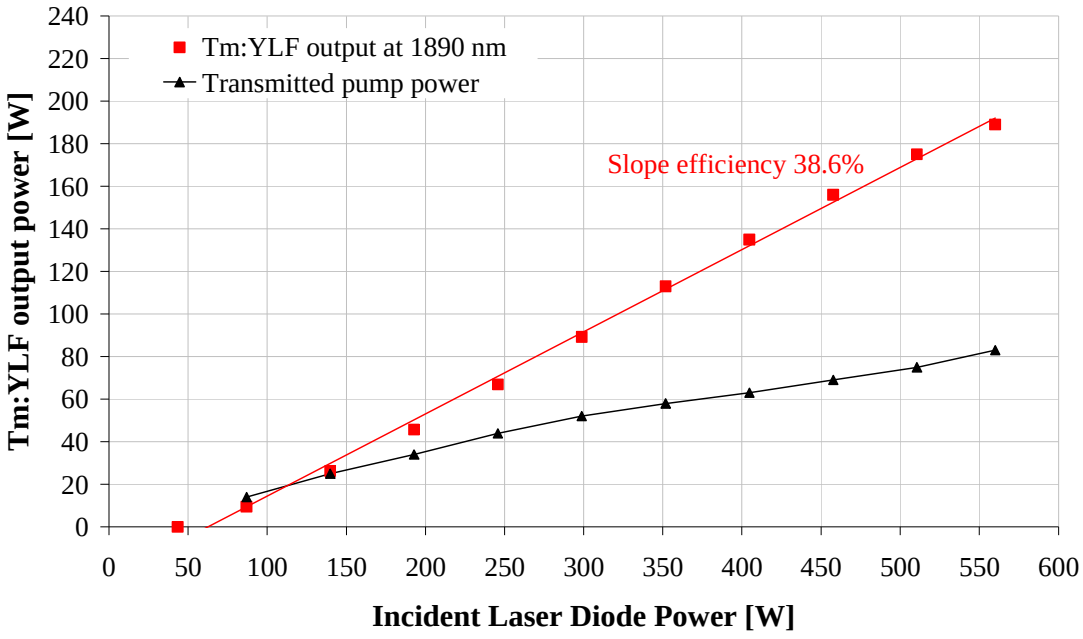

Figure 8.23: Output power of the Tm:YLF slab laser operated on π-polarisation.

The output power of the optimised Tm:YLF slab laser is shown in Figure 8.23 as a function of the incident laser diode pump power. Also indicated on this graph is the transmitted laser diode pump power. The intensity beam profile at full output power is shown in Figure 8.22.

The Tm:YLF slab laser delivered a maximum output power of 189 W with beam quality factor of $M^2_x = 443$ in the horizontal plane and $M^2_y = 3.8$ in the vertical plane. It had a slope efficiency of 39% (45%) and an optical-to-optical efficiency of 34% (40%) with respect to incident (absorbed) pump power. The laser output wavelength for all output powers was measured to be in the range 1888 – 1890 nm which overlapped with the 1890 nm absorption peak of Ho:YLF.

8.3.5 Conclusions

The objective of this research work was reached with the demonstration of a Tm:YLF slab laser end-pumped by two high power laser diode stacks, which produced in different configurations, output powers well in excess to what has been demonstrated before. Several resonator designs were implemented in an effort to reach wavelengths with the Tm:YLF laser which are suitable for pumping a Ho:YLF amplifier crystal.

The Tm:YLF laser with the 90% reflectivity output coupler mirror produced 225 W at 1909 nm, which is the highest power demonstrated for a Tm:YLF laser to date. An

earlier version of this laser utilised a 11 mm-wide (c-axis), 2 mm-thick (a-axis), 20 mm-long (a-axis) 2% doped Tm:YLF slab to produce 148 W output at 1912 nm in an elongated beam with $M^2_x \approx 199$ and $M^2_y \approx 1.7$, and has often been cited as the state of the art [12].

High power operation of a Tm:YLF slab laser operating on π-polarisation at wavelengths shorter than 1900 nm has not been reported prior to this work, which resulted in 189 W output power at 1888 – 1890 nm, with a slight reduction in beam quality due to the strong negative thermal lens. This laser was used as pump source for a high-energy 2 µm amplifier based on both a Ho:YLF and a Ho:LuLF slab crystal [13], as well as a hybrid stable-unstable resonator utilising the same crystals [14]. The development of these devices are described in the next sections.

The record-breaking performance of the Tm:YLF slab laser was attributed to the selection of the optimum crystal dimensions and appropriate Tm^{3+} doping for the available pump power. Furthermore, the high pump power levels reaching almost 600 W would have resulted in thermal fracture of the laser crystal had the custom-designed water-cooled mount not been implemented. Finally, obtaining the maximum output power from the Tm:YLF laser required suitable resonator designs to accommodate the thermal lens, as well as optimum alignment of the counter-propagating pump beams in the Tm:YLF slab crystal with the resonator mode formed by the cavity mirrors.

Further improvements have been identified for the high power Tm:YLF laser and include:

- A resonator with two Tm:YLF slab crystals, each pumped by two high power laser diodes.
- New pump optical arrangement to ensure efficient absorption of the laser diode light, as well as a higher power laser diode stack.
- Utilisation of Volume Bragg Mirrors with defined wavelength suitable for pumping Ho:YLF and Ho:LuLF.
- Hybrid stable-unstable resonator to ensure high beam quality output in both resonator planes.

8.3.6 Contribution

The author contributed to the high power Tm:YLF slab laser development in the following way:

- Jointly specified the Tm:YLF slab crystals.
- Jointly designed the water-cooled mount for Tm:YLF slab crystal exposed to high pump powers.
- Jointly specified and characterised the high power laser diode stacks suitable for pumping the Tm:YLF slab crystals.
- Implemented and analysed the 225 W Tm:YLF slab laser.
- Jointly designed, implemented and analysed the Tm:YLF laser operating at 1914 nm and at 1932 nm.
- Jointly designed, implemented and analysed the Tm:YLF laser operating on π-polarisation at 1888 – 1890 nm.
- Specified (in more detail than listed above) the implementation of improvements for future Tm:YLF slab lasers.

8.3.7 References

[1] Brian M. Walsh, Norman P. Barnes, Baldassare Di Bartolo, "Branching ratios, cross sections, and radiative lifetimes of rare earth ions in solids: Application to Tm3+ and Ho3+ ions in $LiYF^4$", *Journal of Applied Physics*, vol. 83, no 5, pp. 2772-2787, 1 March 1998.

[2] M. Schellhorn, A. Hirth, "Modelling of Intracavity-Pumped Quasi-Three-Level Lasers", *IEEE Journal of Quantum Electronics,* vol. 38, no. 11, pp. 1455-1464, Nov. 2002.

[3] M. Schellhorn, A. Hirth, and C. Kieleck, "Ho:YAG laser intracavity pumped by a diode-pumped Tm:YLF laser". *Opt. Letters*, vol. 28, no. 20, pp.1933-1935, Oct. 15, 2003.

[4] P. A. Budni, C. R. Ibach, S. D. Setzler, E.J. Gustavson, R. T. Castro, and E. P. Chicklis, "50-mJ, Q-switched, 2.09-um holmium laser resonantly pumped by a diode-pumped 1.9-um thulium laser", *Opt. Letters*, vol. 28, no.12, pp. 1016-1018, June 15, 2003.

[5] Brian M. Walsh and Norman P. Barnes, Mulugeta Petros, Jirong Tu and Upendra N. Singh, " Spectroscopy and modelling of solid state lanthanide lasers: Application to trivalent Tm^{3+} and Ho^{3+} in $YLiF^{4}$ and $LuLiF^{4}$", *Journal of Applied Physics*, vol. 95, no. 5, pp.3255-3271, 1 April 2004.

[6] Alex Dergachev, Peter F. Moulton, Vadim Smirnov, Leonid Glebov, "High power CW Tm:YLF laser with a holographic output coupler", CLEO 2004, m-PTR-01.

[7] S. So, J.I. Mackenzie, D.P. Shepherd, W.A. Clarkson, J.G. Betterton, and E.K. Gorton, "A power-scaling strategy for longitudinally diode-pumped Tm:YLF lasers," Appl. Phys. B **84** (3) 389-393 (2006).

[8] S. So, J.I. Mackenzie, D.P. Shepherd, and W. A. Clarkson, J. G. Betterton, E. K. Gorton, and J. A. C. Terry, "Intra-cavity side-pumped Ho:YAG laser", *Optics Express*, vol. 14, no. 22, pp. 10481-10486, 30 Oct. 2006.

[9] C. Bollig, C. Jacobs, H. M. von Bergmann and M. J. D Esser, "High-power end-pumped Nd:YLF laser without lifetime quenching," *CLEO Europe 2005*, CA3-3-TUE (invited).

[10] M. Shellhorn, "High-power diode-pumped Tm:YLF laser" *Applied Physics B* **91** (1) 71-74 (2008).

[11] X.M. Duan, B.Q. Yao, G. Li, T.H. Wang, Y.L. Ju and Y.Z. Wang, "Stable output, high power diode-pumped Tm:YLF laser with a volume Bragg grating" *Applied Physics B* **99** (3) 465–468 (2010).

[12] M. Shellhorn, S. Ngcobo, and C. Bollig, "High-power diode-pumped Tm:YLF slab laser" *Applied Physics B* **94** (2) 195-198 (2008).

[13] W. Koen, H. J. Strauss, C. Bollig, M. J. D. Esser, C. Jacobs, O. J. P. Collett, K. Nyangaza and D. Preussler "200 mJ Single Frequency Ho:YLF & Ho:LuLF Slab Amplifier System at 2064 nm" in *4th EPS-QEOD Europhoton Conference*,

Hamburg, Germany, WeC4, Europhysics Conference Abstract Volume 34C, ISBN 2-914771-64-9, (2010).

[14] M. J. D. Esser, H. J. Strauss, W. Koen, O. J. P. Collett and C. Bollig "End-pumped Ho:YLF & Ho:LuLF Slab Laser" in *4th EPS-QEOD Europhoton Conference*, Hamburg, Germany, WeP29, Europhysics Conference Abstract Volume 34C, ISBN 2-914771-64-9, (2010).

8.4 Development of a Ho:YLF Ho:LuLF slab amplifier

8.4.1 Introduction

Single-frequency pulsed laser systems in the 2 µm region have applications in remote sensing, spectroscopy and defence. Up to 300 mJ of single-frequency energy was reported for a diode-side-pumped Tm-Ho co-doped MOPA system which was QCW-pumped for 1 ms by a total diode power of 9.3 kW [1]. An alternative approach is to end-pump a Ho-doped slab amplifier with a diode-end-pumped Tm-slab laser. Here a single-frequency slab amplifier is reported, based on Ho:YLF and Ho:LuLF delivering up to 210 mJ at 2064 nm with a beam quality factor of $M^2 \leq 1.4$ in both planes, in a scalable architecture.

8.4.2 Amplifier design

Numerical rate-equation calculations indicated that, for the specific Tm:YLF slab pump laser and single-frequency Ho:YLF oscillator-amplifier seed laser, an amplifier crystal length of greater than 80 mm would be optimal for a 0.5% doped Ho:YLF crystal in a single-pass amplification scheme. However, only a 43 x 10 x 2 mm^3 Brewster-cut Ho:YLF crystal was available for the amplifier experiments. In order to improve the amplifier efficiency an AR-coated 20 x 10 x 2 mm^3 Ho:LuLF crystal was added in series, as indicated in Figure 8.24. Both crystals were 0.5 % doped and orientated with their c-axis horizontal, so that the π-polarisation of the amplifier had a low loss on the Ho:YLF's Brewster faces.

The single frequency Ho:YLF ring laser and pre-amplifier system as described in Section 8.2 was used to seed the amplifier. During these experiments it delivered up to 65 mJ per pulse at 50 Hz, with a pulse duration of 370 ns. The ring laser and pre-amplifier was pumped by the commercial 80 W Tm:fibre laser, emitting at ~1940 nm.

The diffraction limited seed beam was focussed with cylindrical lenses to a radius of $w_x = 2.0$ mm and $w_y = 0.390$ mm in the AR-coated Ho:LuLF crystal, which was expanded by the Brewster faces to $w_x = 2.9$ mm in the Ho:YLF crystal. The pump beam from the Tm:YLF slab laser was matched to the seed beam in both crystals using a single spherical lens in an end-pumped configuration.

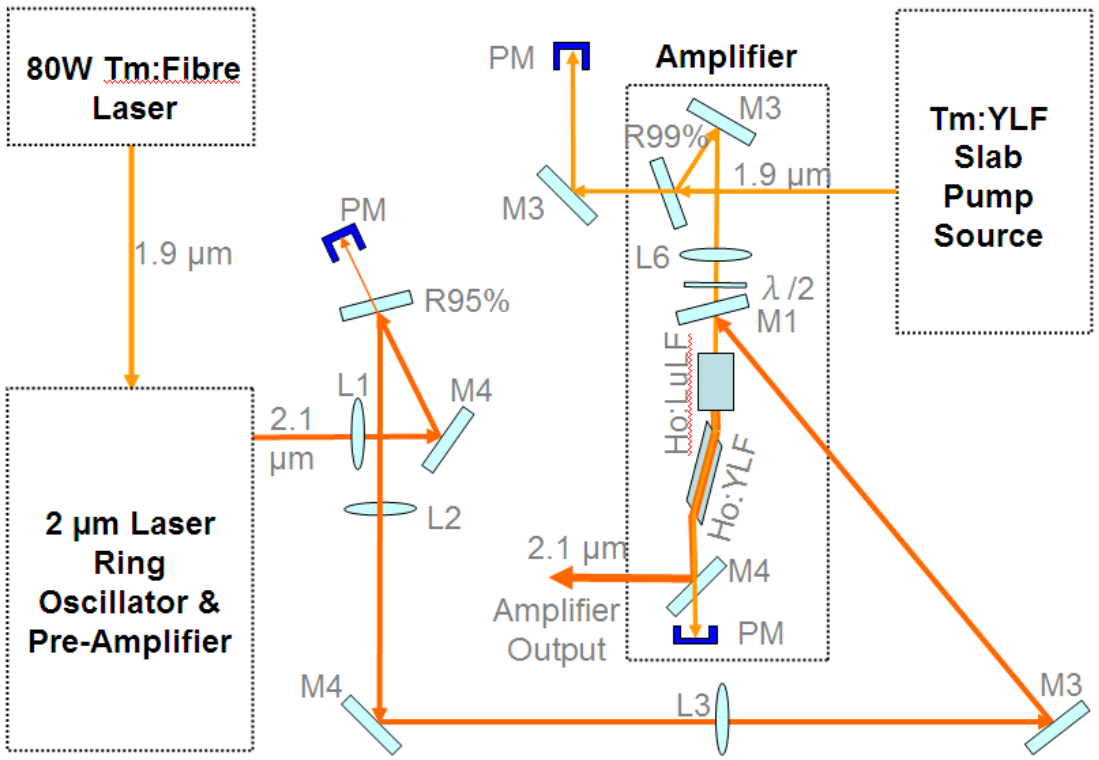

Figure 8.24: Optical layout of the high-energy single-frequency amplifier system.

The available pump laser for the amplifier was the Tm:YLF slab laser as described in Section 8.3. It was end-pumped by two 300 W laser diode stacks and delivered a total of 189 W at 1890 nm, of which 170 W was incident on the amplifier crystals. As described earlier, this laser was similar to the slab laser reported in [2] but redesigned to operate on the π-polarisation at 1890 nm instead of operating on the σ-polarization at 1910 nm. This was achieved by inserting a Brewster plate in the resonator and implementing a laser cavity that accommodated the stronger negative thermal lens associated with the π-polarisation. The resonator consisted of a 300 mm concave output coupler (R=90 %) and a 200 mm concave high reflector.

The change in operational wavelength of the Tm:YLF laser was critical for improved absorption of the pump light in the Holmium YLF and LuLF amplifier crystals, as can be seen in the graphs of absorption cross section of the two gain materials at 1.9 µm [3, 4] in Figure 8.25. Also shown in Figure 8.25 is the emission cross sections of Ho:LuLF and Ho:YLF, indicating that both gain media can amplify the seed on the π-polarisation at a wavelength of 2064 nm.

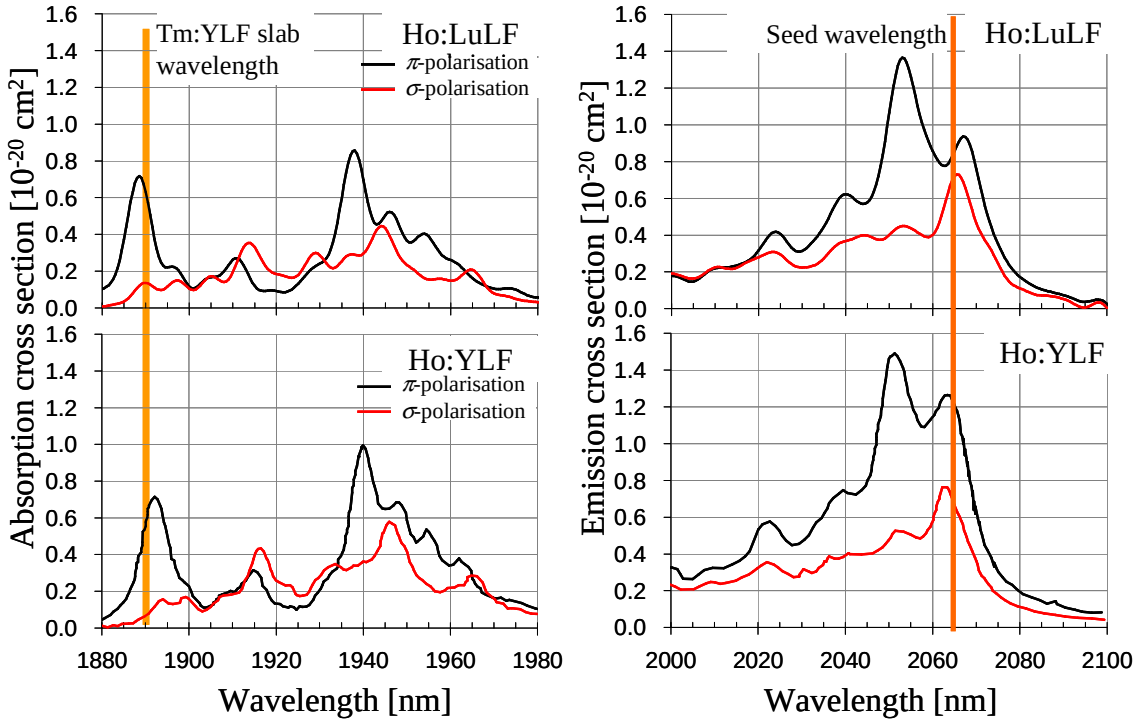

Figure 8.25: Ho:LuLF [3] and Ho:YLF [4] polarisation resolved absorption and emission cross sections. The Tm:YLF pump wavelength of 1890 nm is also indicated.

8.4.3 Experimental results

The amplifier performance was evaluated at increasing pump power from the Tm:YLF laser while the incident seed energy was at a maximum of 65 mJ at 50 Hz. The result of this measurement is shown in Figure 8.26. At full pump power of 170 W the amplified output energy was 210 mJ while only ~75 W of power was absorbed in the single pump pass. The measured gain factor was 3.2.

In a similar experiment with the system operated at 50 Hz, the pump power was kept at a maximum while the incident seed energy was increased, the result of which is shown in Figure 8.27. The measured amplifier gain at low incident seed energy was almost a factor of 5, decreasing to 3.2 at maximum incident energy. Also shown in Figure 8.27 is the performance of the system at different pulse repetition rates of the fibre-laser pumped single-frequency Ho:YLF oscillator-amplifier. Stable, frequency locked operation was possible from 10 Hz up to 300 Hz, over which range the gain factor changed from 2.9 to 3.15.

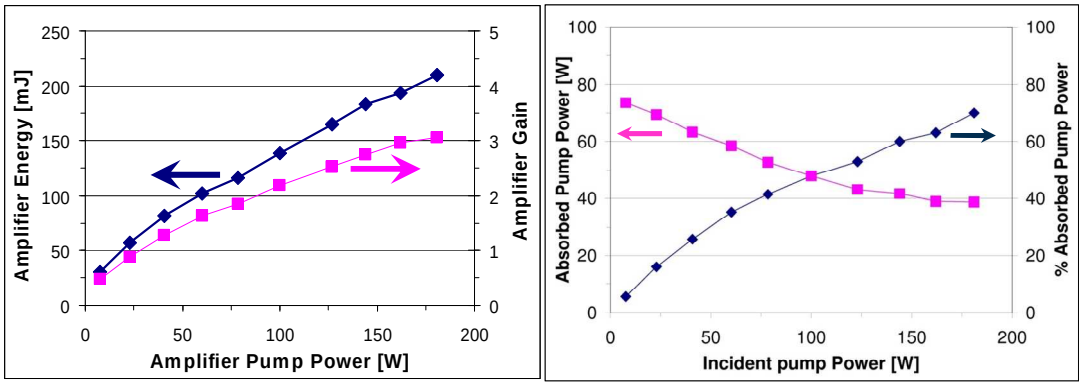

Figure 8.26: Output energy of the Ho:LuLF Ho:YLF amplifier as a function of pump power, at 65 mJ seed energy (left). The transmitted pump power is also indicated (right).

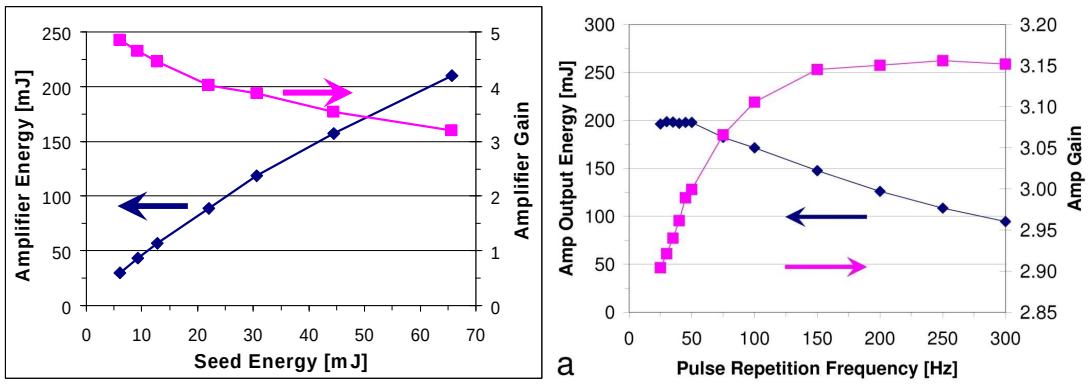

Figure 8.27: Output energy of the Ho:LuLF Ho:YLF amplifier at full pump power as a function of incident seed energy at 50 Hz (left), and of pulse repetition rate (right).

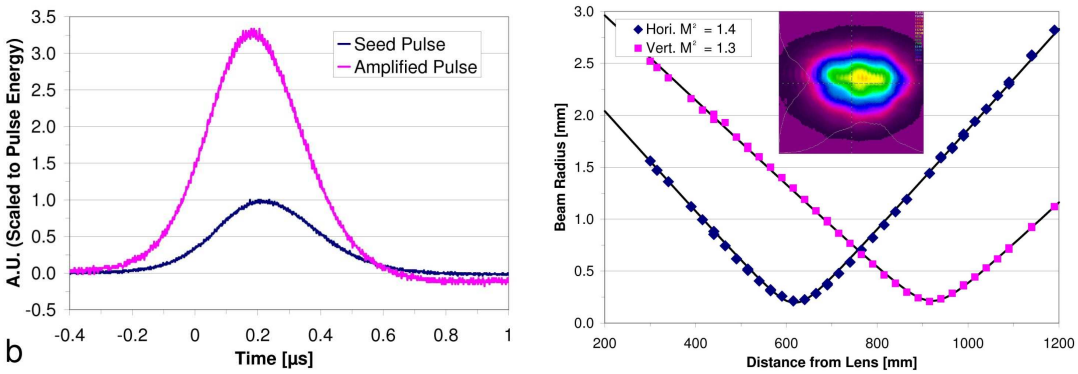

Figure 8.28: Time-resolved shapes of the measured seed and amplfied pulses (left). The M^2 beam quality factors was measured for both the horisontal and vertical planes of the slab amplfier (right).

Shown in Figure 8.28 are the measured seed pulse shapes and the amplfied pulse shapes, indicating that the 370 ns seed pulse was amplfied and only slightly reduced in duration to ~350 ns without distorting the temporal profile significantly. Also shown in Figure 8.28 are the measured M^2 factors for the horizontal and vertical planes for the amplifier output beam, showing that the $M^2 < 1.05$ seed beam was slightly

distorted in the slab amplifier to $M^2_{horizontal}$ = 1.4 and $M^2_{vertical}$ = 1.3. The far-field intensity beam profile (insert) also indicated a deterioration of the beam quality, most likely due to the non-uniform negative thermal lens associated with the π-polarisation of the Ho:LuLF and Ho:YLF amplifier crystals.

8.4.4 Conclusions

A high energy amplifier system based on Ho:YLF and Ho:LuLF slab crystals was demonstrated for the first time to amplify single frequency pulses at 2064 nm. The slab geometry of the amplifier crystals was ideally suited for the high-power Tm:YLF pump laser which produced 170 W incident pump power at 1890 nm in an elongated beam. For efficient amplification, the circular-symmetric, high beam quality seed beam was shaped with cylindrical lenses to match the pump beam in the amplifier crystals.

A maximum gain factor of 3.2 resulted in amplified output pulses at 210 mJ per pulse with 350 – 370 ns duration. The amplified beam quality was equal or better than M^2 1.4 in both planes. It was concluded that it would be preferential to amplify on the σ-polarisation of the Ho:YLF and Ho:LuLF gain media to avoid the strong negative thermal lens observed on the π-polarisation, which was the only option available for these experiments due to the Brewster-cut faces of the Ho:YLF slab crystal.

The possible improvement in performance was identified through the implementation of a multi-pass amplification configuration. Furthermore, it is clear from the more than 63 % transmitted pump light that the absorption of the amplifier should be improved, either by changing the Tm:YLF slab laser pump wavelength (as recommended at the end of Section 8.3 with the use of Volume Bragg Mirrors) or through the implementation of longer gain crystals.

Initial results of an improved amplifier setup, utilising two 50 mm long Ho:YLF slab amplifier crystals in a double-pass amplification scheme are promising. The amplifier was operated on the σ-polarisation and produced ~320 mJ for 170 W of Tm:YLF pump power and ~60 mJ incident seed energy, with a gain factor better than 5. This ongoing collaborative research already resulted in one international conference presentation [5].

8.4.5 Contribution

The author contributed to the high energy Ho:LuLF Ho:YLF slab amplifier development in the following ways:

- Jointly specified the Ho:LuLF and Ho:YLF slab amplifier crystals.
- Jointly designed the water-cooled mount for the Brewster-faced Ho:YLF slab crystal and the micro-channel-cooled mount for the Ho:LuLF slab crystal, suitable for operation high pump powers.
- Jointly designed, specified and implemented the optical layout to couple the seed into the amplifier crystals.
- Characterised the Tm:YLF pump beam in the position of the amplifier crystals.
- Jointly analysed the single-pass amplifier performance and
- Jointly prepared results for publication [5].

8.4.6 References

[1] J. Yu, B. Trieu, Y. Bai, P. Petzar and U.N. Singh, "300 mJ, injection seeded, compact 2 µm coherent Lidar transmitter," Proceedings of SPIE Vol. 6409, 64091A-1 (2006).

[2] M. Schellhorn, S. Ngcobo, C. Bollig, M. J. D. Esser, D. Preussler, K. Nyangaza, "High-power diode-pumped Tm:YLF slab laser," *CLEO Europe*, Munich, Germany, 14-19 June 2009, CA1.3 (2009).

[3] Data supplied by J.I. Mackenzie, ORC Southampton.

[4] Brian M. Walsh, Norman P. Barnes, Baldassare Di Bartolo, "Branching ratios, cross sections, and radiative lifetimes of rare earth ions in solids: Application to Tm^{3+} and Ho^{3+} ions in $LiYF_4$", *Journal of Applied Physics*, vol. 83, no 5, pp. 2772-2787, 1 March 1998.

[5] W. Koen, H. J. Strauss, C. Bollig, M. J. D. Esser, C. Jacobs, O. J. P. Collett, K. Nyangaza and D. Preussler "200 mJ Single Frequency Ho:YLF & Ho:LuLF Slab Amplifier System at 2064 nm" in *4th EPS-QEOD Europhoton Conference*, Hamburg, Germany, WeC4, Europhysics Conference Abstract Volume 34C, ISBN 2-914771-64-9, (2010).

8.5 Demonstration of a hybrid Ho:YLF Ho:LuLF slab laser

The last few years have seen an increased effort in the development of high power and high energy solid-state lasers operating in the 2 µm wavelength region by in-band pumping a Ho-doped material with a Tm-doped laser operating near 1.9 µm. The fluoride host materials YLF and LuLF have gained attention due to a number of favourable properties, such as a weak negative thermal lens and good energy storage for pulsed operation. For example, an end-pumped rod laser based on the relatively new Ho:LuLF material was recently demonstrated to deliver up to 5.4 W of continuous-wave power in near diffraction limited beam [1]. Also, a Tm:fiber laser pumped Ho:LuLF laser has been designed for *Q*-switched operation at 100 Hz, producing 24.8 mJ pulses at 2052 nm in a good beam quality [2].

As an additional collaborative research project, a slab oscillator was developed utilising the same Tm:YLF pump laser and slab Ho:YLF and Ho:LuLF crystals used for the slab amplifier development. The resonator was implemented in a stable concave-plane resonator as well as in a hybrid stable-unstable resonator configuration.

8.5.1 Resonator designs

As discussed in Section 8.3, the high power Tm:YLF slab laser was modified to operate at 1.890 µm by forcing it on to the π-polarisation with an intra-cavity Brewster plate and choosing an appropriate resonator. This pump laser produced up to 180 W incident on the Ho:YLF and Ho:LuLF oscillator crystals which were placed in series to increase the absorption of the pump light, as shown in the optical layout of Figure 8.29. A total of 95 to 108 W was absorbed in a single pump-pass configuration during operation of the Ho:YLF Ho:LuLF laser.

The Ho:LuLF crystal had dimensions 2 x 10 x 20 mm^3 of which the 2 x 10 mm^2 faces were AR coated at 2 µm. The Ho:YLF crystal was cut at Brewster's angle with dimensions 2 x 10 x 43 mm^3. Both crystals were a-cut with the c-axes horizontal, which together with the Ho:YLF's Brewster faces forced the laser to oscillate on the π-polarisation. The incident Tm:YLF pump beam radii were $w_y = 0.5$ mm and $w_x = 2.8$ mm in the two planes and the measured Tm:YLF beam quality factors were $M^2_x \sim 490$ and $M^2_y \sim 2.7$. The slab geometry was preferred for the 0.5% doped Ho:YLF and Ho:LuLF crystals to facilitate easy coupling of the elliptical pump beam

into the oscillator crystals, and to reduce the likelihood of thermal fracture when scaling to multi-hundred watt continuous-wave power levels.

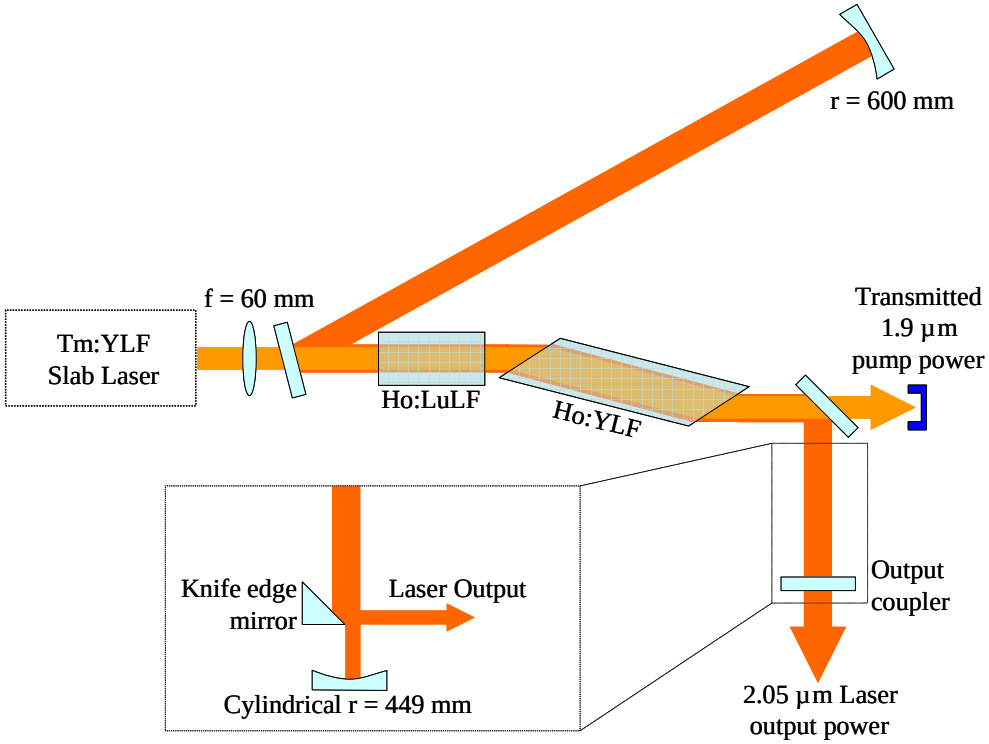

Figure 8.29: Optical layout of the Ho:YLF Ho:LuLF slab oscillator in a stable concave-plane resonator, as well as a hybrid stable-unstable resonator (insert).

The stable concave-plane resonator, as shown in Figure 8.29, consisted of a high-reflective end-mirror with radius of curvature r = 600 mm, flat dichroic pump mirrors and a flat output coupler mirror. Mirrors with reflectivity R = 80%, R = 65%, R = 50% and R = 30% at 2 µm were selected as output couplers. The total resonator length was ~650 mm which became stable for a weak negative thermal lens inside the Ho^{3+} crystals.

The hybrid stable-unstable resonator configuration utilised a cylindrical mirror of curvature r = 449 mm in the position of the flat output coupler mirror, and a knife-edge mirror close to the to the cylindrical mirror couple out the laser beam. The extent to which the knife edge mirror was brought into the unstable beam in the x-plane to produce efficient output coupling was determined experimentally.

8.5.2 Experimental results

Initially the Ho:YLF Ho:LuLF oscillator was tested with the stable concave-plane resonator. The output power as a function of *absorbed* Tm:YLF pump power is shown in Figure 8.30.

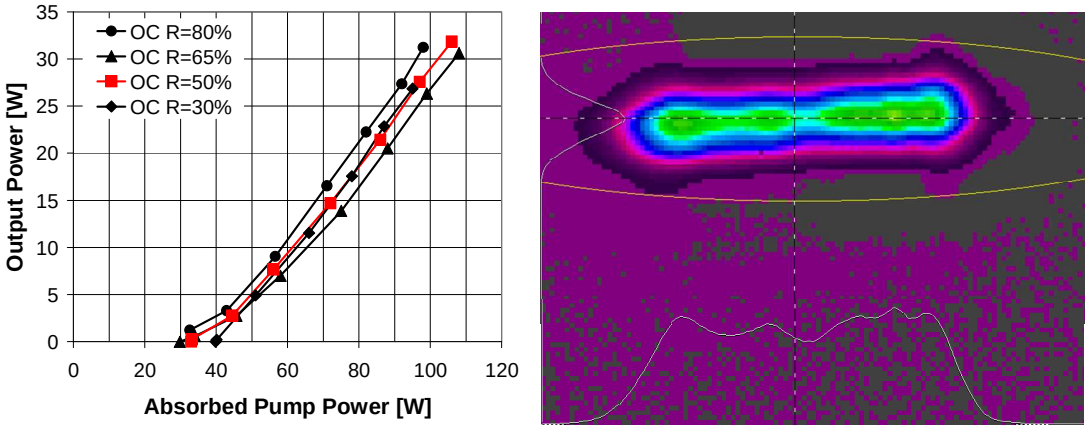

Figure 8.30: Output power of the Ho:YLF Ho:LuLF stable concave-plane resonator as a function of absorbed Tm:YLF pump power (left). The intensity beam profile of the oscillator at maximum output power (right).

The maximum output power of the Ho:YLF and Ho:LuLF laser was 32 W with the R = 50% output coupler which corresponded well to initial numerical simulations of the system. The output of the laser showed some temporal spiking and the wavelength ranged from 2.040 to 2.079 µm for the different output coupler mirrors. The elongated output beam was a consequence of the slab geometry of the laser, which was improved with the implementation of the hybrid-stable unstable resonator.

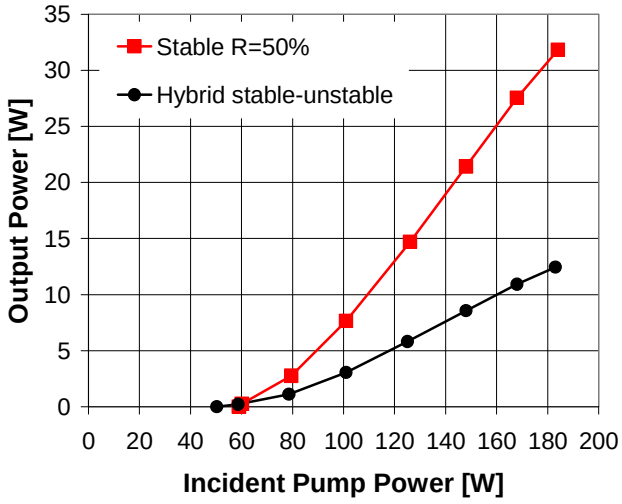

Figure 8.31: Output power of the hybrid Ho:YLF Ho:LuLF stable-unstable resonator as a function of incident Tm:YLF pump power, compared to the best performance of the stable resonator with a 50% output coupler mirror.

The output power of the hybrid Ho:YLF Ho:LuLF stable-unstable resonator is shown in Figure 8.31 as a function of *incident* Tm:YLF pump power. At full pump power the hybrid stable-unstable resonator produced 13 W of continuous-wave output power.

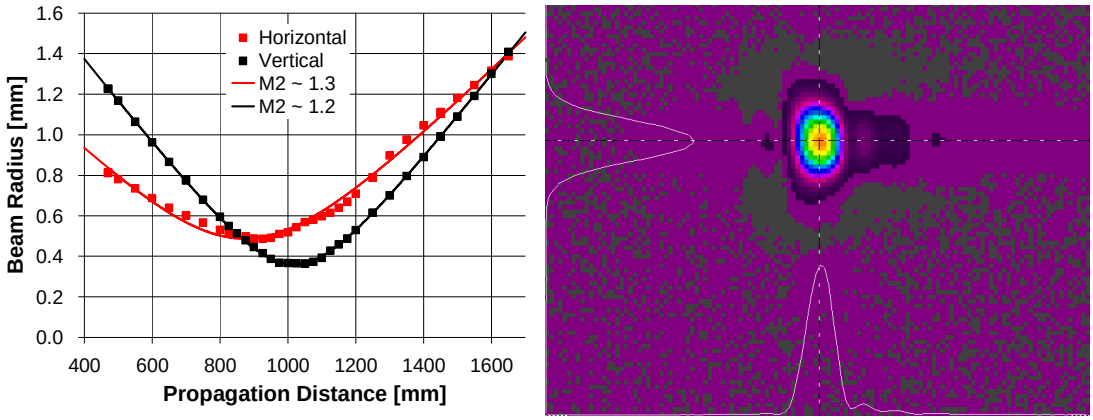

Figure 8.32: Measured beam quality factors and intensity beam profile of the hybrid stable-unstable Ho:YLF Ho:LuLF oscillator at maximum output power.

However, the hybrid stable-unstable resonator produced a superior beam quality which was measured to be M^2 beam quality factors of 1.2 and 1.3 in the vertical and horizontal planes respectively, as indicated in Figure 8.32. The diffraction caused by the knife edge output coupler mirror is clearly visible on the measured far-field beam profile of the hybrid stable-unstable resonator, also shown in Figure 8.32.

8.5.3 Conclusions

A 2 µm oscillator with a Ho:YLF and a Ho:LuLF slab crystal in one cavity end-pumped by a 180 W Tm:YLF slab laser was demonstrated for the first time. The maximum output power of the stable Ho:YLF and Ho:LuLF laser was 32 W with the R = 50% output coupler. The elongated output beam was a consequence of the slab geometry of the pump beam and laser crystals.

The hybrid stable-unstable resonator improved the M^2 beam quality factors to 1.2 and 1.3 in the vertical and horizontal planes respectively, at the cost of reducing the output power to 13 W. During laser oscillation of the hybrid stable-unstable resonator only 89 W of 183 W incident pump power was absorbed. It is believed that multi-pass pumping will increase the efficiency of the hybrid Ho:YLF & Ho:LuLF slab laser.

The research presented here is the initial work on hybrid stable-unstable slab laser architectures. This approach is attractive for scaling the output power of Ho:YLF and Ho:LuLF lasers significantly, using high-power Tm:YLF slab lasers as alternative pump source to, for example, Tm:fibre lasers at 1.9 µm. The research already resulted in an international conference poster presentation [3].

8.5.4 Contribution

The author contributed to the Ho:LuLF Ho:YLF oscillator development in the following ways:

- Taken the lead in the design, implementation and analysis of the Ho:LuLF Ho:YLF stable concave-plane resonator and the hybrid stable-unstable resonator.
- Taken the lead in the preparing and presenting the results for publication [3].

8.5.5 References

[1] J. W. Kim, J. I. Mackenzie, D. Parisi, S. Veronesi, M. Tonelli and W. A. Clarkson, "Efficient in-band pumped Ho:LuLiF4 2µm laser," Optics Letters, Volume 35, number 3, p 420 (2010).

[2] M. Schellhorn, "High-energy, in-band pumped *Q*-switched Ho^{3+}:$LuLiF_4$ 2 µm laser," Opt. Lett. 35, 2609-2611 (2010).

[3] M. J. D. Esser, H. J. Strauss, W. Koen, O. J. P. Collett and C. Bollig "End-pumped Ho:YLF & Ho:LuLF Slab Laser" in *4th EPS-QEOD Europhoton Conference*, Hamburg, Germany, WeP29, Europhysics Conference Abstract Volume 34C, ISBN 2-914771-64-9, (2010).

Publication List

Journal Papers

1. C. Bollig, C. Jacobs, M. J. D. Esser, and H. M. von Bergmann "Power and energy scaling of a diode-end-pumped Nd:YLF laser through gain optimization" *Optics Express* **18** (13), 13993-14003 (Jun 2010).

2. W. Koen, C. Bollig, H. Strauss, M. Schellhorn, C. Jacobs and M. J. D. Esser, "Compact Fibre-Laser-Pumped Ho:YLF Oscillator-Amplifier System," *Applied Physics B* **99** (1-2) 101-106 (April 2010).

3. L. R. Botha, C. Bollig, M. J. D. Esser, R. N. Campbell, C. Jacobs and D. R. Preussler "Ho:YLF pumped HBr Laser," *Optics Express*, **17** (22) 20615–20622 (Oct 2009).

4. M. J. D. Esser, D. Preussler, E. H. Bernhardi, C. Bollig, and M. Posewang "Diode-end-pumped Tm:$GdVO_4$ laser operating at 1818 nm and 1915 nm" *Appl. Phys. B.* **97** (2), 351–356 *(Special Issue)* (Sep 2009).

5. C. Jacobs, C. Bollig, T. Jones, S. Kriel, and M. J. D. Esser "Novel laser rate-equation formalism based on macroscopic parameters applied to laser feedback control design as application example" *IEEE Journal of Quantum Electronics* **45** (10) 1221-1231 (October 2009).

6. E.H. Bernhardi, A. Forbes, C. Bollig, and M. J. D. Esser "Estimation of thermal fracture limits in quasi–continuous–wave end–pumped lasers through a time–dependent analytical model" *Optics Express* **16** (15) 11115-11123 (2008).

7. E. H. Bernhardi, C. Bollig, M. J. D. Esser, A. Forbes, L. R. Botha and C. Jacobs, "A Single-Element Plane-Wave Solid-State Laser Rate Equation Model," *South African Journal of Science* **104** (9,10) 389–393 (Sep/Oct 2008).

Invited International Conference Papers

1. C. Bollig, M. J. D. Esser, C. Jacobs, W. Koen, D. Preussler, K. Nyangaza and M. Schellhorn, "70 mJ Single-Frequency Q Switched Ho:YLF Ring Laser – Amplifier System Pumped by a Single 82-W Tm Fibre Laser," *Middle-Infrared Coherent Sources*, Trouville, France, 8-12 June 2009, Mo3 (*invited*) (2009).

2. E. H. Bernhardi, C. Bollig, M. Eichhorn, M. J. D. Esser, P. Fuhrberg, A. Hirth, C. Kieleck, M. Schellhorn and K. Scholle, "High-Power Diode-Pumped 2 µm Lasers," *17th International Laser Physics Workshop (LPHYS'08), Trondheim, Norway*, p. 232, June/July 2008 (*invited*) (2008).

International Conference Papers

1. M. J. D. Esser, H. J. Strauss, W. Koen, O. J. P. Collett and C. Bollig "End-pumped Ho:YLF & Ho:LuLF Slab Laser" in *4th EPS-QEOD Europhoton Conference*, Hamburg, Germany, WeP29, Europhysics Conference Abstract Volume 34C, ISBN 2-914771-64-9, (2010).

2. W. Koen, H. J. Strauss, C. Bollig, M. J. D. Esser, C. Jacobs, O. J. P. Collett, K. Nyangaza and D. Preussler "200 mJ Single Frequency Ho:YLF & Ho:LuLF Slab Amplifier System at 2064 nm" in *4th EPS-QEOD Europhoton Conference*, Hamburg, Germany, WeC4, Europhysics Conference Abstract Volume 34C, ISBN 2-914771-64-9, (2010).

3. M. J. D. Esser, D. Preussler, A. Sharma, C. Jacobs and C. Bollig "Rugged and Compact Mid-infrared Solid-state Laser for Avionics Applications" in *International Aerospace Symposium of South Africa* (IASSA), 23 – 25 Nov 2009, Pretoria, South Africa (2009).

4. C. Bollig, H.J. Strauss, M. J. D. Esser, W. Koen, M. Schellhorn, D. Preussler, K. Nyangaza, C. Jacobs, E.H. Bernhardi and L.R. Botha, "Compact Fibre-Laser-Pumped Ho:YLF Oscillator-Amplifier System," *CLEO Europe*, Munich, Germany, 14-19 June 2009, CA10.6 (2009).

5. H. J. Strauss, C. Bollig, H. M. von Bergman and M. J. D. Esser, "Comparative study of thermal lensing in low-doped Nd:YVO_4 and Nd:$GdVO_4$ of equal doping concentration," *CLEO Europe*, Munich, Germany, 14-19 June 2009, CA9.5 (2009).

6. M. Schellhorn, S. Ngcobo, C. Bollig, M. J. D. Esser, D. Preussler, K. Nyangaza, "High-power diode-pumped Tm:YLF slab laser," *CLEO Europe*, Munich, Germany, 14-19 June 2009, CA1.3 (2009).

7. M. J. D. Esser, H. Strauss, W. S. Koen, D. Preussler, K. Nyangaza and C. Bollig, "*Q*-switched Ho:YLF Laser Pumped by a Tm:$GdVO_4$ Laser," *Middle-Infrared Coherent Sources*, Trouville, France, 8-12 June 2009, Po4 (2009).

8. H. J. Strauss, W. Koen, C. Bollig, M. J. D. Esser, D. Preussler, K. Nyangaza and C. Jacobs, "Efficient Fiber-Laser-Pumped Ho:YLF Oscillator and Amplifier Utilizing the Transmitted Pump Power of the Oscillator," *CLEO*, Baltimore, USA, 31 May – 5 June 2009, CWH3 (2009).

9. E. H. Bernhardi, C. Bollig, A. Forbes and M. J. D. Esser, "Modelling End-Pumped Solid-State Lasers," in *Proceedings of the 13th Annual Symposium of the IEEE/LEOS Benelux Chapter*, ISBN 978-90-365-2768-2, pp. 147-150, 27-28 November, Enschede, The Netherlands (2008).

10. M. J. D. Esser, D. Preussler, and C. Jacobs "Rugged, compact mid-infrared solid-state laser with simultaneous, modulated output at 2.3 µm and 4.0 µm" in *Technologies for Optical Countermeasures V*, SPIE 7115 7115-07 (2008).

11. C. Bollig, W. Koen, H. Strauss, E. Bernhardi, R. Botha, M.J.D. Esser, D. Preussler, "Exploiting the natural doping gradient of Nd:YLF crystals for high-power end-pumped lasers," *3rd EPS-QEOD Europhoton Conference*, Paris, France, Tup.20 (2008).

12. E. Bernhardi, A. Forbes, C. Bollig, and M. J. D. Esser "A Time-Dependent Analytical Thermal Model To Investigate Thermally Induced Stresses In Quasi-

CW-Pumped Laser Rods" *3rd EPS-QEOD Europhoton Conference*, Paris, France, THp.28 (2008).

13. Forbes, M. J. D. Esser, D. Preussler, S. Ngcobo, C. Bollig "Laser beam propagation characteristics of incoherently added diode bar stacks" in *Laser Beam Shaping IX*, SPIE 7062 7062-48 (2008).
14. M. J. D. Esser, C. Bollig and D. Preussler "Diode-End-Pumped Tm:$GdVO_4$ Laser at Selected Wavelengths," Poster WB6 *Advanced Solid-State Photonics*, Japan 2008 WB6 (2008).
15. E. H. Bernhardi, C. Bollig, L.Harris, M. J. D. Esser, and A. Forbes "Investigating Thermal Stresses in Quasi-CW Pumped Tm:YLF Laser Crystals" *Advanced Solid-State Photonics*, Japan 2008 WB11 (2008).
16. M. J. D. Esser, C. Bollig, D. R. Preussler, C. Jacobs, W. S. Koen, and E. H. Bernhardi "High-power diode-end-pumped Tm:$GdVO_4$ laser operating at 1818 nm and 1915 nm," *Marie Curie Chair Conference Recent advances in laser spectroscopy and laser technology* Lodz, Poland 2007.
17. M. J. D. Esser, C. Bollig and D. Preussler "Direct comparison of the thermal lenses of diode-end-pumped Nd:YVO_4 and Nd:$GdVO_4$ lasers using a simple evaluation technique," talk ThD3 *2nd EPS-QEOD Europhoton Conference, Pisa, Italy* 2006.

Monthly Technical Reports Prepared for External Research Project Sponsor – Lead Author

1. NLC-LTEBB-A07-REP-043 v_1 2010-08-17 (Betelgeuse Progress Report August 2010)
2. NLC-LTEBB-A07-REP-042 v_1 2010-07-02 (Betelgeuse Progress Report June 2010)
3. NLC-LTEBB-A07-REP-041 v_1 2010-05-25 (Betelgeuse Progress Report May 2010)
4. NLC-LTEBB-A07-REP-040 v_1 2010-05-05 (Betelgeuse Executive Report - 2006 to 2010)
5. NLC-LTEBB-A07-REP-039 v_1 2010-05-04 (Betelgeuse Progress Report April 2010)
6. NLC-LTEBB-A07-REP-038 v_1 2010-03-09 (Betelgeuse Progress Report March 2010)
7. NLC-LTEBB-A07-REP-037 v_1 2010-02-05 (Betelgeuse Progress Report February 2010)
8. NLC-LTEBB-A07-REP-036 v_1 2010-01-15 (Betelgeuse Progress Report January 2010)
9. NLC-LTEBB-A07-REP-035 v_1 2009-12-11 (Betelgeuse Progress Report December 2009)
10. NLC-LTEBB-A07-REP-034 v_2 2009-10-21 (Betelgeuse Executive Report - 2006 to 2009)
11. NLC-LTEBB-A07-REP-033 v_2 2009-09-30 (Betelgeuse Progress Report September 2009)
12. NLC-LTEBB-A07-REP-032 v_1 2009-08-27 (Betelgeuse Progress Report August 2009)

13. NLC-LTEBB-A07-REP-031 v_1 2009-07-28 (Betelgeuse Progress Report July 2009 #2)
14. NLC-LTEBB-A07-REP-030 v_1 2009-07-01 (Betelgeuse Progress Report July 2009)
15. NLC-LTEBB-A07-REP-029 v_1 2009-06-04 (Betelgeuse Progress Report June 2009)
16. NLC-LTEBB-A07-REP-028 v_2 2009-05-04 (Betelgeuse Progress Report May 2009)
17. NLC-LTEBB-A07-REP-027 v_1 2009-03-23 (Betelgeuse Progress Report March 2009)
18. NLC-LTEBB-A07-REP-026 v_1 2009-02-23 (Betelgeuse Progress Report February 2009)
19. NLC-LTEBB-A07-REP-025 v_1 2009-01-23 (Betelgeuse Progress Report January 2009)
20. NLC-LTEBB-A07-REP-024 v_1 2008-12-01 (Betelgeuse Progress Report November 2008)
21. NLC-LTEBB-A07-REP-023 v_1 2008-10-27 (Betelgeuse Progress Report October 2008)
22. NLC-LTEBB-A07-REP-022 v_1 2008-10-03 (Betelgeuse Progress Report September 2008)
23. NLC-LTEBB-A07-REP-020 v_2 2008-12-15 (Overseas trip report Sept 2008)
24. NLC-LTEBB-A07-REP-019 v_1 2008-08-22 (Betelgeuse Progress Report August 2008)
25. NLC-LTEBB-A07-REP-018 v_1 2008-07-24 (Betelgeuse Progress Report July 2008)
26. NLC-LTEBB-A07-REP-017 v_1 2008-06-26 (Betelgeuse Progress Report June 2008)
27. NLC-LTEBB-A07-REP-016 v_1 2008-05-23 (Betelgeuse Progress Report May 2008)
28. NLC-LTEBB-A07-REP-015 v_1 2008-04-17 (Betelgeuse Progress Report April 2008)
29. NLC-LTEBB-A07-REP-014 v_1 2008-03-03 (Betelgeuse Progress Report February 2008)
30. NLC-LTEBB-A07-REP-013 v_1 2008-01-29 (Betelgeuse Progress Report January 2008)
31. NLC-LTEBB-A07-REP-012 v_1 2007-12-03 (Betelgeuse Progress Report November 2007)
32. NLC-LTEBB-A07-REP-011 v_1 2007-10-24 (Betelgeuse Progress Report October 2007)
33. NLC-LTEBB-A07-REP-010 v_1 2007-09-28 (Betelgeuse Progress Report September 2007)
34. NLC-LTEBB-A07-REP-009 v_1 2007-08-27 (Betelgeuse Progress Report August 2007)
35. NLC-LTEBB-A07-REP-008 v_1 2007-07-30 (Betelgeuse Progress Report July 2007)
36. NLC-LTEBB-A07-REP-007 v_1 2007-06-25 (Betelgeuse Progress Report 2 June 2007)
37. NLC-LTEBB-A07-REP-006 v_2 2007-06-19 (Betelgeuse Progress Report June 2007)
38. NLC-LTEBB-A07-REP-005 v_1 2007-05-08 (Betelgeuse Progress Report May 2007)
39. NLC-LTEBB-A07-REP-004 v_1 [2007-03-27] (Betelgeuse Progress Report

March 2007)

Technical Project Reports Prepared for External Research Project Sponsor – Lead Author

1. NLC-LTEBB-A02-REP-003 v_1 [2007-02-19] (Evaluation of the 2 µm pump laser)
2. NLC-LTEBB-A02-REP-004 v_1 2008-01-09 (Refine and optimise 2 um pump laser)
3. NLC-LTEBB-A04-REP-002 v_1 [2008-03-04] (Construct 2 µm laser oscillator)
4. NLC-LTEBB-A05-REP-001 v_1 2008-11-25 (Design of high-energy 2 µm amplifier)
5. NLC-LTEBB-A06-REP-004 v_2 (Refine & Optimise 4 um converter phase 1)
6. NLC-LTEBB-A05-REP-002 v_1 2009-10-25 (Test & Evaluate high-energy 2 um amplifier)
7. NLC-LTIC100-REP-006 v_1 2009-03-12 (PG final report) (Advanced mid-IR laser research)
8. NLC-LTTAB-REP-002 v_03 [2008-04-02] (YREF Final Report)
9. LTTAB00 YREF Project Review Report 2006

Technical Project Reports Prepared for External Research Project Sponsor – Co-Author

1. NLC-LTEBB-A01-REP-001 v_2 [2008-10-07] (System Concept Design)
2. NLC-LTEBB-A06-REP-003 v_2 (Test & Evaluate 4 um converter phase 1)
3. NLC-LTEBB-A08-REP-001 v_1 [2010-01-19] (Design 4 um converter phase 2)